Combination of biochemical, molecular and biophysical approaches to investigate the impact of strain background and production process on the yeast cell wall composition and molecular architecture

Marion Schiavone

Université Fédérale

Toulouse Midi-Pyrénées

THÈSE

En vue de l'obtention du

DOCTORAT DE L'UNIVERSITÉ DE TOULOUSE

Délivré par :

Institut National des Sciences Appliquées de Toulouse (INSA de Toulouse)

Présentée et soutenue par :

Marion SCHIAVONE

Le 22 décembre 2014

Titre :

Combination of biochemical, molecular and biophysical approaches to investigate the impact of strain background and production process on the yeast cell wall composition and molecular architecture

---

École doctorale et discipline ou spécialité :

ED SEVAB : Ingénieries microbienne et enzymatique

Unité de recherche :

Laboratoire d'Ingiénierie des Systèmes Biologiques et des Procédés, UMR5504/792

Directeur(s) de Thèse :

Jean Marie FRANCOIS

Etienne DAGUE

Jury :

Hervé ALEXANDRE, Professeur Université de Bourgogne, Dijon	Rapporteur
Grégory FRANCIUS, Chargé de Recherche LCPME-CNRS, Villers-lès-Nancy	Rapporteur
Aude VERNHET, Professeur SupAgro, Montpellier	Présidente
Mathieu CASTEX, Directeur R&D, Lallemand, Blagnac	Invité
Sébastien DEJEAN, Ingénieur de recherche, Université de Toulouse, Toulouse	Invité

Remerciements

Je tiens à remercier le directeur du laboratoire du LISBP de l'INSA de Toulouse, Nic Lindley, et le directeur du LAAS-CNRS à Toulouse, Jean Arlat, de m'avoir accueilli dans leurs laboratoires.

Je suis reconnaissante à mon directeur de thèse, Jean Marie François, de m'avoir accueillie dans son équipe et de m'avoir témoigné sa confiance de l'entretien jusqu'à la soutenance. Je remercie également mon co-directeur de thèse, Etienne Dague, pour son soutien durant ses trois années. Merci à tous les deux pour vos échanges et votre dynamisme scientifique.

Je remercie la société Lallemand d'avoir financé ma thèse. Je suis tout particulièrement reconnaissante à Mathieu Castex, Nathalie Sieczkowski, Anne Julien-Ortiz et Henri Durand qui se sont impliqués dans ce projet.

Je remercie les membres du jury d'avoir accepter de juger mon travail.

Je tiens également à dire un grand merci à toute l'équipe Physiologie et métabolisme des eucaryotes « ead5 » pour tous les moments, professionnels et personnels, partagés ensemble. Un grand merci à Amélie pour son soutien indéfectible, son aide dans les tâches fastidieuses et nos échanges qui me manquent. Je remercie Marjorie pour son dynamisme et tous ses moments au laboratoire même quand il était tard… Je te souhaite une bonne chance pour la suite. Je remercie également tous mes autres collègues Jérôme, Marion, Clément, Agustina, Ceren, Debora, Ran, Jian, Xu, Yvan, Luce et Romain pour nos échanges variés sur les champignons, bactéries et levures. Merci aussi de m'avoir fait voyager à travers vos paroles de l'Argentine à la Chine en passant par la Turquie et le Brésil. Je remercie aussi Marie-Ange pour sa patience ainsi que tous les titulaires de l'équipe : Hélène, Jean-Luc, Thomas, Gustavo et Jean-Pascal pour leur gentillesse.

Je remercie aussi mes amis et collègues du LAAS-CNRS. A Cécile pour tous ses moments au laboratoire dans la cave aux araignées près de l'AFM ou à partager un bon aligot et du caramel au beurre salé. A Flavien et sa bonne humeur, mais aussi à Véronique et Carlos qui ont partagé ma troisième année de thèse…

Je remercie toutes les personnes qui ont su m'aider et partager leurs connaissances quand j'en avais besoin, notamment Lidwine Trouilh et Sophie Lamarre de la plateforme Biopuces pour la partie transcriptomique, Cédric Montanier pour la purification de l'enzyme et Sébastien Déjean pour l'analyse bioinformatique.

Je tiens aussi à remercier mes amis bretons, Nico, Coralie, Katell, Franck, Tiphaine et Solena, qui ont su m'encourager malgré la distance.

Finalement, je suis très reconnaissante à ma famille et tout particulièrement à mes parents de m'avoir aidé et encouragé tout au long de mes études.

Abstract

Due to increasing yeast biomass production resulting from the expansion of the Biorefinery as an alternative to petrol-based energy, the yeast cell wall is receiving an increasing interest as an added value product targeting agro-nutrition markets, such as in animal nutrition and in wine for its probiotic and sorption properties. The study of the yeast cell wall composition and structure is a research topic now addressed for more than twenty years. The data acquired to date show the importance of the strain origin, the culture conditions and processes on the biochemical composition and the biophysical properties of the cell wall. However, the relationships between composition and molecular structure on one hand, and between mechanical properties and molecular architecture of the cell wall on the other hand, are largely incomplete. This is notably due to a lack of (i) methods able to determine quantitatively the exact composition of yeast cell wall and (ii) of biomathematical tools allowing to unravel these relationships. The purpose of this thesis was therefore to combine DNA microarrays, biochemical and biophysical approaches in order to investigate the relationships between these parameters as well as to highlight the impact of strains, growth conditions and processes on the cell wall composition and biophysical properties. To achieve this objective, an acido-enzymatic method was developed to specifically quantify each of the four components of the yeast cell wall, namely mannan, chitin, β-1,3-glucan and β-1,6-glucan. This method was validated on mutant strains disrupted in genes, encoding proteins essential for the cell wall biosynthesis, as well as by studying various stresses. Then, the use of atomic force microscopy (AFM) has allowed investigating the same strains and four strains used in industrial fermentation. They demonstrated distinct nanomechanical and adhesive properties, due to differences in their cell wall structure and composition. By a biostatistical analysis, the interaction between an AFM tip functionalized with a lectin and the cell surface was associated to the levels of mannan in the cell wall. Since concanavalin A binds α-glucose and α-mannose units, these adhesion results were in agreement with biochemical data sets. Content of mannan and adhesion frequency of the lectin-cell wall interaction were also correlated to genes involved in proteins processing, ergosterol and cell wall mannoproteins biosynthesis. Moreover, we found a close association between cell wall elasticity (*i.e.* Young modulus values) and levels of β-1,3-glucans. The genes that were correlated with this association encoded protein implicated in membrane and cytoskeleton assembly, β-glucan biosynthesis and assembly as well as in MAPK signaling pathways. In the last part, the effects of the autolysis and fluid-bed drying processes are presented. The results show that this specific packaging of yeast, sold as Yeast Cell Wall, does not change the composition of the cell wall but induces a modification in topography and surface properties of the cell. Moreover, using AFM we imaged on *S. cerevisiae* cell surface highly adhesive patches forming nanodomains. These nanodomains were attributed through transcriptomic data to Flo11 proteins probably aggregated into β-amyloids clusters.

Table of contents

General introduction

The yeast *Saccharomyces cerevisiae* also well-known as baker's, brewer's and wine yeast, has been employed over millennia, in the food production especially the leavened bread dough and alcoholic beverages (Walker, 1998). This relevant microorganism is used for the annual production of 60 million tons of beer, 30 million tons of wine and 600 000 tons of baker's yeast (Pretorius, 2003). Nowadays, *S. cerevisiae* is also associated with the production of bioethanol (20 billion of liter per year), fertilizer, animal feed, industrial enzymes and metabolites with low molecular weight such as lactic acid (Ostergaard et al., 2000) or flavor compounds (esters, alcohols). Besides its industrial interest, this organism approved by the FDA and the European Union as "*GRAS*" for Generally Recognized As Safe, constituted a model for the study in fundamental and molecular mechanisms of eukaryotic cells. Indeed, the complete sequence of *S. cerevisiae* genome, published in 1996 (Goffeau et al., 1996) has allowed to apprehend the yeast physiology at the genome scale, showing notably the complexity of the cell wall synthesis machinery and its connections with many cellular processes such as cell metabolism and cell reactions to stress (Lesage et Bussey, 2002).

Responsible for maintaining the cell shape, the cell wall of *Saccharomyces cerevisiae* is known to be a complex interplay of 4 major polysaccharides: β-1,3 glucan (up to 1500 glucose units linked in β-1,3), β-1,6 glucan (140 to 350 residues of glucose linked by β-1,6 linkages), mannan (mannose units linked in α-1,2; 1,3; 1,6) and chitin (polymer of 100 to 190 N-acetylglucosamine units linked by β-1,4 linkage) (Klis et al., 2006). Many studies have described the use of the cell wall as feed additive, due to the role of mannoproteins and β-glucan to remove by adsorption toxic molecules such as mycotoxins (Shetty and Jespersen, 2006) or to improve the quality and stability of wine (Alexandre and Guilloux-Benatier, 2006; Chalier et al., 2007), but also the role of β-glucanases to improve the ageing of sparkling wines (Rodriguez-Nogales et al., 2012). Indeed, the cell wall is a dynamic structure and its architecture is continuously remodeled by cell wall remodeling enzymes, with glucanosyltransferase or branching activity (i.e. Gas1, Bgl2, SCWP), in order to integrate polymers recently produced by β-glucanases and chitinases. Moreover, yeast cell walls can display an aggregation with probiotic bacteria (Hatoum et al., 2012; Katakura et al., 2010) or stimulate the immune system (Novak and Vetvicka, 2009).

Although the biotechnological properties of the cell wall products are well known, the molecular mechanisms on which they rely are still poorly understood and are under investigations (Yiannikouris et al., 2006). However, it was shown that the polysaccharides from the cell wall have different proportions and sorption capacity depending on strains, culture conditions (temperature, aeration, carbon sources) and drying processes (Aguilar-Uscanga and Francois, 2003; Pradelles et al., 2008). Until now, most of the studies on cell wall stress have mainly been conducted by biochemical and molecular approaches. They have allowed determining intracellular mechanisms: stress sensors (as Wsc1 or Mid2) detect the environmental changes and trigger the activation of signaling pathways leading to cell wall reinforcement by a compensatory mechanism (Lesage et Bussey, 2006). Therefore, an appropriate imaging of what is happening at the cell surface and the measure of cell surface properties would be complementary to biochemical and molecular data to provide a better understanding of cell wall remodeling mechanism and resistance to stress conditions.

In order to conduct these investigations, we employed different techniques:

We first developed a new biochemical method for the precise quantification of cell wall polysaccharides. Indeed, nowadays, the actual methods to study the cell wall composition use either chemical treatment or enzymatic hydrolysis. Among them, enzymatic methods are only used to study the structure of cell wall polysaccharides, but they were not used to quantify the different polysaccharides of the cell wall, in contrast to chemical methods. Methods using strong acids are used since many years to hydrolyze cell wall polysaccharides into their corresponding monomers which are then analysed by chromatography technique such as HPAEC-PAD (High Performed Anionic Exchange Chromatography coupled to Pulsed Amperometric Detection). These methods of hydrolysis present some drawbacks: first, they damage the monomers released; second, they do not cleave all the chitin polymer leading to an underestimation of this compound; third, they do not allow to distinguish the amount of β-1,3-glucan to β-1,6-glucan. Therefore, our first aim was to develop a new method combining acid and enzymatic hydrolysis to accurately quantify mannans, chitin, β-1,3 and β-1,6-glucan. This new method was validated by phenotypic observations using Congo Red and Calcofluor White. Then, by analysis of the cell wall composition of the laboratory reference strain BY4741 (EUROSCARF collection) compared to different mutants: *fks1*Δ (in which the gene coding for the major catalytic subunit of β-1,3 glucan synthase I is deleted), *gas1*Δ (missing a gene coding for an

β-1,3-glucanosyltransferase), *kre6*Δ (affected in synthesis of β-1,6 glucan), *mnn9*Δ (deficient in the process of N-glycosylation of proteins); *chs3*Δ (deleted mutant of the chitin synthase III gene). The development and validation of this biochemical method has allowed us to characterize the cell wall composition of industrial diploid strains (L71, L69, L62, L60) provided by Lallemand SAS and cultivated in laboratory conditions. The corresponding commercial products (autolysed dry yeasts) of these strains were also analyzed in an effort to better characterize the impact of strain background and environmental conditions (as processes) on the cell wall composition.

The second originality of my thesis work was to use the atomic force microscope (AFM) in combination with the biochemical approach, to investigate the cell surface properties and dynamic of these different mutants and industrial strains. The purpose of this biophysical study was clearly to search for a possible link between the biochemical composition and nanomechanical properties of the yeast cell wall. AFM has been preferred to other microscopies (Scanning Electron Microscopy or Transmission Electron Microscopy), because it allows to investigate living cells at the nanoscale. No solely an imaging tool, AFM is a force machine able to record force measurement and thereby to quantify the interactions between the tip and the sample. Since past few years, it has emerged as useful tool to characterize the biophysical properties of yeast surface such as adhesion, roughness and elasticity or to reveal changes in morphology due to stress conditions (Canetta et al., 2006; Dufrêne, 2002). In addition, it is possible to map biological sites on living cells at molecular resolution with a molecule attached at the end of the tip. All these possibilities with the AFM are relevant to solve the nanoscale architecture of the yeast cell wall from different strains and different environmental conditions, which challenge the cell (processes or exposure to drugs).

Finally, to obtain a comprehensive view of the different phenotypes and industrial properties of the industrial strains, we took advantage of DNA microarray to compare the transcriptomic profiles of these strains under the growth condition. Earlier, the genome transcription profiles of mutants deleted for genes that affect the cell wall composition (Lagorce, 2003) or the expression profile of yeast in presence of cell wall perturbing drugs (Congo Red, Zymolyase, pneumocandins) (García et al., 2004; Rodriguez-Pena, 2005) have shown that a set genes involved in signaling, cell wall biogenesis, metabolism and generation of energy are activated. These studies have contributed to understand the molecular basis of the stress adaptations responses and reveal that the increased chitin content in cell wall mutants may be explained by the concurrent up-regulation of *GFA1* and *CHS3* (Lagorce et al.,

2002). Therefore the use of transcriptomic analysis of about 6 000 genes of the four industrial strains grown in the same culture condition as used in the biochemical and biophysical investigations, may help to identify a core of genes important in cell wall organization and cell surface properties. This characterization helped us to find a link between genomic profiles, cell wall composition as well as structure at the molecular and nano level in order to explain mechanism induces by genetic background (‘strain effect’) or environmental modifications.

In addition the ‘strain effect’ and ‘process effect’ will be investigated to better understand which molecular mechanisms and treatments on the cell can change the yeast cell wall in order to improve targeted productions for biomedical or food applications. For the Lallemand Company, this comprehension will help improving the actual products and developing new products derivative from the yeast cell wall for new applications in oenology or animal nutrition.

Outlines of the thesis

This thesis is divided in different parts.

In **chapter 1**, a literature review on the yeast *Saccharomyces cerevisiae* physiology including the methods of culture and processes employed in industrial fermentation is presented. I will then focus on the cell wall biogenesis, assembly and mechanisms, which govern the molecular architecture, as well as on the biotechnological values of the cell wall components.

In **chapter 2**, I will present my first thesis results which have consisted in the development of a method combining enzymatic and acid hydrolysis to quantify all the components that composed yeast cell wall, namely chitin, mannans, β-1,6-glucan and β-1,3-glucan. I will show that this method has been validated on cell wall defective mutants (*chs3Δ, fks1Δ, kre6Δ, gas1Δ, mnn9Δ*) and has allowed evaluating the impact of ethanol, heat shock and antifungal drug on cell wall composition. This work is published in FEMS Yeast Research Journal.

Chapter 3 deals with the influence of the strain background on yeast cell wall composition and biophysical properties.

In a first part, the possible links between the biophysical properties and the cell wall composition was examined on yeast mutants that are deleted in genes responsible for the chitin synthesis (*chs3Δ*), branching/elongation of β-glucan (*gas1Δ*) and protein mannosylation (*mnn9Δ*). Furthermore, using previous transcriptomic data (Lagorce, 2003) on *gas1Δ* and *mnn9Δ* mutants I tried to correlate gene expression level with cell wall composition and biophysical properties (nanomechanics and surface properties).

In the second part of this chapter, four industrial yeast strains provided by Lallemand SAS were studied. The analysis of the cell wall composition of these strains has shown different profiles, reflected in the difference of the mechanical behavior and adhesion properties measured by AFM. The global gene expression of these strains led to find some correlations and to highlight some genes of interest.

In **chapter 4**, the influence of two culture media and industrial processes such as autolysis and alkalase treatment on cell wall composition of industrial yeasts are investigated and compared to

previous data. Autolysis impact on morphology, nanomechanical and adhesion properties was also studied on these strains by AFM.

Finally, **chapter 5** presents a general conclusion and ideas for future works.

In **chapter 6** are listed the references of this manuscript.

In **appendix (chapter 7)** are gathered material and methods as well as publications I contibuted during my thesis work. These two publications are about the impact of, heat shock and exposure to caspofungin, on the cell wall biochemical composition and nanomechanical properties. These studies are respectively published in BMC Biology (2014) and in Antimicrobial Agents and Chemotherapy (2012).

Chapter I: LITERATURE REVIEW

1. Generality on yeast

1.1. Physiology: generality about growth, metabolism and genetic

The yeast *Saccharomyces cerevisiae* is an unicellular eukaryote fungus that belongs to ascomycete family. The capacity of this yeast to grow quickly and easily on different carbon sources (glucose, fructose and maltose) and its non-pathogenicity have contributed to make it the preferred organism in industry.

The typical yeast growth curve on glucose as the main and sole carbon source can be divided into 4 stages: a lag phase, an exponential phase, a transition or diauxic phase and a stationary phase.

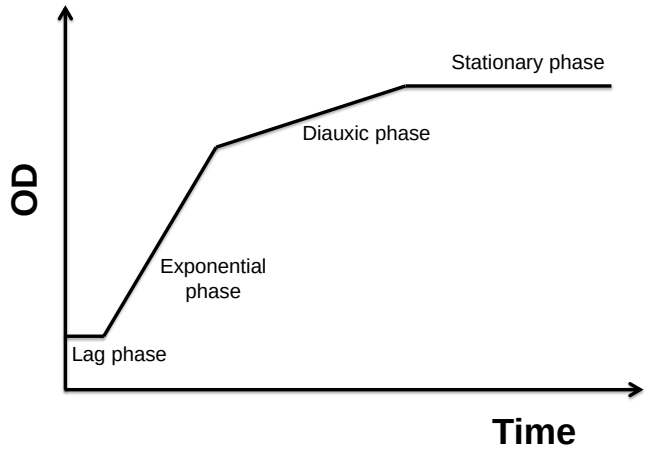

Figure I-1. Typical growth curve of yeast on glucose containing medium

The lag phase is a period during which the yeast cells adapt to the medium, undergo primary budding consuming endogenous carbon sources (trehalose) and then start to assimilate exogenous carbon (glucose) source. The exponential or log phase corresponds generally to a short phase of fermentative metabolism, during which the growth rate is maximal until the yeast have consumed all glucose available. It is followed by a transition phase or 'diauxic shift' when yeast physiology undergoes several changes and notably allows the assimilation of ethanol produced during the exponential phase, which requires full respiratory ability. Then, after yeast cells have consumed all the carbon sources, they enter the stationary phase during which many metabolic processes are down-regulated.

Yeast cells can then enter a quiescent stage or develop apoptotic processes ultimately leading to the cell death (Walker, 1998).

The volume of a yeast cell is mainly occupied by the cytosol containing different compartments: the endoplasmic reticulum and the Golgi apparatus involved in the synthesis and transport of molecules; the vacuoles required for the storage of lytic enzymes and metabolites such as amino acids and polyphosphates; mitochondria where ATP is synthetized. To maintain the internal structure, the cell possesses an internal skeleton called the cytoskeleton and composed of actin filaments and microtubules. Actin filaments allow transport of cellular components through vesicles and myosin motors during bud growth, while microtubules are required for the repartition of chromosomes at time of cell division. In vegetative growth, the yeast *Saccharomyces cerevisiae* is reproduced by budding. The cell division cycle is composed of four stages: G1, S, G2 and M (see Figure 2).

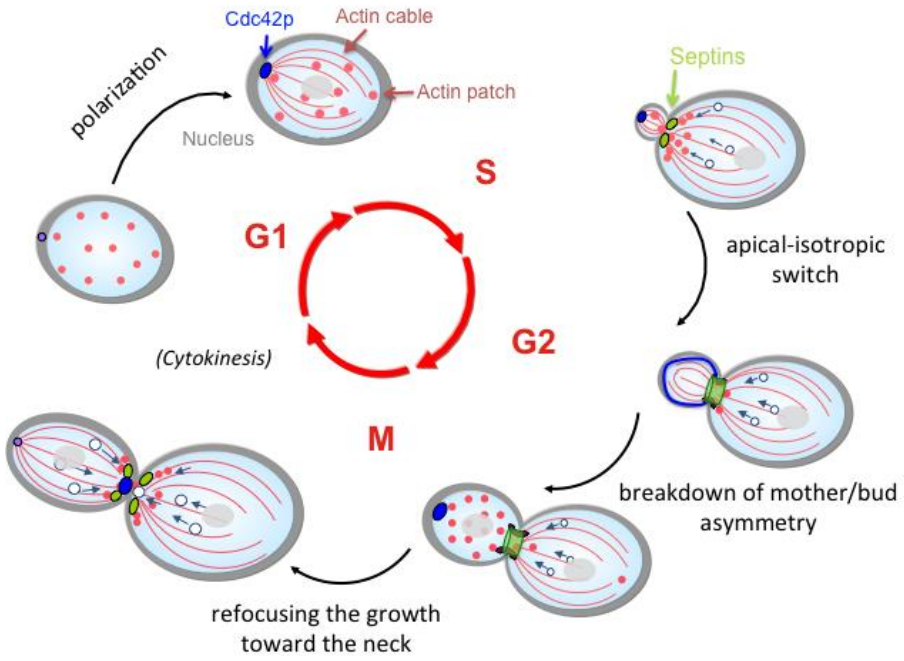

Figure I-2. Morphogenetic events during *Saccharomyces cerevisiae* cell cycle (adapted from (Martin-Yken, 2011) and (Howell and Lew, 2012)

During G1 (Gap), the cell diameter is increased and the cytoskeleton is polarized. It is followed by S phase (Synthesis) when the DNA is duplicated and the bud initiated; in G2 the apical-isotropic switch and a depolarization lead to bud expansion. In M (Mitose), the duplicated chromosomes are separated between the mother and daughter cells leading to the nuclear division. After the mitosis, the growth is refocused toward the neck leading to cytokinesis and cell separation. Membranes and cell walls are separated to form two distinct cells with the same genome. The daughter has a smaller size and

exhibits a birth scar whereas a bud scar rich in chitin remains on the mother cell side (Blanco et al., 2012). The cell cycle of *S. cerevisiae* is under the control of the Cdc28p CDK (cyclin depend kinase), which interacts with different cyclins (Clns and Clbs) that are specific to each phase (see review by Howell and Lew, 2012). Cdc42p is a master regulator of the cell cycle morphogenesis process, because this protein is absolutely required for the polarization of the cytoskeleton and the bud emergence (Howell and Lew, 2012). In G1, Cdc42p is concentrated as a patch at the presumptive bud site on the plasma membrane. At this site, actin cables as well as a cluster formed by actin patches are oriented and a ring of septin filaments is assembled. After the bud emergence, the apical growth switches to isotropic growth: the growth and the deposition of cell wall are not only directed to the tip of the bud anymore, but to the whole bud surface. After the switch, Cdc42p appears distributed around the bud cortex.

Haploïd yeast cells can present two different mating types: they are either MAT**a** or MATα. Congugation can happen between twocells of opposing mating types. This phenomeneon is triggered by the presence in the medium of pheromones. MAT**a** cells secrete **a** type pheromone, to which only MATα cells are sensitive, while MATα cells produce α type pheromone or “α-factor” which, conversely, only MAT**a** cells are sensitive. Sensing of the opposite mating type pheromone induces a cell cycle arrest at G1 stage, and the formation of a conjugation projection or “shmoo”. Fusion of the two haploids cells of opposed mating types results in zygote, and finally a diploid cell (a/α). If the growth conditions are favorable, diploid cells also reproduce by budding with a similar cell cycle. On the contrary, in a nutrient-defective medium lacking for example carbon or nitrogen, Meiosis takes place to allow the apparition of better-adapted progeny by genetic recombination. Sporulation of diploid cells upon meiotic cell cycle liberates four haploid spores, held together in a single ascopore. These spores, when separated, can latter undergo germination to generate new haploids **a** and α cells.

The complete genome sequence of *S. cerevisiae* was the first of any eukaryotic organisms to be published. Its represents 12 068 kb distributed over 16 chromosomes, and encodes a little less than 6000 genes (Goffeau et al., 1996). The genome sequence is still today the best annotated of all published genomes (Cherry et al., 1998) [*Saccharomyces* Genome Database, www.yeastgenome.org].

1.2. Yeast and the mode of culture and production process

Mode of culture: batch, fed-batch and continuous

"Batch" culture is a closed culture system, which contains a limited amount of nutrient added at the start of the culture and where pH is initially adjusted. Thus in batch fermentation, environmental conditions are continuously changing with time, due to metabolic activity and growth of yeast cells; the fermentor is considered as an unsteady-state system. It is used in laboratory to study the yeast physiology or in industry for fermentation purposes that generate biomass, primary and secondary metabolites.

A second commonly used mode of culture is termed "Fed-batch". In this mode, culture is initially inoculated from a previous batch culture, where the cells are grown usually until the end of the exponential growth phase. Then the fermentor is fed, continuously or sequentially, with a solution of substrates or medium without the removal of culture fluid, leading to increase the volume of the liquid contained in the reactor. This mode of culture has been developed to increase the production of biomass by keeping the concentration of the limiting substrate at low levels and thus avoiding the inhibitory effects of high substrate concentrations and overflow metabolism products.

The third most common culture mode, "continuous" culture, involves continuous feeding the yeast culture with fresh nutrients and, at the same time, removing spent medium plus cells from the system, while keeping the culture volume constant. The major characteristic of continuous culture is its 'steady-state': biomass, substrate and product concentration are maintained constants over very long periods of time.

Production processes: methods to collect and to pack yeast products

Industrial yeast products are generally obtained by a controlled aerobic fermentation in batch and fed-batch to ensure a high biomass. In fermentation, sugar cane molasses and beet molasses are the principal carbon sources (mostly sucrose, but also glucose and fructose) for the growth. From the commercial point of view, the type of the molasses used depends on the availability, types, costs, and the presence of inhibitors and toxins. The molasses mixture is diluted with water, clarified to remove any sludge (usually calcium salts), sterilized with high-pressure steam and finally held in tanks until its use in production.

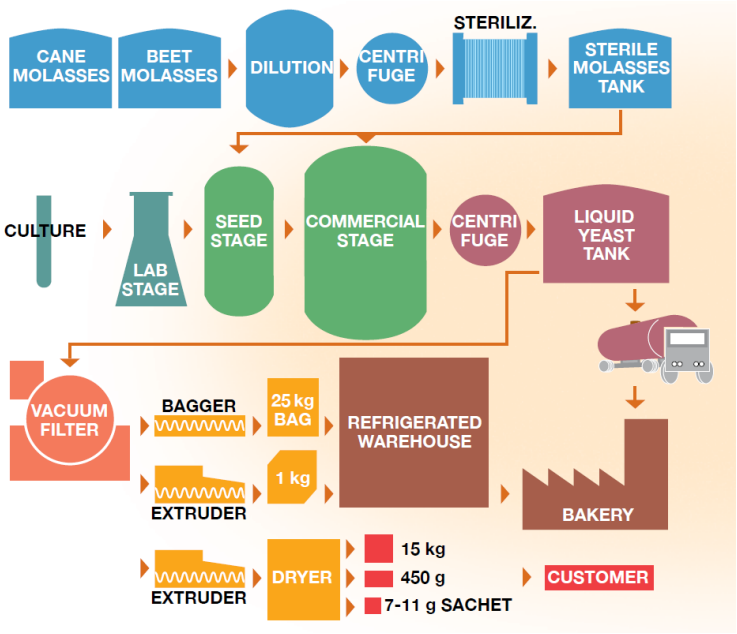

Figure I-3. Schematic flowchart of a commercial yeast plant (from Lallemand Inc.)

As shown in Figure I-3, the commercial yeast production process starts from the single cell culture, which is prepared in the flasks in the laboratory under generally micro-aerobic conditions until sufficient amount of yeast is obtained to seed the first industrial stage of yeast culture. This is a batch fermentation on a mixture of molasses, minerals (Phosphorous, Magnesium, Manganese, Zinc etc) and some B-complex vitamins. Each stage in the lab and the first in the plant require about 24h and are generally carried out as batch processes, with or without the addition of air. Aeration is used to supply the culture with oxygen, which is crucial for synthesis of cell membrane sterols. Generally the first batch stage in the plant process will be aerated but the yeast is still largely fermenting.

The next stage in the plant after this large batch (≈ 10,000 L) stage is the first truly aerobic propagation. The batch will be transferred to another large vessel and diluted with a volume of sterile water. To this the molasses and ammonia required for growth will be supplied in a growth rate dependent manner making this stage a fed-batch process. The control of this feeding is normally achieved through the use of process control software, which maintains the feeding rate such that no, or rather small amounts, of ethanol are produced but the main aim is production of only yeast biomass. At the end of this first fed-batch stage, often called seed or mother propagation, the vessel content are centrifuged to separate and wash the yeast resulting in a yeast solution known as “yeast cream” that has a dry weight of about 20% dry matter, and a beige color. This seed cream yeast can then be used to “seed” further yeast propagations as required. These subsequent propagations are

often termed “commercial” propagations as it is in this stage the modifications can be made to the growth of the yeast in order to prepare them for the various potential applications that that can be subjected to.

Commercial yeasts are available under four forms: creams, compressed yeast, instant dry yeast and autolysed yeast.

The preferred form for many bakeries is the cream, obtained from the fermenters and delivered directly, which contains around 85% of water. The cream can be filtered and pressed into a block called ‘cake’ of compressed yeasts, the most widely used yeast in this form is baker’s yeast containing approximately 70% water and 30% (w/v) dry matter.

The procedure to obtain instant dry yeast is similar to the manufacture of compressed yeast. The yeast cream is filtered, pressed and dried using fluid bed drying. Due to the small size of the particle of the instant dry yeast and to maintain the high level of dry matter in the dry yeast, the packaging is made under vacuum. The yeast can be pretreated with emulsifiers to obtain lower moisture levels (Lee et al. 1996).

Autolysis consists to heat a cell suspension, which cause cell lysis and the self-digestion of the proteins and intracellular constituents of the yeast by the intrinsic enzymes of yeast cells cytoplasm. Those lytic enzymes are nucleases, proteases and glucanases. Nucleases degrade the DNA and RNA into nucleotides, whereas proteases and glucanases can hydrolyze the cell wall components. Influenced by temperature and pH, autolysis has been found to be optimal at 50°C during 24h and pH 6.0 (Tanguler and Erten, 2008) in order to produce yeast extract from *S. cerevisiae*. The autolysates can either be dried or treated to produce soluble yeast extract by separation of the insoluble cell wall fraction. The major compounds liberated during autolysis are nitrogenous compounds, polysaccharides of the cell wall degradation, fatty acids and volatile aromatic compounds such as esters and alcohols which can influence the aromatic profile of sparkling wines (Rodriguez-Nogales et al., 2012)(Pozo-Bayón et al., 2009).

1.3. Cell wall as biotechnological product

Since decades, *Saccharomyces cerevisiae* produces most of the biotechnological products in the world. This yeast is an effective biosorber to reduce some molecules or toxins concentration. Numbers of studies have also demonstrated than besides its biomass, the *S. cerevisiae* cell wall has several beneficial effects and it could be used in many domains as winemaking, animal nutrition and medicine.

In winemaking, the cell wall ability to absorb is well known (Lafon-Lafourcade et al., 1984) and its use as an oenological additive is accepted by the European Union. Esters and aroma compounds (Chalier et al., 2007), thiols (Tirelli et al., 2010) may interact with mannoproteins as well as volatiles phenols such as 4-ethylphenol, which at more than 440 µg/L gives a spicy taste to red wine, but also involve β-1,3-glucan, explaining that *gas1Δ* mutant may sorb 75% less that wild-type strain (Pradelles et al., 2008). This sorption capacity is also dependent on strains, culture conditions and drying processes, which permit to decreased (-)geosmine concentration, a molecule which gives a mouldy taste to wine, for at least 50% by combining different industrial process (Pradelles et al., 2010). It has been demonstrated that the addition of yeast cell walls, mannoproteins or cell wall remodeling enzymes such as β-glucanases can improve the effect of autolytic activity in the wine (Alexandre and Guilloux-Benatier, 2006) and, the physicochemical and sensorial aspects of sparkling wines (Rodriguez-Nogales et al., 2012).

In animal nutrition, the cell wall from whole cells as well as envelope may adsorb different molecules such as mycotoxins which can complex with β-glucan *in vitro* (Armando et al., 2012; Joannis-Cassan et al., 2011; Shetty and Jespersen, 2006; Yiannikouris et al., 2004a, 2006) and observe *in vivo* on rats (Firmin et al., 2010), thus its used as feed additive may lead to the suppression of these toxic molecules from the organism. In addition to the role of the cell wall as detoxifying agent, it was also demonstrated that β-glucan, its major polysaccharides, are biological response modifier (BRMs) with a strong immunostimulating activity (Brown and Gordon, 2003; Novak and Vetvicka, 2009). According to this positive effect on the immune system yeast β-glucan is increasingly considered as a probiotic ingredient (Feldmann, 2012), which provides beneficial effects on health and resistance to diseases and cancer (see reviews (Kogan and Kocher, 2007) and (Chen and Seviour, 2007)). Indeed, β-1,3-glucan has been reported to increase resistance infections by Gram-negative bacteria and exert anti-tumor, antibacterial, antimutagenic, antioxidant activities. Moreover, the yeast cell wall can play a role in the co-aggregation and cohesion with the probiotic bacteria (Millsap, 1998). Yeast cell wall mannoproteins form a capsule-like structure where the bacteria may associate with the polysaccharides (Katakura et al., 2010; Millsap, 1998) which results in an enhancing of the bacterial survival and the stimulation of their growth (Katakura et al., 2010; Suharja et al., 2014).

2. Methods to study the yeast cell wall

The covalent linkages between the cell wall polysaccharides and the highly glycosylated proteins make the study of the cell wall composition and architecture even more difficult. However, genetic, proteomic, immunologic, microscopy and electrophoresis approaches have allow identifying the cell wall proteins. The major polymers in the cell wall have been identified by analysis of the carbohydrates composition.

2.1. Methods to determine the yeast cell wall composition

Several methods aiming at quantifying the cell wall constituents have been published. Most of them used chemical treatments with either separation of alkali soluble and alkali insoluble fractions or acid hydrolysis.

Based on solubility of the cell wall polysaccharides in alkali, mannoproteins and β-glucan can be separated after hydrolysis. Initially studied by Fleet and Manners in the 80's alkali extraction of glucan from *S. cerevisiae* was performed with cold and diluted sodium hydroxide under nitrogen. Later, the alkali treatment was performed on whole cells (Ha et al., 2002) or on purified cell walls (Yiannikouris et al., 2004b) with hot sodium hydroxide (Shokri et al., 2008).

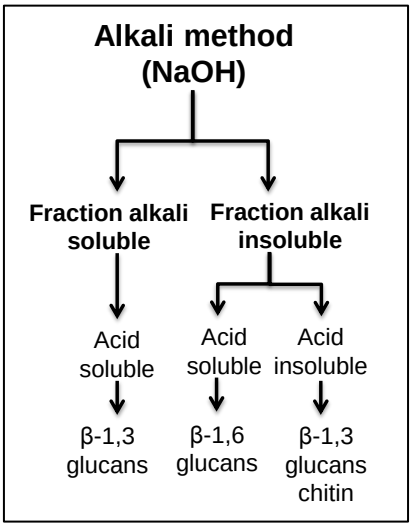

Figure I-4. Scheme of alkali separation of the cell wall polysaccharides

As depicted in the Figure 4, the alkali treatment using sodium hydroxide distinguishes the β-1,3 and the β-1,6-glucan (Hong et al., 1994);(Kim and Yun, 2006). Structural analyses reveal the presence of β-glucan in the alkali soluble acid soluble fraction linked at 80 - 85% in β(1→3), at 8 - 12% in β(1→6) and with 3 - 4% of branched residues linked through C1, C2 and C3 (Fleet and Manners, 1976).

Finally, the alkali-insoluble acid-insoluble fraction includes β-1,3-glucan and chitin (Manners et al., 1973a), whereas more than 85% of the β-1,6-glucan is in the alkali insoluble acid soluble fraction (Manners et al., 1973b). However this method implies different fractionation steps of the polysaccharides making the analysis time consuming and leading to a poor reproducibility.

The use of strong acid to determine the cell wall composition has also been tested (Figure I-5).

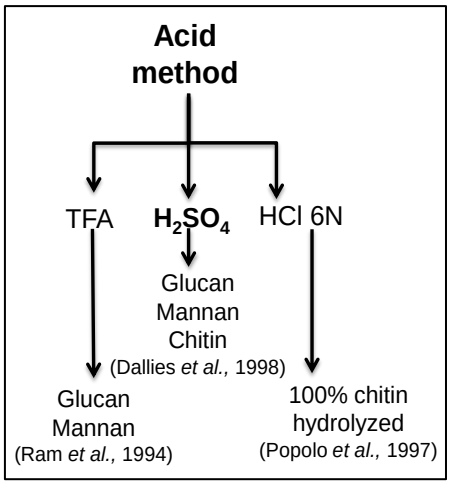

Figure I-5. Scheme of acid methods used in literature

Ram and co-workers (Ram et al., 1994) have characterized yeast mutants which present modifications in their cell wall composition by their β-glucan/mannans ratio after a trifluoroacetic acid hydrolysis of cell walls but no chitin level was determined, this acid was not able to cleave β-1,4-linkages of this polymer. Comparison of chlorhydric, trifluoroacetic and sulfuric acids efficiency have shown that sulfuric acid gives a yield of 93 - 96% through a total hydrolysis of β-1,6-glucan and an hydrolysis of 80% of chitin in glucosamine instead of 10% for TFA and HCl (Dallies et al., 1998). Popolo has shown complete hydrolysis of chitin by chlorhydric acid 6N at 100°C for 16 hours but in this condition 50 to 70% of glucose and mannose residues were degraded (Popolo et al., 1997). The chemical methods give relevant estimation on the different monomers quantities released after the hydrolysis of the polysaccharides present in the yeast cell wall.

Furthermore, enzymatic hydrolyses of the released products by chemical treatment have shown to be relevant to resolve some cell wall polysaccharides structures. Indeed, the degradation of the alkali-soluble fraction by an endo-β(1,3)-glucanase and an endo-β(1,6)-glucanase from *Bacillus circulans* (Fleet and Manners, 1977) has shown that the alkali-soluble glucan is a core structure of β(1→3)glucan with about 2% of branching as β(1→3)-linked side chains. Also it reveals the presence

of 1-2% of cell wall mannan residues attached to some β-1,6-glucan residues in the alkali-soluble glucan. Moreover, by enzymolysis, periodate oxidation and methylation of the alkali insoluble fraction Manners et al. have identified a highly branched β-1,6-glucan (Manners et al., 1973a). This glucan resistant to a β-1,3-glucanase, have been reported to include 130-140 glucose residues linked in β(1→6), with 5-10% of β-1,3-glucosidic linkages and 15-25% of branched glucose residues linked through C1, C3 and C6. More recently, Aimanianda et al. (Aimanianda et al., 2009) have confirm the structure of this branched β-1,6-glucan described by Manners et al. (Manners et al., 1973b). Structural analyses of the released products after incubation with a recombinant endo-β(1,3)-glucanase from *Thermotoga neopolitana* and an endo-β(1,6)-glucanase from *Trichoderma harzianum* have shown that the branched β-1,6-glucan is constituted of 190-200 glucose units with 20% of branching instead of 130-140 glucose residues as previously reported by Manners and coworkers. Magnelli et al. (Magnelli et al., 2002) have also analyze the fraction resistant to Zymolyase digestion and have reported a highly branched β-1,6-glucan with a slight different structure. This difference can be due to the use of Zymolyase instead of a recombinant enzyme that is not contaminated. Therefore specific enzymes devoid to any secondary activities are necessary to hydrolyse cell wall linkages. Indeed, since few years enzymatic methods have appeared to quantify cell wall polysaccharides. For example, Ovalle and co-workers (Ovalle et al., 1998) have qualitatively determined the structure and the resistance of the cell wall to Zymolyase (a β-1,3 glucanase) and shown that stationary phase cells have an increasing resistance to this enzyme. Some enzymatic mixtures such as Glucanex (Kim et al., 2004) or a combination of lyticase, exo-β(1,3)-glucanase and β-glucosidase (Danielson et al., 2010) have allowed determining the proportions of soluble β-glucan in different matrix but without any distinction between the two types of yeast β-glucan. One study proposed by Magnelli (Magnelli et al., 2002) use a sequential treatment of cell walls with specific enzymes followed by dialysis in order to distinguish β-1,3 to β-1,6-glucan. This method is effective and gave a higher level of chitin, but it is not easily applied due because it requires use of label sugars (^{13}C-glucose) during growth of the cells.

2.2. Biophysical approach: Atomic Force Microscopy

The atomic force microscope (AFM) was invented in 1986, by Binnig, Quate and Gerber (Binnig et al., 1986) (see Figure 6).

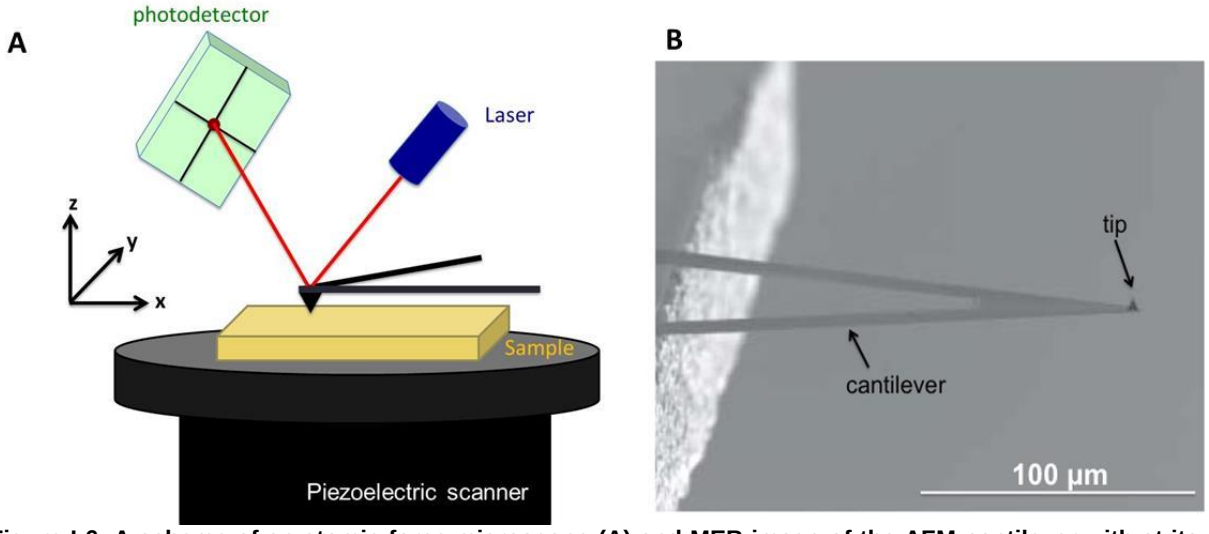

Figure I-6. A scheme of an atomic force microscope (A) and MEB image of the AFM-cantilever with at its end a tip (B).

The main parts of an AFM are the cantilever, the sharp tip, the sample stage and the optical deflection system constituted by a laser and a photodetector also called photodiode. The sample is mounted onto a piezoelectric scanner which allows by applying correct voltage a three dimensional positioning (x y, z). This technology generates a tridimensional image of the sample by scanning the tip over the surface, while the force applied on the surface is maintained constant. The vertical position of the tip is monitored by using a laser beam reflected to its back; when the cantilever moves away from the surface, the position of the laser onto the photodetector shifts from this initial position and the voltage difference from the upper and lower arrays of the photodetector gives a direct measurement of the vertical deflection (deviation) of the cantilever. In addition, force *versus* distance curves can be recorded between the tip and the surface with piconewton sensitivity.

AFM can be operated in air or liquid, making possible its use on living cells in their physiological conditions. Several biological samples have already been imaged and probed with AFM technology such as surface from filamentous fungi (Bugli et al., 2013; Guerriero et al., 2013) or bacteria (Cerf et al., 2009). Here, we will focus on yeasts, as they are our organisms of interest for this work.

Preparation of the sample, cantilever and tip

- **Sample**

As the tip onto the sample exerts a force, the sample has to be firmly immobilized. Immobilization of the sample can be performed by chemical fixation using glutaraldehyde as a cross-linking agent but this method may damage the cell (Liu et al., 2012). Another approach is to immobilize living cells in agar surface (Gad and Ikai, 1995). Another strategy consists in mechanically trapping the cells into a polycarbonate membrane (Alsteens et al., 2008; Pelling et al., 2004; Touhami, 2003). The main problem of this technique is that few cells are immobilized and only those having a diameter similar to the pores are immobilized. In our team, a simple method has been developed to immobilize a large number of individual yeasts on microstructured PDMS stamps with size ranging from 1.5 to 6 µm wide, a pitch of 0.5 µm and a depth ranging from 1 µm to 4 µm. Thus, this technique allows to capture yeats cells by convective/capillary deposition (Dague et al., 2011; Formosa et al., 2014a) without damaging them.

- **Tips and cantilevers**

Tips are made of silicon or silicon nitride. They can be functionalized with chemical groups in order to use them for probing molecular interactions and surface properties. For soft biological samples as yeasts, spherical or conical probes are used. In our study, we employed MLCT cantilevers from Brüker that are cleaned by oxygen plasma before use. They serve as soft nanoindenters of soft surface and they have to be chosen in function of the stiffness of the sample. Since yeast cells are very soft (0.75 ± 0.04 MPa) (Pelling et al., 2004), the spring constant (k_{cant}) has to be around 10-50 $mN.m^{-1}$. Before each experiment, the spring constant of the cantilevers (k_{cant} in $mN.m^{-1}$) and the sensibility (S in $m.V^{-1}$) have to be measured. Several methods exist but the thermal noise is often preferred (Burnham et al., 2003; Hutter and Bechhoefer, 1993).

Imaging mode

Contact mode or tapping mode can be used to image yeasts. In contact mode, the tip is in contact with the surface of the sample and scans this surface horizontally with a constant force. In tapping® mode (or intermittent mode), the cantilever is oscillating near its resonance frequency. The tip oscillates until to get contact with the surface and the modification of the amplitude of oscillation allows measuring the topography (see Figure 7). As the tip has an intermittent contact with the sample, lateral forces

between the tip and the surface are reduced, which avoid to pull apart the cell and to damage the cell surface (Alsteens et al., 2012). JPK Instruments has developed recently the QI™ mode (QI for Quantitative Imaging): in this mode the tip moves from point to point across the surface, the AFM tip being completely detached from the surface before moving to the next point (Chopinet et al., 2013). The main advantage of this mode is to collect the force curves at the same speed and resolution as normal imaging.

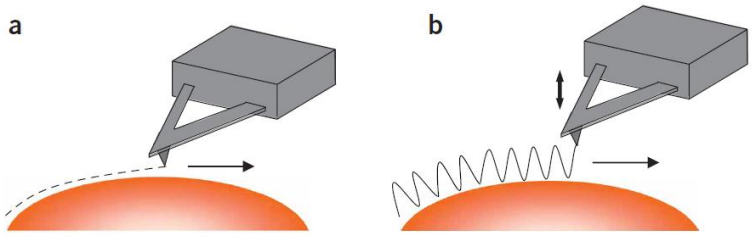

Figure I-7. Contact mode (a) and tapping mode (b) (from (Dufrêne, 2008))

Imaging modes are very useful to collect tridimensional images of yeast cells to determine structural elements on the surface of the yeast cell as the birth and bud scars (Alsteens et al., 2008; Dague et al., 2010; Touhami et al., 2003), but also to investigate the morphological modification upon different stresses. Analysis of AFM image has led to demonstrate that surface roughness of *Saccharomyces cerevisiae* cell increases with ethanol concentration (Canetta et al., 2006), after chemical treatment such as lithium acetate or dithiothreitol (Suchodolskis et al., 2011) and with protease treatment (Ahimou, Touhami, et Dufrene 2003). Erosion observed by AFM after protease digestion is in agreement with the fact that protease digests yeast cell wall. Contact images of encapsulated living *S. cerevisiae* cells in polyelectrolyte multilayers have shown that the surface of coated cells is smooth or granular according to the number of layers and the salt concentration in the liquid (Svaldo-Lanero et al., 2007). The encapsulation of yeast cells in polymeric shells is very important in biotechnology and medicine, since it aims to increase the resistance of yeast cells to environmental conditions without injuring their viability. Since few years, AFM is used as a tool to examine damages produced by a toxin or an antifungal drug. For example, a higher roughness and an irregular surface were observed after exposure to Kpkt, a glycoprotein secreted by the killer yeast *Tetrapisispora phaffii* which presents *in vivo* β-glucanase activity (Comitini et al., 2009). This killer toxin, which is lethal to spoilage yeasts under winemaking conditions, may be used as a novel antiseptic agent in the winemaking and fermentation.

More than a simple imaging technology, the AFM is a force machine able to record force measurements between the tip and the surface. The AFM is then operated in the force spectroscopy mode.

Force spectroscopy

In the force spectroscopy mode, the tip is continuously approached and retracted from the surface and the deflection of the cantilever is monitored in function of the vertical position of the piezoelectric scanner. In fact, it is the voltage on the photodetector that is measured in function of the vertical piezo displacement. This voltage (I in Volts) is converted into a deflection (d) which have the dimension of a length according to: d=S.I where S is the sensibility of the cantilever (in $m.V^{-1}$). Using the spring constant of the cantilever (k_{cant} in $N.m^{-1}$), this deflection can be converted into forces (F) using the Hooke's law: $F=k_{cant} . d$

We thus have access to force-distance curves (Figure 8), which provides several informations:(i) when the tip is in contact with the sample, the sample 'resists' and there is a deformation of both, the cantilever and the sample (C, figure 8). This part of the curve give us access to nanomechanicals properties of the yeasts such as cellular spring constant, elasticity modulus or Young modulus (Mercadé-Prieto et al., 2013; Pelling et al., 2004); (ii) when the tip is moved away from the sample, an hysteresis can be recorded, representing the adhesion of the tip with the sample (E, figure 8). This tip-surface interaction is dependent of the time of contact of the tip, the area of the surface and the surface energy.

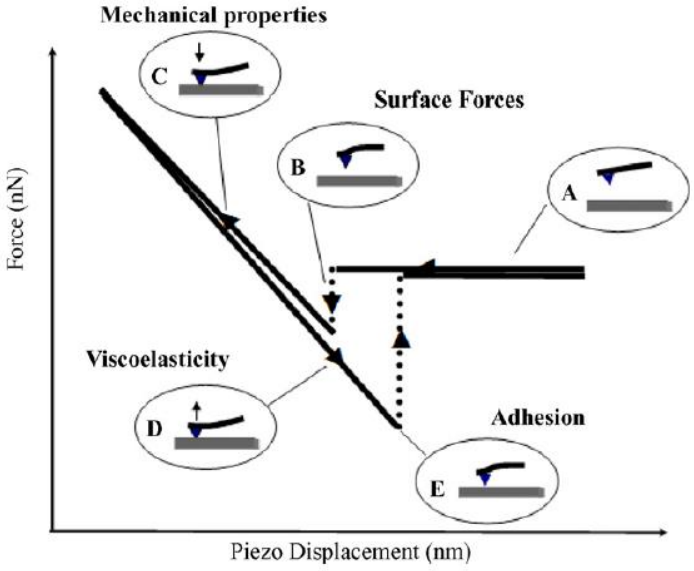

Figure I-8. Schematic diagram of a typical force curve, which can be recorded on local or multiple locations on the cells (from (Gaboriaud and Dufrêne, 2007))

AFM used to measure nanomechanical properties

The cellular spring constant of the sample (k_{cell}) in N/m, also called stiffness, can be calculated from the calibrated cantilever spring constant (k_{cant}) and the slope (s) of the linear part of the force curve:

$$k_{\text{cell}} = k_{\text{cant}}\left(\frac{s}{1-s}\right)$$

The spring constant give information on the stiffness of the yeast cell. By using this method, Karreman et al. (Karreman et al., 2007) found a four times increase of the spring constant of the yeast cell deleted for the heat shock protein Hsp12p involved in the response to stress. This was accompanied by a decrease of β-1,3-glucan and an increase of chitin measured by infrared spectroscopy, confirming that this protein as a role in the cell wall flexibility.

As the tip is pushed on a soft sample, we can determine the indentation (deformation) depth and relies this value to the applied force. By applying the Hertz model, we can calculate the Young modulus in Pascal, which gives information on the elasticity of the cell. The Hertz model is:

$$F = \frac{2E\tan\alpha}{\pi\,(1-\nu^2)}.\delta^2$$

Where indentation (δ in nm) is the deformation of the sample under the tip, the value of the opening angle (α in rad) is a parameter of the tip geometry and the Poisson ratio (v in degree) is arbitrary fixed at 0.5. Thus, fitting each force curve of a batch, e.g. of 1024 force curves, with the Hertz model generates a distribution of Young modulus values that can be adjusted to a Gaussian law in order to describe the mean Young modulus value (E) and standard deviation. The elasticity of the yeast cell wall can vary over the surface of the cell. The bud scar, which has a higher content in chitin, has been shown to have a higher Young modulus value than in the surrounding surface (Alsteens et al., 2008; Touhami et al., 2003). The probing position is crucial and influences the nanomechanical values (Arfsten et al., 2010), therefore repeatability and statistical analyses on independent cells are primordial to conclude on the nanomechanical behavior of a cell population. Besides nanomechanical measurements, the cell wall organization can be probed with a molecule attached to the tip to measure specific interactions with the surface. This method is called single molecule force spectroscopy (SMFS).

Single-molecule force spectroscopy

- **tip functionalization**

AFM tips can be functionalized with chemical groups or biomolecules.

Chemical functionalization with methyl (-CH_3) and hydroxyl (-OH) groups can be made by chemi-adsorption of thiols on gold surface (Alsteens et al., 2007, 2007), covalent attachment of silanes or alcohols on silicon oxides, who serve to attach the biomolecule. Functionalization with biomolecules can be made via a polyethylene glycol crosslinker (Ebner et al., 2008; Hinterdorfer and Dufrêne, 2006; Wildling et al., 2011) or a dendritip (Jauvert et al., 2012). Tips are modified with amino groups and then reacted with the linkers, which carry benzaldehyde groups. Thus chemical groups can react with biomolecules with NH_2 groups, allowing attaching the biomolecule to the end of the tip.

The forces recorded in single molecule force spectroscopy are usually weak (in the range of 100 pN) and thus soft cantilevers (in the range of 10-20 $mN.m^{-1}$) are usually used. Furthermore, the binding of the molecule on the tip has to be stronger than the adhesion force studied. Moreover, the molecules have also to be enough mobile to interact freely with the sample.

Methods have been developed to attach a cell at the end of the cantilever called ‘cell probes’ (cf. Figure 9). These methods also known as single-cell force spectroscopy (SCFS) use tipless AFM cantilevers and makes possible to investigate cell-cell and/or cell-surface interactions (Beaussart et al., 2014; Friedrichs et al., 2010). Individual cells can be attached on the cantilevers via lectins such as concanavalin A and use to evaluate the adhesion of *S. cerevisiae* with silica surface (Götzinger, 2006). This approach has demonstrated that the yeast adhesion is dependent of pH solution and roughness of silica.

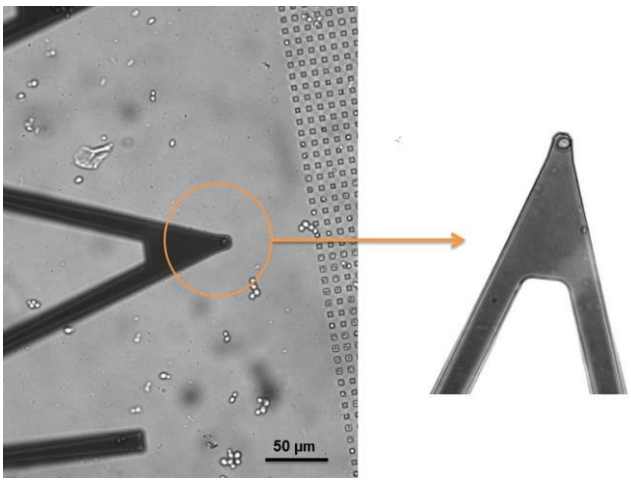

Figure I-9. Cell probe: a yeast cell attached at the tipless AFM cantilevers via concanavalin A

- **Polymer extension models: FJC, FJC+, WLC**

In order to describe the stretching of the molecules on the retract part of the force curves, three major models can be used: the Gaussian chain (GC), the worm-like chain (WLC) and the freely jointed chain (FJC).

In the GC model, the polymer is described as a coil with a random distribution, which can be described as a Gaussian. However, this model is not used to describe polysaccharides stretching, due to its poor descriptional of the polymer at long distance (Abu-Lail and Camesano, 2003). In the case of real polysaccharides stretching, the models FJC and WLC as well as their extension FJC+ and WLC+ are often used (Janshoff et al., 2000; Jena and Hörber, 2006). The WLC model describes a semi-flexible polymer as an irregular and curved filament (Bustamante et al., 1994):

$$F(x) = \frac{k_b T}{l_p}\left[\frac{1}{4(1-\frac{x}{Lc})^2} + \frac{x}{L_c} - \frac{1}{4}\right]$$

Where the persistent length (l_p) represents the stiffness of the molecule, the contour length (L_c) is the total length of the stretched molecule and k_b is the Boltzmann constant, T the absolute temperature.

In the FJC model, the polymer is described as a suit of segments (called 'Kuhn segments') with the same energy and a random orientation: $x(F)=L_c[\coth(Fl_k/k_bT) - k_bT/Fl_k]$

Where F is the extension force (N), x is the extension of polymer (m), k_b is the Boltzmann constant and T the absolute temperature. l_k is the Kuhn length, which represents a length of one segment (m) and L_c (m) is the contour length which is the total length of polymer stretched. For n segments: $L_c=nl_k$.

In WLC+ and FJC+ models, the stiffness of the chain account for a fitting parameter.

Finally, these models can be applied to describe a polymer and depends on the extension of the chain and the magnitude of the pulling force.

- **Application of single-molecule force spectroscopy**

When the tip is functionalized, it can be used to measure specific interactions and the force required to break this interaction can also be measured. For example, in flocculating conditions Touhami *et al.* (Touhami, 2003) have recorded specific adhesion events of 121 and 117 pN attributed to specific binding of the AFM tip functionalized with concanavalin A and mannose residues at the surface of flocculated yeast *S. carlesbergensis*. In a same approach, Alsteens *et al.* (Alsteens et al., 2008) have used concanavalin A tips to investigate the difference of surface properties (Dengis and Rouxhet, 1997) between the bottom-fermenting yeast *S. carlsbergensis* and the top-fermenting yeast *S.*

cerevisiae. AFM has revealed that *S. carlsbergensis* have a homogeneous surface, whereas *S. cerevisiae* has a distribution of mannans all over the surface. However, lower adhesion force and rupture distance were observed and well described by the FJC model for the bottom strain in contrast to the top strain where only the WLC model could be applied to describe elongation forces with rupture distance in the range of 0-400 nm (Francius et al., 2009). These observations show that these two species have different mechanical properties and suggest that mannans chains are stretched for *S. carlsbergensis* instead of polypeptide chains of the entire mannoproteins chains for *S. cerevisiae.*

Recently, AFM techniques were used with molecular tool to study the distribution and function of mechanosensors (Heinisch et al., 2012) such as Wsc1, a transmembrane protein, on the surface of living cells. As the native Wsc1 stress sensor is too short to reach the outer surface of the cell, Wsc1 was elongated with an additional 186 amino acids and an His-tagged, in order to render it accessible to an AFM tip functionalized with Ni^{2+}-nitriloacetate (NTA) groups (Heinisch et al., 2010). Molecular mapping images showed that Wsc1 sensor molecules form clusters of ~200 nm diameter on the cell surface, stimulated under stress conditions (heat and hypo-osmotic shocks) and consistent with the fact that stress activate the cell wall integrity pathway (see part 4.3). This observation indicates that Wsc1 clustering is a response to stress. By mapping the distribution of Wsc1 in three different cysteine-rich domains (CRD) mutants, these authors observe that mutants are distributed over the surface rather than clustered, indicating that the CRD domain is crucial for the sensor clustering (Heinisch et al., 2010).

2.3. Molecular tools: transcription profile and genomic analysis

The achievement of the complete genome sequence of the yeast *Saccharomyces cerevisiae* (Goffeau et al., 1996) has allowed studying yeast physiology at a genome scale. This leads to the construction of a collection of strains (YKO collection), each deleted in one gene, which can be used in many phenotypic tests in order to identify genes relative to cell wall functions. However, among the ~ 6000 genes, about 15% are mandatory for cell viability, therefore their deletions result in absence of growth in most culture medium.

The use of DNA chips to study the transcription profile of strains, *i.e.* the expression as messenger RNA of each gene in a determined condition, has released an enormous amount of information. Indeed, DNA microarrays were used to measure changes in transcripts levels in response to several environmental changes such as heat shocks (from 25°C to 37°C), osmotic shock (with 1M sorbitol),

hydrogen peroxide (0.3 mM H_2O_2) or dithiothreitol (2.5 mM DTT) exposure and nitrogen depletion. Gasch *et al.* (Gasch et al., 2000) have observed that about 900 genes have a similar response to these environmental changes. Among these genes, 600 genes were repressed and divided into 2 clusters. The first cluster consists of genes implied in growth, RNA metabolism, secretion and other metabolic processes. On the contrary to the first cluster of genes, the second cluster was characterized by a slight delay in the decrease of the transcript levels and includes the genes encoding for ribosomal proteins. Approximately 300 genes were induced after the stress conditions and the genes in this group are involved in cellular processes such as carbohydrate metabolism, detoxification of reactive oxygen species, intracellular signalling, protein folding and cell wall modification. Environmental stress response has shown to induce the expression of genes that are governed by Msn2p and Msn4p. Indeed, analysis of the double mutant *msn2Δmsn4Δ* exposed to heat shock and H_2O_2 treatment, results in the modification of the expression of 180 genes compare to the isogenic wild-type. This general stress response has been also reported in the analysis of the modifications of the gene expression in the presence of cell-wall perturbing agents such as Zymolyase and Congo Red (Boorsma et al., 2004; Garcia et al., 2004; Rodriguez-Pena, 2005). These studies reported that the genes induced are related to cell wall biogenesis, metabolism, energy generation and signalling, as well as some genes of unknown function; but overall they highlighted the presence of 18 genes induced in all conditions (Arroyo et al., 2009). Among these genes, 50% were involved in cell wall remodelling (*SED1, CWP1, GFA1, YLR194c, PST1, PIR3, CRH1, HSP150* and *CCW14*). One of the up-regulated genes, *GFA1*, encodes glutamine-fructose 6-phosphate amidotransferase (Gfa1p), which is the first enzyme that catalyzes the chitin biosynthesis (see part 3.1 in this manuscript). Thus an up-regulation of *GFA1* and *CHS3*, encoding chitin synthase III, was correlated to an increase of chitin content in cell wall (Lagorce et al., 2002). Moreover, analysis of the genome-wide transcription profiles of mutants deleted in genes that affect the cell wall composition (*fks1, gas1, mnn9, kre6, knr4*) have reported a modification of about 300 genes (Lagorce, 2003) with a cluster of 80 genes that share a common transcriptional response.

Although all these studies have shown that environmental shifts, deletion of gene relative to the cell wall biosynthesis or an exposure to drugs that damage the cell wall (Garcia et al., 2004) can trigger a common transcriptional response, the regulation of the stress response is specific to gene and to the condition. The expression of genes is regulated by different transcription factors, which are dependent

on the conditions, and different upstream signalling pathways control the response. For example, many genes induced in response to environmental stress described by Gasch *et al.* (Gasch et al., 2000) are dependent on the high osmolarity glycerol (HOG) pathway and the protein kinase C (PKC) pathway (also known as cell wall integrity pathway) (see part 4.3. in this manuscript). These pathways regulate the expression of both the general stress response and the specific response to the stimuli that activate the pathways. For example, the cellular response to Congo Red, a compound that binds to chitin, is ensured *via* the Mid2 sensor and the cell wall integrity (CWI) pathway. However, alterations of the cell wall by Zymolyase (a main β-1,3-glucanase with protease activity) activates the CWI pathway but also requires the HOG pathway (García et al., 2009). The analysis of transcriptional profiles in mutants of the HOG and CWI pathways (*sho1*Δ*, hog1*Δ*, wsc1*Δ*, mid2*Δ*, slt2*Δ*, hog1*Δ*slt2*Δ*, ste11*Δ) has allowed characterizing the links between both signaling pathways in the regulation of the transcriptional response. Thus, damage of the cell wall by Zymolyase is sensed by the sensors of the Sho1 branch of the HOG pathway, which activate Slt2 and result in the transcriptional adaptation response through Rlm1.

In conclusion, DNA microarrays are very useful tools to characterize the transcriptional profile of cells under diverse stresses, and thus to contribute to a better understanding of the molecular response to stress and the cells adaptation mechanisms.

2.4. Phenotypic observations: use of drugs

Inhibitors of chitin synthase

Nikkomycins and polyoxins are antifungal drugs which competitively inhibit *in vitro* chitin synthases but have *in vivo* effects only at very high doses (50 µM) (Kim et al., 2002), (Cabib, 1991). These compounds have been useful for the study of the enzymatic chitin synthesis: they prevent septum formation during the budding process, when the mother and daughter cells are separated. Recently, it was observed that Nikkomycin Z treated cells are morphologically similar to *crh1* (or *utr2*) cells (Okada et al., 2014), defective in polysaccharides cross-linking, which demonstrate the key role of chitin-glucan linkage in morphogenesis (Cabib and Arroyo, 2013). This suggest also that this drug may inhibit the reaction of linkage between chitin and β-1,3-glucan.

Table I-1. Cell wall perturbing drugs implied in inhibition of chitin synthesis

Name	Function	Reference
Nikkomycin Z	Competitive inhibitor of chitin synthase	(Cabib, 1991; Cabib and Arroyo, 2013; Kim et al., 2002; Okada et al., 2014)
Polyoxin B	Competitive inhibitor of chitin synthase	(Cabib, 1991)

Inhibitors of β-glucan synthesis

Among antibiotics, one family gathers fungicides lipopetides which inhibit β-1,3-glucan synthesis. Papulacandin B (Baguley et al., 1979),(Kopecká, 1984), Aculeine (Mora et al., 1991), Echinocandin B, synthetic and semi-synthetic derivatives belong to this family. For example, Caspofungin is a semi-synthetic derivate of the echinocandin. Commercialized by Merck and Co, it is the first β-1,3-glucan synthase inhibitor to be approved by Food and Drug Administration (FDA) in USA. In an effort to characterize genes involved in β-1,3 glucan synthesis, *S. cerevisiae* mutants resistant to these drugs were isolated. This allowed to identify *FKS1*, also known as *ETG1* for *E*chinocandin *T*arget *G*ene *1* and coding for the major catalytic subunit of the β-1,3-glucan synthase. These compounds have also permitted to identify *PBR1* gene for Papulacandin B Resistant 1, and *GNS1* likely involved in β-1,3-glucan synthesis (el-Sherbeini and Clemas, 1995). However, mutations in 22 genes caused hypersensitivity to Papulacandin B but, surprisingly, no correlation was found with changes levels in glucan, mannan and chitin (Lussier et al., 1997a);(Ram et al., 1994) leading to the conclusion that Papulacandin B-hypersensitivity was not specific to the cell wall mutants. Moreover sensitivity and resistance of strains to β-1,3-glucanases can be used as easy phenotypic test to characterize a mutation on β-1,3-glucan content in yeast cell walls (Lussier et al., 1997a; Ram et al., 1994).

Bussey and coworkers (Boone, 1990) have selected several mutant resistant to the yeast K1killer toxin in order to identify genes important for the biosynthesis of β-1,6-glucan. This screen turned to isolate several mutants harbouring reduced levels of β-1,6-glucan bearing mutations in genes named *KRE* for Killer Resistance. Finally, a pyridobenzimidazole derivative named D75-4590 has shown an inhibitor activity on β-1,6-glucan synthesis leading to cell aggregation, multiple budding in *S. cerevisiae* and an inhibition of hyphae elongation in *Candida albicans* (Kitamura et al., 2009).

Table I-2. Inhibitors of β-glucan synthesis

Name	Function	Reference
Aculeine		(Mora et al., 1991)
Papulacandin B	Noncompetitive inhibitor of β-1,3-glucan synthase	(Baguley et al., 1979),(Kopecká, 1984) (Castro et al., 1995)
Echinocandin B	Noncompetitive inhibitor of β-1,3-glucan synthase	(Douglas et al., 1994)
Caspofungin	Noncompetitive inhibitor of β-1,3-glucan synthase	(Denning, 2003; Saravolatz et al., 2003)
K1 killer toxin	Noncompetitive inhibitor of β-1,6-glucan synthesis	(Boone, 1990)
D75-4590	Noncompetitive inhibitor of β-1,6-glucan synthesis	(Kitamura et al., 2009)

Inhibitors of protein glycosylation

Hygromycin B and geneticin G418 are antibiotics of the aminoglycosides family. Yeast strains which present defaults in protein N-glycosylation, are much more sensitive to aminoglycosides (Ballou et al., 1991; Dean, 1995; Dean, 1999). Therfore, these antibiotics enable to study the cell wall and to reveal defects in cell surface. Hygromycin B has been used for that purpose on sensitive mutants defective in β-1,6-glucan and O-glycosylated chains synthesis (Lussier et al., 1997a).

Calcofluor White and Congo red:

Table I-3. Congo Red and Calcofluor White : cell wall perturbing agents

Name	Chemical structure	Function	Reference
Calcofluor White	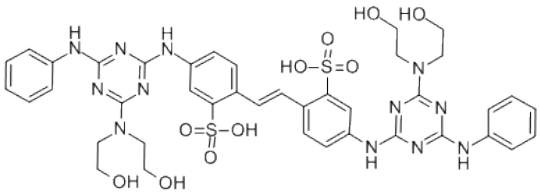	Inhibitor of CWI pathway	(Ram and Klis, 2006; Ram et al., 1994; Roncero and Duran, 1985)
Congo Red	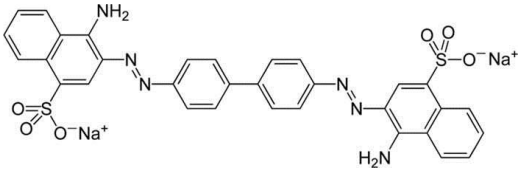	Inhibitor of CWI pathway	(Kopecka and Gabriel, 1992; Ram and Klis, 2006; Roncero and Duran, 1985)

Congo red and Calcofluor white are antifungal drugs, which interact with β-1,4-glucopyranoside units of the chitin polymer (Ram and Klis, 2006). Addition of these drugs induce morphological changes in *S. cerevisiae* such as a default of separation of daughter cell from the mother cell (Roncero and Duran, 1985) as well as a weakened cell wall. Interestingly, a significant increase in chitin deposition in

the lateral cell wall occurs in the presence of Calcofluor White and Congo Red. Therefore, susceptibility assays based on these drugs have been used for screening different mutants and their modification in the cell wall composition (Ram et al., 1994). Remarkably, a wide range of cell wall mutants show a hypersensitivity to Congo Red and Calcofluor White, related to the increase of the chitin content in their cell wall due to the activation of the cell wall-stress response. They include mutants defective in chitin synthase (*chs3*), synthesis of β-1,3-glucan (*fks1, gas1*) or β-1,6-glucan (*kre6, cwh41*), mannosylation of protein (*mnn9*) and GPI-anchor synthesis (*gpi1, gpi3*). Indeed Congo Red and Calcofluor White exert their effects through a similar mechanism leading to the loss of the cell wall integrity (see part 4.3 in this manuscript): they induce phosphorylation of Slt2/Mpk1p, an effect that is mediated by the Mid2p sensor, and can be diminished by 1 M sorbitol. Remodeling of the cell wall in response to these agents is dependent on Mpk1 kinase (de Nobel *et al*., 2000).

Although both drugs are used, Calcofluor White has been preferred because of the ambiguous role of Congo Red. Indeed, Congo Red is known to stimulate the chitin synthesis but also to interact *in vivo* with β-glucan and to inhibit enzymes related to the cell wall assembly which allow the cross-linking between chitin to β-1,3 and β-1,6-glucan. Imai et al. (Imai, 2004) have shown that Congo Red preferentially targets chitin rather than β-1,3-glucan, which allow the characterization of *RCR1* gene (for Resistance Congo Red 1) in *S. cerevisiae*.

3. Biosynthesis of the cell wall polysaccharides

In fungi, the cell wall is composed of polysaccharides cross-linked to a matrix. As indicated in the table 4, the cell wall of different species share some similarities and may contain chitin, β-1,3-glucan, β-1,6-glucan, α-1,3-glucan, mixed β-1,3/β-1,4-glucan and glycoprotein as major constituents (Free, 2013). For example, the cell wall of the pathogenic yeast *Candida albicans* is very similar to those of *Saccharomyces cerevisiae* and many aspects of the cell wall construction and the stress signaling are conserved between these two species. In filamentous fungi, all components have not yet been characterized but it appears that important differences have been identified. These differences are also present in the cell wall of the filamentous fungi.

Table I-4. The cell wall components of different species (adapted from (Free, 2013)). Percent of each component in the cell wall and in parentheses the number of genes, which encoded the synthesis of these components, are indicated. Not amount (na) and not identified (ni).

	S. cerevisiae	*C. albicans*	*S. pombe*	*A. fumigatus*	*C. neoformans*	*N. crassa*
Chitin	1-2% (CHS1-3)	2-6% (4)	conidia (2)	7-15% (7)	na (8)	4% (7)
β-1,3-glucan	50-55% (FKS1-3)	30-39% (1)	46-54% (1)	20-35% (1)	na (1)	87% (1)
β-1,6-glucan	10-15%			0	na	0
α-1,3 glucan	0	0	(1)	35-46% (3)	na (ni)	(1)
mannoproteins	40-30%	35-40%	0	0	0	0
galactomannan	0	0		20-25%		
Mixed β-1,3/β1,4-glucan	0	0	0	na (ni)	0	na
melanin	0	infection	0	conidia (6)	ascospore	infection

In the yeast *Saccharomyces cerevisiae,* the cell wall constitutes an envelope of 100 to 200 nm of thickness that surrounds the plasma membrane. This structure is essential for cell integrity and may account for 15 to 25% of the cell dry mass (Aguilar-Uscanga and Francois, 2003). The cell wall composition of this yeast cultivated in rich medium at 30°C in laboratory is given in the table I-5.

Table I-5. Cell wall composition of *S. cerevisiae* determined by chemical hydrolysis (Aguilar-Uscanga and Francois, 2003; Klis et al., 2002, 2006)

Macromolecule	% of cell wall (dry weight)	Degree of polymerization	Average *Mr* (kDa)	Level of branching
Mannans	30-50	highly variable	highly variable	high
β(1,6)-Glucan	5-10	150	24	moderate
β(1,3)-Glucan	30-45	1500	240	high
Chitin	1.5-6	120	25	linear

The yeast cell wall is a complex interplay of 4 major polysaccharides: β-1,3-glucan (1500 glucose units linked in β-1,3), β-1,6-glucan (140 to 350 residues of glucose linked by β-1,6 linkage), mannan (mannose units linked in α-1,2; 1,3; 1,6) and chitin (polymer of 100 to 190 N-acetylglucosamine units linked by β-1,4 linkage) (Klis et al., 2002)(Lesage and Bussey, 2006).

The structure and the composition of the cell wall may vary with respect of the cell cycle (Cid et al. 1995; Klis, Boorsma, et De Groot 2006), strains (Nguyen et al., 1998) as well as on the culture

conditions such as temperature, pH, medium and batch conditions (Aguilar-Uscanga and Francois, 2003).

3.1. Chitin

Chitin is one of the most abundant biopolymer in the planet, which has a crucial role in fungal cell walls but also is presented in crustacean and insect exoskeletons. The biological value of chitin and its role as possible target for antifungal drugs, have motivated numbers of researchers to investigate the pathways and mechanism of chitin biosynthesis and degradation.

Chitin is a linear polymer constituted of 120 N-acetylglucosamine residues attached by a β(1→4) linkage (Figure I-10).

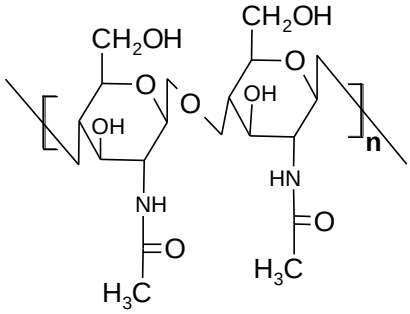

Figure I-10. Structure of chitin, a linear polymer of β(1,4)-linked N-acetyl-D-glucosamine molecules that consists of approximately 120 residues.

Several studies have been reported that, in *Saccharomyces cerevisiae*, chitin represents 1-2% of the cell wall where it serves as a key component for yeast survival probably because of its central role in septation that takes place during budding (Cabib and Arroyo, 2013; Shaw et al., 1991). Indeed, during unstressed growth, chitin is deposited as a ring at the site of bud emergence, then as a disk (the primary septum), and finally in the lateral cell wall of the mother cell after septation (Kapteyn et al., 1997; Kollar et al., 1995, 1997; Orlean, 2012).

In *S. cerevisiae*, the metabolic pathway for chitin synthesis is composed of 5 reaction steps depicted in Figure I-11.

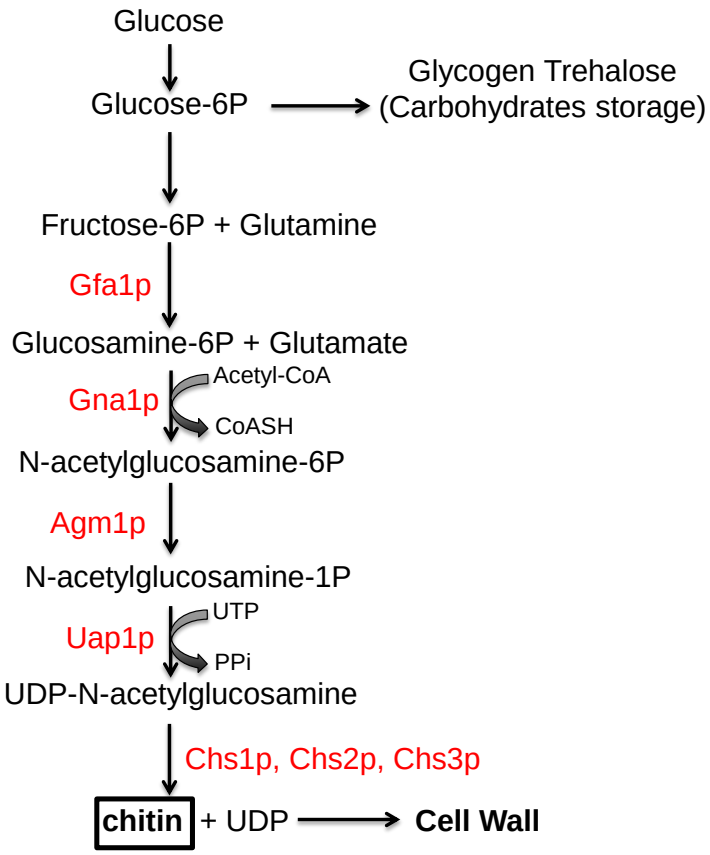

Figure I-11. Mechanisms involved in the chitin synthesis

This synthesis starts with Gfa1p who catalyze UDP-N-acetylglucosamine from fructose-6 phosphate (F6P) (Milewski et al., 2006): F6P is converted to Gln6P by glutamine F6P amidotransferase Gfa1, Gln6P is N-acetylated by Gna1 to form GlNac-6P, which is converted in GlNac-1P by the N-acetylglucosamine phosphate mutase Agm1 and finally UDP-GlcNac is formed by the UDP-N-acetylglucosamine pyrophosphorylase Uap1. The last step is catalyzed by chitin synthase. Yeast *S. cerevisiae* has 3 chitin synthases Chs1, Chs2 and Chs3, that are multispanning membrane proteins with a cytoplasmic domain and that catalyze the transfer of GlcNAc from the sugar nucleotide donor UDP-GlcNAc to elongate chitin chains.

As reviewed below, each chitin synthase has a specific function in chitin synthesis that is associated with a specific period of the yeast life cycle.

Chitin synthase 1

Chs1 is an enzyme expressed in early G1 phase and involved in the chitin synthesis for the repair of the septum after cytokinesis (Cabib et al., 1992).

Chitin synthase II

Chs2 is expressed during mitosis and produced chitin in the primary septum (about 5% of the chitin (Orlean, 2012)), that separates the mother and the daughter cells. Chs2 is synthesized in the endoplasmic reticulum during metaphase. Its release from endoplasmic reticulum is coordinated with the exit of mitosis and provokes upon inactivation of mitotic kinase by Sic1 (Zhang et al., 2006). After its release, Chs2 is delivered to the plasma membrane at the mother cell-bud junction. Dbf2 (Oh et al., 2012), Inn1, Cyk3 (Devrekanli et al., 2012) are involved in activation of Chs2 for primary septum formation.

Chitin synthase III

Chs3 is involved in the synthesis of 90% of chitin in the cell wall (Roncero et al., 1988). This protein is required for the production of chitin inserted into lateral walls in early G1 phase and in the chitin ring at the bud site in late G1. This ring is not essential for cell division but reinforces the neck region, promoting the correct assembly of the cell wall layers in this localization. The chitin ring is attached directly into β-1,3-glucan network, whereas chitin in the lateral wall is mostly linked to β-1,6-glucan chains (Cabib, 2005).

The synthesis in the endoplasmic reticulum of Chs3 implies the palmitoylation, *i.e.* the covalent attachment of fatty acid to membrane protein by Pfa4 and then the interaction with Chs7 allows exit the endoplasmic reticulum. These two components, Pfa4 and Chs7, are limiting factors for Chs3 but are not required for exit of Chs1 and Chs2 from the endoplasmic reticulum (Lam, 2006). In the Golgi, Chs3 interacts with Chs5 and Chs6 to form exomer complexes, which promote incorporation of Chs3 into secretory vesicles, for the transport to the plasma membrane at the site of chitin ring is formed. At the plasma membrane, Chs4 activates Chs3 (Reyes et al., 2007) and mediates its localization on the plasma membrane prior to the formation of the chitin ring at the site of the bud emergence. The interaction between Chs3 and Chs4 mediates the anchorage of Chs4 to septins through Bni4, a scaffold protein.

Table I-6. Genes involved in chitin synthesis

Gene	Biological function	Reference
GFA1	Glutamine-Fructose-6-phosphate Amidotransferase	(Arnaud Lagorce et al. 2002; Cid et al. 1995)
GNA1	GlucosamiNe-6-phosphate Acetyltransferase	(Mio et al., 1999; Peneff et al., 2001)
AGM1	N-AcetylGlucosamine-phosphate Mutase	(Boles et al., 1994; Hofmann et al., 1994)
UAP1	UDP-N-Acetylglucosamine Pyrophosphorylase	(Cid et al., 1995; Mio et al., 1998)
CHS1	chitin synthase I, requires for the production of chitin to repair the septum	(Cabib et al., 1992; Cid et al., 1995; Ziman et al., 1996)
CHS2	chitin synthase II, requires for the synthesis of the primary septum	(Bulawa and Osmond, 1990; Cabib, 1991; Shaw et al., 1991)
CHS3	chitin synthase III, requires for the production of the chitin ring and into the lateral walls	(Reyes et al., 2007; Ziman et al., 1996)
CHS4	activator of chitin synthase III, recruits Chs3p to the bud neck via interaction with Bni4p	(Reyes et al., 2007; Trilla et al., 1997)
CHS5	chitin Synthase related, Exomer mediates transport of Chs3p from the Golgi to the plasma membrane	(Santos et al., 1997)
CHS6	chitin Synthase related, Exomer mediates transport of Chs3p from the Golgi to the plasma membrane	(Cid et al., 1995)
CHS7	chitin Synthase related, Regulates the exit of Chs3p from the ER	(Trilla et al., 1999)
DBF2	Mitotic exit kinase, phosphorylates Chs2p to regulate primary septum formation	(Oh et al., 2012), (Meitinger et al., 2013)
INN1	activates chitin synthase activity of Chs2p during cytokinesis	(Devrekanli et al., 2012)
CYK3	activates chitin synthase activity of Chs2p during cytokinesis	(Devrekanli et al., 2012)
PFA4	Protein fatty acyltransferase, palmitoyltransferase	(Lam, 2006)

3.2. β-1,3-glucan

The main structural component of the yeast cell wall is constituted by β-1,3-glucan, which is long chains of 1500 glucose units linked in β(1→3) (Klis et al., 2006) and moderately branched (Fleet, 1991).

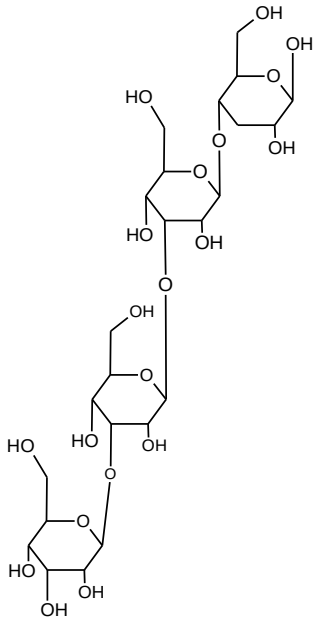

Figure I-12. Structure of β-1,3-glucan chains

Branching of the polymer (about 3% branching points) ensures that β-1,3-glucan molecules can only locally associate through hydrogen bonds, resulting in the formation of an amorphous and fibrillar ultrastructure (Klis et al., 2006; Kopecká, 2013). The β-1,3-glucan chains have a flexible shape that is comparable to a wire spring which can exist in various states of extension. The helices of β-1,3-glucan are composed of three hydrogen-bonded chains (a triple helix) or a single polysaccharide chain.

The glucan synthase complex consists of a catalytic subunit Fks1/Fks2 encoded by *FKS1/FKS2* and of a regulatory subunit GTPase encoded by *RHO1*. This latter protein is also requires for the activation of Pkc1 in the CWI pathway. Both subunits are essential for the complex activity. The Rho1-FKS1 corresponds to the major isoform of β-glucan synthases in the yeast cells. The β-1,3-glucan synthase complex encoded a β-glucanosyltransferase activity, which catalyses the transfer of a glucosyl unit from UDP-glucose to the β-1,3-glucan chain. The subunit Fks1 or Fks2 is an integral membrane protein that are co-localized in site of polarized growth and coincide with actin patches (Dijkgraaf et al., 2002) in budding cells.

Despite the glucan complex has been identified since several years, how the β-glucan chain is initiated is still today an opening question. However, the regulation of *FKS1* and *FKS2* has been extensively studied. It was found that Fks1 is induced during vegetative growth and cell cycle as its transcript levels peaks in late G1 and in early S phases (Lesage and Bussey, 2006).

Fks2 is induced under starvation, during sporulation or in response to mating pheromones. The double mutant *fks1Δ fks2Δ* is not viable, indicating that Fks1 and Fks2 are essential. However the deletion of either gene is not lethal, but the mutant *fks1Δ* leads to a slow growth, a decrease of glucan with an increase of the chitin and mannoprotein levels in the cell wall (Dijkgraaf et al., 2002), whereas *fks2Δ* mutant shows defects only in spore wall formation.

FKS3 has been identified based on sequence similarity to *FKS1* and *FKS2*, and seem to have a role in wall assembly of spore, but its exact function remains unclear. Ishihara et al have proposed that Fks3 acts as an upstream regulator to the β-1,3-glucan synthase, which is encoded by *FKS2* (Ishihara et al., 2007).

Gas in the β-1,3 glucan biosynthesis

An *in vitro* assay for transglucosidase activity using a recombinant enzyme have shown that Gas1 can catalyse the formation of a β-1,3-glycosidic bond between the reducing end of a β-1,3-glucan chain and the non-reducing end of a β-1,3 glucan molecule. Therefore Gas1 is a glucanosyltransferase also called β-1,3 glucan elongase (Mouyna, 2000; Plotnikova et al., 2006). A *gas1* mutation leads to phenotypes characteristic of a weakened cell wall: cells are abnormally round, have reduced viability, and display increased sensitivity to cell wall-affecting drugs and elevated temperatures (Popolo et al., 2000; Ram et al., 1998).

Besides to Gas1, there are other Gas proteins, encoded by *GAS2*, *GAS3*, *GAS4*, and *GAS5*, with a β-1,3glucanosyltransferase activity implied in cell wall assembly (Ragni et al., 2007a). *GAS3* and *GAS5* like *GAS1* is expressed during vegetative growth in the plasma membrane, whereas *GAS2* and *GAS4* are expressed exclusively during sporulation and are required for normal spore wall formation (Ragni et al., 2007b). These five proteins are GPI-anchored and Ragni *et al.* has shown that Gas1 can be transferred to wall polysaccharide thanks to a transglycosylation (Rolli et al., 2009).

Table I-7. Genes implied in the biosynthesis of β-1,3 glucan

Gene	Biological function	Reference
FKS1	Catalytic subunit of β-1,3-glucan synthase	(Dijkgraaf et al., 2002; Douglas et al., 1994; Eng et al., 1994; Johnson and Edlind, 2012)
FKS2 (GSC2)	Catalytic subunit of β-1,3-glucan synthase	(Huang et al., 2005)
FKS3	similar to 1,3-β-D-glucan synthase catalytic subunits Fks1p and Gsc2p	(Ishihara et al., 2007)
RHO1	GTP-binding protein of the rho subfamily of Ras-like proteins (Ras HOmolog)	(Rodríguez-Peña et al., 2010)
GAS1	Beta-1,3-glucanosyltransferase (Glycophospholipid-Anchored Surface protein)	(Plotnikova et al., 2006; Popolo and Vai, 1999; Ram et al., 1998; Rolli et al., 2009)(Mouyna, 2000)
GAS2	Glycophospholipid-Anchored Surface protein	(Mouyna, 2000; Ragni et al., 2007b)
GAS3	Glycophospholipid-Anchored Surface protein	(Mouyna, 2000; Ragni et al., 2007a)
GAS4	Glycophospholipid-Anchored Surface protein	(Mouyna, 2000; Ragni et al., 2007b)
GAS5	Glycophospholipid-Anchored Surface protein	(Mouyna, 2000; Ragni et al., 2007a)

After their export through the plasma membrane, β-1,3-glucan chains can be cross-linked to chitin by Crh1 and Crh2 (Cabib, 2009). They can also be linked to β-1,6-glucan and PIR proteins but the enzymes implicated in these cross-linkages are not yet known.

3.3. β-1,6-glucan

Chains of β-1,6-glucan are constituted of a β-1,6 backbone branched with β-1,6 side chains via a 3,6-substituted glucose on average every fifth glucose (see Figure 6) (Magnelli, Cipollo, et Abeijon 2002; Aimanianda et al. 2009). These chains are shorter than β-1,3-glucan (150 to 350 units of glucose linked in β(1→6)) and represent about 10-15% of the cell wall polysaccharide (Magnelli et al., 2002) (Manners, 1974). It was proposed that β-1,6-glucan serve as a 'glue' in the cell wall architecture (Lesage and Bussey, 2006).

In homology with β-1,3-glucan synthesis, a β-1,6-glucan synthase able to hydrolyse β-1,6-glucan from UDP-Glucose was search for. This investigation led to controversial results. Vink and coworkers used a dot-blot immunoassay with anti-β-1,6-glucan antibody to demonstrate the formation of a β-1,6-glucanase sensitive polymer upon incubation of a membrane extracts with UDP-Glucose (Vink et al., 2004). This assay was validated by the correlation between level of β-1,6-glucan synthetized *de novo* and the reduction of β-1,6-glucan synthesis *in vivo*, in β-1,6-glucan synthesis defective mutants. In this

assay, besides membrane extracts and UDP-glucose as a donor, GTP was required to stimulate the reaction, suggesting a role of a GTP-binding protein. Moreover, in membranes from cells overexpressing Rho1 GTPase, it was found a higher level of β-1,6-glucan synthetic activity, supporting the idea of a dependence of β-1,6-glucan synthase to Rho1.

In a more recent study of Latgé and coworkers an *in vitro* synthesis of the β-1,6-glucan was carried out by incubation of permeabilized cells with radiolabeled UDP-glucose (Aimanianda et al. 2009). It was demonstrated a *de novo* polymerization of an insoluble radiolabeled β-1,6-glucan that has a structure similar to purified β-1,6-glucan from wild-type cell walls, whereas a *kre9* mutant showed a no UPD-glucose dependent β-1,6-glucan synthetic activity (Aimanianda et al. 2009). However, in this study the synthetic activity was not stimulated by the presence of GTP. The exact enzymatic function underlying this polymerization remains to be identified. While the exact biosynthetic pathway of β-1,6-glucan synthesis is not yet undiscovered, some genes involved are known. This biosynthesis is initiated at the endoplasmic reticulum and implied several ER-proteins, which were discovered through a genetic screen using the yeast K1 killer toxin as the drug and searching for Killer Resistance (KRE) clones. This screen turned to isolate mutants harboring reduced levels of β-1,6-glucan (Boone, 1990). Indeed, mutations in *KRE1* have shown a decrease of 40% in β-1,6-glucan levels compare to the wild-type (Roemer and Bussey, 1991), whereas deletion of *KRE5*, a gene encoding for a large soluble ER-resident protein, result in abnormal morphology and severe growth defect accompanied with large reduced levels of β-1,6-glucan (Meaden et al., 1990). In addition, the pair of the functional proteins, encoded by Kre6/Skn1, was found to be required for normal amount of β-1,6-glucan in the cell wall with a predominant role of Kre6 in the β-1,6-glucan synthesis, as its absence lead to a 50% decrease of the wild-type β-1,6-glucan amount (Roemer and Bussey, 1991; Roemer et al., 1993).

Besides Kre family, small integral membrane proteins of the endoplasmic reticulum encoded by *BIG1, ROT1* and *KEG1* have presented defective β-1,6-glucan amount in their cell walls when they are mutated, indicating a role in the β-1,6-glucan synthesis. It was observed that *keg1Δ* has 2-fold reduction of the β-1,6-glucan, similar to *kre6Δ* (Nakamata et al., 2007). Mutations in *BIG1* and *ROT1* have shown severe reductions in β-1,6-glucan compensate by an increase of β-1,3-glucan and chitin levels, indicating that these genes are related to the β-1,6-glucan synthesis but are not β-1,6-glucan synthase since there is small amount of the polymer found (Machi, 2004; Pagé et al., 2003). Rot1, Big1 and Keg1 may act as stabilizer to the proteins involved in β-1,6-glucan synthesis.

Table I-8. Genes implied in β-1,6-glucan biosynthesis

Gene	Biological Function	Reference
KRE1	cell wall glycoprotein invoved in β-1,6-glucan biosynthesis	(Roemer et al., 1993)
KRE9	cell wall glycoprotein invoved in β-1,6-glucan biosynthesis	(Brown et al., 1993)
KRE5	cell wall glycoprotein invoved in β-1,6-glucan biosynthesis	(Meaden et al., 1990)
KRE6	integral membrane protein required for β-1,6-glucan biosynthesis	(Kurita et al., 2011; Roemer and Bussey, 1991; Roemer et al., 1993)
BIG1	integral membrane protein of the ER	(Azuma et al., 2002; Machi, 2004)
ROT1	molecular chaperone in the ER, involved in N-glycosylation and O-mannosylation	(Machi 2004; Pagé et al. 2003)
KEG1	Kre6-binding ER protein responsible for Glucan synthesis	(Nakamata et al., 2007)

Importantly, it can be noticed that mutations in genes related to the mannoprotein synthesis such as *OCH1, MNN9, MNN2*, present increased levels of β-1,6-glucan (Magnelli et al., 2002; Pagé et al., 2003), showing the importance of a compensatory mechanism between these two polymers.

3.4. Mannoproteins

The fibrillar outer layer of the yeast cell wall is made of mannoproteins, the second most present component in the cell wall, very useful in many industrial applications due to their beneficial effects in winemaking and their role in flocculation. Biochemical and genetic approaches have been used to determine the structure of mannoproteins in *Saccharomyces cerevisiae* and many reviews have been published on this topic.

3.4.1. Synthesis of the precursor

UDP-N-acetylglucosamine, UDP-Glucose and Dol-P-Mannose are used as donors in mannoproteins biosynthesis.

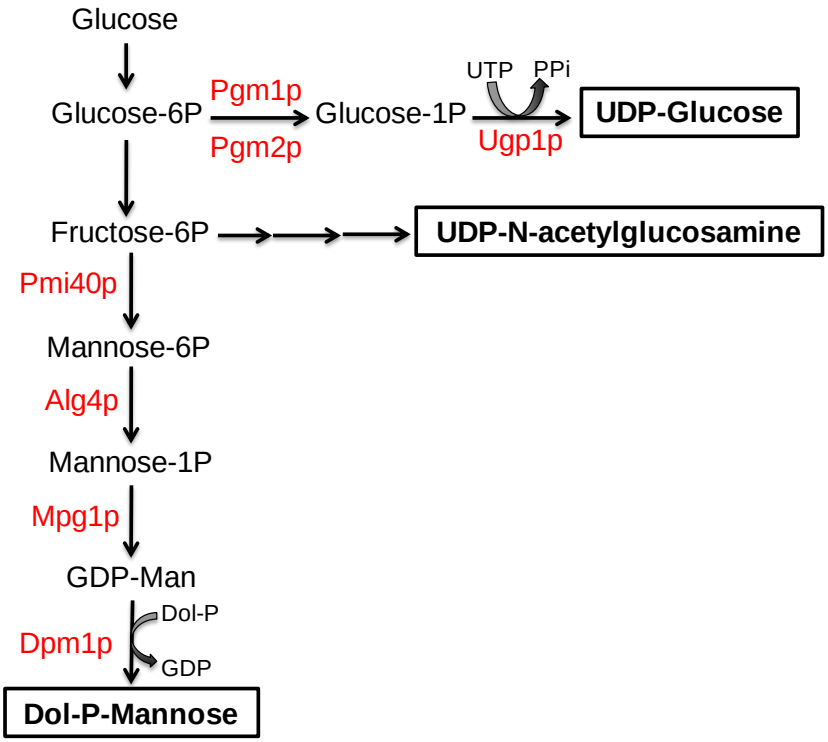

Figure I-13. Synthesis of the Dol-P-Mannose donor for the reactions in the lumen implied in GPI anchor, O- and N-glycosylation pathways.

As depicted in Figure I-13, Fructose-6P is required for the formation of Dol-P-Mannose and this conversion is catalyzed by the successive action of Pmi40, Alg4, Psa1 and Dpm1 (see Figure 13) (Orlean, 1990). Dol-P-Mannose is a key mediator in the protein glycosylation of the proteins: N-glycosylation, O-glycosylation and the synthesis of GPI anchors (Orlean, 2012).

Table I-9. Genes involved in the synthesis of mannoproteins precursors

Gene	Biological function	Reference
PGM1	PhosphoGlucoMutase, Catalyses the conversion of Glc-1P to Glc-6P	(Boles et al., 1994)
PGM2	Paralog to PGM1	(Boles et al., 1994)
UGP1	UDP-Glucose Pyrophosphorylase, catalyses the reversible formation of UDP-Glc from Glc-1P and UTP	(Daran et al., 1995)
ALG4	Phosphomannomutase; involved in synthesis of GDP-mannose and dolichol-phosphate-mannose	(Bernstein et al., 1985; Burda and Aebi, 1999)
MPG1	Mannose-1-Phosphate Guanyltransferase, synthesizes GDP-Man from GTP and Man-1P	(Hashimoto et al., 1997; Yoda et al., 2000)
DPM1	Dolichol Phosphate Mannose synthase, catalyzes the formation of Dol-P-Man from Dol-P and GDP-Man	(Orlean, 1990)

3.4.2. Protein glycosylation

Mannoproteins are constituted of highly glycosylated proteins attached to mannosyl chains composed of mannose units linked in α(1→2), α(1→3) and α(1→6). There are two type of glycosylation.

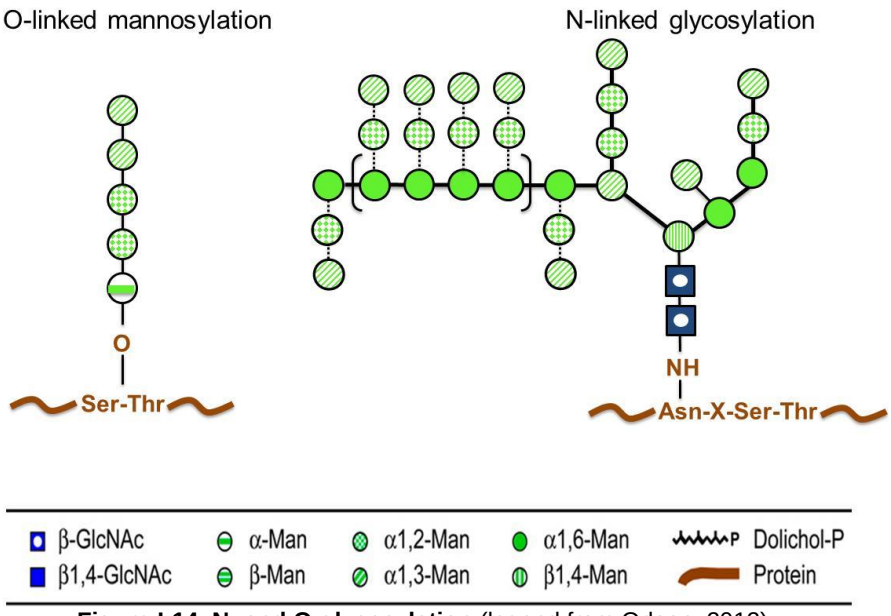

Figure I-14. N- and O-glycosylation (legend from Orlean, 2012).

N-glycosylated chains are constituted of an oligosaccharide core, composed of 8 to 13 units of mannose and 2 units of N-acteylglucosamine. As shown in Figure I-14, this core is attached on amide group of asparagine (Asn) of a sequence of three amino acids: Asn-X-Thr/Asn-X-Ser, where X is an amino acid except proline (Herscovics and Orlean, 1993). O-glycosylated chains are shorter mannose chains (4 or 5 mannose units) attached by α-1,2 and α-1,3 linkages, which are bonded to serine and threonine residues through a α-mannosyl bond.

3.4.2.1. N-glycosylation

N-glycosylation requires firstly assembling a 14-sugar oligosaccharides on a carrier Dol-PP in the endoplasmic reticulum membrane, then to transfer this oligosaccharide to asparagine in lumen of the endoplasmic reticulum.

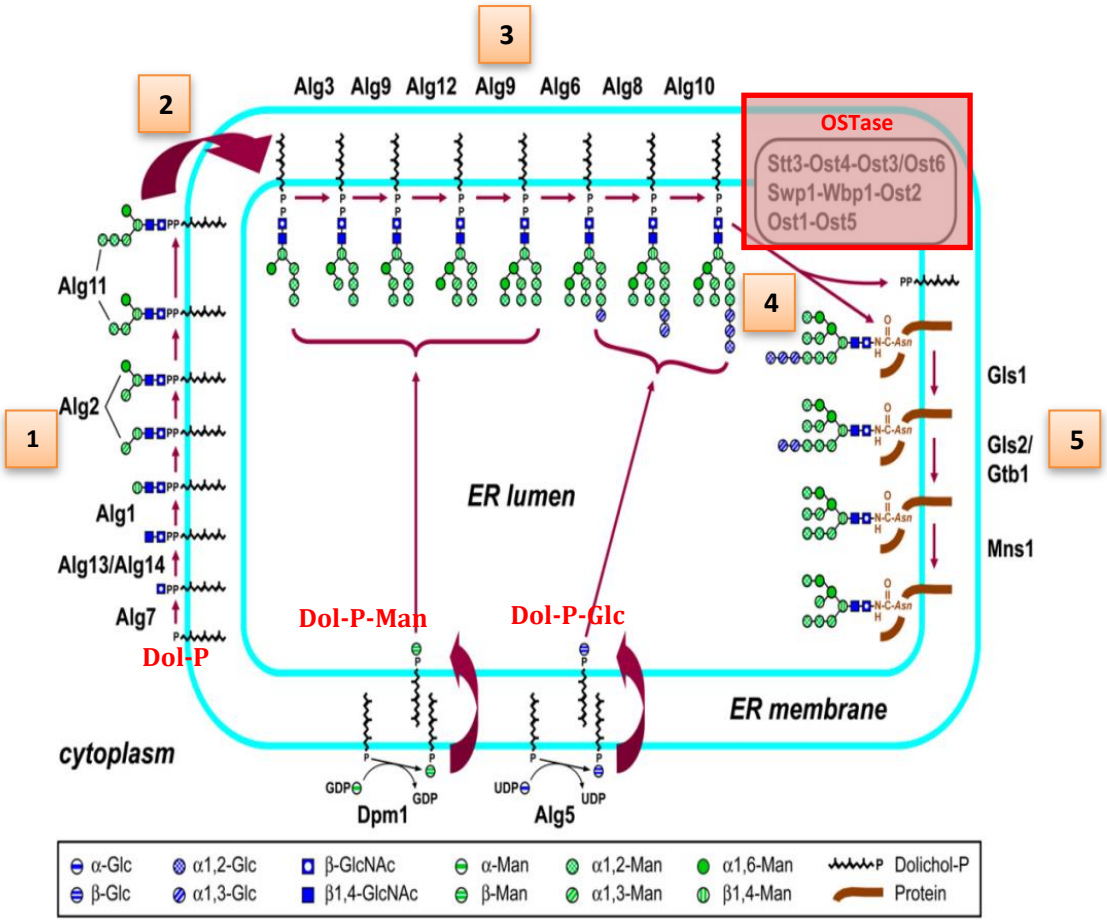

Figure I-15. Scheme of the N-glycosylation with the assembly of a sugar oligosaccharide on a carrier Dol-PP in the endoplasmic reticulum (ER) and its transfer to asparagine in the ER lumen. The number 1 to 5 indicate the different steps of the glycosylation (adapted from Orlean, 2012).

The synthesis of protein N-glycosylated is initiated in the cytoplasm face of the endoplasmic reticulum by the addition of two N-acetylglucosamine units and five units of mannose on the dolichol-phosphate (Dol-P) anchored at the membrane (Orlean, 2012) (Figure I-15, step 1). The formed Dol-P-$GlcNAc_2$-Man_5 translocated to the lumenal face of the endoplasmic reticulum by a still unclear mechanism. Then 4 more mannose of the Dol-P-mannose (Dol-P-Man) are added by mannosyltransferases (Alg3p, Alg9p, Alg12p) and three units of glucose of the Dol-P-Glucose (Dol-P-Glc) are sequentially added by the consecutive action of Alg6p, Alg8p et Alg10p to obtain Dol-P-$GlcNAc_2$-Man_9-Glc_3 (Figure I-15, step 3). The Dol-P-$GlcNAc_2$-Man_9-Glc_3 is finally transferred on the asparagine of the protein by an enzymatic complex, oligosaccharyltransferase (OSTase), where subunits are encoded by *STT3*, *OST4*, *OST3/OST6*, *SWP1*, *WBP1*, *OST2*, *OST1* and *OST5* (Figure I-15, step 4). After this transfer, the three units of glucose are cleaved: the first unit is cleaved by the glucosidase 1 encoded by *GLS1* whereas the two others glucose is cleaved by glucosidase II encoded by *GLS2/GTB1*. In the last step,

one mannose unit is cleaved by the α-mannosidase encoded by *MNS1* (Figure I-15, step 5). Finally N-linked glycosylated proteins come from the endoplasmic reticulum and are extended with a single α-1,6-linked mannose by Och1p (see Figure I-16).

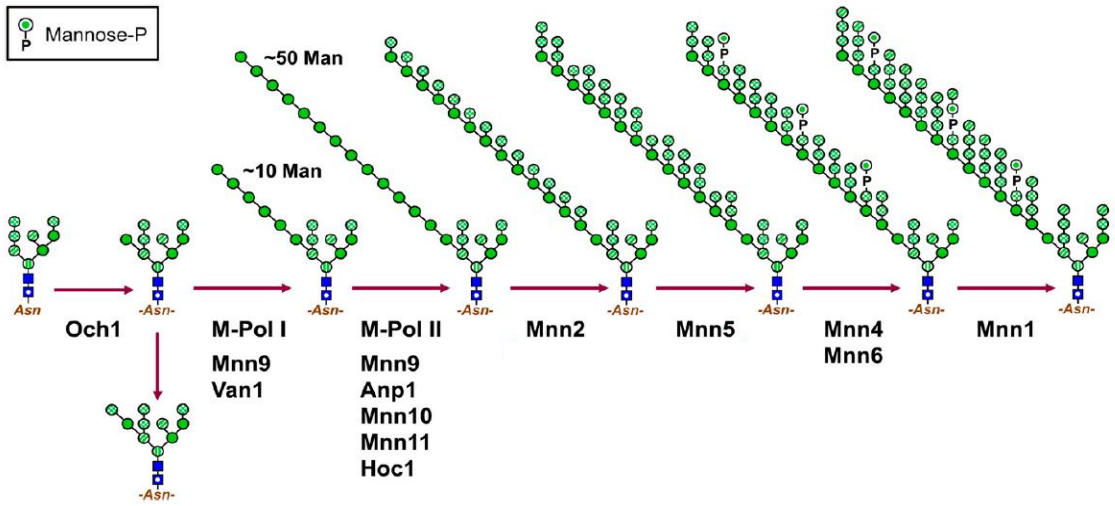

Figure I-16. Elongation in the Golgi of the N-glycosylated proteins to form mannoproteins (from Orlean, 2012).

This residue is elongated with mannose units by a mannosyltransferase complex M-Pol I (Mnn9p and Van1p) to form a backbone of at least 10 α-1,6-linked mannose residue then further extend with α-1,6 linked mannose by a mannosyltransferase complex II M-Pol II (Mnn9p, Anp1p, Mnn10p, Mnn11p, Hoc1p). Additional mannosyltransferases (Mnn2p, Mnn5p, Mnn4p, Mnn6p, Mnn1p) add branches of α-1,2 and α-1,3-linked mannose and phosphomannose to this backbone (Figure I-16).

Mannoproteins of *S. cerevisiae* have been shown to carry up to 200 mannose residues on each of their N-glycans.

Table I-10. Genes involved in N-glycosylation. ER for Endoplasmic Reticulum

Gene	Biological function	localisation	Reference
ALG3	asparagine α-1-3-mannosyltransferase	ER	(Herscovics and Orlean, 1993)
ALG6	asparagine α-1,3-glucosyltransferase	ER	(Herscovics and Orlean, 1993)
ALG8	asparagine glucosyltransferase	ER	(Herscovics and Orlean, 1993)
ALG9	asparagine mannosyltransferase	ER	(Herscovics and Orlean, 1993)
ALG10	asparagine α-1,2-glucosyltransferase	ER	(Herscovics and Orlean, 1993)
ALG12	asparagine α-1,6-mannosyltransferase	ER	(Herscovics and Orlean, 1993)
GLS1	α-glucosidase I	ER	(Herscovics and Orlean, 1993)
GLS2	Glucosidase II subunit	ER	(Herscovics and Orlean, 1993)
GTB1	Glucosidase II subunit	ER	(Herscovics and Orlean, 1993)
HOC1	α-1,6-mannosyltransferase, homolog to OCH1	Golgi apparatus	(Herscovics and Orlean, 1993)
MNN1	α-1,3-mannosyltransferase	Golgi apparatus	(Lussier et al., 1999)
MNN2	α-1,2-mannosyltransferase	Golgi apparatus	(Lussier et al., 1999; Rayner and Munro, 1998)
MNN5	α-1,2-mannosyltransferase	Golgi apparatus	(Lussier et al., 1999; Rayner and Munro, 1998)
MNN6	mannosylphosphate transferase	Golgi apparatus	(Byrne and Wolfe, 2005; Lussier et al., 1997b)
MNN8/ ANP1	α-1,6-mannosyltransferase, subunit	Golgi apparatus	(Orlean, 2012)
MNN9	α-1,6-mannosyltransferase	Golgi apparatus	(Lussier et al., 1999; Van Rinsum et al., 1991; Striebeck et al., 2013)
MNN10	mannosyltransferase complex subunit	Golgi apparatus	(Jungmann et al., 1999)
MNN11	mannosyltransferase, subunit	Golgi apparatus	(Jungmann et al., 1999)
MNS1	α-1,2-mannosidase	Golgi apparatus	(Orlean, 2012)
OST1	oligosaccharyltransferase I	ER	(Orlean, 2012)
OST2	oligosaccharyltransferase II	ER	(Orlean, 2012)
OST3	oligosaccharyltransferase III	ER	(Orlean, 2012)
OST4	oligosaccharyltransferase IV	ER	(Orlean, 2012)
OST5	oligosaccharyltransferase V	ER	(Orlean, 2012)
OST6	oligosaccharyltransferase VI	ER	(Orlean, 2012)
SWP1	oligosaccharyltransferase, Δsubunit	ER	(Orlean, 2012)
VAN1	mannan polymerase I component	Golgi apparatus	(Orlean, 2012)
WBP1	oligosaccharyltransferase, β-subunit	ER	(Orlean, 2012)

3.4.2.2. O-glycosylation

The synthesis of O-mannosylated chains is initiated in the endoplasmic reticulum by six Protein of the O-MannosylTransferase (PMT). PMTs transfer mannose residues from Dol-P-Mannose on a serine or threonine residue of the protein (Gentzsch and Tanner, 1996; Girrbach and Strahl, 2003). The synthesis of O-glycosylated chains continues in the Golgi apparatus by the addition of four or fifth α-linked mannose provided by GDP-Mannose by the Ktr1 and Mnn1 families (Lussier et al., 1999). The proteins Ktr1p, Ktr3p and Kre2p are responsible for the transfer of the first two α-1,2-mannose. The elongation is pursued by the addition of one or two mannose linked in α(1→3) by Mnn1p, Mnt2p and Mnt3p.

Table I-11.Genes implied in O-mannosylation

Gene	Biological function	localisation	Reference
PMT1	protein O-mannosyltransferase,	ER	(Bourdineaud et al., 1998)
PMT2	protein O-mannosyltransferase, paralog to PMT3	ER	(Lussier et al., 1995)
PMT3	protein O-mannosyltransferase	ER	(Girrbach and Strahl, 2003)
PMT4	protein O-mannosyltransferase	ER	(Girrbach and Strahl, 2003)
PMT5	protein O-mannosyltransferase, paralog to PMT1	ER	(Girrbach and Strahl, 2003)
PMT6	protein O-mannosyltransferase	ER	(Girrbach and Strahl, 2003)
KTR1	α-1,2-mannosyltransferase	Golgi apparatus	(Lussier et al., 1999)
KTR3	α-1,2-mannosyltransferase	Golgi apparatus	(Lussier et al., 1999)
KRE2 (MNT1)	α-1,2-mannosyltransferase	Golgi apparatus	(Lussier et al., 1999)
MNN1	α-1,3-mannosyltransferase	Golgi apparatus	(Lussier et al., 1999)
MNT2	mannosyltransferase	Golgi apparatus	(Romero et al., 1999)
MNT3	α-1,3-mannosyltransferase	Golgi apparatus	(Lussier et al., 1999; Romero et al., 1999)

The different mechanisms required for the protein mannosylation lead to obtain long chain of mannoprotein, who can be attached to the cell wall by covalent linkage.

3.4.3. Covalent attachment of CWP

The proteins attached to the cell wall polysaccharides are named CWP (CWP for Cell Wall Protein) and are divided in three classes: mannoproteins attached to β-1,6-glucan via a GPI anchor (GPI-

CWP), mannoproteins covalently attached to β-1,3-glucan (PIR-CWP), and small amount of mannoproteins attached by ionic or disulfide linkages.

GPI anchor

The majority of mannoproteins covalently attached to the glucan network are bound to it trough a GPI anchor remnant (GPI for Glycosyl-Phosphatidyl-Inositol). These proteins are Ser-Thr rich, and possess an N-terminal signal peptide, terminated by a hydrophobic sequence which is replaced by a GPI anchor during secreteion through the endoplasmic reticulum. The core structure of the GPI anchor is a chaincomposed of a phosphate ethanolamine, five mannose residues, one glucosamine unit and an inositol, followed by a lipidic part which includes diacylglycerol and a ceramid (Herscovics and Orlean, 1993). In the case of cell wall GPI proteins, this lipid part is cleaved of, and GPI-CWP are connected to the cell wall by a β-1,6-glucan chain via a phosphodiester link (Pittet and Conzelmann, 2007).

PIR family

Proteins with Internal Repeats (PIR), are attached to β-1,3-glucan. The PIR-CWPs are characterized by the following sequence structure: a N-terminal signal peptide, a Kex2 cleavage site, an internal repeat region and a C-terminal conserved region.

Since Pir proteins can be liberated from the cell walls by mild alkali extraction (Kapteyn et al., 1999) and are highly O-glycosylated, it is suggested that they are retained through an O-glycosidic bound to β-1,3-glucan. It has also be reported that Pir proteins are linked to the cell wall via disulfide bridges because they can be released by a reducing agent such as β-mercaptoethanol (Castillo et al., 2003). Deletion of the repetitive sequence units in Pir4p (Castillo et al., 2003) and Pir1p (Sumita et al., 2005), leads to a release of these proteins into the culture medium, suggesting a role of the internal repeats in the connection between PIR-CWP and β-1,3 glucan.

Minor attachment

A third kind of connection was reported for the linkage with others cell wall proteins via disulfide bonds. Secretory CWPs are reported to be linked through an alkali-sensitive linkage, whereas others secretory CWPs no covalently bound to the cell wall have been found.

Specific cell wall proteins: Flo proteins

In most of the industrial applications, after the growth, the yeast cells have to be removed for further processing of the product. The solid-liquid separation processes may involve sedimentation, centrifugation, filtration or others clarification strategies, which are time consuming, expensive and can affect the quality of the final product. Therefore, these methods are replaced by the use of yeasts able to flocculate and thus easy to separate from the medium.

While the interest of flocculation in industrial fermentation processes is well known, the precise molecular mechanism of this phenomenon is still not fully characterized. Flocculation is a characteristic yeast cells behavior, defined as a asexual, homotypic, reversible, calcium dependent and multivalent process of aggregation of yeast cells to form flocs (multicellular masses of thousands of cells) that rapidly sediment to the bottom of the medium (Soares, 2011). Two main hypothesis may explain the molecular mechanism of flocculation, but the lectin-like theory by Miki *et al.* (Miki Bl et al., 1982) is often preferred. These authors proposed that specific surface sugar binding proteins called lectins (also called adhesins or flocculins) on the flocculent cells recognize and interact with α-mannans carbohydrates on the surface of other cells. Lectins achieve their active conformation inthe presence of calcium ions; hence this element is essential to this process.

Flocculation can be inhibited by a solution of EDTA or sugars like mannose in the medium. Strains able to flocculate can be classified through their phenotypes of inhibition: Flo1 phenotype (flocculation inhibits by mannose and derivatives), NewFlo phenotype (inhibition by mannose, maltose, sucrose, glucose but not galactose) and mannose insensitive (no inhibition by sugars). Flo1 phenotype is governed by the gene *FLO1*, which belongs to the FLO family. This flocculin family also includes *FLO5*, *FLO9*, *FLO10* and *FLO11*. The sequence of flocculin family is composed of a central domain, N- and C- hydrophobic terminal domains. The C-terminal region contains a GPI anchor site which covalent binds Flo proteins to β-1,6 glucan of the yeast cell wall *via* a GPI remnant. The central domain contains repeated sequences and many serine/threonine residues, providing sites for O-glycosylation, and around 14 potential N-glycosylation sites (Watari et al., 1994). The interaction between a purified N-terminal domain of the protein Flo1p with monomannoses and mannans chains of *S. cerevisiae* have confirmed that this domain is responsible for the sugar-binding activity of Flo1p (Goossens et al., 2011). Besides the genetic background of the strains (FLO family), different environmental factors may influence the phenomenon of flocculation like the kind of sugars present,

ethanol level, temperature and presence of cations in particular Ca^{2+}. Studying an ale-brewing strain with a NewFlo phenotype, Claro *et al.* (Claro et al., 2007) have shown that continuous mild heat shock (37°C) or short heat shock (52°C, 5 min) impairflocculation. Although the mechanisms are still unclear, some articles have reported a positive effect of ethanol on flocculation (Li et al., 2012).

4. Architecture of the cell wall and remodeling enzymes

4.1. Architecture of the yeast cell wall

According to electronic microscopy analysis, the structure of the yeast cell wall presents two layers: the internal layer is amorphous and colorless, when the outer layer is condensed and constituted by fibrils perpendicular to the surface (Osumi, 1998). The internal layer is composed of β-1,3 and β-1,6-glucan that is complexed to chitin and provides the maintenance of the cell shape and mechanical strength of the cell. The external layer is mainly constituted by mannosylated CWP (Cell Wall Protein) anchored to the β-glucan. This outer layer is thought to act as a selective filter protecting cells against chemical or enzymatic attacks like glucanase (Fernandez and Cabib, 1984), as well as a binder of toxins (Yiannikouris et al., 2006)

4.2. Hydrolytic enzymes of the yeast cell wall

Despite its rigidity and its capacity to protect against exterior harsh conditions, the cell wall architecture is continuously remodeled by glucanases, chitinase and chitin/glucan branching enzymes which monitor progression of the glycosidic linkages between the different polymers of the yeast cell wall (Teparić and Mrša, 2013). Glucanases are involved in different morphogenesis events. They are necessary for a controlled endo or exo hydrolysis. Exo-glucanase hydrolyses β-glucan by sequentially cleaving glucose residues from the non-reducing end, whereas endo-glucanase cleaves β-linkages at random sites along the polysaccharide chains and release smaller oligosaccharides and glucose units. Chitinase cleaves the β-1,4 linkages of the linear chitin polymer, releasing N-acetylglucosamine residues (Adams, 2004).

Chitinase and glucanases in *Saccharomyces cerevisiae* have been classified in the CAZY database (http://www.cazy.org/) into different Glycosyl Hydrolases (GH) families: chitinases (Cts1 and Cts2) belong to GH18 family, exo-β-1,3 glucanases (Exg1, Exg2, Ssg1) are in GH5 family, whereas endo-β-1,3 glucanases are divided in GH17 family (Bgl2, Scw4, Scw10, Scw11) and GH81 family (Eng2 and

Eng1). The Gas family (Gas1-5), required for β-1,3 synthesis, are members of GH72 family (Ragni et al., 2007a). They have a β-1,3 glucanosyltransferase activity, which consist in cleaving an internal glycosidic linkage of a β-1,3 glucan chain as a glycosyl hydrolase, but instead of a water molecule, a carbohydrate is transferred to the new reducing end (Mazáň et al., 2011).

4.2.1. β-1,3-Glucanases

4.2.1.1. Endo-β(1,3) glucanase

GH17 family (Bgl2, Scw4, Scw10, Scw11)

Bgl2 is an endo-β-1,3-glucanase (Mrsa et al., 1993). This protein has been found in isolated cell walls and its structure has been elucidated (Klebl and Tanner, 1989)., It was recently shown that β-sheets are present in Bgl2p structure, allowing it to form fibrils particularly in the presence of cell wall polysaccharides (Kalebina et al., 2008) from pH 5.0 to neutral pH, ability which is lost at pH 7.6 (Bezsonov et al., 2013). Bgl2 and Gas1 are considered the major glucanosyltransferases participating in the cell wall assembly (Plotnikova et al., 2006). Deletion of *BGL2* leads to an increase in chitin with no modification of glucan levels, but alkali soluble glucan, which comprises the majority of β-1,6-glucan, was found to be increased (Orlean, 2012). Moreover, an up-regulation of the gene *BGL2* expression has been observed in the mutants *kre6Δ, mnn9Δ* and *gas1Δ*, all presenting higher amount of chitin levels in their cell walls.

Scw4, Scw40 and Scw11 proteins are soluble cell wall (SCW) proteins of the GH17 family, SDS extractable, similarity to β-1,3-glucanases, but no evidence for an enzymatic *in vitro* activity has been found yet.

GH81 family (Eng2 and Eng1)

The GH81 family includes proteins with endo-β-1,3-glucanase activity found in yeast and fungi, but also present in plant and bacteria. In the yeast *Saccharomyces cerevisiae*, Baladron et al. (Baladron et al., 2002) have identified *ENG1* and *ENG2 as* coding for endo-β-1,3-glucanases. Eng1 is an extracellular highly glycosylated protein, while Eng2 is an intracellular protein induced during sporulation. A deletion of *ENG1* leads to aggregate cells and its protein has been localized at the daughter side of the septum, indicating that Eng1 is involved, with chitinase, in the dissolution of the

septum causing the separation of the daughter from the mother cell (Baladron et al., 2002; Cabib and Arroyo, 2013).

Although Eng2 hydrolyzes linear β-1,3-glucan of at least five units of glucose (Martín-Cuadrado et al., 2008), this protein is not essential for the sporulation because no important effect has been observed in *eng2Δ* mutant.

4.2.1.2. Exo-β(1,3) glucanase

In *Saccharomyces cerevisiae*, three exo-β-1,3-glucanases, Exg1, Exg2 and Ssg1, have been characterized. Exg1, the major exo-β-1,3 glucanase, is secreted to the periplamic space and released into the culture medium, although Exg2 is anchored to the plasma membrane via a GPI anchor (Larriba et al., 1993) and Ssg1 is specific to sporulation of diploids (San Segundo et al., 1993). Exo-β-1,3 glucanase activity for Exg1, Exg2 and Ssg1 have been detected *in vitro*, but Exg1 and Exg2 have also shown a β-1,6-glucanase *in vitro* activity. Overexpression and deletion of *EXG1* has led to a slight decrease and increase of β-1,6-glucan amount, respectively (Jiang et al., 1995); suggesting a role for these enzyme in the cell wall glucan assembly (Lesage and Bussey, 2006).

4.2.2. Chitinases

In *Saccharomyces cerevisiae*, *CTS1* and *CTS2* genes have been shown to encode endochitinases, which can degrade chitin in N-acetyl-D-glucosamine residues. Cts1p is a cell wall protein highly glycosylated, present in the vegetative growth, which destroys the chitin at the primary septum, synthesized by Chs2p (Kuranda and Robbins, 1991). Cts2p is induced during sporulation (Dünkler et al., 2008) but its action is still not known.

4.2.3. Remodelling enzymes

Chitinase may cleave the β-1,4-linkage inside the chitin polymer, but this chitin may also be attached to β-1,3-glucan and β-1,6-glucan. The enzymes responsible for these connections are Crh1, Crh2 and Crr1 of the GH16 family. Crh1 and Crh2 possesses a transglycosylase activity (Cabib et al., 2008), homolog to glycosyltransferase, while Crr1 is their functional homolog expressed during sporulation and responsible for the cross-linkage between chitin/β-1,3-glucan in the ascospore cell wall. Using two novel method, based on the affinity between β-1,3-glucan chains (curdlan method) or based on the deacetylation of chitin to form chitosan followed by a direct extraction of this product with acetic acid or after digestion with different glucanase (chitosan method), Cabib could determine the amount

of chitin free and bound to the different glucan (Cabib, 2009). This study allowed to show that chitin polymer linked to β-1,3-glucan and β1,6-glucan has a similar size, but shorter than the free chitin. This evidence suggests that chitin transferred by Crh1 and Crh2 to the β-glucan is only a small fragment of the nascent chitin. By applying these new methods, it was confirmed that chitin linked to β-1,6-glucan is predominant in lateral walls, whereas its cross-linkage with β-1,3-glucan is major at the bud neck (Cabib, 2005).

Therefore, a mutation in *CRH* gene conduct to a decreased chitin linked to β-1,6-glucan or its absence in *crh1Δcrh2Δ* mutant. In mutants defective in cell wall synthesis, such as *fks1Δ* and *gas1Δ*, the deletion of either *CRH1* or *CRH2* exacerbates the morphologic defect in these mutants (Cabib et al., 2007). However, as expected, in the absence of chitin substrate, a mutation in *CRH1* or/and *CRH2* did not affect the phenotype of *chs3Δ* mutant (Blanco et al., 2012). The function of Crh2 may be dominant to Crh1, as suggest by Blanco et al, because of the more abnormal shape of *cla4Δcrh2Δ* cells than *cla4Δcrh1Δ. CLA4* encode a protein kinase, which is required for the correct localization and assembly of the septin ring (Schmidt et al., 2003).

Table I-12. Enzymes implied in the yeast cell wall architecture in *Saccharomyces cerevisiae*.

Gene	Biological activity/function	Mode of action	CAZY family	References
BGL2	β-1,3 glucanase/cell maintenance	Endo	GH17	(Bezsonov et al., 2013; Kalebina et al., 2008; Klebl and Tanner, 1989; Mrsa et al., 1993)
SCW4	β-1,3 glucanase		GH17	(Cappellaro et al., 1998)
SCW10	β-1,3 glucanase		GH17	(Cappellaro et al., 1998)
SCW11	β-1,3 glucanase		GH17	(Cappellaro et al., 1998)
ENG1	β-1,3 glucanase/cell separation	Endo	GH81	(Baladron et al., 2002)
ENG2	β-1,3 glucanase	Endo	GH81	(Baladron et al., 2002; Martín-Cuadrado et al., 2008)
EXG1	β-1,3 glucanase	Exo	GH5	(Jiang et al., 1995; Larriba et al., 1993)
EXG2	β-1,3 glucanase	Exo	GH5	(Larriba et al., 1993)
SSG1	β-1,3 glucanase/sporulation	Exo	GH5	(San Segundo et al., 1993)
CTS1	Chitinase/cell separation	Endo	GH18	(Kuranda and Robbins, 1991)
CTS2	Chitinase/cell separation	Endo	GH18	(Dünkler et al., 2008)
CRH1	Chitin cross-linking/wall assembly		GH16	(Blanco et al., 2012; Cabib, 2009; Cabib et al., 2007, 2008)
CRH2	Chitin cross-linking/wall assembly		GH16	(Blanco et al., 2012; Cabib, 2009; Cabib et al., 2007, 2008)
CRR1	Chitin cross-linking/spore wall assembly		GH16	(Gómez-Esquer et al., 2004)

4.3. Signalling pathways involved in the yeast cell wall architecture

During growth, cells are subjected to different environmental constraints. In order to survive, the cell wall can change in composition and architecture in response to these environmental stresses. These cellular responses are mediated by a set of adaptive changes called 'compensatory mechanism' or 'cell wall salvage response', consisting in three major outcomes: (i) the proportion between the polysaccharides in the cell wall is changed, with a rise of the chitin content; (ii) the type of association between the cell wall polymers is modified, illustrated in *gas1Δ* mutant by a 20-fold increase of the linkage chitin/cell wall protein as compared to the isogenic wild-type strain; (iii) the transient redistribution of the cell wall synthesis (such as β-1,3-glucan synthase complex) and repair machinery to the whole cell periphery. These observations show that the cell wall is a dynamic structure, which can be repaired and adapted under stress conditions by a set of complex mechanisms. Numbers of studies have been published about the regulation of these processes (Cid et al., 1995; Fuchs and Mylonakis, 2009; Levin, 2005, 2011).

First, the yeast cells sense these changes at the cell surface, and transmit the signal to intracellular effectors. In *S. cerevisiae*, different signalling pathways have been reported to be involved, including the pheromone response, cell wall integrity (CWI) and high osmolarity glycerol (HOG) pathways. These signalling pathways are based on protein kinases cascades and result in the activation of a final effector, a mitogen-activated protein kinase (MAPK). They share some common elements such as *STE11*, which encodes a mitogen activated protein kinase kinase kinase (MAPKKK) involved in the MAPK pathways governing pheromone response, HOG and filamentous growth. Nevertheless their responses are distinct, depending on the upstream elements (sensors) and downstream elements (transcription factors), which are specific to each pathway.

In response to a stress or perturbing conditions that may damage the cell wall such as heat shock, hypotonic shock, mutations of cell wall related genes or exposure to cell wall perturbing drugs (Calcofluor White, Congo Red, caffeine or β-1,3-glucanase), the MAPK cascade dependent on the protein kinase C encoded by *PKC1* is activated (Figure 17). This pathway is also known as the cell wall integrity (CWI) pathway, since it is vital for maintenance of the integrity of the cell. The CWI pathway can be activated within seconds when the extracellular osmolarity is abruptly decreased (Davenport et al., 1995), or in 10 – 30 minutes after a temperature increase (Kamada et al., 1995) .

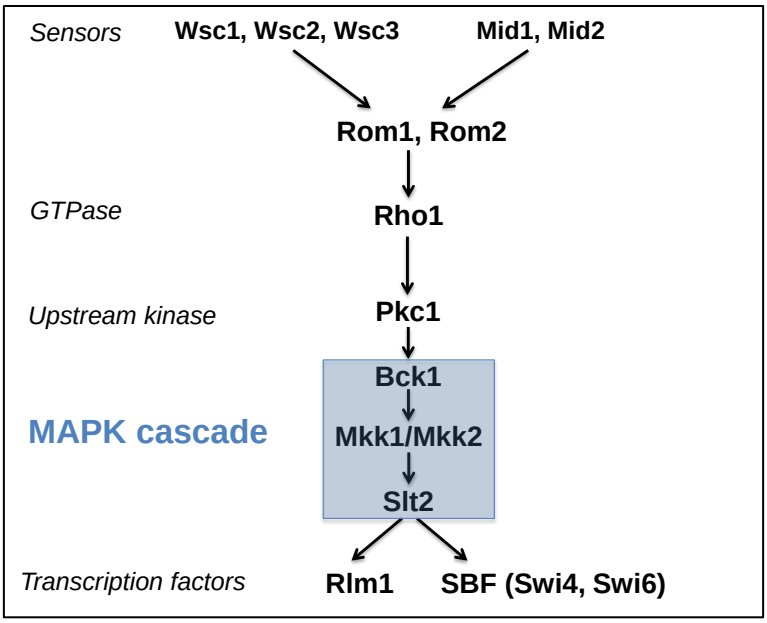

Figure I-17. Cell wall integrity (CWI) signalling pathway involved in the detection and response to stresses that damage the cell wall (adapted from (Levin, 2005))

The activation of the linear Pkc1-MAPK pathway is triggered at the plasma membrane through cell surface sensors, which are Wsc1, Wsc2, Wsc3, Mid1 and Mid2. Among these sensors, the major ones are encoded by *MID2* and *WSC1*, since a simultaneous deletion of these two genes leads to lethality. The signal is transmitted to the GTP protein encoded by Rho1 through Rom1/Rom2 that activates the exchange between GDP and GTP on Rho1. Then Rho1, directly activates Pkc1, the yeast homolog of mammalian Protein Kinase C. Remarkably, Rho1 protein also constitutes the regulatory subunit of the β-1,3-glucan synthase (with the catalytic subunits Fks1 and Fks2 (Lesage and Bussey, 2006)). Loss of function of either *PKC1* or another of the components of the MAPK cascade results in a cell lysis defect due to a cell wall construction deficiency. The activation of Pkc1-MAPK cascade by cell wall stress leads to the dual phosphorylation of Slt2/Mpk1, which is then in its active kinase Slt2/Mpk1 state. One of the consequences of signalling through the MAPK cascade is the activation of the transcription factors Rlm1 and SBF. Signalling through Rlm1 regulates the expression at least 25 genes, most of which are implicated in cell wall biogenesis (Levin, 2005). Also under the control of Slt2-MAPK cascade, SBF transcription factor complex (composed of Swi4 and Swi6) activates gene expression at the G1/S transition of the cell cycle. The targeted genes are involved in bud emergency, membrane and cell wall biosynthesis.

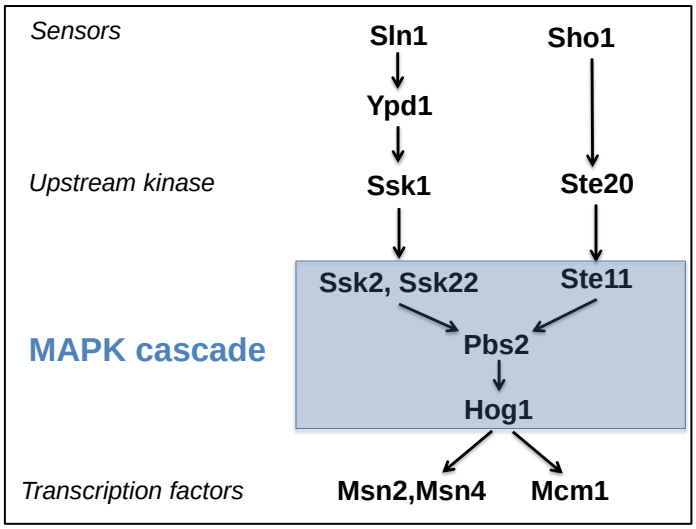

Figure I-18. High Osmolarity Glycerol (HOG) pathway (adapted from (Levin, 2005))

On the opposite, when cells are challenged by hyperosmotic condition, the high osmolarity glycerol pathway (HOG) is activated. The increase in external osmolarity is detected by two independent osmosensors, Sln1 and Sho1, which in turn regulate the activity of the HOG1 MAPK pathway (Posaset al., 1996) and lead to the phosphorylation of the Hog1p kinase. The MAP kinase Hog1 then activates several genes, including regulators of glycerol synthesis resulting in accumulation of glycerol, which is the main osmoprotector compound of yeast cells. In addition, activation of the HOG1 MAPK cascade also induces transcription of several genes through stress response elements (STREs) (Schulleret al. 1994). *STREs* genes are characterized by a common sequence element (AGGGG) or its reverse complement (CCCCT) in their promoter region.

5. Conclusion of the literature review and objectives of the thesis

In this literature review, we reported studies relative to *Saccharomyces cerevisiae* cell wall. Although numbers of publications on this subject have shown that the yeast cell wall is a dynamic and complex structure of cross-linked polysaccharides, some of the molecular and biochemical mechanisms at stake are still under investigations. Indeed, the structure and composition of the yeast cell wall have been reported to vary in function of cell cycle, strains and culture conditions. However the mechanisms that could explain this influence are still not clear. This understanding is crucial in order to be able to optimize the production of cell wall components as feed additive or to find antifungal targets. As a first important step towards this understanding, we developed a new analytical method to have a reliable and precise estimation of the content of each polysaccharide in the yeast

cell wall, to assess the impact of stress and the consequences of different mutations (chapter 2). This method has then be used to characterize the effect on cell wall composition of different stress such as a short-exposure to heat (42°C, 1hr) and a treatment by caspofungin (at MICx0.5 and MICx4), an antifungal drug that targets the β-1,3-glucan synthase complex. These results were correlated with nanomechanicals measurements by Atomic Force Microscopy and were published (in appendix). The second step is to investigate the influence of strains on cell wall assembly and composition (chapter 3). We have combined genome-wide transcriptomic analysis, AFM technology and cell wall composition measurements of strains deleted in important genes for the cell wall biogenesis. Then, we used an integrative approch to search for correlation between these data that would help to finding molecular clues that account for the cell wall structure and its nanomechanical properties link (chapter 3A). Since the yeast cell wall has an important biotechnological value, four industrial strains have been studied by similar approaches (chapter 3B). Finally, with the aim to characterize the stress impact of industrial processes, we have examined the effect of autolysis on the cell wall composition and biophysical properties for two industrial strains of interest (chapter 4).

Chapter II: DETERMINATION OF THE YEAST CELL WALL COMPOSITION

Objective:

The development and validation of a simple and reliable method for quantitative determination of *Saccharomyces cerevisiae* cell wall polysaccharides is described. This new protocol combines acid and enzymatic hydrolyses to determine accurately the cell wall polysaccharides: mannans, chitin, β-1,3-glucan and β-1,6-glucan.

Material and methods:

The screening of 11 enzymes commercially available that possess hydrolytic activities on different substrates (mannans, chitin, laminarin as β-1,3-glucan and pustulan as β-1,6-glucan) has allow to select 4 specific enzymes avoid to any secondary activities. The production and purification of a recombinant endo-β-1,6-glucanase from *Trichoderma harzianum* was made according to (Bom et al. 1998), due to the lack of commercial enzyme. The chromatography profiles show that chitin and β-1,3-glucan were hydrolysed into their corresponding monomers N-acetylglucosamine and glucose, respectively, by the combined action of a chitinase from *Streptomyces griseus* and endo/exo-β-1,3-glucanase from *Trichoderma species.* The digestion of β-1,6-glucan substrate by the endo-β(1,6)-glucanase results in gentiobiose, a disaccharide linked in β(1→6), as a major peak, which is hydrolysed in glucose by addition of a β-glucosidase from *Aspergillus niger*. After checking in the cell wall preparation (from the wild-type strain), lipids and proteins by thin layer chromatography (TLC) and micro-Kejdahl respectively, we have analysis the residues released by different enzymatic configurations. Finally, we have compared the amount of β-1,3 and β-1,6-glucan obtained by alkali method in order to establish the enzymatic procedure to hydrolyse chitin, β-1,3-glucan and the remaining β-1,6-glucan, combined to sulfuric acid treatment to determine mannans.

Results:

This novel method was validated by showing that the content of β-(1,3), β-(1,6)-glucan or chitin was dramatically decreased in yeast mutants defective in cell wall synthesis genes (*chs3Δ, fks1Δ, kre6Δ, gas1Δ, mnn9Δ*), which was correlated with phenotypic observations using Congo Red and Calcofluor White. Moreover, this method is a valuable tool to assess the environmental effects on yeast cell wall composition. We found that heat shock at 42°C in *S. cerevisiae* resulted in twofold increase of chitin, whereas ethanol stress had apparently no effect on yeast cell wall composition.

RESEARCHARTICLE

A combined chemical and enzymatic method to determine quantitatively the polysaccharide components in the cell wall of yeasts

Marion Schiavone[1,2,3,4], Amelie Vax[1,2,3], Cecile Formosa[1,5,6,7,8], Helene Martin-Yken[1,2,3], Etienne Dague[1,5,6] & Jean M. Francois[1,2,3]

[1]INSA, UPS, INP, Universite de Toulouse, Toulouse, France; [2]UMR792 Ingenierie des Systemes Biologiques et des Procedes, INRA, Toulouse, France; [3]UMR5504, CNRS, Toulouse, France; [4]Lallemand SAS, Blagnac, France; [5]LAAS, CNRS, Toulouse, France; [6]UPS, INSA, INP, ISAE, LAAS, Universite de Toulouse, Toulouse, France; [7]UMR 7565, SRSMC, CNRS, Vandœuvre-les-Nancy, France; and [8]Faculte de Pharmacie, UMR 7565, Universite de Lorraine, Nancy, France

Correspondence: Jean M. Francois, LISBP-INSA, 135 Avenue de Rangeuil, F-31077 Toulouse Cedex 04, France.
Tel.: +33(0) 5 61 55 9492;
fax: +335 615 59400;
e-mail: fran_jm@insa-toulouse.fr

Received 21 May 2014; revised 2 July 2014; accepted 3 July 2014.

DOI: 10.1111/1567-1364.12182

Editor: Carol Munro

Keywords
cell wall; β-(1,3)-glucan; β-(1,6)-glucan; chitin; chitinase; b-glucanases.

Abstract

A reliable method to determine cell wall polysaccharides composition in yeast is presented, which combines acid and enzymatic hydrolysis. Sulphuric acid treatment is used to determine mannans, whereas specific hydrolytic enzymes are employed in a two sequential steps to quantify chitin and the proportion of β-(1,3) and β-(1,6)-glucan in the total β-glucan of the cell wall. In the first step, chitin and β-(1,3)-glucan were hydrolysed into their corresponding monomers N-acetylglucosamine and glucose, respectively, by the combined action of a chitinase from *Streptomyces griseus* and a pure preparation of endo/ exo-β-(1,3)-glucanase from *Trichoderma species.* This step was followed by addition of recombinant endo-β-(1,6)-glucanase from *Trichoderma harzianum* with β-glucosidase from *Aspergillus niger* to hydrolyse the remaining b-glucan. This latter component corresponded to a highly branched β-(1,6)-glucan that contained about 75–80% of linear β-(1,6)-glucose linked units as deduced from periodate oxidation. We validated this novel method by showing that the con-tent of β-(1,3), β-(1,6)-glucan or chitin was dramatically decreased in yeast mutants defective in the biosynthesis of these cell wall components. Moreover, we found that heat shock at 42 °C in *Saccharomyces cerevisiae* and treatment of this yeast species and *Candida albicans* with the antifungal drug caspofungin resulted in 2- to 3-fold increase of chitin and in a reduction of β-(1,3)-glucan accompanied by an increase of β-(1,6)-glucan, whereas ethanol stress had apparently no effect on yeast cell wall composition.

Introduction

The cell wall is vital for growth, survival and morphogenesis of fungi. In the yeast *Saccharomyces cerevisiae*, this external structure is a complex interplay of four major polysaccharides: β-(1,3) glucan which is a linear chains of around 1500 glucose units linked in β-(1,3), β-(1,6) glucan composed of 140–350 residues of glucose linked by a β-(1,6) linkage, mannans which comprises mannose units linked in α-(1,2); α-(1,3); α-(1,6) and chitin, a polymer of 100–90 N-acetylglucosamine units linked by β-(1,4) linkages. Moreover, the cell wall also harbours several proteins that are implicated in molecular recognition and adhesion (Levin, 2005; Klis et al., 2006, 2009). Other polymers of glucose (α-(1,3) and α-(1,4)-glucan) as well as galactomannans are part of the cell wall structure of other fungal species such as *Schizosaccharomyces pombe* and *Aspergillus species* (Free, 2013). Over the last 15 years, the complexity of the cell wall architecture has emerged from detailed genetic, molecular and biochemical studies, which led to the discovery of several interconnections between the wall components to form macromolecular

complexes (see Free, 2013; Orlean, 2012; for a recent review on this topic). In addition, the molecular architecture of the cell wall is constantly remodelled according to growth conditions, morphological development or in response to cell surface stresses. This cell wall remodelling process is mainly under the control of the cell wall integrity (CWI) signalling pathway that transmits the sig-nal from cell surface sensors to a MAP kinases cascade (Levin, 2011), with the main consequence to reorganize cell wall architecture through changes in cell wall carbohydrates content, in cross-links between chitin and β-glucan polymers, and in a transient redistribution of the cell wall repair machinery to the site of the cell wall injuries (Klis et al., 2006; Lesage & Bussey, 2006).

The yeast cell wall is endowed with remarkable biochemical properties, which are exploited in different biotechnological industrial sectors. In winemaking, cell wall mannoproteins are used to reduce astringency caused by tannins (Dupin et al., 2000) and to capture some wine aromatic contaminants that give a mouldy taste to wine. In animal nutrition, cell wall β-glucan serves as a valuable microbiological binder of mycotoxins (Yiannikouris et al., 2004). This polymer is also well known to have strong immunostimulating activities that could be beneficial for health and resistance to diseases and cancer (Brown & Gordon, 2003; Chen & Seviour, 2007). Taken together, these biological functions of the yeast cell wall appeal for a precise quantitative determination of its composition, owing to the fact that cell wall mass and the proportion of each of its component may dramatically vary according to growth conditions and process methods (Nguyen et al., 1998; Aguilar-Uscanga & Francois, 2003).

Several methods aiming at isolating cell wall and quantifying its composition have been already developed. Most of them make use of chemical treatments of the cell wall with strong acids such as hydrochloric, hydrofluoric, trifluoroacetic and sulphuric acids, which can break down the cell wall polymers into their monomers of glucose, mannose and glucosamine (De Ruiter et al., 1992; Ram et al., 1994; Dallies et al., 1998; Freidmund et al., 2005). However, these acidic methods suffer from at least three major problems. Firstly, they are unable to make distinction between β-(1,3) and β-(1,6)-glucan. Secondly, they are rather harsh and may destroy the monomers and hence underestimate the content of the corresponding polysaccharide in the wall if not well controlled in terms of duration and temperature. Thirdly, most of these methods are not efficient enough to hydrolyse all chitin, leading to an underestimation of this polymer. To esti-mate the proportion of β-(1,3) and β-(1,6)-glucan, Fleet and Manners (Fleet & Manners, 1976) developed a chemical fractionation method that consisted in the separation of the cell wall into an alkali-soluble and alkali-insoluble fraction, and the latter was again separated into an alkali-insoluble acid-insoluble and alkali-insoluble acid-soluble fractions that contain the bulk of β–(1,6)-glucan, whereas β-(1,3)-glucan is essentially present in the alkali-soluble and alkali-soluble acid-insoluble fraction. Aimanianda et al. (2009) applied an enzymatic digestion after this fractionation procedure to determine β-(1,3)- and β-(1,6)-glucan using recombinant endo-β(1,3)-glucanase from Thermotoga neopolitana and endo-β-(1,6) glucanase from Trichoderma harzianum. However, this fractionation procedure is time-consuming and imperfect as it leaves some 10–20% of β-(1,6)-glucan in the alkali-insoluble acid-soluble fraction (Catley, 1988; Ha et al., 2002). To be more accurate on these polysaccharides quantification, Hong et al. (1994) and Magnelli et al. (2002) have pro-posed a method based on the chemical and enzymatic fractionation of the cell wall obtained from yeast cells cul-tivated with radiolabeled glucose. Although this method allowed to trace and quantify each component in the dif-ferent fractions, they could not be applied for regular cell wall analysis because they require cultivating yeast cells with a radiolabeled sugar prior to hydrolysis.

With the objective to determine more precisely chitin levels and to distinguish β-(1,6) from β-(1,3)-glucan in cell wall b-glucan, we report a simple and reliable method that is based on the sequential treatment of cell walls with specific hydrolytic enzymes, namely chitinase, endo and exo-β-(1,3)-glucanases followed by a mixture of endo-β-(1,6)-glucanase and b-glucosidase. Combined with the chemical treatment that hydrolyses mannans into mannoses units, this new method allowed faithfully quan-tifying each of the different polymers that compose the cell wall. This method has been applied to determine the cell wall composition of mutants defective in genes involved in the cell wall synthesis and remodelling, as well as to assess effects of ethanol stress, heat shock and the antifungal drug caspofungin on the cell wall composition of yeasts.

Material and methods

Chemicals and biochemicals

Laminarin (from *Laminaria digitata*), chitin (from shrimp shells) and mannan (from *S. cerevisiae*) were purchased from Sigma-Aldrich. Pustulan isolated from *Umbilicaria papullosa* was from Calbiochem. All these polysaccharides were verified for their relative purity after acid hydrolysis as described in Dallies et al. (1998). Values around 65–78% of the dry powders were obtained based on the quantification of the sugars monomers released after this acid hydrolysis (see Table 1). Note that all commercial polysaccharides were kept in a jar under vacuum to main-tain them dry. Except for β-D-gentiobiose, which was

Table 1. Screening of commercial enzymatic preparation on β-(1,3) glucan, β-(1,6) glucan, chitin and mannans

Commercial name (company)	Origin	Description of enzymes activities present in the commercial preparation	Laminarin (*Laminaria digitata*) µg glucose mg^{-1} powder	Pustulan (*Umbilicaria pustulata*) µg glucose mg^{-1} powder	Chitin (Shrimp shells) µg GlcNac mg^{-1} powder	Mannan (*S. cerevisiae*) µg mannose mg^{-1} powder
Glucanex	Enzyme preparation	Endo-β(1,3)-glucanase β-(1,6)glucanase Cellulase Protease Chitinase	570.9 ± 13.6	576.0 ± 20.2	556.9 ± 7.2	574.7 ± 20.2
Glucazyme	Enzyme preparation	Endo & Exo-β-(1,3)-glucanase Chitinase β-glucosidase	757.4 ± 8.9	799.9 ± 20.3	26.5 ± 2.5	23.8 ± 5.3
Zymolyase	*Arthobacter luteus*	β-(1,3)-laminari pentao-hydrolase Mannanase Protease	409.2 ± 35.7	39.9 ± 16.9	13.9 ± 2.8	0
Laminarinase	*Trichoderma species*	Endo-β-(1,3) glucanase Cellulase α-amylase	752.3 ± 11.3	740.9 ± 33.7	6.0 ± 2.3	15.7 ± 9.2
	Hordeum vulgare	Endo-β-(1,3) glucanase	249.6 ± 19.2	48.5 ± 11.3	0	0
Exo-β-(1,3) glucanase	*Trichoderma species*	Exo-β-(1,3) glucanase	745.3 ± 33.4	46.2 ± 18.5	0	6.9 ± 1.6
Endo-β-(1,3) glucanase	*Trichoderma species*	Endo-β-(1,3) glucanase	626.9 ± 21.7	48.2 ± 5.9	0	0
Endo-β-(1,6) glucanase	*Trichoderma harzianum*	Recombinant Endo-β-(1,6)glucanase	0	559.8 ± 42.2	0	0
β-glucosidase	*Aspergillus niger*	β-(1,4)-glucanase	663.3 ± 62.0	311.5 ± 50.2	0	0
Chitinase	*Trichoderma viride* *Streptomyces griseus*	Chitinase Chitinase	0 0	0 0	161.3 ± 19.5 975.0 ± 17.5	0 0
Sulphuric acid method			720.9 ± 25.4	695.6 ± 13.3	491.3 ± 25.0	651.3 ± 22.4

obtained from Carbosynth, other biochemicals were purchased from Sigma-Aldrich (France) and were of the purest quality. The following enzyme preparation known to act on β-glucan were purchased from Megazyme (Ireland): Glucazyme (K-EBHLG), exo-β-(1,3)-glucanase from *Trichoderma species* (E-EXBGL), endo-β-(1,3)-glucanase from *Trichoderma species* (E-LAMSE), recombinant endo-β-(1,3)-glucanase from *Hordeum vulgare* (E-LAMHV) and β-glucosidase from *Aspergillus niger* (E-BGLUC). Glucanex was from Novozymes (L1412), Zymolyase 20T (L5263), laminarinase from *Trichoderma species* (L5272), chitinase from *Streptomyces griseus* (C6137) and from *Trichoderma viride* (C8241) were obtained from Sigma-Aldrich. Recombinant endo-β-(1,6)-glucanase from *Trichoderma harzianum* expressed in *Pichia pastoris* (a kind gift from Dr J. Chapman, Unilever, the Netherlands) was prepared according to Bom et al. (1998).

Strains, culture conditions and phenotypic tests

The BY4741 and its isogenic YKO strains [deletion mutants made with the kanMX6 cassette according to (Wach, 1996)] were obtained from Open Biosystem). Unless otherwise stated, the yeast cells were cultivated in YPD medium (1% w/v of yeast extract; 1% w/v of peptone, 2% w/v glucose) and were collected at the exponential growth phase ($OD_{600\ nm}$ around 1.5 corresponding to 2 9 10^7 cells.mL^{-1}) by centrifugation at 4°C (1000 g for 10 min) and washed two times with cold sterile water. The pellets were kept frozen at 20°C until use. Sensitivity of yeast cells to Congo Red (CR; Sigma-Aldrich) or Calcofluor White (CFW; US Bio) was carried out on YPD agar plates using the concentration of the drug reported in the corresponding figure.

Isolation of cell walls

Each pellet was resuspended in 0.5 mL cold water and transferred to lysis matrix tubes (MPBio, 6960-500) containing 0.5 mm glass beads. Cells were disrupted using a Fastprep system (MP Biomedicals) for 20 s with intervals of 1 min on ice. The disruption cycle was repeated until more than 95% of the cells were lysed as estimated by methylene blue coloration according to (Cot et al., 2007). Usually, about 10 cycles were needed to reach this yield. The cell suspension was collected, and the glass beads were extensively washed with cold deionized water. The supernatant and washings were pooled and centrifuged at 4000 g for 15 min. The cell wall-containing pellet was again washed two times with cold deionized water. Pellets were frozen in nitrogen liquid and then lyophilized until complete dryness.

Chemical treatment of cell walls

Acid sulphuric hydrolysis of the cell wall was carried out as described previously (Dallies et al., 1998). This acid hydrolysis released glucose from β-glucan, mannose from mannans and glucosamine from chitin (since the N-acetyl residue in N-acetyl-glucosamine is acid-labile).

Enzymatic treatment of commercial polysaccharides and yeast cell wall

Pustulan, laminarin, chitin, mannan and yeast β-glucan (alkali-soluble from Megazyme) were prepared as a 1–10 $mg.mL^{-1}$ solution in 50 mM potassium acetate pH 5.0. Unless otherwise stated, commercial enzymes were added at 1 U and incubation was carried out at 37 °C for 8–16 h. One unit is defined as the amount of enzyme that releases 1 μmol of product which is either glucose or N-acetylglucosamine per min under the condition of the assay. An aliquot was taken for measurement of glucose residues and N-acetylglucosamine (see below).

Enzymatic treatment of yeast cell wall to determine chitin, β-(1,3) and β-(1,6)-glucan

The procedure for quantitative determination of chitin, β-(1,3)- and β-(1,6)-glucan from purified yeast cell wall is based on a two steps process as depicted in Fig. 1.

Step 1: enzymatic treatment for chitin and β-(1,3)-glucan determination

The lyophilised cell wall (about 10 mg of dry mass) was resuspended in 200 μL of potassium acetate 50 mM pH 5.0. After heating at 65 °C for 5 min, 1 U chitinase from *Streptomyces griseus*, 5 U of exo-β-(1,3)-glucanase and 5 U endo-β-(1,3)-glucanase from *Trichoderma species* were added. Hydrolysis was carried out at 37 °C for 6–12 h.

Step 2: enzymatic hydrolysis for β-(1,6)-glucan estimation

To the remaining hydrolysate in step 1, 2 U of purified endo-β-(1,6)-glucanase prepared as described above and 1 U of β-glucosidase from *A. niger* (Megazyme, E-BGLUC) were added. Hydrolysis was carried out at 37 °C for 6–12 h.

Quantification of sugars by HPAEC-PAD

After each enzymatic digestion, a sample was withdrawn and centrifuged in a microfuge (10 min at 10 000 g at

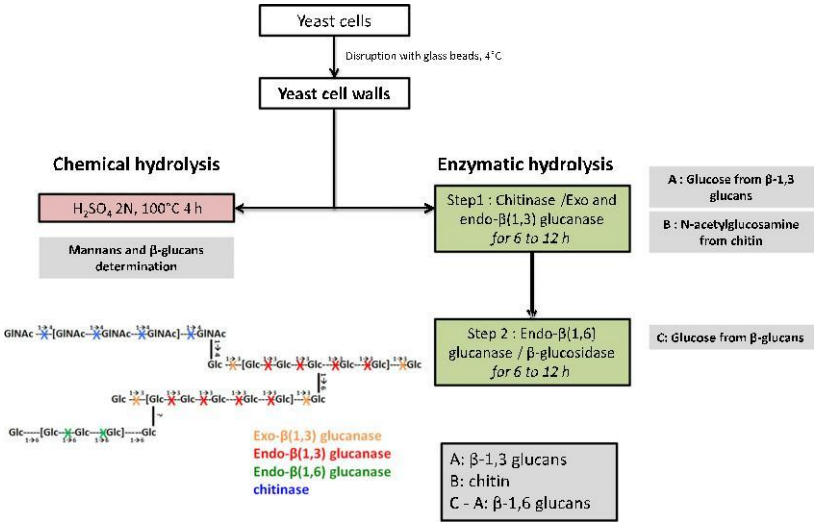

Fig. 1. General scheme for cell wall preparation and fractionation by acid and serial enzymatic hydrolysis to determine its polysaccharide composition. Chitin, β-(1,3)-glucan and β-(1,6)-glucan chains are schematically represented by the specific linkages between monomers of glucose (Glc) and N-acetylglucosamine (GlNAc). The crosses of different colours correspond to the specific enzymes cleaving these linkages (with the name of these enzymes given in the Insert). The figure which illustrates cell wall linkages is adapted from Lesage & Bussey (2006).

4 °C). The supernatant was analysed by HPAEC-PAD on an ICS 5000 system (Thermofisher Scientific, Courtaboeuf, France). Separation of the released monosaccharides (glucose, mannose and glucosamine) and oligosaccharides were performed on a CarboPac PA100 analytical column (250 x 4 mm) with a guard column CarboPac PA100 using NaOH (100 mM) and NaOAc/NaOH (500 mM/100 mM) as solvent A and B, respectively. The chromatographic conditions set up by Aimanianda et al. (2009) were followed. The column was pre-equilibrated by 98% A and 2% B. Following sample injection, a gradient run (flow rate 1 mL min^{-1}) was performed as follows: 0–2 min, isocratic step (98% A-2% B), 2–15 min 98% A-2% B to 65% A-35% B, 15– 22 min 65% A 35% B to 57% A-43% B, 22–23 min 57% A-43% B to 100% B, and 23–25 min 100% B. Sugar residues were detected on a pulsed amperometric system equipped with a gold electrode.

Colorimetric method to determine chitin levels

Chitin was determined by the colorimetric method as described by Reissig et al. (1955) and adapted for a microplate reader method, using N-acetylglucosamine as a standard. Briefly, a 125 μL of the digestion mixture was heated with 25 μL of 0.8 M potassium tetraborate pH 9.0 at 100 °C for 8 min. After cooling down the samples to room temperature, 750 μL of Reissig reagent diluted 10 times in glacial acetic acid was added, and the tubes were incubated 40 min at 37 °C. The absorbance was read at 585 nm. The 10X Reissig's solution was prepared by dissolving 10 g of 4-dimethylaminobenzaldehyde in 12.5 mL of HCl 10 N and 87.5 mL of glacial acetic acid.

Other miscellaneous methods

Preparation of alkali-soluble and insoluble fractions from purified yeast cell wall was carried out as described in Magnelli *et al.* (2002). The nitrogen content of the cell walls was determined by a micro-Kjeldahl method in a Leco nitrogen auto analyser FP428 (Leco Corporation) according to the manufacturer procedure with EDTA as internal standard (9.56% N). The protein content was calculated as the N content x 6.25, based on the estima-tion that the average nitrogen content of proteins in food material is around 16% (\http://www.fao.org/docrep/006/y5022e/y5022e03.htm). Glucose oxidase peroxidase kit Sigma-Aldrich was routinely used for determination of glucose after hydrolysis of various polysaccharide substrates (mannan, chitin, laminarin and pustulan) by chemical or enzymatic treatment. Periodate oxidation of carbohydrate was performed according to Hong et al. (1994).

Results

Screening of enzymes that harbour hydrolytic activities specific on chitin, β-(1,3) and β-(1,6)-glucan

As our goal was to find enzymes able to specifically hydrolyse β-(1,3)-glucan, β-(1,6)-glucan and chitin, we screened a large set of commercially available enzymatic preparations harbouring hydrolytic activities on laminarin, a linear β-1,3-glucan; pustulan, a β-1,6-glucan; chitin and mannans (Table 1). As the exact purity of these commercial polysaccharide products was either not available or questionable, these products were subjected to

acid hydrolysis using the sulphuric acid hydrolysis method described earlier (Dallies et *al*., 1998), and the released glucose from β-glucan and mannose from mannans were quantified by HPAEC. With the exception of chitin whose hydrolytic yield with this method has been estimated to 45–55% (Aguilar-Uscanga & Francois, 2003), and assuming complete hydrolysis of the other polysaccharides and minor degradation of the released of monomers in this highly acidic condition, the purity of laminarin, pustulan and mannans was estimated in the range of 65–73% of dry powder (Table 1). Also, it was necessary to establish assay conditions that would be common for all the enzymes tested. After preliminary assays following the recommendation of the manufacturers, we finally decided to use 50 mM potassium acetate buffer, at pH 5.0 and to run the reaction at 37 °C for 16 h, since in all cases, the hydrolysis reaction carried out with 1–5 U of enzyme in the presence of 1–10 mg mL^{1} of substrate reached a plateau after 8–12 h (data not shown). Accordingly, we found that Glucanex®, a glucanase preparation obtained from Novozymes, hydrolysed all the different polysaccharides with yield very close to that obtained by chemical treatment, indicating that contrary to their commercial description, this enzyme preparation may also contain chitinase and manannases. Another enzymatic cocktail termed Glucazyme® from Megazyme was effective on laminarin and pustulan but almost inactive on chitin and mannans, indicating that they contain endo-β-(1,3)/β-(1,6)- and exo-β-glucanases in accordance with its commercial prescription, whereas the chitinase, that is, explicitly mentioned in this cocktail had, in our hand, no activity on chitin. This result confirmed that this enzymatic preparation could be used to hydrolyse β-glucan from yeast cell wall as proposed by Megazyme. The last enzymatic cocktail tested was Zymolyase 20T, commonly used to prepare yeast spheroplasts (Ovalle et al., 1998). This cocktail was found to only partially hydrolyse laminarin and had also a weak action on pustu-lan and chitin, showing that this enzyme preparation was not appropriate for our purpose.

We then assayed four enzymes with reported endo-β-(1,3) glucanase activity. Whereas purified laminarinase from *Trichoderma sp*. exhibited efficient hydrolytic action on both β-(1,3) and β-(1,6) glucan substrates, the puri-fied enzyme from *Hordeum* was highly specific for β-(1,3) linkages and was unable to fully hydrolyse laminarin, according to its pure endo-β-(1,3)-glucanosidase activity. On the other hand, we found an exo-β-(1,3)-glucanase from *Trichoderma* that was highly efficient on laminarin with almost no action on pustulan. An endo-β-(1,3)-glucanase purified from this fungus was also tested and showed hydrolytic action on laminarin albeit with less glucose released than with the exo-β-(1,3)-glucanase. Interestingly, the combination of the endo and exo-β-(1,3)-glucanases led to a release of glucose units from laminarin that was about 20% higher than after acid treatment, which indicated higher polysaccharides recovery upon enzymatic hydrolysis than after acid hydrolysis (Table 2). Chromatography analysis showed mainly glucose after digestion of laminarin with both exo and

Table 2. Combination of selected enzymes to hydrolyse β-1,3 (laminarin), β-1,6-glucan (pustulan) and alkali-soluble yeast β-glucan

	Cell wall substrates (source)			
Type of hydrolysis action	Laminarin (Laminaria digitata) µg glucose mg^{-1} powder	Pustulan (Umbilicaria pustulan) µg glucose mg^{-1} powder	Yeast β-glucan* (S. cerevisiae) µg glucose mg^{-1} powder	Chitin (Shimp shells) µg GlNAc mg^{-1} powder
Exo + endo-β-(1,3) glucanases + chitinase	898.1 ± 56.1 (1.24)	58.0 ± 12.1 (0.09)	474 ± 21.7 (0.76)	980.2 ± 20.0 (2.0)
Exo + endo-β-(1,3) glucanases + b-glucosidase	895.1 ± 44.1 (1.24)	358.0 ± 52.1 (0.09)	nd	0
Endo-β-(1,6)-glucanase	0	560 ± 42.2 (0.87)	nd	0
Endo-β-(1,6) glucanase + b-glucosidase	620.1 ± 23.7 (0.86)	868.8 ± 44.9 (1.24)	nd	0
Exo + endo-β-(1,3)-glucanases + endo-β-(1,6) glucanase + β-glucosidase	nd	nd	589 ± 4.9 (0.96)	nd
Acid hydrolysis	720.9 ± 25.4	695.6 ± 13.3	614.6 ± 3.5	491.3 ± 25.0

For enzymatic assay, the polysaccharides were resuspended at 1 $mg.mL^{-1}$ in 50 mM acetate buffer pH 5.0. The value indicated in parentheses corresponded to of the ratio of polysaccharides after enzymatic digestion to that after acid hydrolysis. The results shown are the mean SD of at least three independent experiments, each made in triplicate.
nd, not done.
*Yeast β-glucan is an alkali-soluble fraction of yeast cell wall purchased from Megazyme and which contained 620 mg glucose units.mg^{-1} powder according to this manufacturer.

endo-β-(1,3)-glucanase. A tiny peak that eluted just before glucose was also detected that likely could be a contaminant in the polysaccharide solution as it was also present in the control reaction without enzyme. In contrast, the digestion of laminarin with endo-β-(1,3)-glucanase alone resulted in the presence of two main peaks, one as glucose and a second that likely corresponded to a short oligosaccharide (see Supporting Information, Fig. S1). As indicated in Table 2, further addition of the β-glucosidase did not improve degradation yield of laminarin but it partially hydrolysed pustulan, suggesting that this commercial preparation may contain some β-(1,6)-glucanase activity.

Due to the absence of a commercially available β-(1,6)-glucanase, we produced the recombinant endo-β-(1,6)-glucanase from *Trichoderma harzianum* expressed in *Pichia pastoris* according to the protocol of Bom et al. (1998). It is shown in Table 1 that this recombinant protein was only active on pustulan, releasing about 80% glucose, when compared to the amount released by acid hydrolysis. The chromatography profile of pustulan digestion with this endo-β-(1,6)-glucanase showed that the major product detected was gentiobiose (G2), a β-(1,6) disaccharide which agreed with the endo-β-glucanase action of this enzyme (Lora et al., 1995) (Fig. S2). Interestingly, the addition of a commercial preparation of β-glucosidase from *Aspergillus* led to a complete disappearance of gentiobiose and reduction in the intensity of the other peaks, with a concomitant increase of the glucose peak (Fig. S2). Overall, this enzymatic digestion caused a 25% higher hydrolysis of pustulan than the acidic method (Table 2). This result indicated that the commercial preparation of β-glucosidase from *A. niger* may also contain some β-(1,6)-glucanase activity in addition to the reported β-(1,3) and β-(1,4) hydrolytic activities. This higher value shows that the enzymatic hydrolysis is more efficient than the acidic method to hydrolyse pustulan, because this chemical treatment could destroy glucose residues during its release from the polymer. Finally, two chitinases were commercially available but only the enzyme purified from *Streptomyces griseus* was able to hydrolyse chitin with a yield close to 98% of the amount of the powder present in the reaction (Table 1), suggest-ing that this polymer was completely hydrolysed into its monomer N-acetylglucosamine. This result was verified by chromatography on HPAEC that showed only one peak corresponding to N-acetylglucosamine (see Fig. S3). In addition, this result confirmed that the acid hydrolysis method using sulphuric acid underdetermined chitin levels by about 50%. The reason why the enzyme from *Trichoderma viride* was unable to fully hydrolyse chitin, whatsoever the time of incubation was not explored further. To complete this analysis, we incubated a suspension of commercial yeast β-glucan with the mixture of endo and exo-β-(1,3)-glucanases for 16 h, at pH 5.0 and found that the amount of glucose released was about 76% of the total β-glucan estimated by acid hydrolysis (Table 2). After further addition of β-glucosidase and endo-β-(1,6)-glucanase to this mixture, the total glucose released was very close to the amount obtained after acid hydrolysis which was also in accordance with manufacturer's indication (i.e. 62% of the dry powder consisted in β-glucan). From this total hydrolysis, we could deduce that the amount of β-(1,6)-glucan in this alkali-soluble yeast β-glucan was around 23%.

Setting up the enzymatic procedure on mixed polysaccharides and on purified yeast cell wall

As a first step to set up the enzymatic hydrolysis of yeast cell wall, we evaluated the hydrolytic efficiency of our selected enzymes on a mix of the four polysaccharides components at proportion that mimicked their content in the yeast cell wall. We applied two different modes of enzymatic digestion to this mixture (Fig. 2). In mode 1, the digestion was started by adding chitinase from *Streptomyces griseus*, followed after 6 h by addition of endo and exo β-(1,3)-glucanase and then terminated with endo β-(1,6)-glucanase and β-glucosidase. Before each enzyme addition, a sample was withdrawn and the amount of monosaccha-rides released was determined by HPAEC. As reported in Fig. 2, the recovery of β-(1,3) and β-(1,6)-glucan after enzymatic hydrolysis was very close to the initial amount of total β-glucan initially added (550 mg), whereas that of chitin content was slightly above than initially added in the mixture. However, it is important to notice that the amount of chitin determined after whole incubation procedure with both β-(1,3) and β-(1,6)-glucanases enzymes was the same as after incubation with chitinase alone (data not shown), indicating that the action of the latter enzyme was not impaired by the presence of the other polysaccharides.

We then set out the enzymatic procedure on purified cell wall of the wild-type BY4741 strain. The purity of our cell wall preparation was checked qualitatively by the nearly absence of lipids (see Fig. S4). The amount of the proteins present was measured by a micro-Kjeldahl method (Miller & Houghton, 1945) and found to be around 14% of the cell wall dry mass (see Table 3). As depicted in Fig. 2, we evaluated the specific enzymatic digestion of chitin, β-(1,3) and β-(1,6)-glucan on the purified yeast cell walls according to two different sequential modes of enzymes addition. According to mode 1, the content of chitin determined after incubation with chitinase was around fourfold lower than after treatment of the cell wall with both chitinase and endo/exo-β-(1,3) and β-(1,6)-glucanase as performed in mode 2 ($P < 0.01$). This result confirmed previous findings that

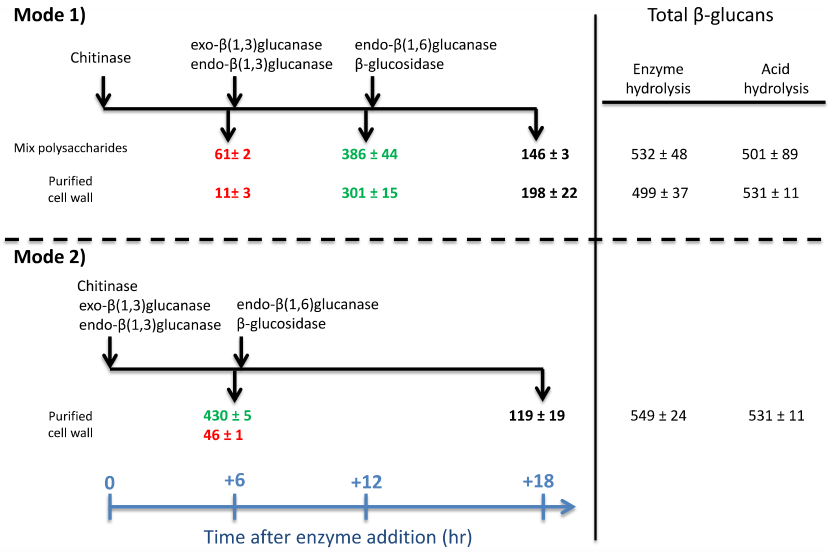

Fig. 2. Sequential enzymatic hydrolysis of chitin and β-glucan. Configuration of enzymatic hydrolysis used in the mix of cell wall polysaccharides and purified yeast cell wall. The polysaccharide mix was made to mimic cell wall composition. It was composed of 40% (w/v) mannans, 40% (w/ v) β-(1,3)-glucan as laminarin, 15% (w/v), β-(1,6)-glucan as pustulan and 5% (w/v) chitin in 50 mM acetate buffer at pH 5.0 in a total volume of 2 mL (Note: these amount was based on the purity of each components which were 90% for laminarin, 87% for pustulan, 98% for chitin). Chitinase (1 U), exo–β-(1,3)-glucanase (5 U)/endo-β-(1,3)-glucanase (5 U), endo β-(1,6)-glucanase (2 U) and β-glucosidase (1 U) were added at the time indicated. Incubation was carried out at 37 °C, and before each addition of enzymes, samples were withdrawn. In red, are values of the N-acetylglucosamine residues from chitin determined by the colorimetric Reissig's method, and in green, are values of glucose residues from β-glucan determined by HPAEC analysis. Values are given in $\mu g.mg^{-1}$ of polysaccharide mix or purified cell wall from two independents experiments. Note that mode 2 was retained as the method for hydrolysis of purified wall from yeast cells.

complete chitin hydrolysis required auxiliary polysaccharide hydrolases in addition to chitinase (Cabib & Sburlati, 1988) and agreed with the existence of cross-linkages between chitin and β-glucan (Sietsma & Wessels, 1990; Kollar et al., 1995; Cabib et al., 2007; Cabib, 2009). Also, this enzymatic procedure showed that the content of chi-tin in wild-type yeast cultivated on glucose was in the range of 5% of cell wall dry mass, rather than 1–2% as commonly reported (Lesage & Bussey, 2006; Orlean, 2012). This difference could be explained by incomplete hydrolysis of chitin by sulphuric acid treatment (see Table 1). In addition, the sequential addition of hydrolytic enzymes in mode 1 led to an apparent under-estimation of β-(1,3)-glucan and an overestimation of β-(1,6)-glucan, in comparison to mode 2.

From these results, it can be estimated that the proportion of β-(1,6)-glucan in the total cell wall β-glucan was around 20–22% of the total β-glucan in yeast wall. This value is about 15–20% higher than the one reported in previous works that employed cell wall fractionation followed by chemical or enzymatic hydrolysis (Fleet & Manners, 1976; Brown et al., 1993; Hong et al., 1994; Magnelli et al., 2002; Aguilar-Uscanga & Francois, 2003). This difference could be due to the fact that the enzymatic mixture of endo-β-(1,6)-glucanase and β-glucosidase was able to hydrolyse not solely the linear β-(1,6)-glucose linked units but also glucose residues, that is, triply linked at C1, C3 and C6 on the β-(1,6)-glucan backbone, as initially described by Manners et al. (1973a, b) and confirmed by Aimanianda et al. (2009). To verify this hypothesis, we subjected our purified cell wall to a chemical fractionation with sodium hydroxide, which yielded an alkali-insoluble fraction according to Hong et al. (1994). This fraction that contained the bulk of β-(1,6)-glucan was then treated with endo/exo β-(1,3)-glucanase, and the digested fraction was filtered through Microcon-10 membrane to separate a low-molecular-mass fraction (glucose units from β-(1,3) glucan hydrolysis) from the high-molecular-mass fraction retained on the membrane and which mainly consisted of β-(1,6)-glucan chains. Part of this latter fraction was treated with endo-β-(1,6)-glucanase and β–glucosidase, while the other part was subjected to periodate oxidation. As each glucose res-idue in the linear β-(1,6)-glucan has three hydroxyl groups on adjacent carbon atoms (C2, C3 and C4), periodate can oxidize and cleaves C-C bonds between C2 and C3 as well as C3 and C4, resulting in the liberation of the C3 atom in the form of formic acid that can be quantified by HPLC. Results of this experiment presented in Fig. S5 showed that the levels of β-(1,6)-glucan determined by the enzymatic hydrolysis were around 25% higher than those estimated after periodate oxidation. These results

Table 3. Determination of polysaccharides and protein content in some selected yeast mutants affected in cell wall formation

Strains	Genetic defect and references	Chemical treatment			Enzymatic method				Protein (%)
		Mannans	β-glucans	Chitin	β (1,3) glucan	β (1,6) glucan	β-(1,3) + β-(1,6) glucan	Chitin	
BY4741	Wild type	304 ± 36	418 ± 16.3	17.0 ± 8.4	357 ± 11	138 ± 4	*495*	45 ± 5	14.4 ± 1.0
BY*fks1*Δ	β-1,3 glucan synthase isoform 1 (Eng *et al.*, 1994)	383 ± 18***	305 ± 8.3***	20 ± 8.8	225 ± 6***	143 ± 19	*368*	98 ± 3***	20.8 ± 0.3
BY*gas1*Δ	β-1,3 glucanosyltranferase (Mouyna *et al.*, 2000)	368 ± 18**	263 ± 34***	27 ± 8	189 ± 2.5***	154 ± 24	*343*	156 ± 0.9***	12.4 ± 0.6
BY*kre6*Δ	Putative β-glucan synthase, localizes to ER, plasma membrane (Roemer & Bussey, 1991)	454 ± 10***	283 ± 48***	11.1 ± 2.0	296 ± 19***	38 ± 21***	*335*	97 ± 6***	12.0 ± 1.7
BY*mnn9*Δ	Subunit of Golgi mannosyltransferase complex; (Jungmann & Munro, 1998)	170 ± 38**	328 ± 88	13 ± 0.5	299 ± 21***	123 ± 1.5*	*422*	62 ± 2***	43.2 ± 4.6
BY*chs3*Δ	Chitin synthase 3; required for synthesis of the majority of cell wall chitin	343 ± 36	402 ± 60	bd	316 ± 25*	136 ± 24	*452*	3.6 ± 0.5***	23.5 ± 1.6

Yeast strains were cultivated in YPD at 30 °C and harvested at $OD_{600\ nm}$ of 1.0. The results shown are the mean ± SD from of 3 to 5 independent biological experiments with each made technically three times. Protein content was determined by micro-Kjeldahl method and calculated as N content × 6.25 and expressed in % of cell wall dry mass. Statistical analysis was carried out using the *t*-test student to assess the significance in difference of cell wall composition between mutants and wild type. These analyses gave *P* values which were marked by $*P < 0.01$; $**P < 0.001$ and $***P < 10^{-4}$.
bd, below detection.

showed that the enzymatic hydrolysis allowed the measurement of the so-called highly branched β-(1,6)-glucan (Manners et al., 1973b) from which about 75–80% corresponded to linear β-(1,6)-glucose linked units.

Validation of the combined chemical and enzymatic method on cell wall defective mutants

Based on the enzymatic protocol described above (Fig. 2, mode 2), and our previous procedure to purify cell wall (Dallies et al., 1998) from yeast culture, we set up an updated protocol (Fig. 1) that combines enzymatic and chemical hydrolysis to quantify mannans, chitin, β-(1,3) and β-(1,6)-glucan in the wall of wild-type and mutant strains harbouring defects in the synthesis of specific cell wall polymers. These results are summarized in Table 3. As a general rule, the hydrolysis of cell wall β-glucan by the enzymatic method yielded roughly 10–25% higher recoveries than acid hydrolysis ($P < 0.01$). Also, levels of chitin were underestimated with the acid method as already noticed in an earlier report (Aguilar-Uscanga & Francois, 2003). On the other hand, the enzymatic digestion with chitinase clearly reinforced previous data that these mutations, except *chs3*Δ, led to a 3- to 5-fold increase in chitin content (Popolo et al., 1997; Dallies et al., 1998; Klis et al., 2006), whereas the *chs3*Δ mutant defective in chitin synthase III contained < 10% of the wild-type levels of chitin. In addition, it is relevant to notice a good correlation between the sensitivity of these cell wall mutants to CFW and CR, two colloidal dyes that are known to bind preferentially to chitin microfibrils (Roncero et al., 1988; Kopecka & Gabriel, 1992; Hoch et al., 2005; Costa-de-Oliveira et al., 2013), and chitin content, as higher this content, greater is the sensitivity to these drugs (Fig. 3). Table 3 also shows that the content of β-(1,3)-glucan decreased by about 45% in a *fks1*Δ mutant that is defective in the major β-(1,3) glucan synthase (Eng et al., 1994). This reduction was to the same extent as that previously reported using chemical methods (Dallies et al., 1998) or fractionation followed by chemical method (Magnelli et al., 2002). The re
maining production of β-(1,3)-glucan is likely due to the activity of the minor β-(1,3)-glucan synthase encoded by *FKS2* that is activated in a *fks1*Δ null mutant (Mazur et al., 1995). An even higher reduction of β-(1,3)-glucan (55%) was recorded in a *gas1*Δ mutant, which is defective in a β-1,3-beta-glucanosyltransferase implicated in the elonga-tion of β-(1,3)-glucan chains (Mouyna et al., 2000), whereas β-(1,6)-glucan content was barely modified in both *fks1*Δ and *gas1*Δ mutants. On the contrary, β-(1,6)-glucan was decreased by about 4-times ($P < 0.0001$) in a *kre6*Δ mutant that is defective in β-(1,6)-glucan biosyn-

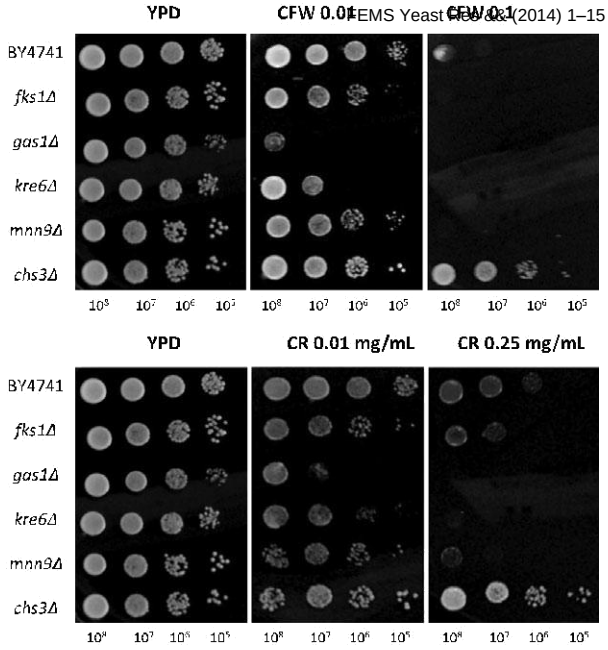

Fig. 3. Sensitivity of wild-type and cell wall defective mutants to CFW and CR. Exponentially growing cells on YPD ($OD_{600\ nm}$ around 1 U) were collected by centrifugation, resuspended in sterilize water at 10^8 cells mL^{-1}. Series of 10-fold dilutions were spotted on YPD agar plates in the absence or presence of various concentrations of CFW or CR as indicated. Picture was taken after 2 days of growth at 30 °C. For identity of the gene mutation, see Table 3.

thesis (Roemer & Bussey, 1991). Therefore, these results can be taken as direct means to validate our enzymatic method of β-(1,3) and β-(1,6)-glucan quantification. The cell wall composition of the *mnn9*Δ mutant which is defective in the elaboration step of protein mannosylation in the Golgi (Orlean, 2012), resulted in a twofold decrease of mannans, and in a noticeable 10–15% decrease of β-(1,3) and β-(1,6)-glucan as compared to wild-type cells. This result was apparently at variance to previous reports indicating a compensatory change in cell wall composition, as a reduction in mannans could be partially compensated by an increase of β-glucan (Dallies et al., 1998; Popolo et al., 2001; Klis et al., 2006). Although this statement was not totally incorrect, as seen for instance with *fks1*Δ, *gas1*Δ and *kre6*Δ mutants for which a reduction of β-glucan was accompanied by an increase of mannans, we actually found that the protein content in the cell wall of a *mnn9*Δ mutant was found to be threefold higher than in wild-type (Table 3).

Effect of various stresses on levels of chitin, β-(1,3) and β-(1,6)-glucan

To enlarge our study, we conducted a biochemical analysis of cell wall composition in response to various environmental stresses as well as to the treatment with caspofungin, an antifungal drug acting specifically on β-(1,3)-glucan synthase (Deresinski & Stevens, 2003). When yeast cells were transferred from 30 to 42 °C, we recently showed using atomic force microscopy (AFM) technology, the formation of a circular structure at the cell surface that takes its origins at a single punctuated source and propagates into concentric manner to reach a diameter of 2–3 μm (Pillet et al., 2014). In addition, as reported in Table 4, the heat shock at 42 °C caused a 45% reduction of the β-(1,3)-glucan that was accompanied by 20% rise in β-(1,6)-glucan ($P < 0.01$) and by a twofold increase of chitin ($P < 0.001$). In contrast, exposure of a yeast culture to 9% ethanol did not cause any significant change of its cell wall composition, even though the nanomechanical properties as determined by AFM were dramatically altered (C. Eltsztein, C. Formosa, M. Schiavone, H. Martin-Yken, M. Morais, E. Dague & J. M. Francois, manuscript in preparation). Finally, we assessed the effects of caspofungin on cell wall composition in both *S. cerevisiae* and in the pathogenic yeast *Candida albicans* (Fig. 4), as we reported that the nano-mechanical properties of both types of yeast determined using AFM technology were strongly altered after exposure to this drug (Formosa et al., 2013). While we already reported a rise of chitin that was roughly proportional to the dose of caspofungin added to the cells, here, we showed that this treatment also strongly impacted the β-glucan layers with a 50% decrease of β-(1,3)-glucan content that was compensated in part by a 20% increase of β-(1,6)-glucan at drug concentration corresponding to a MIC/2. One can notice that effects of caspofungin on the β-glucan content were more pronounced than in a *fks1*Δ

Table 4. Effect of heat shock and ethanol stress on cell wall polysaccharides composition

	% of total cell wall polysaccharides			
Condition	Mannans	b-(1,3)-glucan	b-(1,6)-glucan	Chitin
Control	34.3 2.9	38.7 4.6	22 9	5.1 0.3
Ethanol 9%	34.9 1.4	38.0 2.1	22 2.0	4.9 1.1
Heat shock	44.6 2.6*	20.3 3.5**	25 3.2*	10.1 0.5**

At the exponential phase of growth on YPD ($OD_{600\ nm}$ 1.5 unit), the BY4741 cells were exposed to 9% ethanol for 5 h exposure or subjected to a heat shock at 42 °C for 1 h. The cells were then collected to measure chitin, β-(1,3)-and β-(1,6)-glucan by the enzymatic method, and mannans by acid method as described in 'Material and methods'. Results shown are the mean SD from three independent experiments, with each sample analysis technically performed three times. Significance of the difference was statistically calculated by the t-test student to give P values which were represented by *$P < 0.01$ and **$P < 0.001$.

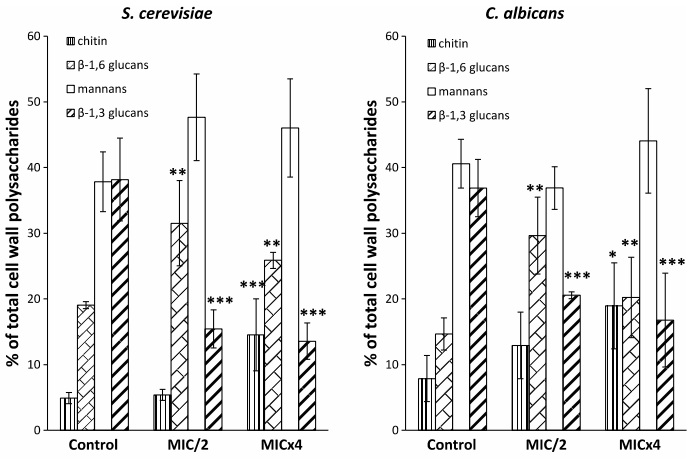

Fig. 4. Effect of caspofungin treatment on cell wall polysaccharides composition. *Saccharomyces cerevisiae* BY4741 or *Candida albicans* (strain from the ABC platform bugs bank, gift of Dr Duval, University of Nancy) were cultivated in YPD. At $OD_{600\ nm}$ of 1 unit, part of the yeast culture was treated with caspofungin at concentration corresponding to 0.5 or 4× MIC [as determined in a previous report (Formosa *et al.*, 2013)]. After 16 h of incubation, cultures were collected, cell walls were purified and chitin, β-(1,3) and β-(1,6)-glucan were measured as described in 'Material and methods'. The results shown are the mean ± SD of two independent experiments, each technically performed three times. Statistical significance of the difference in cell wall components between control and treated cells were calculated by the *t*-test student and yielded *P* value that were represented on the histograms by $*P < 0.01$, $**P < 0.001$ and $***P < 10^{-4}$

mutant lacking the major β-(1,3)-glucan synthase. This can be explained in part by the action of the antifungal drug to also inhibit the activity of the minor β-glucan synthase encoded by *FKS2*. This significant modification of cell wall composition induced by caspofungin can be related with the increased mechanical resistance of the cells after treatment with this drug (Formosa et al., 2013).

Discussion

The yeast cell wall is a complex structure made of 4 types of polysaccharides: mannans, β-(1,3)-glucan, β-(1,6)-glucan and chitin whose proportions of each of them, and linkages between them can dramatically change according to growth conditions, stresses, etc. (Klis et al., 2006; Orlean, 2012). In addition, as several cell wall components may have biotechnological values, there is a crucial need to precisely quantify the content of each of these polymers. The method presented in this study was developed to respond to this question by combining specific enzymatic hydrolysis and chemical hydrolysis. While a similar approach was previously attempted by others to characterize cell wall structure and/or quantify cell wall polysaccharides composition (Fleet & Manners, 1977; Hong et al., 1994; Magnelli et al., 2002), we here provided additional inputs that allow conducting a simple protocol to achieve this goal, without requiring any fractionation, dialysis procedure or labelling of the yeast cells to trace the fate of the polysaccharides during their separation. The main inputs were (i) to identify and select a very active chitinase to fully hydrolyse chitin into its monomer N-acetylglucosamine, which can be thereafter determined by a simple colorimetric method. There were some previous attempts to employ chitinase from *Serratia marcescens* to hydrolyse chitin from the cell wall (Molano et al., 1977; Magnelli et al., 2002). While this enzyme is no longer commercially available, two other chitinases are available in the Sigma catalogue. We found that only the chitinase preparation from *Streptomyces griseus* was highly active on pure chitin and did not exhibit any side activity on β-glucan and mannans. In addition, we showed that maximal hydrolysis of chitin in the yeast cell wall required the incubation of this bacterial chitinase with endo/exo-β-glucanases, likely because the latter enzymes allowed better access of chitinase to chitin microfibrils, as proposed earlier (Cabib & Sburlati, 1988). Accordingly, we found that the chitin content in exponentially growing yeast cells on glucose was in the range of 5% of the cell wall dry mass, which is 2–3 times higher than commonly considered (Lesage & Bussey, 2006; Orlean, 2012). This data may suggest that previous methods based on acid hydrolysis were likely not effective enough to release all chitin that is bound to β-(1,3) and β-(1,6)-glucan, and which gives rise to a tightly knit mesh (Klis et al., 2006; Cabib & Arroyo, 2013). This new evaluation of the chitin content in the cell wall may better fit with the crucial role of this polymer in yeast morphogenesis (Blanco et al., 2012; Cabib & Arroyo, 2013). It remains unknown whether this enzymatic mixture comprising chitinase and β-glucanases can release the last N-acetylglucosamine resi-

dues that are linked at the nonreducing end of β-(1,3)-linked glucan through a β-(1,4) linkage (Kollar et al., 1995).

The second important accomplishment was to use a combination of 'relatively pure' endo and exo-β-(1,3)-glucanases from *Trichoderma reesei* that exhibited high specificity and efficient cleavage of the β-(1,3)-glycosidic bonds of the β-(1,3)-glucan polymers. This mix of enzymes was shown to completely hydrolyse laminarin, a linear β-(1,3)-glucosyl polymer and to release 80% of β-glucan present in the alkali-soluble fraction of purified yeast cell walls, in accordance with the level of β-(1,3)-glucan determined by previous chemical analysis of this fraction (Fleet & Manners, 1977). This combination of enzymes was more useful than the single recombinant endo-β-(1,3)-glucanase, which only releases laminaribi-ose and laminaritriose from linear β-(1,3)-glucan (Mag-nelli et al., 2002; Aimanianda et al., 2009). The last input of the method was to find an enzymatic treat-ment to quantify β-(1,6)-glucan as glucose units. To this end, the recombinant endo-β-(1,6)-glucanase from Trichoderma harzianums was combined with a β-glucosidase to split the disaccharide gentiobiose (G2) that is the major product of the endolytic action of β-(1,6)-glucanase on commercial β-(1,6)-glucan (pustulan). However, it turned out that the proportion of β-(1,6)-glucan in total β-glucan determined in purified yeast cell wall with our enzymatic method were around 22– 27% (see Fig. 1 and Table 1). This value is about 15– 20% higher than previously reported either by chemical analysis (Fleet, 1991) or by combination of enzymatic and acid hydrolysis of ^{13}C-labelled yeast cells (Hong et al., 1994; Magnelli et al., 2002). This overestimation was confirmed by periodate oxidation of β-(1,6)-glucan fraction obtained after cell wall digestion with endo/ exo-β-(1,3)-glucanases. This chemical reagent is specific to attack vicinal hydroxyl groups on the glucose resi-dues. Thus, in the case of linear β-(1,6)-linked glucose units, it specifically oxidizes and cleave C-C bonds between C2, C3 and C4, releasing a stoichiometric amount of formic acid. A simple explanation for this overestimation can be found in previous works of Manners et al. (1973b) and Aimanianda et al. (2009), showing that β-(1,6)-glucan is a highly branched polymer composed of 65–70% of glucose residues linked by C1 and C-6, 15% of nonreducing terminal glucopyranose residues, 5% of glucose linked by C-1 and C-3 and 10–15% of residues that are triply linked at C-1, C-3 and C-6. By subtracting the 15–20% glucose excess from this β-(1,3,6)-linked glucose units that is apparently cleaved by the β-glucosidase, the linear β-(1,6)-glucan content dropped to a proportion of 18–20% of total cell wall β-glucan, in agreement with data reported by Magnelli et al. (2002). As a conclusion, we could consider that our enzymatic method provides an overall quantification of the highly branched β-(1,6)-glucan that include β-(1,6)-linked glucose units and other glucose units linked at C1, C3 and C6 on the β-glucan backbone.

Using this novel method, we confirmed the huge rise of chitin levels in yeast mutants defective in the synthesis of β-(1,3)-glucan (*fks1*Δ), β-(1,6)-glucan (*kre6*Δ) and mannans (*mnn9*Δ) (Dallies et al., 1998), as well as in *gas1*Δ which lacks a major glucanosyltransferase that plays an important role in cell wall remodelling (Popolo & Vai, 1999; Carotti et al., 2004; Plotnikova et al., 2006). More interestingly, this method has highlighted significant changes in the relative proportion of β-(1,3) and β-(1,6)-glucan in these different mutants as well as in response to stresses. As expected, a mutant deleted for *KRE6* encoding a protein needed in β-(1,6)-glucan synthesis (Roemer & Bussey, 1991; Kurita et al., 2011) has a low level of β-(1,6)-glucan, which supports the validation of our enzymatic method. However, in response to other mutations, as well to heat shock and treatment with caspofungin, we noticed a significant reduction in the β-(1,3)-glucan content, whereas levels of the 'highly branched' β-(1,6)-glucan increased, with a concurrent increase of chitin. Taking into account that expression of genes encoding cell wall remodelling enzymes such as Crh1, Crh2, Cwp1, Gas1 and Bgl2 are strongly upregu-lated under these conditions (Lagorce et al., 2003; Rein-oso-Martin et al., 2003; Rodriguez-Pena et al., 2010), this increased level of β-(1,6)-glucan is in accordance with an amplified cross-linkages between this polymer and chitin and between β-(1,6)-glucan and β-(1,3)-glucan (Kollar et al., 1995, 1997), in response to the cell wall compensatory mechanism that is triggered under these conditions (Klis et al., 2006; Lesage & Bussey, 2006; Orlean, 2012).

Acknowledgements

We thank Henri Durand, Mathieu Castex, Nathalie Sieczkowski and Anne Ortiz-Julien from Lallemand SAS for critical discussions during this work. We thank Carole Bannelier from INRA of Toulouse (UMR 1289 TANDEM) for the nitrogen measurement. This work was supported in part by a grant no. 10051296 from Region Midi Pyrenees to J.M.F. and an ANR Young Scientist project ANR-11-JSV5-001-01, no. (SD) 30 02 43 31 to E.D. E.D. is researcher at the Centre National de la Recherche Scientifique (CNRS). M.S. and C.F. are respectively supported by a grant from Lallemand SAS (Cifre fellowship) and from 'Direction Generale de l'Armement' (DGA). The authors declare no commercial and financial conflict of interest.

References

Aguilar-Uscanga B & Francois JM (2003) A study of the yeast cell wall composition and structure in response to growth conditions and mode of cultivation. Lett Appl Microbiol 37: 268–274.

Aimanianda V, Clavaud C, Simenel C, Fontaine T, Delepierre M & Latge JP (2009) Cell wall beta-(1,6)-glucan of Saccharomyces cerevisiae: structural characterization and in situ synthesis. J Biol Chem 284: 13401–13412.

Blanco N, Reidy M, Arroyo J & Cabib E (2012) Crosslinks in the cell wall of budding yeast control morphogenesis at the mother-bud neck. J Cell Sci 125: 5781–5789.

Bom IJ, Dielbandhoesing SK, Harvey KN, Oomes SJ, Klis FM & Brul S (1998) A new tool for studying the molecular architecture of the fungal cell wall: one-step purification of recombinant trichoderma beta-(1-6)- glucanase expressed in Pichia pastoris. Biochim Biophys Acta 1425: 419–424.

Brown GD & Gordon S (2003) Fungal beta-glucan and mammalian immunity. Immunity 19: 311–315. Brown JL, Kossaczka Z, Jiang B & Bussey H (1993) A mutational analysis of killer toxin resistance in Saccharomyces cerevisiae identifies new genes involved in cell wall (1?6)-beta- glucan synthesis. Genetics 133: 837–849.

Cabib E (2009) Two novel techniques for determination of polysaccharide cross-links show that Crh1p and Crh2p attach chitin to both beta(1-6)- and beta(1-3)glucan in the Saccharomyces cerevisiae cell wall. Eukaryot Cell 8: 1626– 1636.

Cabib E & Arroyo J (2013) How carbohydrates sculpt cells: chemical control of morphogenesis in the yeast cell wall. Nat Rev Microbiol 11: 648–655.

Cabib E & Sburlati A (1988) Enzymatic determination of chitin. Methods Enzymol, 161: 457–459.

Cabib E, Blanco N, Grau C, Rodriguez-Pena JM & Arroyo J (2007) Crh1p and Crh2p are required for the cross-linking of chitin to beta(1-6)glucan in the Saccharomyces cerevisiae cell wall. Mol Microbiol 63: 921–935.

Carotti C, Ragni E, Palomares O, Fontaine T, Tedeschi G, Rodriguez R, Latge JP, Vai M & Popolo L (2004) Characterization of recombinant forms of the yeast Gas1 protein and identification of residues essential for glucanosyltransferase activity and folding. Eur J Biochem 271: 3635–3645.

Catley BJ (1988) Isolation and analysis of cell walls. Yeast, A Pratical Approach (Campbell D & Duffus JH, eds), pp. 163–184. IRL Press, Washington, DC.

Chen J & Seviour R (2007) Medicinal importance of fungal beta-(1?3), (1?6)-glucan. Mycol Res 111: 635– 652.

Costa-de-Oliveira S, Silva AP, Miranda IM, Salvador A, Azevedo MM, Munro CA, Rodrigues AG & Pina-Vaz C (2013) Determination of chitin content in fungal cell wall: an alternative flow cytometric method. Cytometry A 83: 324–328.

Cot M, Loret MO, Francois J & Benbadis L (2007) Physiological behaviour of Saccharomyces cerevisiae in aerated fed-batch fermentation for high level production of bioethanol. FEMS Yeast Res 7: 22–32.

Dallies N, Francois J & Paquet V (1998) A new method for quantitative determination of polysaccharides in the yeast cell wall. Application to the cell wall defective mutants of Saccharomyces cerevisiae. Yeast 14: 1297–1306.

De Ruiter GA, Schols HA, Voragen AG & Rombouts FM (1992) Carbohydrate analysis of water-soluble uronic acid-containing polysaccharides with high-performance anion-exchange chromatography using methanolysis combined with TFA hydrolysis is superior to four other methods. Anal Biochem 207: 176–185.

Deresinski SC & Stevens DA (2003) Caspofungin. Clin Infect Dis 36: 1445–1457.

Dupin IV, Stockdale VJ, Williams PJ, Jones GP, Markides AJ & Waters EJ (2000) Saccharomyces cerevisiae mannoproteins that protect wine from protein haze: evaluation of extraction methods and immunolocalization. J Agric Food Chem 48: 1086–1095.

Eng WK, Faucette L, McLaughlin MM, Cafferkey R, Koltin Y, Morris RA, Young PR, Johnson RK & Livi GP (1994) The yeast FKS1 gene encodes a novel membrane protein, mutations in which confer FK506 and cyclosporin A hypersensitivity and calcineurin- dependent growth. Gene 151: 61–71.

Fleet GH (1991) Cell walls. The Yeast (Rose AH & Harrison JS, eds), pp. 199–277. Academic Press, New York.

Fleet GH & Manners DJ (1976) Isolation and composition of an alkali-soluble glucan from the cell walls of Saccharomyces cerevisiae. J Gen Microbiol 94: 180–192.

Fleet GH & Manners DJ (1977) The enzymic degradation of an alkali-soluble glucan from the cell walls of Saccharomyces cerevisiae. J Gen Microbiol 98: 315–327.

Folch J, Lees M & Sloane-Stanley GH (1957) A simple method for the isolation and purification of total lipids from animal tissues. J Biol Chem 226: 509–511.

Formosa C, Schiavone M, Martin-Yken H, Francois JM, Duval RE & Dague E (2013) Nanoscale effects of caspofungin against two yeast species, Saccharomyces cerevisiae and Candida albicans. Antimicrob Agents Chemother 57: 3498–3506.

Free SJ (2013) Fungal cell wall organization and biosynthesis. Adv Genet 81: 33–82.

Freidmund S, Janett S, Arrigoni E & Amado R (2005) Optimised quantification for yeast-derived 1,3-b-D-glucan. Eur Food Res Technol 220: 101–105.

Ha CH, Lim KH, Kim YT, Lim ST, Kim CW & Chang HI (2002) Analysis of alkali-soluble glucan produced by Saccharomyces cerevisiae wild-type and mutants. Appl Microbiol Biotechnol 58: 370–377.

Hoch HC, Galvani CD, Szarowski DH & Turner JN (2005) Two new fluorescent dyes applicable for visualization of fungal cell walls. Mycologia 97: 580–588.

Hong Z, Mann P, Shaw KJ & Didomenico B (1994) Analysis of b-glucan and chitin in Saccharomyces cerevisiae cell wal

mutant using high-performance liquid chromatography. Yeast 10: 1083–1092.

Jungmann J & Munro S (1998) Multi-protein complexes in the cis Golgi of Saccharomyces cerevisiae with alpha-1,6-mannosyltransferase activity. EMBO J 17: 423–434.

Klis FM, Boorsma A & de Groot PW (2006) Cell wall construction in Saccharomyces cerevisiae. Yeast 23: 185–202.

Klis FM, Sosinska GJ, de Groot PW & Brul S (2009) Covalently linked cell wall proteins of Candida albicans and their role in fitness and virulence. FEMS Yeast Res 9: 1013–1028.

Kollar R, Petrakova E, Ashwell G, Robbins PW & Cabib E (1995) Architecture of the yeast cell wall. The linkage between chitin and beta(1?3)-glucan. J Biol Chem 270: 1170–1178.

Kollar R, Reinhold BB, Petrakova E, Yeh HJ, Ashwell G, Drgonova J, Kapteyn JC, Klis FM & Cabib E (1997) Architecture of the yeast cell wall. Beta(1?6)-glucan interconnects mannoprotein, beta(1?)3-glucan, and chitin. J Biol Chem 272: 17762–17775.

Kopecka M & Gabriel M (1992) The influence of congo red on the cell wall and (1-3)-beta-D-glucan microfibril biogenesis in Saccharomyces cerevisiae. Arch Microbiol 158: 115–126.

Kurita T, Noda Y, Takagi T, Osumi M & Yoda K (2011) Kre6 protein essential for yeast cell wall beta-1,6-glucan synthesis accumulates at sites of polarized growth. J Biol Chem 286: 7429–7438.

Lagorce A, Hauser NC, Labourdette D, Rodriguez C, Martin-Yken H, Arroyo J, Hoheisel JD & Francois J (2003) Genome-wide analysis of the response to cell wall mutations in the yeast Saccharomyces cerevisiae. J Biol Chem 278: 20345–20357.

Lesage G & Bussey H (2006) Cell wall assembly in Saccharomyces cerevisiae. Microbiol Mol Biol Rev 70: 317– 343.

Levin DE (2005) Cell wall integrity signaling in Saccharomyces cerevisiae. Microbiol Mol Biol Rev 69: 262–291.

Levin DE (2011) Regulation of cell wall biogenesis in Saccharomyces cerevisiae: the cell wall integrity signaling pathway. Genetics 189: 1145–1175.

Lora JM, de la Cruz J, Llobell A, Benitez T & Pintor-Toro JA (1995) Molecular characterization and heterologous expression of an endo-beta- 1,6-glucanase gene from the mycoparasitic fungus Trichoderma harzianum. Mol Gen Genet 247: 639–645.

Magnelli P, Cipollo JF & Abeijon C (2002) A refined method for the determination of Saccharomyces cerevisiae cell wall composition and beta-1,6-glucan fine structure. Anal Biochem 301: 136–150.

Manners DJ, Masson AJ & Patterson JC (1973a) The structure of a beta-(1 leads to 3)-D-glucan from yeast cell walls. Biochem J 135: 19–30.

Manners DJ, Masson AJ, Patterson JC, Bjorndal H & Lindberg B (1973b) The structure of a beta-(1–6)-D-glucan from yeast cell walls. Biochem J 135: 31–36.

Mazur P, Morin N, Baginsky W, el Sherbeini M, Clemas JA, Nielsen JB & Foor F (1995) Differential expression and function of two homologous subunits of yeast 1,3-beta-D-glucan synthase. Mol Cell Biol 15: 5671–5681.

Miller L & Houghton AL (1945) The micro-Kjeldahl determination of the nitrogen content of amino acids and proteins. J Biol Chem 159: 373–383.

Molano J, Duran A & Cabib E (1977) A rapid and sensitive assay for chitinase using tritiated chitin. Anal Biochem 83: 648–656.

Mouyna I, Fontaine T, Vai M, Monod M, Fonzi WA, Diaquin M, Popolo L, Hartland RP & Latge JP (2000) Glycosylphosphatidylinositol-anchored glucanosyltransferases play an active role in the biosynthesis of the fungal cell wall. J Biol Chem 275: 14882–14889.

Nguyen TH, Fleet GH & Rogers PL (1998) Composition of the cell walls of several yeast species. Appl Microbiol Biotechnol 50: 206–212.

Orlean P (2012) Architecture and biosynthesis of the Saccharomyces cerevisiae cell wall. Genetics 192: 775– 818.

Ovalle R, Lim ST, Holder B, Jue CK, Moore CW & Lipke PN (1998) A spheroplast rate assay for determination of cell wall integrity in yeast. Yeast 14: 1159–1166.

Pillet F, Lemonier S, Schiavone M, Formosa C, Martin-Yken H, Francois JM & Dague E (2014) Uncovering by atomic force microscopy of an original circular structure at the yeast cell surface in response to heat shock. BMC Biol 12: 6.

Plotnikova TA, Selyakh IO, Kalebina TS & Kulaev IS (2006) Bgl2p and Gas1p are the major glucan transferases forming the molecular ensemble of yeast cell wall. Dokl Biochem Biophys 409: 244–247.

Popolo L & Vai M (1999) The Gas1 glycoprotein, a putative wall polymer cross-linker. Biochim Biophys Acta 1426: 385– 400.

Popolo L, Gilardelli D, Bonfante P & Vai M (1997) Increase in chitin as an essential response to defects in assembly of cell wall polymers in the ggp1delta mutant of Saccharomyces cerevisiae. J Bacteriol 179: 463–469.

Popolo L, Gualtieri T & Ragni E (2001) The yeast cell-wall salvage pathway. Med Mycol 39: 111–121.

Ram A, Wolters A, ten Hoopen T & Klis FM (1994) A new approach for isolating cell wall mutants in Saccharomyces cerevisiae by screening for hypersensitivity to Calcofluor white. Yeast 8: 1030.

Reinoso-Martin C, Schuller C, Schuetzer-Muehlbauer M & Kuchler K (2003) The yeast protein kinase C cell integrity pathway mediates tolerance to the antifungal drug caspofungin through activation of Slt2p mitogen-activated protein kinase signaling. Eukaryot Cell 2: 1200–1210.

Reissig JL, Storminger JL & Leloir LF (1955) A modified colorimetric method for the estimation of N-acetylamino sugars. J Biol Chem 217: 959–966.

Rodriguez-Pena JM, Garcia R, Nombela C & Arroyo J (2010) The high-osmolarity glycerol (HOG) and cell wall integrity (CWI) signalling pathways interplay: a yeast dialogue between MAPK routes. Yeast 27: 495–502.

Roemer T & Bussey H (1991) Yeast beta-glucan synthesis: KRE6 encodes a predicted type II membrane protein required for glucan synthesis in vivo and for glucan synthase activity in vitro. P Natl Acad Sci USA 88: 11295–11299.

Roncero C, Valdivieso MH, Ribas JC & Duran A (1988) Isolation and characterization of Saccharomyces cerevisiae mutants resistant to Calcofluor white. J Bacteriol 170: 1950–1954.

Sietsma JH & Wessels JG (1990) The occurrence of glucosaminoglycan in the wall of Schizosaccharomyces pombe. J Gen Microbiol 136: 2261–2265.

Wach A (1996) PCR-synthesis of marker cassettes with long flanking homology regions for gene disruptions in S. cerevisiae. Yeast 12: 259–265.

Yiannikouris A, Andre G, Buleon A, Jeminet G, Canet I, Francois J, Bertin G & Jouany JP (2004) Comprehensive conformational study of key interactions involved in zearalenone complexation with beta-D-glucan. Biomacromolecules 5: 2176–2185

Supporting Information

Additional Supporting Information may be found in the online version of this article:

Fig. S1. Chromatography profiles resulting from enzymatic hydrolysis of β-(1,3)-glucan.

Fig. S2. Chromatography profiles resulting from enzymatic hydrolysis of β-1,6-glucan.

Fig. S3. Chromatography profiles resulting from enzymatic hydrolysis of chitin.

Fig. S4. Evaluation of lipids contamination in purified yeast cell wall (Folch et al., 1957).

Fig. S5. Schematic diagram of yeast cell wall fractionation and analysis of the alkali-insoluble acid-soluble fraction for the content of β-(1,6)-glucan content by periodate oxidation (fraction C) and by enzymatic hydrolysis with endo β-(1,6)-glucanase and β-glucosidase (fraction A).

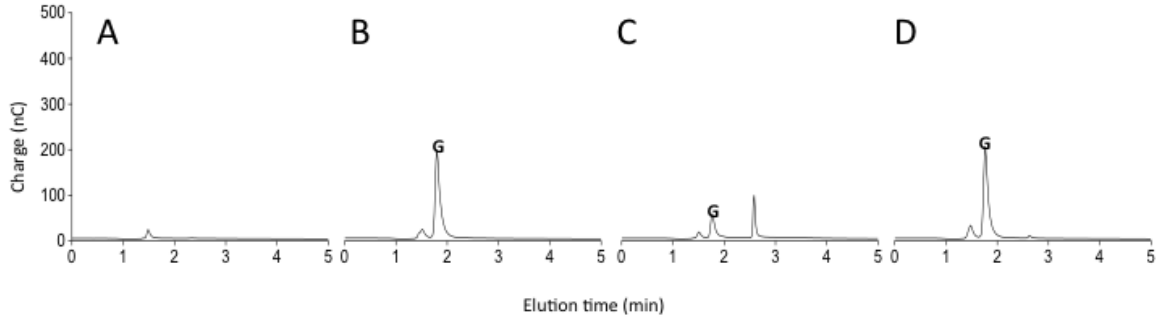

Figure S1 (Schiavone et al., 2014)

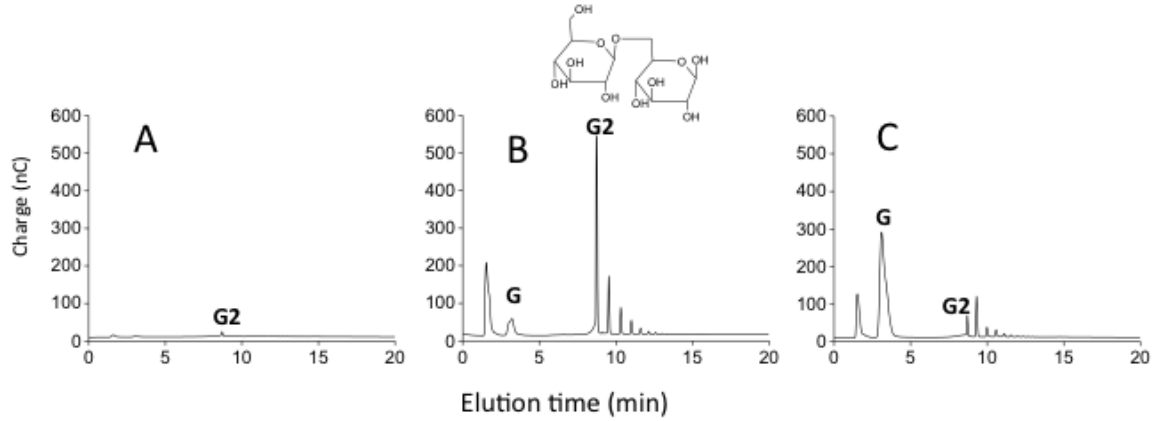

Figure S2 (Schiavone et al., 2014)

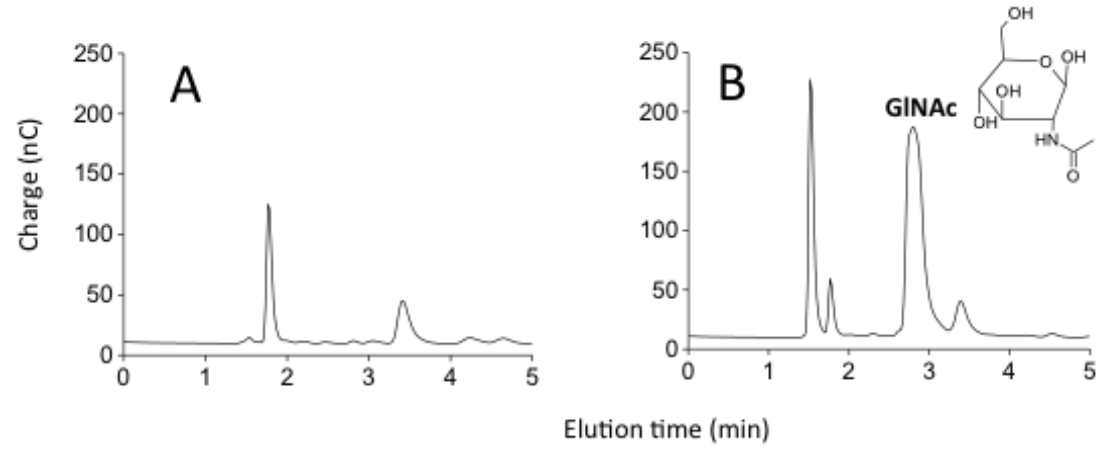

Figure S3 (Schiavone et al., 2014)

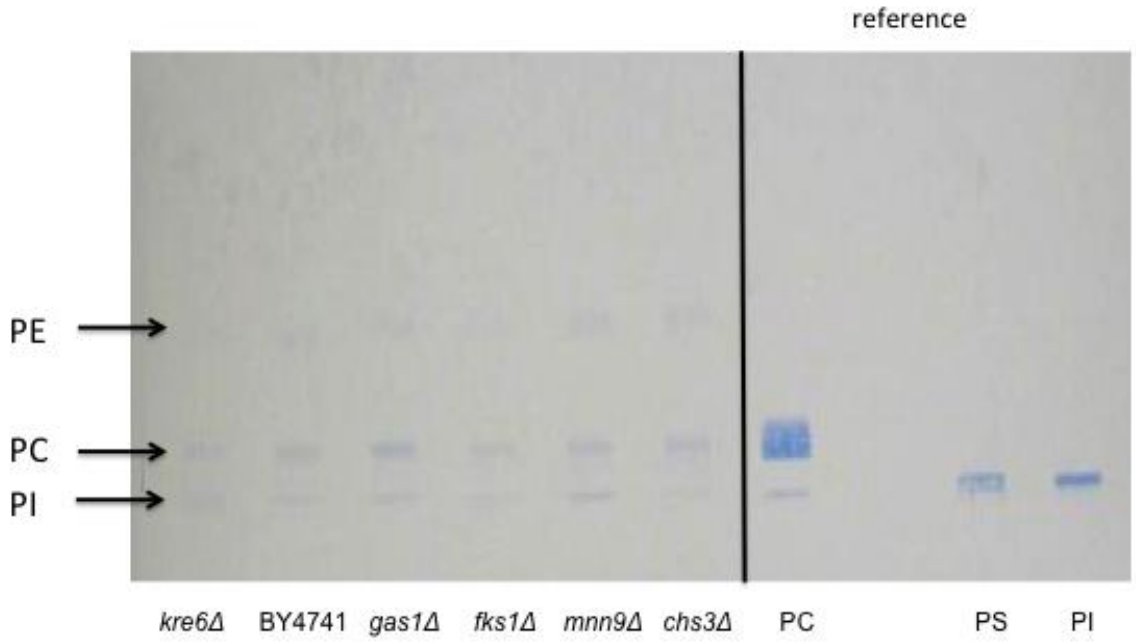

Figure S4 (Schiavone et al., 2014)

Lipids were extracted from 100 mg of purified yeast cell wall according (Folch *et al.* 1957) on a Thin-Layer Chromatograohy (TLC) using chloroform/mehanol/water at (95/20/2.5) (v/v/v) as running solvent. Revelation of phospholipids was made with molybdenum blue. PC, phosphatidylcholine; PS, phopshatidylserine; PI, phosphatidylinositol.

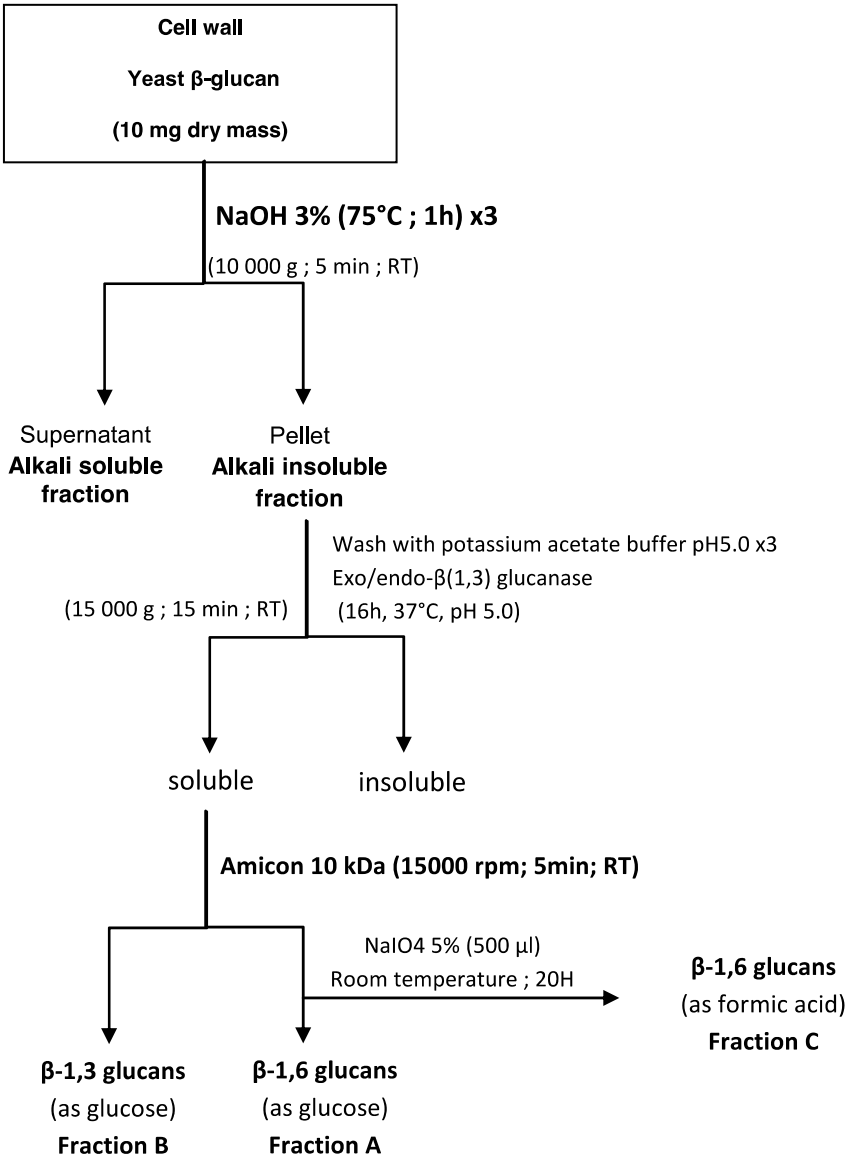

BY4741 Cell wall

Fraction B	Fraction C	After endo-β(1,6) glucanase / β-glucosidase
384.3 ± 10.6	99.0 ± 5.5	125.91 ± 36.1

Control Yeast β-glucan from Megazyme (K-EBHLG)

Fraction B	Fraction C	After endo-β(1,6) glucanase / β-glucosidase
610.8 ± 21.1	111.83 ± 27.37	135.31 ± 28.8

The values are expressed as µg/mg and are the mean ± SD of three independent experiments made in triplicate.

Figure S5 (Schiavone et al., 2014)

Chapter III: EFFECT OF THE STRAIN BACKGROUND ON THE CELL WALL

This chapter deals with the influence of strains on cell wall assembly and composition. For this purpose, we determined the cell wall composition by the new acido-enzymatic method (chapter 2). In addition, the cell surface properties of the yeast strains were assessed by using AFM technology and combined to transcriptomic profiles. These different data on yeast cells were correlated through statistical methods, which allow us to enlight a set of genes implied in cell surface properties and cell wall composition.

Two parts divide this chapter:

A. Study of strains deleted to one gene encoding for cell wall biosynthesis (*gas1Δ, chs3Δ, mnn9Δ*)

Firstly, we aimed at investigate the relationship between cell wall composition, cell biophysical properties and transcriptomic profiles on yeast strains deleted for one gene essential for the cell wall biogenesis.

B. Study of four industrial strains

Secondly, we investigate the strain specificity and cell wall architecture of four industrial strains (L71, L69, L60, L62) provided by Lallemand company.

Chapter IIIA: STUDY OF CELL WALL MUTANTS (*gas1Δ, chs3Δ, mnn9Δ*)

Integration of genomics and biophysical-chemical data to unravel molecular cues that account for structural organization and nanomechanical properties of the yeast cell wall

Marion Schiavone[1, 2, 3, 4, 5]; Sébastien Déjean[1, 6]; Etienne Dague[1, 4], Jean Marie François*[1,2,3]

[1]Université de Toulouse; INSA, UPS, INP, 135 avenue de Rangueil, F-31077 Toulouse, France

[2]INRA, UMR792 Ingénierie des Systèmes Biologiques et des Procédés, F-31077 Toulouse, France ;

[3]CNRS, UMR5504, F-31400 Toulouse, France 135 avenue de Rangueil, F-31077 Toulouse, France ;

[4]CNRS; LAAS ; 7 avenue du colonel Roche, F-31400 Toulouse, France ;

[5]Lallemand SAS, 19 rue des briquetiers, 31702 Blagnac, France

[6]Institut de Mathématiques de Toulouse, 118 route de Narbonne, F-31062 Toulouse, France

*Correspondance to Jean Marie François; LISBP INSA, 135 Avenue de Rangeuil, F-31077 Toulouse cedex 04 ; Email: fran_jm@insa-toulouse.fr; Phone: +33(0) 5 61 55 94 92

Keywords: Cell wall, atomic force microscopy, genome, architecture, yeast, biostatistics

ABSTRACT

The cell wall is a dynamic structure that confers resistance to the cell against environmental changes by adapting the cell wall composition and by changing its nanomechanical properties. However, how the molecular architecture of the cell wall is related to its biochemical composition and account for its nanomechanical properties is a challenging open question. As a first step towards this goal, we used a set of well-characterized cell wall mutants from which transcriptomic data were available, and then measured their cell wall composition and obtained quantitative data on cell elasticity, cell surface adhesion and interaction of concanavalin A with mannoproteins using atomic force microscopy (AFM). We subsequently combined the datasets through their ratio against the wild-type strain and performed a comparative analysis. We made different observations. First, single molecule force spectroscopy experiments showed the impact of mutation in the deployment through the mannoproteins using AFM tips functionalized with concanavalin A. Long chains of polysaccharides were unfolded with concanavalin A tips on the surface of *gas1*Δ mutant cell, while on *mnn9*Δ cell a small percentage of specific interaction mannan-lectin were observed with shorter rupture lengths (below 100 nm). Second, we confirmed our integrative approach by finding an association between the levels of mannan and frequency events in lectin-cell surface interactions. Thirdly, we showed that cell wall elasticity values correlated with β-1,3-glucan although cross-linkages between cell wall component is likely determining the quantitative value of this nanomechanical properties. Finally, genes found to be associated to physico-biochemical variables were distinct to those previously identified as implicated in the cell wall remodeling mechanism.

I. INTRODUCTION

The cell wall of *Saccharomyces cerevisiae* is a complex interplay of four polysaccharides that are cross-linked to provide integrity to the cell. These polysaccharides are β-1,3 and β-1,6-glucan which are formed by glucosyl units attached either in β-1,3 or β-1,6-linkages. They represent around 50-60% of total cell wall polysaccharides. The second polysaccharide in abundance (around 40-50%) is mannoproteins that are composed of linear chains of α-1,6-mannosyl units with α-1,4; α-1,6; α-1,2; α-1,3 branches and are attached to proteins through either an asparagine (N-glycosylation) or serine/threonine (O-glycosylation) residue. The fourth component is chitin which is a linear polymer of 100-150 units of β-1,4-N-acetylglucosaminyl residues. Chitin is indispensable for yeast cells in spite of its low abundance (1 to 4 % of the total cell wall polysaccharide), likely because of its key role in

septation that takes place during budding (Cabib and Arroyo, 2013; Shaw et al., 1991). According to electronic microscopy observations (Osumi, 1998), the yeast cell wall presents an amorphous and colorless internal layer of about 70-100 nm thick that is composed of a complex network of chitin, β-1,3 and β-1,6-glucan (Klis et al., 2002). The outer layer is condensed and mainly composed of cell wall mannoproteins (CWP) anchored to β-glucan.

The cell wall is a dynamic structure that is remodeled in order to avoid cell lysis and eventually cell death. Modification of the cell wall appears during cell growth and morphogenesis, but also in response to environmental stress or various injuries caused by drugs, lytic enzymes or mutations in genes implicated in its synthesis. Genetic analyses led to the finding that the MAPkinase cascade dependent on PKC1 is the main signaling pathway that controls this cell wall remodeling (Levin, 2004; Lesage & Bussey, 2006). In addition, genome wide transcriptomic analysis of this cell wall remodeling caused by mutations in genes specifically implicated in synthesis of cell wall component or by cell wall perturbing agents led to the identification of a 'core of about 50 upregulated genes' that are considered to be critically important in this cellular response (Bermejo et al., 2010; Garcia et al., 2004; Lagorce, 2003). Among them were identified several genes encoding glycosyltransferase/hydrolase, that were called 'cell wall remodeling enzymes'. These changes at the transcriptional level can be associated with biochemical modifications that take place in response to cell wall remodeling and which are: (i) an increase of chitin amount in cell wall which can contribute up to 20% of the cell wall when important genes encoding for its biosynthesis are deleted (Popolo et al., 1997); (ii) a modification of linkages between cell wall components and (iii) an increase of cell wall remodeling enzymes accompanied with a redistribution of cell wall synthesis and repair machinery. Yeast cell wall is also endowed with biomechanical properties that can nowadays address using Atomic Force Microscopy, invented by Gruber and colleagues at IBM Zurich (Binnig et al., 1986). Initially developed in Material Sciences, this technology has evolved to be able to operate in liquid using life cells in their natural environment (Dufrene 2001;Dague et al. 2007). A seminal work illustrating cell wall mechanical properties was reported by Pelling *et al.* (Pelling et al., 2004). These authors reported nanomechanical motions of the *S. cerevisiae* cell wall with a periodicity in the range of 0.8 to 1.6 kHz and amplitudes of approximately 3 nm, which were of biological origin and could implicate the yeast actin cytoskeleton. More recently, we carried out AFM nano-indentation experiments on yeast mutants deleted in specific genes implicated in synthesis of cell wall component (i.e. *CHS3*, for chitin; *FKS1*, for β-1, 3 glucan, *MNN9*, for

mannans; *KRE6* for β-1,6 glucan) or cell wall remodeling enzymes (*GAS1, CRH1/CRH2*). In this study, we showed that the elasticity properties of the cell wall was not dependent on a specific cell wall component, which was at variance of the established consideration that β-glucan layers were responsible for the 'rigidity' of the cell wall (Fleet 1991;Klis et al. 2006). Other biophysical properties can be addressed using single molecule force spectroscopy (SMFS). This technique consists to probe the cell surface with either chemically modified or functionalized tips with a given biomolecule that has a specific interaction with a component exposed at the cell surface, such as concanavalin-A for mannoproteins (Alsteens et al. 2008). With this approach, valuable qualitative and quantitative data on adhesion properties, physical organization of the cell surface as well as identification of clusters of cell surface protein can be obtained (Alsteens et al., 2010; Formosa et al., 2014).

Giving these different approaches that deliver apparent independent but complementary data which contribute to identify the mechanisms of cell wall biogenesis and remodeling, we could argue that using appropriate biomathematical tools developed under the mixOmics package (Lê Cao et al., 2009) that permits to create correlation matrixes between biological data obtained at different hierarchical levels such as metabolomics/transcriptomics data (Guo et al., 2014) we should be able to find out molecular cues (genes or proteins) that account for the biomechanical properties of the cell wall, as well as which and how the different cell wall component contribute to cell wall nanomechanical property. As a first step towards this goal, we used a set of well-characterized cell wall mutants from which transcriptomic data were available (Lagorce et al), measured cell wall composition in these mutants using our recent chemical-enzymatic method (Schiavone et al., 2014) and obtained quantitative data on cell elasticity, cell surface adhesion and interaction with mannoproteins using atomic force microscopy (AFM). This integrative approach allows highlighting some unexpected associations between ratio of β-glucan/mannan with elasticity, whereas events of adhesion were mainly related to mannans, and genes found to be associated to these physico-biochemical variables were distinct to those previously identified as implicated in cell wall remodeling mechanism.

II. MATERIAL AND METHODS

Yeast strains

The strains used in this work are listed below.

Table IIIA-1: Yeast strains used in this work; their genotype and origin

Strain	Genotype	Origin
BY4741	MAT**a** *his3Δ1; leu2Δ0 ; met15Δ0 ura3Δ0*	EUROSCARF
***chs3*Δ**	BY4741 *chs3::KanMX4*	Open Biosystem
***gas1*Δ**	BY4741 *gas1::KanMX4*	Open Biosystem
***mnn9*Δ**	BY4741 *mnn9::KanMX4*	Open Biosystem

Cell wall isolation and quantification of polysaccharides

Yeast cells are cultivated in rich media (YPD; 2% glucose, 1% peptone, 1% yeast extract) and collected during the exponential phase until $2x10^7$ cells (OD_{600}=1). Then, cells were collected at the exponential phase harvested by centrifugation (5 min, 4500 g, 4°C) and washed two times with sterilized water. Yeast cell walls were isolated and purified as described in (Francois, 2006). Cells were disrupted by 15 - 20 cycles of 20 seconds at maximal speed using a Fastprep system (MP Biomedicals) until at least 95% of cells were broken. Cell wall polysaccharides mannan, chitin, β-1,3- and β-1,6-glucan in the purified cell walls were determined by a method, combining acid and enzymatic hydrolysis, developed by (Schiavone et al., 2014). Quantification of the released monomers (mannose, glucose and N-acetylglucosamine) was determined by HPAEC coupled to amperometric detection as described by (Dallies et al., 1998) and Reissig's method, respectively.

AFM measurements

Sample preparation

Strains were stocked at -80°C, revivified on Yeast Peptone Dextrose agar (242720530, Difco) and grown in 5 mL of Yeast Peptone Dextrose broth (242820530, Difco) at 30°C under shaking. Yeasts cells were collected at the exponential phase (OD600~1), washed two times in acetate buffer (18 mM CH_3COONa, 1 mM $CaCl_2$, 1 mM $MnCl_2$, pH 5.2), resuspended in the same buffer, and immobilized on polydimethylsiloxane (PDMS) stamps prepared as described in (Dague et al., 2011). Briefly, freshly oxygen activated microstructured PDMS stamps were covered by a total of 100 µL of the solution of cells. The cells were then deposited into the microstructures of the stamp by convective/capillary assembly.

AFM imaging and force spectroscopy

Images and force-distance curves were recorded at room temperature in acetate buffer (18 mM, pH 5.2) using an AFM Nanowizard III (JPK Instruments, Berlin, Germany) and MLCT AUWH cantilevers

(Bruker, Santa Barbara, USA). The spring constants of the cantilevers were systematically measured by the thermal noise method (Hutter and Bechhoefer, 1993) and were found to be in the range of 0.01-0.02 $N.m^{-1}$.

Images were recorded in Quantitative Imaging™ mode (Chopinet et al., 2013) and the maximal force applied to the cell was limited to 1.5 nN.

Mechanical properties were mapped by recording an array of 32 x 32 force-distance curves using a maximal applied force of 0.5 nN. Elasticity histograms were generated by analyzing the force (F) curves according to the Hertz model with an indentation (δ) of 50 nm and taking into account a conical tip geometry with an half-opening angle α of 0.31 rad and a Poisson ratio (v) of 0.5:

$$F = \frac{2E \tan \alpha}{\pi (1 - \nu^2)} . \delta^2$$

The value of the Young modulus (E) is determined as the maximal value of the histogram.

For probing cell surface polysaccharides, AFM tips were functionalized with the lectin concanavalin A from Canavalia ensiformis (Sigma-Aldrich) via a dendritip as described in (Jauvert et al., 2012). The coupling with the lectin was made by immersion of the dendritip in 100 µL of concanavalin A solution (100 $\mu g.mL^{-1}$ in 0.1 M carbonate buffer). After 1 hr of incubation, 100 µL of $NaBH_4$ 3.5 $mg.mL^{-1}$ solution was added and incubated 15 min in order to reduce the unreacted groups. Finally, the cantilever was washed three times and stored in acetate buffer. To analyze the stretching of polysaccharides at the surface of the cell, elongation forces were described using the freely jointed chain (FJC) model or the worm like chain (WLC) model (Janshoff et al., 2000).

The FJC model described the polymer as a suit of segments (called 'Kuhn segments') with the same energy and a random orientation: $x(F) = L_c[\coth(Fl_k/k_bT) - k_bT/Fl_k]$

Where F is the extension force (N), x is the extension of polymer (m), k_b is the Boltzmann constant and T the absolute temperature. l_k is the Kuhn length, which represents a length of one segment (m) and L_c (m) is the contour length which is the total length of polymer stretched. For n segments: $L_c = nl_k$.

The WLC model introduced by (Bustamante et al., 1994) which describes the polymer as a curved filament and the force F vs the extension x is given by: $F(x) = k_bT/l_p [0.25 (1-x/L_c)^{-2} + x/L_c - 0.25]$

Where L_c is the contour length, l_p is the persistent length, k_b is the Boltzmann constant, T the absolute temperature. This model has already been successfully used for the stretching of polysaccharides of yeasts especially *S. cerevisiae* and give the best fitting of force curves (Alsteens et al., 2008; Francius

et al., 2009). Blocking control experiments were performed by injecting 100 mM D-mannose (Sigma-Aldrich) solution into the cell surface.

Data collection and methods for association or correlations

The transcriptomic data of the mutant strains *gas1*Δ and *mnn9*Δ were obtained from a previous transcriptomic analysis (Lagorce et al. 2003). Triplicates transcriptomic analysis of each mutant were retrieved and expressed as the fold change between mutant and wild-type (differentially expressed genes data set in Tables IIIA.S1-S4). The biophysical data that corresponded to Young modulus (E), % of adhesion events, adhesion force, maximum of rupture distance, contour length and biochemical data that corresponded to β-1,3 glucan, β-1,6-glucan, total β-glucan, mannan, chitin, ratio β-glucan/mannan were also collected, their median value calculated and then expressed as ratio value between mutant/wild-type (Tables IIIA.S5 and S6). Genes were considered to be induced or repressed if the ratio changed by at least a factor two. Association/correlation between the genes data sets (12 lines) and combined the biophysical and biochemical data sets (11 columns) were determined using the mixOmics package with R software (http://www.math.univ-toulouse.fr/~biostat/mixOmics/). Canonical correlation analysis (CCA) and partial least square (sparse-PLS) regression were performed in order to measure associations among the set of variables. These two multidimensional methods are used for an exploratory analysis and are based on the same principle of principal component analysis (PCA) in order to research high correlation (covariance) between variables. Functional classification of genes was carried using Funspec database (http://funspec.med.utoronto.ca/) with a p-value cut-off of 0.01 and a Bonferroni correction.

III. RESULTS AND DISCUSSION

Reexamination of the biochemical composition of cell wall in mutants defective in cell wall-related genes

As shown in table IIIA-2, a defect in protein mannosylation (mnn9Δ mutant) induces a two-fold decrease of the mannan content whereas this mutation have no effect on β-1,3-glucan levels, in accordance to an earlier work Pagé et al., 2003). Previous investigations from Ballou *et al.* (Ballou et al., 1990) found that the major oligosaccharide obtained from this mutant was $Man_{13}GlcNAc$, which correspond to a core structure of α-1,6-linked mannan units with side chains of α-1,2 and α-1,3-mannan residues and a N-acetylglucosamine (GlcNAc) unit attached at the reducing end of the α-

mannosyl chain by a β-1,4-linkage. The decrease of mannan level was accompanied by a two-fold increase of chitin. Likewise, there was a significant increase of chitin in *gas1*Δ mutant in which level of β-1,3-glucan significantly decreased, whereas content of β-1,6-glucan was only slightly affected by deletion of *GAS1*. This results is thus consistent with the fact that *GAS1* encodes a glucanosyltransferase that is implicated in the elongation of the β-1,3-glucan (Mouyna, 2000; Plotnikova et al., 2006) and thus likely does not alter the β-1,6-glucan process. As expected a defect of chitin synthase 3 that is responsible for the major synthase activity of chitin in vegetative cells lead to a 10-fold decrease of this component, which was accompanied by a slight increase of mannan (Table IIIA-2).

Table IIIA-2. Cell wall composition (expressed in µg/mg of purified cell wall) and determination of Young Modulus values (E) of mutants defective in cell wall-related genes and its isogenic wild-type

Strain	Function properties	E (kPa)	chitin	β-1,3 glucan	β-1,6 glucan	mannan
BY4741	wild-type	483 ± 61	39.5 ± 6.9	307.0 ± 50.7	153.3 ± 4.3	304.2 ± 36.5
gas1Δ	β-1,3-glucanosyl-transferase	345 ± 71	156.3 ± 0.9	189.6 ± 25	174.1 ± 54.5	367.7 ± 18.2
chs3Δ	Chitin synthase III	189 ± 83	3.6 ± 0.5	256.3 ± 34.6	120.5 ± 34.1	343.3 ± 32.8
mnn9Δ	Mannosyltransferase	866 ± 92	61.7 ± 1.7	299.4 ± 20.7	123.2 ± 1.3	170.2 ± 58.0

These biochemical analyses of the cell wall in response to these specific mutations in cell wall related genes complemented previous reports (Dallies et al., 1998; Magnelli et al., 2002). They confirmed that yeast cell wall is subjected to cell wall remodeling characterized by a significant change in chitin levels and by a partial compensation of the one component (*i.e.* mannan or β-glucan).

AFM investigation of cell wall defective mutants

The biophysical properties of the three mutants were investigated by atomic force microscopy in order to complement our previous study (Dague et al., 2010). Cells were firstly imaged by AFM using Quantitative Imaging mode (Fig. IIIA-1). AFM height images of *gas1*Δ, *chs3*Δ and *mnn9*Δ mutants show characteristic phenotypes; cells become larger and are abnormally round as compared to the oblong shape of the corresponding isogenic wild-type (Fig. IIIA-1a). To gain insights on the organization of the yeast cell wall, we performed nano-indentations experiments by AFM to determine the elasticity of the cell wall. As the AFM tip is pushed on the yeast cell, the deformation depth (indentation) can be determined and plotted as a function of the force applied on the cell. The use of

the Hertz Model for each indentation versus force curve (1024 curves per cell) generates a distribution of Young Modulus values. These values gave information on the stiffness of the cell and can be adjusted to a Gaussian law to obtain a mean Young modulus value (E) and standard deviation (Fig.IIIA-1c and Table IIIA-1). Since the stiffness of the yeast cell wall can be impacted by the bud scar that has higher Young modulus than the surrounding surface (Alsteens et al., 2008; Touhami et al., 2003), our measurements were performed on area devoid of bud scars and on several independent cells, to get statistical value on the nanomechanical properties of yeast cells. Our results showed that the Young modulus of exponential cells from *chs3*Δ and *gas1*Δ mutants were about 2-fold lower than wild-type (Fig IIIA-1c), but 1.7-fold higher for *mnn9*Δ cells as compared to wild-type value. The decrease of the elasticity in *gas1*Δ and *chs3*Δ cells was agreed with our previous results (Dague et al., 2010), while in this same report, we found that elasticity was similar between wild-type and *mnn9*Δ mutant. In accordance with our previous statement, we could not rely the change in elasticity properties of the yeast cell with that of a specific component of the cell wall, indicating that this nanomechanical property of the cell must be on the molecular organization of the cell wall.

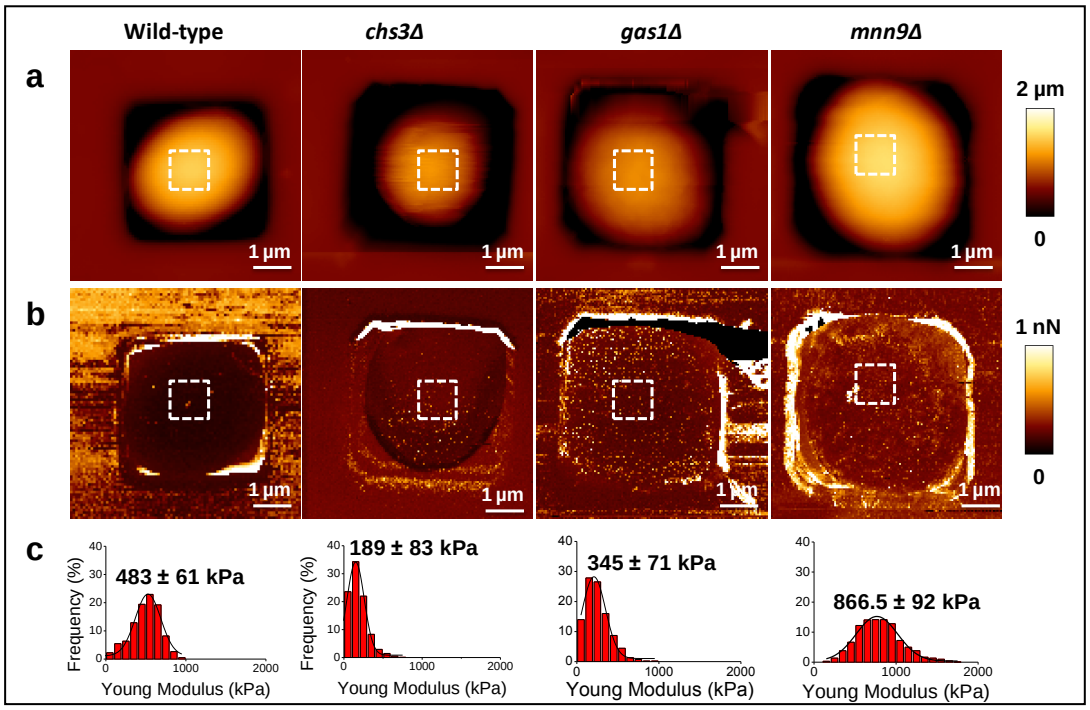

Figure IIIA-1. Nanomechanical properties: elasticity differences.

AFM images of height (a) and adhesion (b) recorded with QI™ mode (JPK Instruments). Distribution of Young Modulus values (c) fitted with a Gaussian law. Wild-type strain (BY4741) and the cell wall-related mutants (*gas1*Δ, *mnn9*Δ and *chs3*Δ) were grown and harvested as described in Materiel and Methods.

Investigation of cell wall architecture by single-molecule force spectroscopy experiments

The outer layer of the yeast cell wall is mainly constituted of mannoproteins associated with the β-glucan layer through β-1,6-glucan chains. These mannoproteins are responsible for most of the cell surface properties and protect the cell from external attacks such as chemical or enzymatic onsets like β-glucanase (Fernandez and Cabib, 1984). To map and unfold polysaccharides at the cell surface, we used AFM tips functionalized with lectin Concanavalin A (ConA). Con A is a plant lectin isolated from the jack bean which has specificity for the α-pyranose forms of D-mannose and D-glucose, but has no affinity for β-linked glucose residues of *S. cerevisiae* cell wall (Sharon and Lis, 2007). Here, we investigated the distribution, adhesion and extension of mannan on the surface of the cell wall-related mutants as compared to the wild-type (Fig. IIIA-2). Adhesion force maps (Fig. IIIA-2 b, g, l and q), adhesion force histograms (Fig. IIIA-2 c, h, m, r) and typical retract force curves (Fig. IIIA-2 d, I, n, s) were recorded between AFM tips functionalized with the lectin and the surface of the wild-type and the three cell-wall related mutants. In the wild-type, the adhesion force histogram had a maximal value centered around 50-60 pN (n=1024), which correspond to a single lectin-mannose interaction (Francius et al., 2009). Adhesion force of 100-200 pN range were attributed to the unfolding of two or three mannose residues (Alsteens et al., 2008). The frequency of adhesion event recorded in the wild-type was around 23 %. In *chs3*Δ mutant, single or double adhesion events with a frequency of 22.5 % were observed with rupture distance in the 0-200 nm range. On the contrary on *gas1*Δ mutant cell, multiple adhesion events were detected with larger adhesion forces and much longer rupture lengths ranging from 20 to 400 nm. These elongation forces were well described with the worm like chain (WLC) model, but not with the freely jointed chain (FJC) model. The WLC model describes a polymer as a filament that is continuously flexible, with successive segments that pointed in the same direction. This model is relevant to describe polymers with high stiffness. In contrast, with the FJC model the polymer can only dismantle at the joints between distinct segments called 'Kuhn segments'. Therefore, the fact that elongation forces were well fitted with a WLC model and not with a FJC model, could indicate that glycoproteins are stretched rather than pure carbohydrates. This result can be explained by the increase of cell wall mannoproteins and the difference in their anchorage into the cell wall in *gas1*Δ as compared to the wild-type. In *S.cerevisiae*, the majority of the cell wall mannoproteins are anchored into the cell wall through covalent linkages to β-1,3 and β-1,6-glucan that are linked to chitin.

However, unlike to wild-type cells in which only 1-2% of covalently bound cell wall proteins were attached to chitin through β-1,6-glucan, in *gas1*Δ mutant where β-1,3-glucan is reduced and chitin is significantly increased, this percentage of cross-links raised to about 40% (Kapteyn et al., 1997). The response of *GAS1* deletion, *i.e.* increase of chitin and cell wall mannoproteins as well as their cross-linkage, results to a weakened and disassembled cell wall but avoid cell lysis. These mechanisms are essential for cell viability. Indeed, the double mutation *gas1*Δ *kre6*Δ, that affects the β-1,6-glucan synthesis, is lethal and a disruption of *CHS3* in *gas1*Δ leads to an important reduction of growth rate and a disorganization of the cell wall structure (Kollar et al., 1997; Popolo et al., 1997). In contrast to the others mutant strains, only 8% of adhesion events were detected on *mnn9*Δ mutant with rupture (or contour) lengths below 100 nm and a mean value of 44.8 ± 7.3 nm. This finding correlates with a disruption of *MNN9* that decreases mannan content attached on the proteins (Table IIIA-1). To validate that the interaction detected between ConA tip and cell surface was due to mannoproteins, we repeated these experiments in the presence of a large excess of D-mannose added to the cell surface before AFM analysis and found that the adhesion frequency was almost completely abolished, and the 5% remaining can be ascribed to some unspecific interaction on the cell surface by the conA tip (Fig. IIIA-S1, in supplementary data).

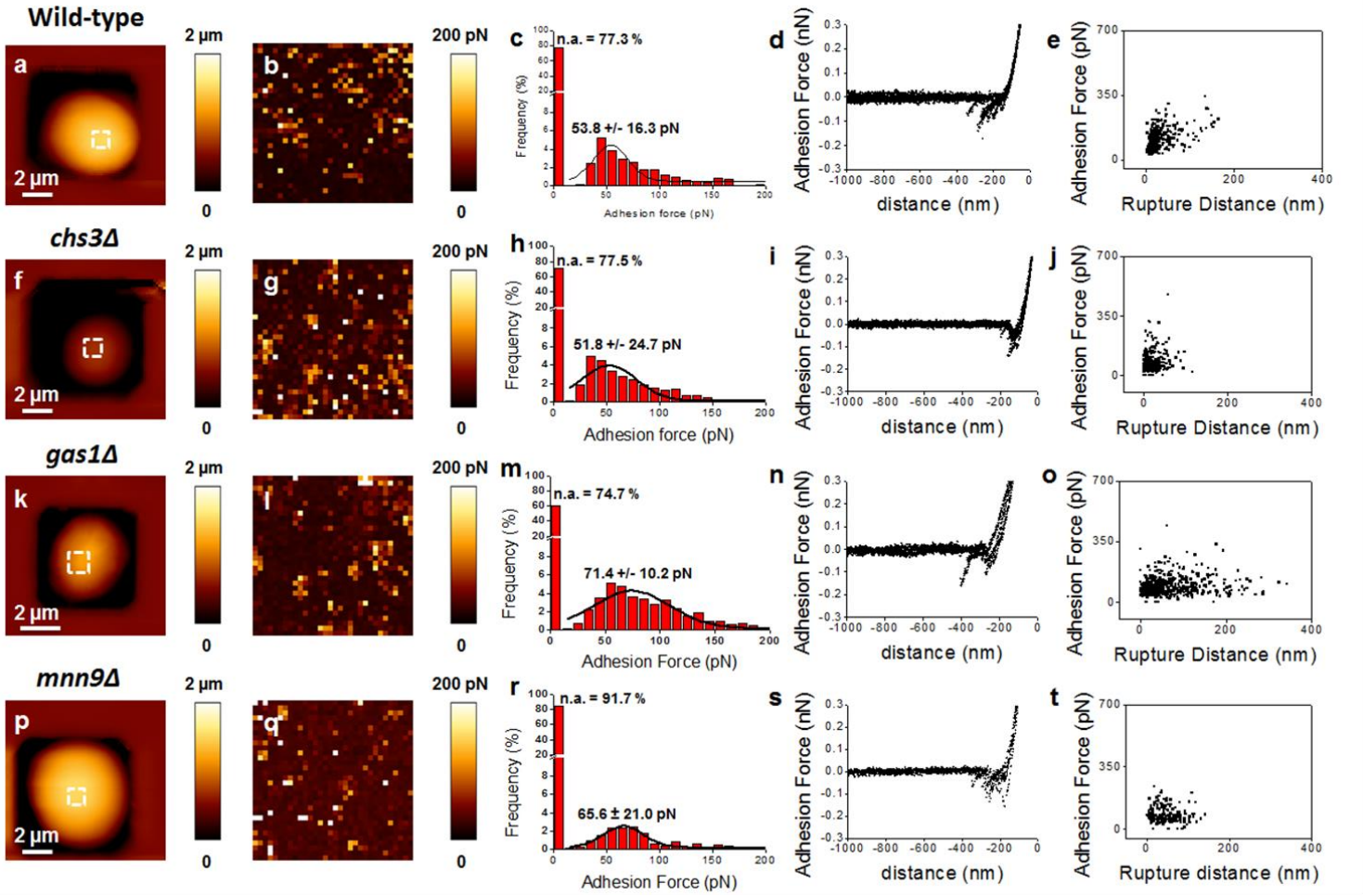

Figure IIIA-2. Stretching polysaccharides on mutants defective in cell wall relative genes with ConA tips
AFM height images (a, f, k, p) of wild-type (BY4741) and mutants defective in chitin synthase III (*chs3*Δ), β-1,3 glucanosyltransferase (*gas1*Δ), mannosyltransferase (*mnn9*Δ).
Adhesion force map of 1µm x 1µm (b, g, l, q); adhesion force histogram (n=1024) recorded with a ConA tip on cell (c, h, m, r); superposition of 10 typical retract force curves (d, l, n, s); repartition of adhesion forces in function of rupture distance (e, j, o, t). Very similar histograms and repartitions were obtained using different tips on 8 cells from 3 independent experiments (8192 curves were analyzed with JPK data processing)

Correlation between gene expression, biophysical properties and cell wall composition

As cell wall organization, structure and physical properties are linked somehow to the cell wall composition and dependent on the genome expression, we sought to identify these correlations by an integrative approach recently developed (González et al., 2012). Transcriptomic data on *gas1*Δ and *mnn9*Δ mutants were retrieved from a previous genome-wide transcriptome analysis that was carried some 10 years ago using nylon membrane arrays (Lagorce et al. 2003). These data are accessible in supplementary data as differentially expressed genes between mutants and wild-type (see Table IIIA.S1-S4). Genes were induced or repressed if the ratio was changed at least by a factor 2. However, the transcriptomic data on *chs3*Δ are not available yet. Ratio of the median values between mutant (*gas1*Δ and *mnn9*Δ) and wild-type for each of the quantitative biochemical (i.e. cell wall components) and biophysical (Young modulus, adhesion events, contour length) data were also established (see Table IIIA-S5 and Table IIIA-S6).

To search for the associations between cell wall related measurements and differentially expressed genes, we conducted a canonical correlation analysis (CCA). CCA is a multivariate statistical technique employed for studying associations between two matrices, such as between sets of transcriptomic and metabolomics data (González et al., 2012). A recent example is the use of this analysis to compare metabolic and transcriptomic datasets with cell wall composition measurements in order to obtain new insights into cell wall synthesis in rice (Guo et al., 2014). Here, we used this analysis to find association between biochemical composition and biophysical properties of the cell (adhesion and nanomechanical properties) and gene expression change in *gas1*Δ and *mnn9*Δ. As shown in Figure IIIA-3, the data are represented in a 2D clustering. In the 1D (horizontal) is shown the association between biochemical and biophysical variables, whereas the second dimension illustrated the association of differentially expressed genes with the physico-biochemical variables. This correlation analysis highlights a close association between frequency of adhesion events and mannans, which was expected taking into account that the interaction with the ConA tip is due the presence of mannoproteins present at the cell surface. Also a close association between chitin and contour length of the cell is found. As contour length represents the length of molecule expansion resulting from the retraction of the conA tip (here mannoproteins), one can suggest that this association is due to the importance of chitin as a cross-link with β-1,3-glucan and mannans linkage.

On the other hand, β-1,6-glucan has no specific association to any of the biophysical variables, except a weak relationship with the adhesion force and with rupture distance. This later association can be related to the fact that β-1,6 glucan is implicated in the links between mannoproteins and the inner layer composed of β-1,3 glucan (Kollar et al., 1997). We also found a close association of the cell elasticity (Young modulus) with the ratio β-glucan/mannan. Genes found to be associated with these physico-biochemical variables were interestingly all found to be upregulated in the *gas1*Δ mutant, but not in *mnn9*Δ (see Table IIIA-3). Thus, this association analysis provides different information than the transcriptomic profiles of the cell wall-related mutants, which have highlighted 33 commonly up-regulated genes that were directly linked to cell wall architecture and remodeling (Lagorce et al., 2003). Another relevant information from this association analysis was to find that the list of retrieved genes are positively correlated with number of adhesive events, contour of length, chitin, mannans and negatively correlated with β-1,3 glucan, ratio β-glucan/mannan and cell wall elasticity (i.e. Young modulus). Looking more carefully to these genes, we identified 5 genes (*FRE1, FTR1, ACO2, HAL5, PTK2*) implicated in ion transport and ion homeostasis, 5 genes (*NSG2, YEH1, ERG12, ECT1, TCB1*) related to membrane structure and sterol metabolism, 2 genes implicated in the actin-related function in membrane cytoskeleton and cell polarization (*SLA2* and *ENT3*), 2 major heat shock encoding genes (*HSP82, HSP90*) and a gene (*CIS3*) encoded a cell-wall mannoprotein with internal repeat.

IV. CONCLUSION

In this study, we tentatively investigated the relationships that can exist between cell wall composition, cell surface properties and gene expression by taking these variables from two mutants specifically defective in genes implicated in the synthesis of mannans (*mnn9*Δ) and β-1,3-glucan elongation (*gas1*Δ). Because the gene expression data of these two mutants were retrieved from a previous transcriptomic analysis as ratio between expression in mutants and wild-type, we had to express the physico and biochemical data as ratio between mutant and wild-type as well to be coherent in our integrative analysis. Using Canonical correlation analysis (CCA) and partial least square (sparse-PLS) regression analysis developed in the mixOmics package, we correlated, as expected, mannans with frequency of adhesion events, which is an indication that our statistical tool is meaningful. Thus, it was interesting to find out that the elasticity property of the cell is associated with the ratio between β-glucan and mannans. This actually makes sense because these two cell wall

polymers are organized into two layers, with mannoproteins as the outer layer and β-glucan as the inner layer of the cell wall. In addition, mannoproteins are considered as soft material whereas β-1,3-glucan has a rigid and fibrillar structure. Therefore, their relative abundance in cell wall can be decisive for cell wall elasticity. This tentative explanation does not exclude chitin as being an important component in this nanomechanical property of the cell wall because chitin present in lateral walls is bound to β-1,6-glucan, which in turn makes the linkage between β-1,3-glucan and mannans (Kollar et al. 1997;Cabib et al. 2007). These linkages may contribute also to the nanomechanical property of the cell wall because a *crh1crh2* mutant that is defective in the protein catalyzing the cross-linkage between chitin and β-1,6 glucan (Cabib et al. 2007) harbors a reduced cell wall elasticity (Dague et al., 2010). Finally, the genes that correlated either positively or negatively with these physical and biochemical parameters were different from those that contribute to the 'cell wall remodeling mechanism' that is activated in response to any conditions that is harmful for the cell wall.

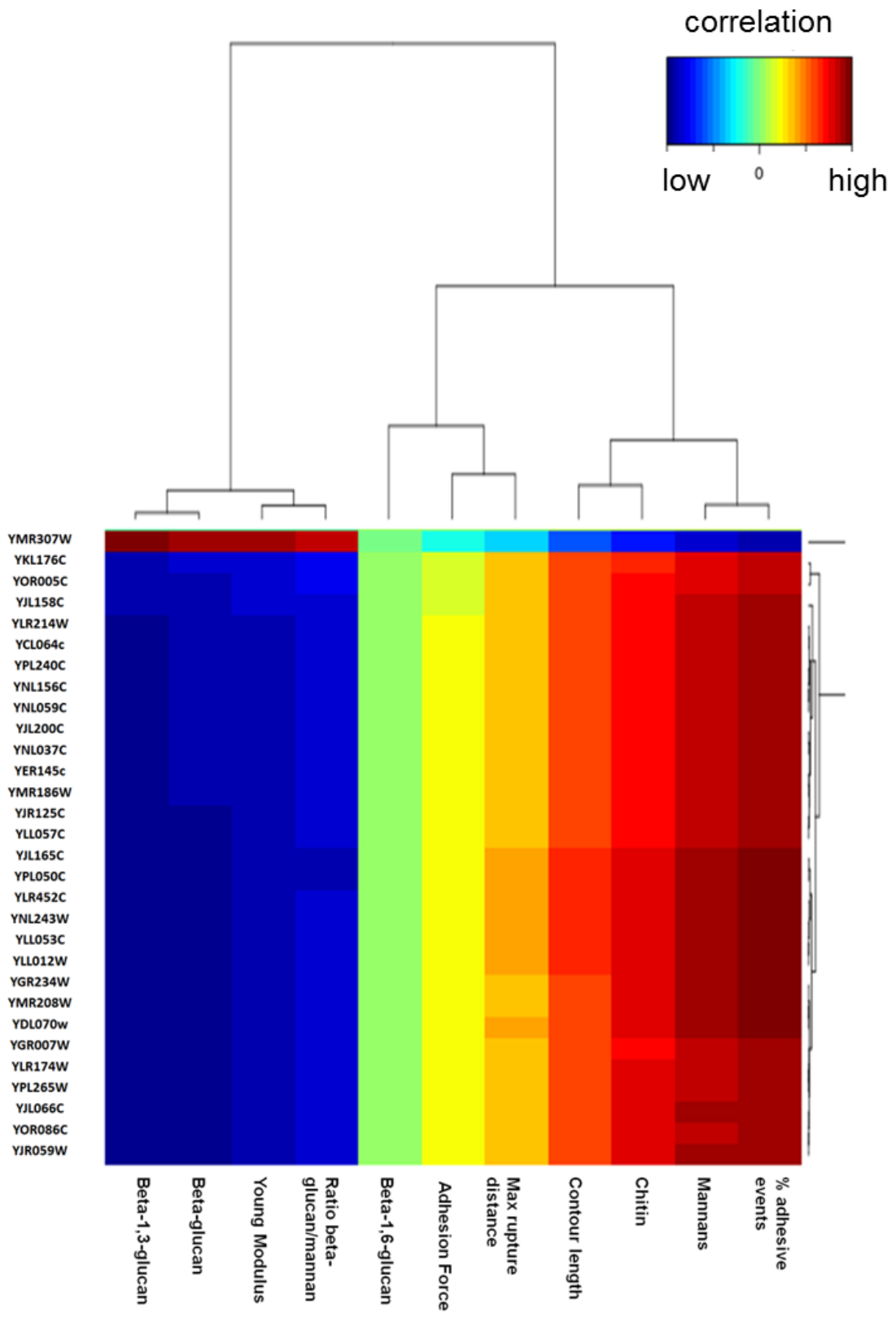

Figure IIIA-3. Correlation of gene expression level, cell wall composition and nanomechanical measurements. The heatmap represents the genes that were selected by S-PLS method in *gas1*Δ mutant as compared to its isogenic wild-type (BY4741). Red color indicates positive correlation while blue color indicates a negative correlation.

Table IIIA-3. Biological function and fold change of genes associate with the cell wall composition and nanomechanical measurements (see Figure IIIA-3).

ORF/Gene	Biological function	Fold change (*gas1*Δ/wt)	Fold change (*mnn9*Δ/wt)
YMR307W/GAS1	β-1,3-glucanosyltransferase, required for cell wall assembly	0.03	0.96
YKL176C/LST4	Protein transport (from Golgi to plasma membrane)	2.21	0.83
YOR005C/DNL4	DNA ligase	2.07	0.98
YJL158C/CIS3	Protein with Internal Repeats; mannose-containing glycoprotein constituent of the cell wall	3.45	0.63
YLR214W/FRE1	Ion transport (copper and iron)	1.95	0.48
YCL064C/CHA1	Amino acids metabolism	2.61	0.42
YPL240C/HSP82	Involved in protein folding; induced by heat shock	2.28	0.40
YNL156C/NSG2	Protein involved in sterol biosynthesis	2.05	1.11
YNL059C/ARP5	Actin-related protein involved in chromatin remodeling	1.71	0.97
YJL200C/ACO2	Catalyze the isomerization of citrate to isocitrate ; implied in ion binding	1.12	0.42
YNL037C/IDH1	Glutamate biosynthesis	1.81	0.84
YER145C/FTR1	Ion transport (iron)	1.44	0.52
YMR186W/HSP90	Involved in protein folding, induced by heat shock	1.53	0.40
YJR125C/ENT3	Implied in protein binding, required for actin organization	1.42	0.59
YLL057C/JLP1	Detoxification	4.03	1.04
YJL165C/HAL5	Protein kinase involved in ion homeostasis	3.53	1.46
YPL050C/MNN9	α-1,6-mannosyltransferase, involved in the elongation of mannan backbone	0.98	0.29
YLR452C/SST2	GTPase activator of Gpa1p, involved in signal transduction	1.17	0.32
YNL243W/SLA2	Adaptator protein involved in membrane cytoskeleton assembly and cell polarization	1.88	0.92
YLL053C	Protein of unknown function	3.23	0.83
YLL012W/YEH1	Hydrolase involved in sterol metabolism	4.43	1.29
YGR234W/YHB1	Involved in nitric oxide detoxification	0.77	0.16
YMR208W/ERG12	Protein kinase involved in sterol biosynthesis	1.98	0.95
YDL070W/BDF2	Protein involved in transcription, induced in response to DNA replication stress	4.81	1.39
YGR007W/ECT1	catalyze phosphatidylethanolamine biosynthesis, implied in the maintenance of plasma membrane	1.40	0.84
YLR174W/IDP2	Metabolism	17.72	2.55
YPL265W/DIP5	Amino acid transport	0.84	0.20
YJL066C/MPM1	Mitochondrial protein with unknown function	4.09	1.82
YOR086C/TCB1	Lipid-binding protein involved in endoplasmic reticulum-plasma membrane tethering	1.73	0.84
YJR059W/PTK2	Protein kinase involved in regulation of ion transport	1.88	0.73

Table IIIA-S1. Upregulated genes in *mnn9*Δ mutant as compared to the wild-type strain (BY4741).
Data from (Lagorce *et al.* 2003)

ORF	gene	Factor of induction	ORF	gene	Factor of induction
YCL020W	TY2A	2	**YOR120W**	GCY1	2,5
YGL127C	SOH1	2	**YPL149W**	APG5	2,5
YJL023C	PET130	2	**YBR160W**	CDC28	2,6
YLL041C	SDH2	2	**YGR040W**	KSS1	2,6
YLR119W	SRN2	2	**YEL058W**	PCM1	2,7
YLR300W	EXG1	2	**YGL166W**	CUP2	2,7
YMR011W	HXT2	2	**YGR288W**	MAL13	2,7
YMR064W	AEP1	2	**YMR072W**	ABF2	2,7
YMR199W	CLN1	2	**YOR208W**	PTP2	2,7
YNL003C	PET8	2	**YPL155C**	KIP2	2,7
YNL053W	MSG5	2	**YPR198W**	SGE1	2,7
YOL025W	LAG2	2	**YDL215C**	GDH2	2,8
YOR237W	HES1	2	**YER144C**	UBP5	2,8
YPL111W	CAR1	2	**YGL205W**	POX1	2,8
YPR001W	CIT3	2	**YIR027C**	DAL1	2,8
YPR183W	DPM1	2	**YHR044C**	DOG1	2,9
YBR023C	CHS3	2,1	**YJL106W**	IME2	2,9
YBR222C	PCS60	2,1	**YKL096W**	CWP1	2,9
YCL040W	GLK1	2,1	**YKL104C**	GFA1	2,9
YCR098C	GIT1	2,1	**YMR165C**	SMP2	2,9
YDR178W	SDH4	2,1	**YFL014W**	HSP12	3
YFL020C	PAU5	2,1	**YLR438W**	CAR2	3
YHL027W	RIM101	2,1	**YOR036W**	PEP12	3
YKL178C	STE3	2,1	**YDL245C**	HXT15	3,1
YLR332W	MID2	2,1	**YMR173W**	DDR48	3,1
YLR457C	NBP1	2,1	**YPL057C**	SUR1	3,1
YML016C	PPZ1	2,1	**YMR053C**	STB2	3,2
YML027W	YOX1	2,1	**YNL250W**	RAD50	3,2
YMR200W	ROT1	2,1	**YHR030C**	SLT2	3,3
YNL210W	MER1	2,1	**YPR167C**	MET16	3,3
YNR002C	FUN34	2,1	**YPR189W**	SKI3	3,3
YOL013C	HRD1	2,1	**YGR070W**	ROM1	3,4
YPL256C	CLN2	2,1	**YJL155C**	FBP26	3,4
YPR006C	ICL2	2,1	**YJR156C**	THI11	3,4
YAL039C	CYC3	2,2	**YDR085C**	AFR1	3,5
YDR106W	ARP10	2,2	**YER159C**	NCB1	3,5
YGR008C	STF2	2,2	**YER179W**	DMC1	3,5
YHL016C	DUR3	2,2	**YIR017C**	MET28	3,5
YHR006W	STP2	2,2	**YFL058W**	THI5	3,6
YHR176W	FMO	2,2	**YGL038C**	OCH1	3,6
YJR052W	RAD7	2,2	**YDR218C**	SPR28	3,8
YKL016C	ATP7	2,2	**YMR008C**	PLB1	3,8
YLR258W	GSY2	2,2	**YKR097W**	PCK1	4

YLR459W	CDC91	2,2	**YLR303W**	MET25	4,2
YMR092C	AIP1	2,2	**YPL054W**	LEE1	4,2
YNL036W	NCE3	2,2	**YEL060C**	PRB1	4,3
YOR035C	SHE4	2,2	**YOL016C**	CMK2	4,4
YPL089C	RLM1	2,2	**YDR077W**	SED1	4,5
YBL066C	SEF1	2,3	**YDR059C**	UBC5	4,6
YBR201W	DER1	2,3	**YPL163C**	SVS1	4,6
YGR166W	KRE11	2,3	**YDL234C**	GYP7	4,7
YHR055C	CUP1B	2,3	**YNL015W**	PBI2	4,7
YJL223C	PAU1	2,3	**YGR144W**	THI4	4,8
YJR073C	OPI3	2,3	**YMR056C**	AAC1	4,8
YKL150W	MCR1	2,3	**YNL160W**	YGP1	5
YMR023C	MSS1	2,3	**YDR277C**	MTH1	5,2
YMR054W	STV1	2,3	**YMR081C**	ISF1	5,2
YPL167C	REV3	2,3	**YMR055C**	BUB2	5,4
YBR050C	REG2	2,4	**YBR295W**	PCA1	6,1
YDL181W	INH1	2,4	**YKR013W**	PRY2	6,3
YEL049W	PAU2	2,4	**YDL049C**	KNH1	7,1
YFR030W	MET10	2,4	**YLR393W**	ATP10	7,5
YGL248W	PDE1	2,4	**YKR061W**	KTR2	8
YGR014W	MSB2	2,4	**YGR032W**	GSC2	8,4
YGR028W	MSP1	2,4	**YGR248W**	SOL4	8,6
YHR053C	CUP1A	2,4	**YDL021W**	GPM2	9
YIL171W	HXT12	2,4	**YGR213C**	RTA1	9,2
YJR159W	SOR1	2,4	**YGR249W**	MGA1	9,4
YLR178C	TFS1	2,4	**YNL202W**	SPS19	10,3
YML054C	CYB2	2,4	**YMR104C**	YPK2	10,8
YMR052W	FAR3	2,4	**YDL169C**	UGX2	11,3
YAR027W	FUN55	2,5	**YPR074C**	TKL1	14
YGR282C	BGL2	2,5	**YAR050W**	FLO1	15,4
YHR043C	DOG2	2,5	**YOR211C**	MGM1	16,7
YLR174W	IDP2	2,5	**YEL019C**	MMS21	26,6
YLR461W	PAU4	2,5	**YNR075W**	EDL1	42,1
YMR170C	ALD5	2,5			

Table IIIA-S2. Genes downregulated in *mnn9*Δ mutant as compared to the wild-type strain (BY4741).
Data from (Lagorce et al. 2003)

ORF	gene	Factor of repression	**ORF**	gene	Factor of repression
YLR304C	ACO1	-2	**YLL024C**	SSA2	-2,4
YJR060W	CBF1	-2	**YNR044W**	AGA1	-2,5
YLR274W	CDC46	-2	**YAL003W**	EFB1	-2,5
YBR291C	CTP1	-2	**YMR186W**	HSC82	-2,5
YNL280C	ERG24	-2	**YPL240C**	HSP82	-2,5
YJL157C	FAR1	-2	**YER103W**	SSA4	-2,5
YCL027W	FUS1	-2	**YPL061W**	ALD6	-2,6
YPR160W	GPH1	-2	**YIL119C**	RPI1	-2,7
YJL214W	HXT8	-2	**YDR422C**	SIP1	-2,7
YBR146W	MRPS9	-2	**YBR081C**	SPT7	-2,7
YBL080C	PET112	-2	**YDR505C**	PSP1	-2,8
YBL035C	POL12	-2	**YBR140C**	IRA1	-2,9
YBL007C	SLA1	-2	**YPL021W**	SRD2	-2,9
YGR162W	TIF4631	-2	**YCL037C**	SRO9	-2,9
YBL067C	UBP13	-2	**YLR452C**	SST2	-3,1
YGL255W	ZRT1	-2	**YPL161C**	BEM4	-3,2
YBR145W	ADH5	-2,1	**YPL174C**	NIP80	-3,2
YCR048W	ARE1	-2,1	**YIL114C**	POR2	-3,2
YLL050C	COF1	-2,1	**YNL248C**	RPA49	-3,2
YAL013W	DEP1	-2,1	**YLR249W**	YEF3	-3,2
YMR058W	FET3	-2,1	**YAR071W**	PHO11	-3,3
YLR214W	FRE1	-2,1	**YHR215W**	PHO12	-3,3
YDR225W	HTA1	-2,1	**YDR464W**	SPP41	-3,3
YBR268W	MRPL37	-2,1	**YNL145W**	MFA2	-3,4
YBL020W	RFT1	-2,1	**YPR149W**	NCE2	-3,4
YGL229C	SAP4	-2,1	**YAL005C**	SSA1	-3,4
YOR008C	SLG1	-2,1	**YPL050C**	MNN9	-3,5
YFL026W	STE2	-2,1	**YCL001W**	RER1	-3,5
YDR310C	SUM1	-2,1	**YBL101C**	TY2B	-3,9
YDL007W	YTA5	-2,1	**YBL002W**	HTB2	-4,5
YOR204W	DED1	-2,2	**YKL092C**	BUD2	-4,6
YDL106C	GRF10	-2,2	**YDR285W**	ZIP1	-4,6
YHR096C	HXT5	-2,2	**YJL113W**	TY4B	-4,8
YDL182W	LYS20	-2,2	**YPL265W**	DIP5	-5
YOR346W	REV1	-2,2	**YAL029C**	MYO4	-5,3
YBL034C	STU1	-2,2	**YJR062C**	NTA1	-5,3
YCL050C	APA1	-2,3	**YGR234W**	YHB1	-6,4
YGL195W	GCN1	-2,3	**YDR522C**	SPS2	-6,6
YBL003C	HTA2	-2,3	**YBL063W**	KIP1	-7,2
YBR093C	PHO5	-2,3	**YOR302W**	CPA1	-8,5
YLL016W	SDC25	-2,3	**YNL172W**	APC1	-8,8
YCR081W	SRB8	-2,3	**YCR028C**	FEN2	-10,5
YCL064C	CHA1	-2,4	**YDR292C**	SRP101	-12,5

YPR124W	CTR1	-2,4	**YKL209C**	STE6	-13
YMR232W	FUS2	-2,4	**YLR098C**	CHA4	-13,4
YPL171C	OYE3	-2,4	**YML123C**	PHO84	-13,4
YGR233C	PHO81	-2,4	**YKL095W**	YJU2	-16,5
YPR135W	POB1	-2,4	**YFL050C**	ALR2	-29,1
YOR207C	RPC128	-2,4	**YAR042W**	OSH1	-85,8
YFL005W	SEC4	-2,4			

Table IIIA-S3. Genes upregulated in *gas1*Δ mutant as compared to the wild-type strain (BY4741).
Data from (Lagorce et al. 2003)

ORF	gene	Factor of induction	ORF	gene	Factor of induction
YAL005C	SSA1	2	**YDR293C**	SSD1	2,6
YAL040C	CLN3	2	**YEL049W**	PAU2	2,6
YBL061C	SKT5	2	**YER098W**	UBP9	2,6
YCL027W	FUS1	2	**YGL167C**	PMR1	2,6
YCR081W	SRB8	2	**YGL253W**	HXK2	2,6
YDL126C	CDC48	2	**YGR055W**	MUP1	2,6
YDR039C	ENA2	2	**YHL027W**	RIM101	2,6
YDR040C	ENA1	2	**YHR006W**	STP2	2,6
YDR283C	GCN2	2	**YIL031W**	SMT4	2,6
YDR403W	DIT1	2	**YIL072W**	HOP1	2,6
YEL046C	GLY1	2	**YIL136W**	OM45	2,6
YER091C	MET6	2	**YJR121W**	ATP2	2,6
YER159C	NCB1	2	**YLR028C**	ADE16	2,6
YFL014W	HSP12	2	**YNL204C**	SPS18	2,6
YGR092W	DBF2	2	**YNL277W**	MET2	2,6
YGR274C	TAF145	2	**YOR337W**	TEA1	2,6
YHR032W	ERC1	2	**YDR261C**	EXG2	2,7
YHR082C	KSP1	2	**YDR351W**	SBE2	2,7
YIR031C	DAL7	2	**YDR389W**	SAC7	2,7
YJL187C	SWE1	2	**YGL112C**	TAF60	2,7
YJR005W	APL1	2	**YGR258C**	RAD2	2,7
YJR028W	TY1A	2	**YIL125W**	KGD1	2,7
YJR132W	NMD5	2	**YJL129C**	TRK1	2,7
YKL038W	RGT1	2	**YJR159W**	SOR1	2,7
YKR034W	DAL80	2	**YKL182W**	FAS1	2,7
YLR157C	ASP3B	2	**YLR461W**	PAU4	2,7
YLR160C	ASP3D	2	**YMR017W**	DBI9	2,7
YLR195C	NMT1	2	**YNL036W**	NCE3	2,7
YLR259C	HSP60	2	**YNL237W**	YTP1	2,7
YLR263W	RED1	2	**YNR058W**	BIO3	2,7
YLR304C	ACO1	2	**YOR134W**	BAG7	2,7
YML109W	ZDS2	2	**YPR074C**	TKL1	2,7
YMR011W	HXT2	2	**YDR001C**	NTH1	2,8
YMR016C	SOK2	2	**YDR009W**	GAL3	2,8
YMR208W	ERG12	2	**YDR074W**	TPS2	2,8

YMR275C	BUL1	2	**YGR183C**	QCR9	2,8
YNL074C	YMK1	2	**YHL032C**	GUT1	2,8
YNL250W	RAD50	2	**YJL127C**	SPT10	2,8
YOR141C	ARP8	2	**YJL223C**	PAU1	2,8
YOR153W	PDR5	2	**YJR094C**	IME1	2,8
YOR204W	DED1	2	**YJR156C**	THI11	2,8
YOR231W	MKK1	2	**YKL198C**	PTK1	2,8
YOR274W	MOD5	2	**YOR348C**	PUT4	2,8
YOR329C	SCD5	2	**YCR005C**	CIT2	2,9
YOR363C	PIP2	2	**YDR251W**	PAM1	2,9
YPL248C	GAL4	2	**YJL026W**	RNR2	2,9
YCR073C	SSK22	2,1	**YJL164C**	SRA3	2,9
YDL021W	GPM2	2,1	**YKR013W**	PRY2	2,9
YDL043C	PRP11	2,1	**YKR097W**	PCK1	2,9
YDL245C	HXT15	2,1	**YLR178C**	TFS1	2,9
YDR505C	PSP1	2,1	**YLR362W**	STE11	2,9
YGR087C	PDC6	2,1	**YML016C**	PPZ1	2,9
YGR152C	RSR1	2,1	**YMR170C**	ALD5	2,9
YGR282C	BGL2	2,1	**YOL051W**	GAL11	2,9
YGR289C	AGT1	2,1	**YPR168W**	NUT2	2,9
YHL022C	SPO11	2,1	**YEL042W**	GDA1	3
YIR027C	DAL1	2,1	**YJL214W**	HXT8	3
YJL137C	GLG2	2,1	**YJR077C**	MIR1	3
YJR158W	HXT16	2,1	**YKL103C**	LAP4	3
YKL067W	YNK1	2,1	**YLL065W**	GIN11	3
YKL135C	APL2	2,1	**YLR332W**	MID2	3
YKL185W	ASH1	2,1	**YML057W**	CMP2	3
YKR061W	KTR2	2,1	**YNL053W**	MSG5	3
YKR098C	UBP11	2,1	**YPL111W**	CAR1	3
YLR138W	NHA1	2,1	**YPR159W**	KRE6	3
YLR158C	ASP3C	2,1	**YDR085C**	AFR1	3,1
YLR347C	KAP95	2,1	**YDR388W**	RVS167	3,1
YMR297W	PRC1	2,1	**YGR166W**	KRE11	3,1
YNL007C	SIS1	2,1	**YIL140W**	SRO4	3,1
YNL012W	SPO1	2,1	**YJL102W**	MEF2	3,1
YNL251C	NRD1	2,1	**YKL148C**	SDH1	3,1
YOR127W	RGA1	2,1	**YNR002C**	FUN34	3,1
YOR237W	HES1	2,1	**YOR208W**	PTP2	3,1
YPL015C	HST2	2,1	**YBR046C**	ZTA1	3,2
YPL149W	APG5	2,1	**YJL099W**	CHS6	3,2
YPR001W	CIT3	2,1	**YJR052W**	RAD7	3,2
YPR054W	SMK1	2,1	**YJR103W**	URA8	3,2
YPR155C	NCA2	2,1	**YKL079W**	SMY1	3,2
YBR001C	NTH2	2,2	**YPR191W**	QCR2	3,2
YBR112C	CYC8	2,2	**YDR077W**	SED1	3,3
YCL057W	PRD1	2,2	**YDR258C**	HSP78	3,3

YCR088W	ABP1	2,2	**YDR480W**	DIG2	3,3
YDR178W	SDH4	2,2	**YER065C**	ICL1	3,3
YDR443C	SCA1	2,2	**YKL164C**	PIR1	3,3
YDR507C	GIN4	2,2	**YLL041C**	SDH2	3,3
YER167W	BCK2	2,2	**YLR258W**	GSY2	3,3
YJL172W	CPS1	2,2	**YOR027W**	STI1	3,3
YJL221C	FSP2	2,2	**YOR035C**	SHE4	3,3
YKL085W	MDH1	2,2	**YBR297W**	MAL33	3,4
YKL101W	HSL1	2,2	**YCL040W**	GLK1	3,4
YKL157W	APE2	2,2	**YDL169C**	UGX2	3,4
YLR060W	FRS1	2,2	**YER144C**	UBP5	3,4
YLR248W	RCK2	2,2	**YFR031C**	RPL5B	3,4
YMR092C	AIP1	2,2	**YJL219W**	HXT9	3,4
YMR280C	CAT8	2,2	**YKL093W**	MBR1	3,4
YMR302C	PRP12	2,2	**YLR133W**	CKI1	3,4
YOR061W	CKA2	2,2	**YOL067C**	RTG1	3,4
YOR207C	RPC128	2,2	**YBR165W**	UBS1	3,5
YOR219C	STE13	2,2	**YGL192W**	IME4	3,5
YPL040C	ISM1	2,2	**YHR030C**	SLT2	3,5
YPR069C	SPE3	2,2	**YIL150C**	DNA43	3,5
YAL034C	FUN19	2,3	**YJL034W**	KAR2	3,5
YAL063C	FLO9	2,3	**YJL165C**	HAL5	3,5
YBL034C	STU1	2,3	**YOL156W**	HXT11	3,5
YBR169C	SSE2	2,3	**YPL089C**	RLM1	3,5
YCL043C	PDI1	2,3	**YAL032C**	FUN20	3,6
YCR048W	ARE1	2,3	**YGL006W**	PMC1	3,6
YDL230W	PTP1	2,3	**YGR040W**	KSS1	3,6
YDR069C	DOA4	2,3	**YKL129C**	MYO3	3,6
YDR081C	PDC2	2,3	**YLR155C**	ASP3A	3,6
YDR343C	HXT6	2,3	**YML120C**	NDI1	3,6
YDR350C	TCM10	2,3	**YGR014W**	MSB2	3,7
YEL061C	CIN8	2,3	**YIR019C**	STA1	3,7
YGR288W	MAL13	2,3	**YMR319C**	FET4	3,7
YHR016C	YSC84	2,3	**YOL126C**	MDH2	3,7
YIL066C	RNR3	2,3	**YBR208C**	DUR1,2	3,8
YJL176C	SWI3	2,3	**YJL089W**	SIP4	3,8
YJR026W	TY1A	2,3	**YLR438W**	CAR2	3,8
YLR342W	FKS1	2,3	**YMR137C**	PSO2	3,8
YLR459W	CDC91	2,3	**YGL248W**	PDE1	3,9
YMR020W	FMS1	2,3	**YGR143W**	SKN1	3,9
YMR035W	IMP2	2,3	**YKL188C**	PAT1	3,9
YNL241C	ZWF1	2,3	**YLR006C**	SSK1	3,9
YNR076W	PAU6	2,3	**YPR005C**	HAL1	3,9
YOR014W	RTS1	2,3	**YBR023C**	CHS3	4
YOR040W	GLO4	2,3	**YLR039C**	RIC1	4
YPL018W	CTF19	2,3	**YDL220C**	CDC13	4,1

YPL119C	DBP1	2,3	**YEL011W**	GLC3	4,1
YPL240C	HSP82	2,3	**YBR222C**	PCS60	4,2
YBL005W	TY1A	2,4	**YDR059C**	UBC5	4,2
YCR104W	PAU3	2,4	**YHL016C**	DUR3	4,2
YDL215C	GDH2	2,4	**YOR036W**	PEP12	4,2
YER011W	TIR1	2,4	**YDR277C**	MTH1	4,3
YER020W	GPA2	2,4	**YIL107C**	PFK26	4,4
YER095W	RAD51	2,4	**YKL104C**	GFA1	4,4
YFL020C	PAU5	2,4	**YBL075C**	SSA3	4,6
YFL058W	THI5	2,4	**YDR216W**	ADR1	4,6
YGL063W	PUS2	2,4	**YNR001C**	CIT1	4,6
YGL166W	CUP2	2,4	**YLL019C**	KNS1	4,7
YHR211W	FLO5	2,4	**YPL054W**	LEE1	4,7
YIL046W	MET30	2,4	**YDR448W**	ADA2	4,8
YIL114C	POR2	2,4	**YJR091C**	JSN1	4,8
YJR062C	NTA1	2,4	**YMR165C**	SMP2	4,8
YKL062W	MSN4	2,4	**YJL078C**	PRY3	4,9
YKL126W	YPK1	2,4	**YMR008C**	PLB1	4,9
YKR050W	TRK2	2,4	**YLR120C**	YAP3	5
YLR092W	SEL2	2,4	**YBR294W**	SUL1	5,2
YLR337W	VRP1	2,4	**YGL163C**	RAD54	5,3
YML054C	CYB2	2,4	**YPL163C**	SVS1	5,3
YML100W	TSL1	2,4	**YMR056C**	AAC1	5,4
YMR053C	STB2	2,4	**YBL015W**	ACH1	5,6
YMR105C	PGM2	2,4	**YJL106W**	IME2	5,6
YMR109W	MYO5	2,4	**YOL016C**	CMK2	5,6
YNL282W	(POP2)	2,4	**YDR138W**	HPR1	5,8
YNR006W	VPS27	2,4	**YIR028W**	DAL4	5,9
YNR032W	PPG1	2,4	**YPL057C**	SUR1	6,2
YNR072W	HXT17	2,4	**YIL155C**	GUT2	6,3
YOL122C	SMF1	2,4	**YLR393W**	ATP10	6,4
YOR058C	ASE1	2,4	**YJL155C**	FBP26	6,6
YOR328W	PDR10	2,4	**YKL163W**	PIR3	6,8
YPL179W	PPQ1	2,4	**YLR142W**	PUT1	6,8
YPR198W	SGE1	2,4	**YKR009C**	FOX2	7,2
YBL074C	AAR2	2,5	**YLL026W**	HSP104	7,2
YBR012W	TY1A	2,5	**YGR032W**	GSC2	7,4
YBR114W	RAD16	2,5	**YDR171W**	HSP42	7,5
YBR126C	TPS1	2,5	**YPR065W**	ROX1	8,1
YDL138W	RGT2	2,5	**YGR213C**	RTA1	8,2
YDR270W	CCC2	2,5	**YDL234C**	GYP7	8,3
YDR436W	PPZ2	2,5	**YDR461W**	MFA1	8,3
YEL058W	PCM1	2,5	**YJL153C**	INO1	8,7
YER103W	SSA4	2,5	**YKL095W**	YJU2	8,8
YGL062W	PYC1	2,5	**YFL031W**	HAC1	8,9
YGR097W	ASK10	2,5	**YKL197C**	PAS1	9,1

YGR270W	YTA7	2,5	**YEL060C**	PRB1	11,2
YHL036W	MUP3	2,5	**YKL217W**	JEN1	15,6
YHR176W	FMO	2,5	**YBR295W**	PCA1	17,1
YIR017C	MET28	2,5	**YLR174W**	IDP2	17,7
YJL141C	YAK1	2,5	**YGL212W**	VAM7	18,9
YKL064W	MNR2	2,5	**YBL066C**	SEF1	21,5
YKL142W	MRP8	2,5	**YLR240W**	VPS34	21,9
YLL024C	SSA2	2,5	**YAR042W**	OSH1	23,2
YLR216C	CPR6	2,5	**YMR104C**	YPK2	24
YAL039C	CYC3	2,6	**YGR059W**	SPR3	102
YBR299W	MAL32	2,6	**YLR234W**	TOP3	141,8
YCL064C	CHA1	2,6			

Table IIIA-S4. Genes downregulated in *gas1*Δ mutant as compared to the wild-type strain (BY4741).
Data from (Lagorce et al. 2003)

ORF	gene	Factor of repression	ORF	gene	Factor of repression
YKL134C	MIP1	-2	**YER114C**	BOI2	-2,5
YHR093W	AHT1	-2	**YDR301W**	CFT1	-2,5
YGR108W	CLB1	-2	**YGL070C**	RPB9	-2,5
YBR252W	DUT1	-2	**YBR084C**	RPL19B	-2,5
YCR028C	FEN2	-2	**YPL178W**	SAE1	-2,5
YKR039W	GAP1	-2	**YDR292C**	SRP101	-2,5
YGR252W	GCN5	-2	**YGR105W**	VMA21	-2,5
YCL059C	KRR1	-2	**YCR097W**	A1	-2,6
YAL025C	MAK16	-2	**YGL119W**	ABC1	-2,6
YLR329W	REC102	-2	**YNL271C**	BNI1	-2,6
YDR418W	RPL15A	-2	**YBR290W**	BSD2	-2,7
YDR471W	RPL27B	-2	**YGR292W**	MAL12	-2,7
YNL162W	RPL41A	-2	**YBR093C**	PHO5	-2,7
YJL190C	RPS24A	-2	**YGR034W**	RPL33B	-2,7
YMR190C	SGS1	-2	**YPR187W**	RPO26	-2,7
YOR008C	SLG1	-2	**YGL194C**	RTL1	-2,7
YLL021W	SPA2	-2	**YFL-TYA**	TY2A	-2,7
YDR218C	SPR28	-2	**YMR161W**	HLJ1	-2,8
YDR390C	UBA2	-2	**YPR166C**	MRP2	-2,8
YFR028C	CDC14	-2,1	**YDR208W**	MSS4	-2,8
YDR254W	CHL4	-2,1	**YCL004W**	PEL1	-2,8
YEL027W	CUP5	-2,1	**YPR189W**	SKI3	-2,8
YDR191W	HST4	-2,1	**YGR246C**	BRF1	-3
YHL003C	LAG1	-2,1	**YCR098C**	GIT1	-3,1
YCR003W	MRPL32	-2,1	**YNL262W**	POL2	-3,1
YDL208W	NHP2	-2,1	**YBR140C**	IRA1	-3,2
YIR008C	PRI1	-2,1	**YFR036W**	CDC26	-3,3
YBR181C	RPS101	-2,1	**YER058W**	PET117	-3,3
YPL081W	RPS13B	-2,1	**YCR039C**	MATALPHA2	-3,4
YDL083C	RPS16B	-2,1	**YHR141C**	RPL41B	-3,4

YDR025W	RPS18A	-2,1	**YKL049C**	CSE4	-3,6
YDR450W	RPS18EA	-2,1	**YKL001C**	MET14	-3,6
YLR367W	RPS24B	-2,1	**YHR147C**	MRPL6	-3,7
YHR021C	RPS27B	-2,1	**YMR123W**	PKR1	-3,7
YGL100W	SEH1	-2,1	**YLR353W**	BUD8	-3,8
YHR153C	SPO16	-2,1	**YOL081W**	IRA2	-3,9
YBR191W	URP1A	-2,1	**YIR023W**	DAL81	-4,2
YER031C	YPT31	-2,1	**YIL119C**	RPI1	-4,3
YLL009C	COX17	-2,2	**YHR208W**	TWT1	-4,4
YIR032C	DAL3	-2,2	**YHR139C**	SPS100	-5
YNL112W	DBP2	-2,2	**YML123C**	PHO84	-5,4
YAL033W	FUN53	-2,2	**YBR092C**	PHO3	-5,6
YBR146W	MRPS9	-2,2	**YGL009C**	LEU1	-6,2
YER023W	PRO3	-2,2	**YHR215W**	PHO12	-6,5
YDL105W	QRI2	-2,2	**YPL016W**	SWI1	-6,7
YKL006W	RPL14A	-2,2	**YAR071W**	PHO11	-6,8
YBR048W	RPS18B	-2,2	**YKL120W**	PMT	-7
YGL229C	SAP4	-2,2	**YBL038W**	MRPL16	-10,2
YPL085W	SEC16	-2,2	**YAR050W**	FLO1	-10,7
YDL191W	SOS1	-2,2	**YAL051W**	OAF1	-11,3
YDR523C	SPS1	-2,2	**YGR098C**	ESP1	-11,6
YBR164C	ARL1	-2,3	**YOR373W**	NUD1	-14,4
YGL130W	CEG1	-2,3	**YOR349W**	CIN1	-15,1
YFL001W	DEG1	-2,3	**YJL114W**	TY4A	-21,5
YER014W	HEM14	-2,3	**YGL205W**	POX1	-26,3
YKR082W	NUP133	-2,3	**YCL014W**	BUD3	-30,6
YHR037W	PUT2	-2,3	**YMR307W**	GAS1	-37,8
YGL083W	SCY1	-2,3	**YLR098C**	CHA4	-207,9
YAL059W	SIM1	-2,3	**YAR008W**	FUN4	-514,4
YLR306W	UBC12	-2,3	**YHR014W**	SPO13	-850,6
YER123W	YCK3	-2,3	**YBR021W**	FUR4	-893,2
YGL043W	DST1	-2,4	**YDR150W**	NUM1	-2054,4
YBL080C	PET112	-2,4	**YAR010C**	TY1A	-2355,8
YCR029C	RIM1	-2,4	**YER155C**	BEM2	-2760,5
YHL001W	RPL14B	-2,4	**YCR097W**	A1	-4924,6
YKL020C	SPT23	-2,4	**YKL010C**	SOS1	-5286,1
YER112W	USS1	-2,4	**YEL031W**	SPF1	-6586
YDR106W	ARP10	-2,5	**YER109C**	FLO8	-6849,1

Table IIIA-S5: Median ratio value between mutant/wild-type of biophysical and biochemical data.

strain	YM (kPa)	% of adhesion events	adhesion force (pN)	maximum of rupture distance (nm)	contour length (nm)	roughness (nm^2)
gas1Δ	0.7	3.1	1.1	1.9	1.1	3.7
chs3Δ	0.4	2.7	1	1.1	0.8	2.1
mnn9Δ	1.7	0.8	1.1	1.5	0.8	2.8

Table IIIA-S6: Median ratio value between mutant/wild-type of biophysical and biochemical data.

strain	chitin	β-1,3 glucans	β-1,6 glucans	total β-glucans	mannans	ratio β-glucans/mannans
gas1Δ	5.6	0.6	1.7	1.2	1.7	0.7
chs3Δ	0.2	1.3	1.5	1.6	1.2	0.8
mnn9Δ	3.1	1.0	0.8	1.9	0.8	1.9

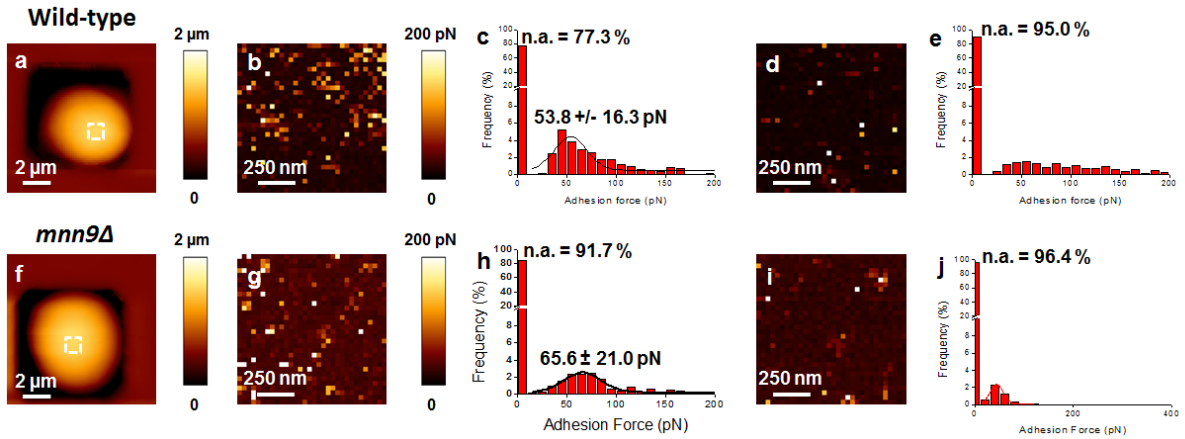

Figure IIIA-S1. Blocking interaction mannan-lectin tips
(a, f) AFM height images recorded with QI™ mode (JPK Instruments) with (b, d, g, i) adhesion force map of 1µm x 1µm and (c, e, h, j) adhesion force histogram (n=1024) recorded with a ConA tip on the cell wall of wild-type strain (a-e) and *mnn9*Δ mutant (f-j). Experiments were performed in the absence (b, c, g, h) or in presence (d, e, i, j) of 100 mM mannose.

References:

Alsteens, D., Dupres, V., Mc Evoy, K., Wildling, L., Gruber, H.J., and Dufrêne, Y.F. (2008). Structure, cell wall elasticity and polysaccharide properties of living yeast cells, as probed by AFM. Nanotechnology 19, 384005.

Ballou, L., Hernandez, L.M., Alvarado, E., and Ballou, C.E. (1990). Revision of the oligosaccharide structures of yeast carboxypeptidase Y. Proc. Natl. Acad. Sci. U. S. A. 87, 3368–3372.

Binnig, Quate, and Gerber (1986). Atomic force microscope. Phys. Rev. Lett. 56, 930–933.

Bustamante, C., Marko, J.F., Siggia, E.D., and Smith, S. (1994). Entropic elasticity of lambda-phage DNA. Science 265, 1599–1600.

Cabib, E., and Arroyo, J. (2013). How carbohydrates sculpt cells: chemical control of morphogenesis in the yeast cell wall. Nat. Rev. Microbiol. 11, 648–655.

Chopinet, L., Formosa, C., Rols, M.P., Duval, R.E., and Dague, E. (2013). Imaging living cells surface and quantifying its properties at high resolution using AFM in QITM mode. Micron.

Dague, E., Bitar, R., Ranchon, H., Durand, F., Yken, H.M., and Francois, J.M. (2010). An atomic force microscopy analysis of yeast mutants defective in cell wall architecture. Yeast Chichester Engl. 27, 673–684.

Dague, E., Jauvert, E., Laplatine, L., Viallet, B., Thibault, C., and Ressier, L. (2011). Assembly of live micro-organisms on microstructured PDMS stamps by convective/capillary deposition for AFM bio-experiments. Nanotechnology 22, 395102.

Dallies, N., Francois, J., and Paquet, V. (1998). A new method for quantitative determination of polysaccharides in the yeast cell wall. Application to the cell wall defective mutants of Saccharomyces cerevisiae. Yeast Chichester Engl. 14, 1297–1306.

Francius, G., Alsteens, D., Dupres, V., Lebeer, S., De Keersmaecker, S., Vanderleyden, J., Gruber, H.J., and Dufrêne, Y.F. (2009). Stretching polysaccharides on live cells using single molecule force spectroscopy. Nat. Protoc. 4, 939–946.

Francois, J.M. (2006). A simple method for quantitative determination of polysaccharides in fungal cell walls. Nat. Protoc. 1, 2995–3000.

González, I., Cao, K.-A.L., Davis, M.J., and Déjean, S. (2012). Visualising associations between paired “omics” data sets. BioData Min. 5, 19.

Guo, K., Zou, W., Feng, Y., Zhang, M., Zhang, J., Tu, F., Xie, G., Wang, L., Wang, Y., Klie, S., et al. (2014). An integrated genomic and metabolomic framework for cell wall biology in rice. BMC Genomics 15, 596.

Hutter, J.L., and Bechhoefer, J. (1993). Calibration of atomic‐force microscope tips. Rev. Sci. Instrum. 64, 1868–1873.

Jauvert, E., Dague, E., Séverac, M., Ressier, L., Caminade, A.-M., Majoral, J.-P., and Trévisiol, E. (2012). Probing single molecule interactions by AFM using bio-functionalized dendritips. Sens. Actuators B Chem. 168, 436–441.

Kapteyn, J.C., Ram, A.F., Groos, E.M., Kollar, R., Montijn, R.C., Van Den Ende, H., Llobell, A., Cabib, E., and Klis, F.M. (1997). Altered extent of cross-linking of beta1,6-glucosylated mannoproteins to chitin in Saccharomyces cerevisiae mutants with reduced cell wall beta1,3-glucan content. J. Bacteriol. 179, 6279–6284.

Klis, F.M., Mol, P., Hellingwerf, K., and Brul, S. (2002). Dynamics of cell wall structure in Saccharomyces cerevisiae. FEMS Microbiol. Rev. 26, 239–256.
Kollar, R., Reinhold, B.B., Petrakova, E., Yeh, H.J., Ashwell, G., Drgonova, J., Kapteyn, J.C., Klis, F.M., and Cabib, E. (1997). Architecture of the yeast cell wall. Beta(1-->6)-glucan interconnects mannoprotein, beta(1-->)3-glucan, and chitin. J. Biol. Chem. 272, 17762–17775.

Lagorce, A. (2003). Genome-wide Analysis of the Response to Cell Wall Mutations in the Yeast Saccharomyces cerevisiae. J. Biol. Chem. 278, 20345–20357.

Magnelli, P., Cipollo, J.F., and Abeijon, C. (2002). A Refined Method for the Determination of Saccharomyces cerevisiae Cell Wall Composition and [beta]-1,6-Glucan Fine Structure. Anal. Biochem. 301, 136.

Mouyna, I. (2000). Glycosylphosphatidylinositol-anchored Glucanosyltransferases Play an Active Role in the Biosynthesis of the Fungal Cell Wall. J. Biol. Chem. 275, 14882–14889.

Osumi, M. (1998). The ultrastructure of yeast: Cell wall structure and formation. Micron 29, 207–233.

Pagé, N., Gérard-Vincent, M., Ménard, P., Beaulieu, M., Azuma, M., Dijkgraaf, G.J.P., Li, H., Marcoux, J., Nguyen, T., Dowse, T., et al. (2003). A Saccharomyces cerevisiae Genome-Wide Mutant Screen for Altered Sensitivity to K1 Killer Toxin. Genetics 163, 875–894.

Pelling, A.E., Sehati, S., Gralla, E.B., Valentine, J.S., and Gimzewski, J.K. (2004). Local nanomechanical motion of the cell wall of Saccharomyces cerevisiae. Science 305, 1147–1150.

Popolo, G., D, G., P, B., and M, V. (1997). Increase in chitin as an essential response to defects in assembly of cell wall polymers in the ggp1delta mutant of Saccharomyces cerevisiae. J. Bacteriol. 179, 463–469.

Schiavone, M., Vax, A., Formosa, C., Martin-Yken, H., Dague, E., and François, J.M. (2014). A combined chemical and enzymatic method to determine quantitatively the polysaccharide components in the cell wall of yeasts. FEMS Yeast Res. n/a – n/a.

Shaw, J.A., Mol, P.C., Bowers, B., Silverman, S.J., Valdivieso, M.H., Durán, A., and Cabib, E. (1991). The function of chitin synthases 2 and 3 in the Saccharomyces cerevisiae cell cycle. J. Cell Biol. 114, 111–123.

Touhami, A., Nysten, B., and Dufrêne, Y.F. (2003). Nanoscale Mapping of the Elasticity of Microbial Cells by Atomic Force Microscopy. Langmuir 19, 4539–4543.

Chapter IIIB: STUDY OF FOUR INDUSTRIAL STRAINS

Integration of transcriptomic, biophysical and biochemical data to unravel molecular cues implicated in cell wall organization and properties between different industrial strains

Marion Schiavone[1, 2, 3, 4, 6]; Sébastien Déjean[1,5]; Nathalie Sieczkowski[6] ; Mathieu Castex[6]; Etienne Dague[1, 4], Jean Marie François*[1,2,3]

1 Université de Toulouse; INSA, UPS, INP, 135 avenue de Rangueil, F-31077 Toulouse, France

2 INRA, UMR792 Ingénierie des Systèmes Biologiques et des Procédés, F-31077 Toulouse, France ;

3 CNRS, UMR5504, F-31400 Toulouse, France 135 avenue de Rangueil, F-31077 Toulouse, France ;

4 CNRS; LAAS ; 7 avenue du colonel Roche, F-31400 Toulouse, France ;

5 Institut de Mathématiques de Toulouse, 118 route de Narbonne, F-31062 Toulouse, France

6 Lallemand SAS, 19 rue des briquetiers, 31702 Blagnac, France

*Correspondance to Jean Marie François; LISBP INSA, 135 Avenue de Rangeuil, F-31077 Toulouse cedex 04 ; Email: fran_jm@insa-toulouse.fr; Phone: +33(0) 5 61 55 9492

Running Title:

Keywords: Cell wall, β-glucan, chitin, yeast, atomic force microscopy, microarrays, architecture.

ABSTRACT

Since the past twenty years, original industrial applications for yeast cell wall have been created. Different companies sell autolysed yeast enriched of cell wall as prebiotic in animal nutrition or in wine making to improve the sensorial effects of wine. However, the cell wall composition and characteristics of industrial strains are not well known. In this study, we acquired different quantitative data on 4 industrial strains by measuring the cell wall composition and biophysical properties such as cell elasticity, cell surface adhesion and interaction with an AFM tip functionalized with concanavalin A. We combined these datasets with transcriptomic data and performed a comparative analysis in order to search for correlation between cell wall composition cell surface characteristics and genes that are involved in these properties. Each industrial strain was characterized by their specific nanomechanical property, cell wall composition and transcriptome profile. Using a mathematical method based on covariance association, we found close associations between cell elasticity and β-1,3-glucans with genes implied in membrane, cytoskeleton assembly (*SLA1*), β-1,6-glucan biosynthesis (*KRE11*) and MAPK signalling pathways (*STE11, HOG1, DIG1*). On the other hand, a correlation between mannan and chitin in the cell wall was identified with the frequency of adhesion events at the cell surface and genes correlating with these physico-chemical traits were involved in protein processing, ergosterol biosynthesis and cell wall mannoproteins biosynthesis.

I. INTRODUCTION

In the past years, given the fact that yeast cell wall has been shown to have a favourable effect on stability and quality of wines, the interest of this structure has greatly increased. Yeast cell walls were used for the first time by Lafon-Lafourcade in 1984 (Lafon-Lafourcade et al., 1984) to remove medium-chain fatty acid inhibitors of alcoholic and malolactic fermentations. Now, different industrial companies sell them but their composition and characteristics are not always well known. The outer layer of this envelope is mainly made of mannoproteins (proteins highly N- or O-glycosylated with mannose residues linked in α-1,2, α-1,3 and α-1,6) when the inner layer is a network of cross-linked polysaccharides constituted by β-1,3 and β-1,6-glucan (glucose units connected either by a β-1,3 or β-1,6-linkage) with a minor content of chitin (a β-1,4-N-acetylglucosamine polymer) (Klis et al., 2006; Lesage and Bussey, 2006). Each of these polysaccharides presents interesting biotechnological properties. In the winemaking, cell wall mannoproteins have been reported to interact with aroma

compounds (Chalier et al., 2007) and thiols (Tirelli et al., 2010). Some studies have also shown the use of these compounds to form a protective capsule for the probiotic bacteria (Katakura et al., 2010; Millsap, 1998), resulting in an enhancement of the bacterial survival and the stimulation of their growth (Katakura et al., 2010; Suharja et al., 2014). Moreover it was demonstrated the strong immunostimulatory activity of β-glucan (Brown and Gordon, 2003; Novak and Vetvicka, 2009) that constituted the major component of the cell wall, providing different beneficial effects on health and resistance to diseases and cancer (see reviews (Kogan and Kocher, 2007) and (Chen and Seviour, 2007)). However, biochemical analyses have allowed determining that the cell wall composition and properties are dependent to the yeast strains (Nguyen et al., 1998), which can significantly impact on their industrial properties. Therefore in order to guide the emergence of original application for the yeast cell walls, it is mandatory to get a better understanding of how the cell wall characteristics such as cell wall elasticity, adhesion and composition of industrial strains can be associate to gene expression.

To reach this goal, we used an original combination of an acido-enzymatic method to measure the amount of each polysaccharide that formed the cell wall (Schiavone et al., 2014) and atomic force microscopy (AFM) (Binnig et al., 1986), which allows imaging the structure of living cells and measure their local surface properties such as elasticity (Arfsten et al., 2010; Mercadé-Prieto et al., 2013) and polysaccharides properties (Alsteens et al., 2008). In a previous study combining cell wall composition measurements, nano-indentation and Single Molecule Force Spectroscopy (SMFS) experiments on yeast mutants such as *gas1*Δ, *chs3*Δ and *mnn9*Δ, we have confirmed our previous statement (Dague et al., 2010) that nanomechanical properties are more correlated to the cross-linked and remodeling of cell wall polysaccharides than the biochemical composition. Moreover, we used the transcriptome profiles of these mutants to identify the cellular differences. In this way, we have highlighted that genes upregulated in *gas1*Δ and involved in membrane cytoskeleton assembly and mannoprotein glycosylation are associated with higher amounts of mannans in the cell wall and lectin-interactions.

Genome-wide transcriptome analysis can reveal relationship between gene and cellular function. Based on this principle, and using dedicated biostatistical tools it is possible to predict functional gene clusters and groups of genes that contribute to biological processes. However these approaches used one type of data. Instead, integrative approaches can associate two types of datasets such as microarrays, metabolomics or proteomic data. In this work, we used an integrative approach that

combined transcriptomic and cell wall measurements datasets to highlight correlation between genes expression, cell wall composition and cell surface characteristics, with the expectation to underscore molecular cues that can contribute to a better understanding of cell wall structure and organization, such as genes that are linked determine to physico-chemical properties of the cell wall. To this end, cell wall composition measurements (*i.e.* mannans, chitin, β-1,3-glucan, β-1,6-glucan), quantitative data on biophysical properties (*i.e.* cell wall elasticity, percentage of interaction concanavalinA with mannans, length of the molecule unfolded) and transcriptome profile of 4 different, albeit all wine industrial strains, and of a laboratory strain were gathered for this integrative analysis.

II. MATERIAL AND METHODS

Strains and growth conditions

Four strains named L71, L69, L62 and L60 were provided by Lallemand Inc. (Montréal, Canada) and three of them are *Saccharomyces cerevisiae* with oenological origin. The strain *Saccharomyces cerevisiae* BY4743 (MAT**a**/α his3Δ1/his3Δ1 leu2Δ0/leu2Δ0 LYS2/lys2Δ0 met15Δ0/MET15 ura3Δ0/ura3Δ) from Euroscarf collection was used as diploid control. Cells were grown at 30°C with agitation in a rich medium (YPD; 2% glucose, 1% peptone, 1% yeast extract).

Cell wall isolation and quantification of polysaccharides

Two independent biological cultures were carried out in 200 ml of YPD in a 1 L shake flasks on a rotary shaker set at 200 rpm at 30°C. Cells were collected during the exponential phase until $2x10^7$ cells (OD_{600}=1). Cells were harvested by centrifugation 10 min at 4000 rpm and washed at least two times with sterile water. The pellets were kept to isolate cell walls. Cell walls were isolated and purified by centrifugation and extensive washing as described in (Francois, 2006). Polysaccharides mannan, chitin, β-1,3- and β-1,6-glucan in the purified cell walls were determined as described in (Schiavone et al., 2014). Quantification of the released monomers (mannose, glucose and N-acetylglucosamine) was determined by high performance anionic exchange chromatography (HPAEC) coupled to amperometric detection as described by (Dallies et al., 1998) and colorimetric method, respectively (Reissig et al., 1955).

AFM measurements

Sample preparation

Strains were stocked at -80°C, revivified on Yeast Peptone Dextrose agar (242720530, Difco) and grown in 5 mL of Yeast Peptone Dextrose broth (242820530, Difco) at 30°C under shaking. Yeasts

cells were collected at the exponential phase (OD_{600}~1), washed two times in acetate buffer (18 mM CH_3COONa, 1 mM $CaCl_2$, 1 mM $MnCl_2$, pH = 5.2), resuspended in the same buffer, and immobilized on polydimethylsiloxane (PDMS) stamps prepared as described in (Dague et al., 2011). . Briefly, freshly oxygen activated microstructured PDMS stamps were covered by a total of 100 µL of the solution of cells. The cells were then deposited into the microstructures of the stamp by convective/capillary assembly.

AFM imaging and force spectroscopy

Images and force-distance curves were recorded at room temperature in acetate buffer using an AFM Nanowizard III (JPK Instruments, Berlin, Germany) and MLCT AUWH cantilevers (Brüker, Santa Barbara, USA). The spring constants of the cantilevers were systematically measured by the thermal noise method (Hutter and Bechhoefer, 1993) and were found to be in the range of 0.01-0.02 $N.m^{-1}$. Images were recorded in Quantitative Imaging™ mode (Chopinet et al., 2013) and the maximal force applied to the cell was limited to 1.5 nN. Mechanical properties were mapped by recording an array of 32x32 force-distance curves using a maximal applied force of 0.5 nN. Elasticity histograms were generated by analyzing with OpenFovea software (Roduit et al., 2012) the force (F) curves according to the Hertz model with an indentation (δ) of 50 nm and taking into account a conical tip geometry with an half-opening angle α of 0.31 rad and a Poisson ratio (v) of 0.5:

$$F = \frac{2E \tan \alpha}{\pi \, (1 - \nu^2)} . \delta^2$$

The value of the Young modulus (E) is determined as the maximal value of the histogram.

For probing cell surface polysaccharides, AFM tips were functionalized with the lectin concanavalin A from *Canavalia ensiformis* (Sigma-Aldrich) via a dendritip as described in (Jauvert et al., 2012). The coupling with the lectin was made by immersion of the dendritip in 100 µL of conA solution (100 $\mu g.mL^{-1}$ in 0.1 M carbonate buffer). After 1 hour of incubation, 100 µL of $NaBH_4$ (3.5 $mg.mL^{-1}$) solution was added and incubated 15 min in order to reduce the unreacted groups. Finally, the cantilever was washed three times and stored in acetate buffer. To analyze the stretching of polysaccharides at the surface of the cell, elongation forces were described using the freely jointed chain (FJC) model or the worm like chain (WLC) model (Janshoff et al., 2000).

The FJC model described the polymer as a suit of segments (called ‘Kuhn segments’) with the same energy and a random orientation: $x(F) = L_c[\coth(Fl_k/k_bT) - k_bT/Fl_k]$

Where F is the extension force (N), x is the extension of polymer (m), k_b is the Boltzmann constant and T the absolute temperature. l_k is the Kuhn length, which represents a length of one segment (m) and L_c (m) is the contour length which is the total length of polymer stretched. For n segments: $L_c=nl_k$.

The WLC model introduced by (Bustamante et al., 1994)which describes the polymer as a curved filament and the force F vs the extension x is given by: $F(x) = k_bT/l_p [0.25 (1-x/L_c)^{-2} + x/L_c -0.25]$

Where L_c is the contour length, l_p is the persistent length, k_b is the Boltzmann constant, T the absolute temperature. This model has already been successfully used for the stretching of polysaccharides of yeasts especially *S. cerevisiae* and give the best fitting of force curves (Alsteens et al., 2008; Francius et al., 2009).

DNA microarray analysis

Three independent biological cultures were carried out in 50 ml of YPD in a 250 mL shake flasks on a rotary shaker set at 200 rpm at 30°C. Yeast cells (about 10 OD_{600} units) were collected at OD600=1 by centrifugation (3,000 rpm, 4°C, 2 min), followed by a washing step with 1 mL of sterilized water. The cell pellets were immediately frozen in liquid nitrogen and stored at -80°C until RNA extraction.

Total RNA extraction and DNA microarray

Frozen cells were mechanically disrupted using a ball mill (MicroDismembrator Braun, Melsungen, Germany). Total RNA was extracted using SV Total RNA Isolation System (Promega) following the protocol of the Manufacturer. The quantity of extracted RNA was controlled using Nanodrop ND-1000 (Nanodrop Technologies) and the quality was determined by microcapillarity electrophoresis using a Bioanalyzer 2100 (Agilent Technologies, Wilmington, USA). Incorporation of Cyanine 3 was performed during reverse transcription of total RNA using the Low Input Amp Labeling kit (Agilent Technologies, Wilmington, USA) and following the One-Color Microarray-Based Gene Expression Analysis Protocol. Labeled cDNA from the microarray experiments was purified and hybridized on Agilent glass slides, which bear the whole *Saccharomyces cerevisiae* genome (see details at http://www.biocompare.com/ProductDetails/760330/S-cerevisiae-Saccharomycescerevisiae-Whole-Genome.html). Hybridization was carried out in an automatic hybridization chamber (Agilent Technologies, Wilmington, USA) for 17 hr at 65°C. The hybridization signals were detected by scanning using Innoscan 900 laser Scanner (Innopsys Instruments), and transformed to numerical values using Feature Extraction V.11.5.1.1. The microarrays hybridization and processing were carried out at the Transcriptome-Biochips Platform of Toulouse (http://biopuce.insa-toulouse.fr).

Data analysis

Transcriptome analyses were done in R computing environment (www.R-project.org) using the limma package (www.bioconductor.org). The estimates used for the foreground and background intensities were the median of pixels intensity. Raw data were imported into R and spot quality weights were performed assigning a weight of 1 or 0 to each spot. Low-quality spots, non-uniform spots, spots with low signal/background ratio or spots with low signal-to-noise ratio and empty or non-validated spots were down weighted. Data were preprocessed by base 2 logarithmic transformation and within-array normalized was performed using the weighted global median (spots with zero weight were not included in the normalization). To achieve consistency of expression values between arrays, quantile normalization across all the microarrays for each strain was performed. After normalization, the expression of a gene was calculated by the median of replicate spots within each microarray. Gene expression data for both strains were pairwise compared using the limma package (Smyth, 2005). Genes with significant evidence for differential expression were identified with a modified T-test in conjunction with an empirical Bayes method to moderate the standard errors of the estimated log-fold changes. The p-values for the contrast of interest were adjusted for multiple testing by the "BH" method (Hochberg and Benjamini, 1990).

Relationships between gene expression, biochemical and biophysical data

By using the package mixOmics by R software (Lê Cao et al., 2009; González et al., 2012), a partial least square (PLS) regression was performed in order to identify and measure the associations among the set of variables. This multidimensional method is used for an explorative analysis and is based on the same principle of principal component analysis (PCA) in order to research high covariance between variables. Specific functions were based on the Saccharomyces Genome Database (http://www.yeastgenome.org).

III. RESULTS AND DISCUSSION

Strain dependency of cell wall composition and cell wall nanomechanical properties

The cell wall composition of the four industrial strains was determined by acid and enzymatic hydrolyses. From this determination, we observed differences in levels of each constituent. As shown in Table III B-1, levels of mannan in the cell walls prepared from industrial strains account for 39-45% of their cell wall. This result is in agreement with the fact that the content in mannoproteins of wine yeasts is usually higher than in other types of yeast, because this component is favourable in wine

fermentation such as in the stability of wine against protein haze (Gonzalez-Ramos et al., 2009). Additionally, β-1,3-glucan and β-1,6-glucan have different proportions, suggesting a different structure and/or cross-linking between the polysaccharides. Therefore, all these results confirm that the cell wall composition is highly specific to the strain.

Table IIIB-1. Cell wall composition of wine yeasts.

Strain	chitin	β-1,3-glucan	β-1,6-glucan	mannans
L71	48.2 ± 21.4	248.2 ± 46.8	197.8 ± 73.9	318.3 ± 62.4
L69	30.0 ± 8.6	308.0 ± 46.6	142.0 ± 14.3	370.5 ± 43.6
L60	44.4 ± 6.7	297.5 ± 99.8	190.8 ± 54.0	449.4 ± 67.1
L62	136.2 ± 59.3	210.6 ± 27.5	187.5 ± 66.4	433.6 ± 48.8

Cell wall composition was determined in exponentially growing yeast cells in YPD as described in Material and Methods. Data are expressed as µg of residues per mg of cell wall dry mass and they are the mean values ± SD obtained from two independent experiments made in biological triplicates.

To evaluate potential linkage between the cell wall composition and to cell wall structure we determined the elasticity of the cell wall by performing nano-indentations experiments by AFM. As the AFM tip is pushed on the yeast cell, the deformation depth (indentation) can be determined and plotted as a function of the force applied on the cell. As already explained earlier (see also Material and Methods section), the use of the Hertz Model for each indentation versus force curve (1024 curves per cell), generates a distribution of Young Modulus values. These values gave information on the elasticity of the cell and can be adjusted to a Gaussian law in order to describe the mean Young modulus value and standard deviation (Figure IIIB-1). The measurements were performed on area devoid of bud scars and on independent cells, for statistical significance of the data. The elasticity of exponential cells showed a high variability between the strains. Indeed, the four industrial strains exhibited a different Young modulus, which ranged from 637 kPa for strain L71 to 239 and 230 for strain L69 and L62 strain respectively. As it is not clear to find a direct link between cell all composition and cell wall elasticity properties, the difference in the Young modulus between the strains can be ascribed to the molecular organization of the cell wall, namely the linkages between cell wall components, as we already proposed, based on analyses carried out on cell wall related mutants (Dague et al., 2010 and chapter IIIA).

Cell surface properties are highly specific to the strain

Due to the beneficial effects of mannoproteins during wine fermentation, increase interest has been observed for these complex carbohydrates. To unfold individual mannan oligosaccharides, AFM

tips were functionalized with Concanavalin A (ConA). We investigated the distribution, adhesion and extension of mannans on the surface of industrial yeast cells (Fig. IIIB-2). Adhesion force maps, adhesion force histograms and typical retract force curves were recorded with AFM tips functionalized with the lectin on the surface of the industrial strains. The adhesion force histograms indicate a maximal value centred above 50-60 pN (n=1024), which corresponded to a single lectin-mannose interaction (Francius et al., 2009). Adhesion force of 100-200 pN range were attributed to the unfolding of two or three mannose residues (Alsteens et al., 2008). In L71 and L60 strain, single or double adhesion events were observed with rupture distance in the 0 to 100 nm range. On the contrary on L69 cell, which is highly adhesive (see adhesion image recorded in QI™ mode), multiple adhesion events were detected with greater adhesion forces and much longer rupture lengths ranging from 20 to 400 nm that fitted quite well with the worm-like chain (WLC) model, but not with the freely jointed chain (FJC) model. In this model, the polymer is described as a filament that is continuously flexible, with successive segments that pointed in the same direction. This is particular relevant when polymers have a high stiffness. In contrast, with the FJC model the polymer can only disorder at the joints between distinct segments called 'Kuhn segments'. Therefore, the fact that that elongation forces were at long rupture distances and were well fitted with a WLC model could indicate that long chains of mannoproteins are stretched rather than mannan oligosaccharides. This result can be explained by the increase of cell wall mannoproteins and the difference in their anchorage into the cell wall in L69 as compared to the other industrial strains.

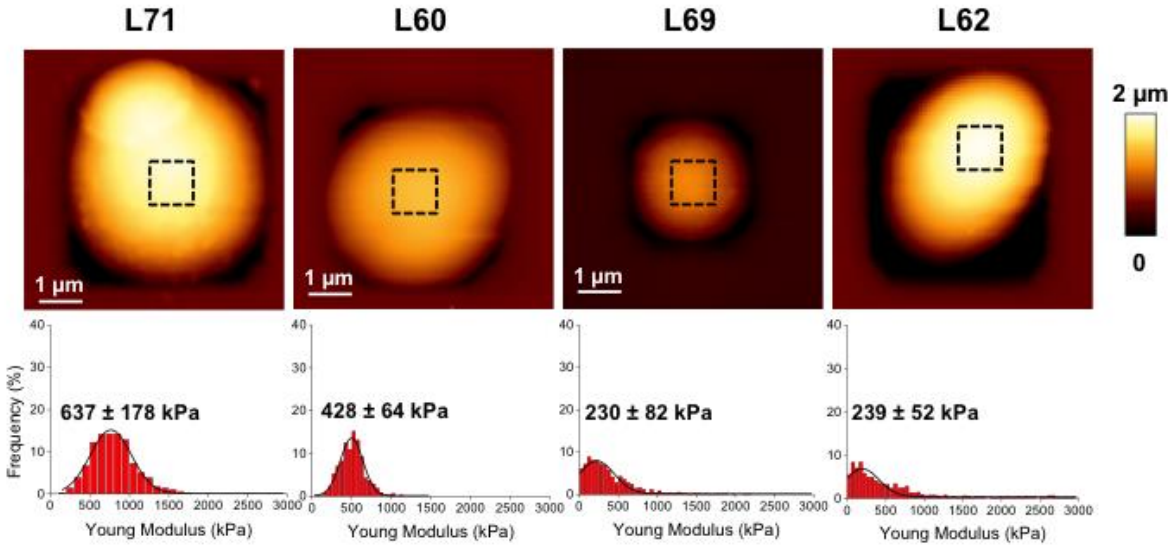

Figure IIIB-1. Cell wall elasticity of industrial strains

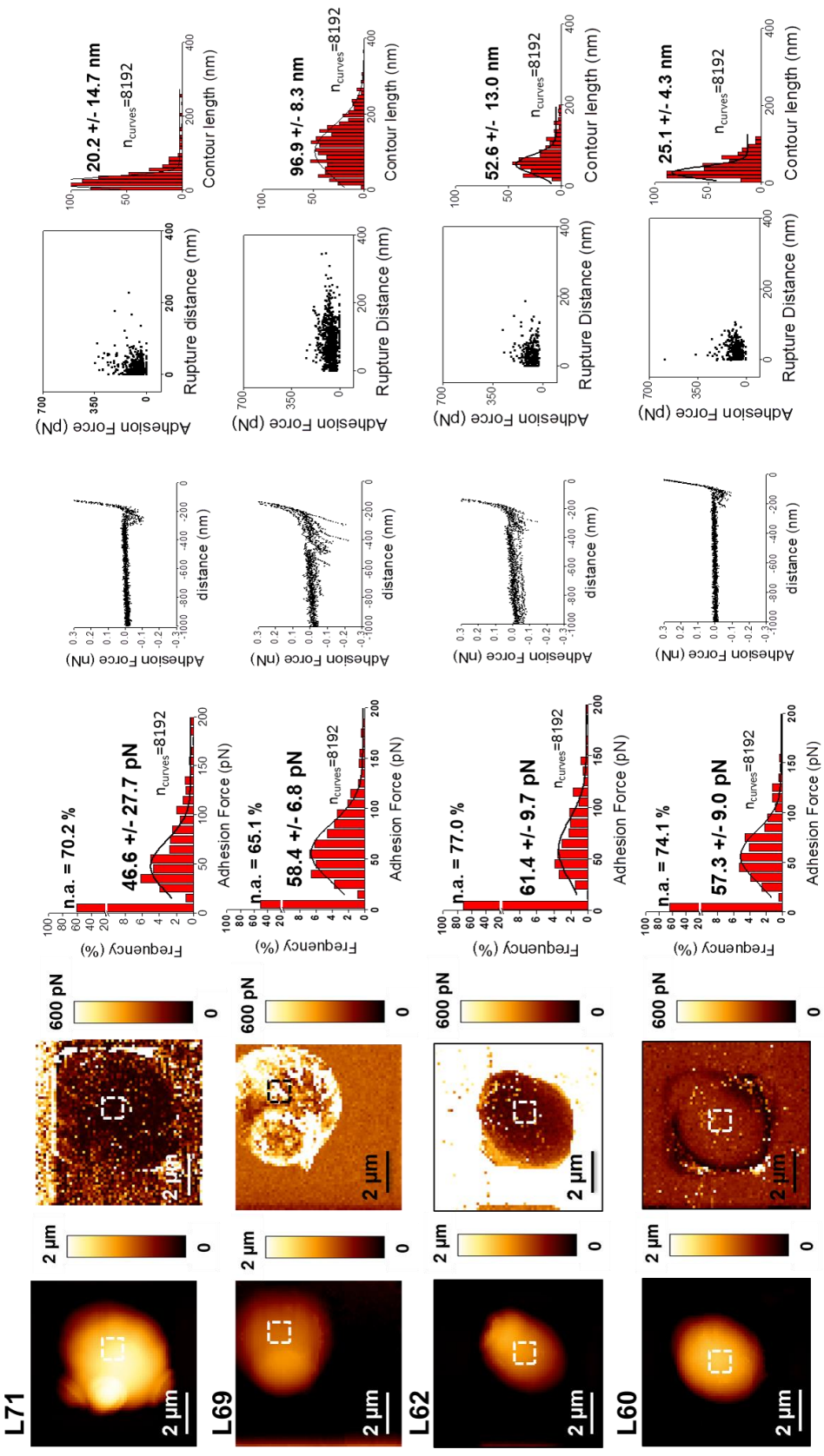

Figure IIIB-2. Probing cell wall architecture of industrial strains with AFM tips functionaliezd with concanavalin A lectin
AFM height (A) and adhesion (B) images of 4 industrial strains. Adhesion force of conA-tips with cells obtained on 8 cells from 3 independent experiments (8192 curves were analyzed with JPK data processing). Superposition of 10 typical retract force curves (C). Repartition of adhesion forces in function of rupture distance (E). Contour length of the stretch molecule (F).

Global gene expression changes in industrial wine yeasts

As our purpose was to correlate nanomechanical properties of the yeast cell wall to genetic data, we sought to determine the transcriptome of each industrial strain using cDNA. The transcriptomic data were acquired from three independent experiments and were analyzed using a principal component method developed by (Lê Cao et al., 2011) and termed 'sparse-PLS regression analysis' that allows highlighting similarities and dissimilarities between samples (here between transcriptomes from each strain). As shown in the figure IIIB-3, in which the three transcriptome replicates per strain were represented in a Sparse PLS regression graphical, the position of the five strains to each other could be nicely attributed. The transcriptome of the diploid laboratory strain BY4743 is found significantly distant from the four industrial yeasts (L71, L69, L62, L60), whereas between these latter industrial strain, we could see a proximity of transcriptome for strains L60 and L62, with the transcriptome of strain L69 slightly different but close to that of these two former strains. In contrast, the strain L71 exhibits a transcriptome that is far distant to both these three other industrial strain as well as to the lab strain BY4743.

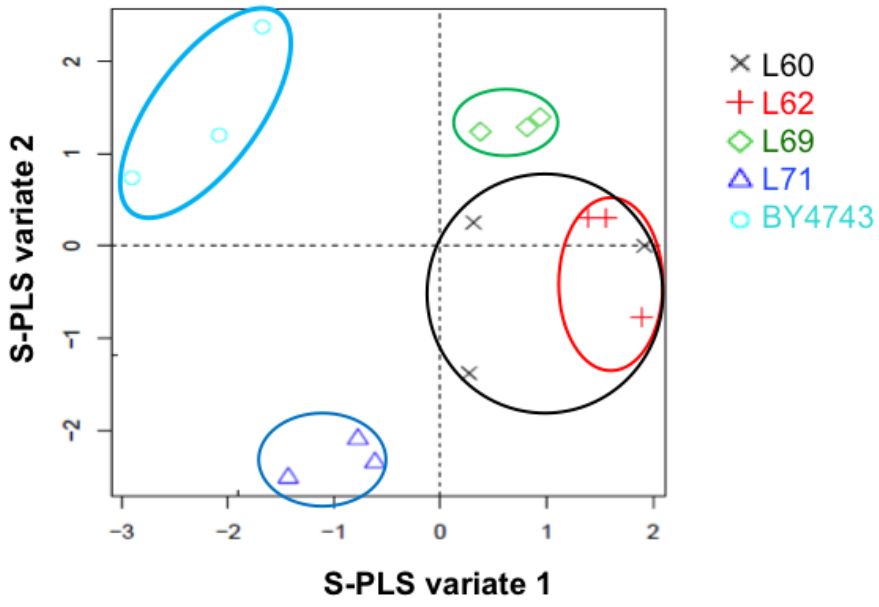

Figure IIIB-3. Sample representation.
Sample representation using Sparse PLS regression with no variable selection.

To examine more carefully the specificity among transcriptome of industrial strains, we have expressed the transcriptomic data of each of them, relative to that of the laboratory diploid strain BY4743, used as reference (since it is the strain with the sequenced genome). We retained genes that were differentially expressed by a factor of two-fold ratio (higher or lower expression than those of the

lab strain) at a *p*-value of 5% after data normalisation. From transcriptomic data, we observed a large number of differentially expressed genes between strains. Of these, 162, 210, 190 and 166 genes were upregulated in L71, L69, L62 and L60, respectively as compared to the laboratory strain BY4743. Among the differentially expressed genes, many genes were common in the wine strains (Figure IIIB-4). For example, L71 strain has 162 differentially expressed genes with 105 genes common to L69, 87 genes similar to L62 strain and 85 genes common to L60 strain. Comparative analysis of the differentially expressed genes revealed 71 genes common to the four industrial strains that were either higher or lower expressed than in the BY4743. This list of 71 common genes is shown in figure IIIB-5.

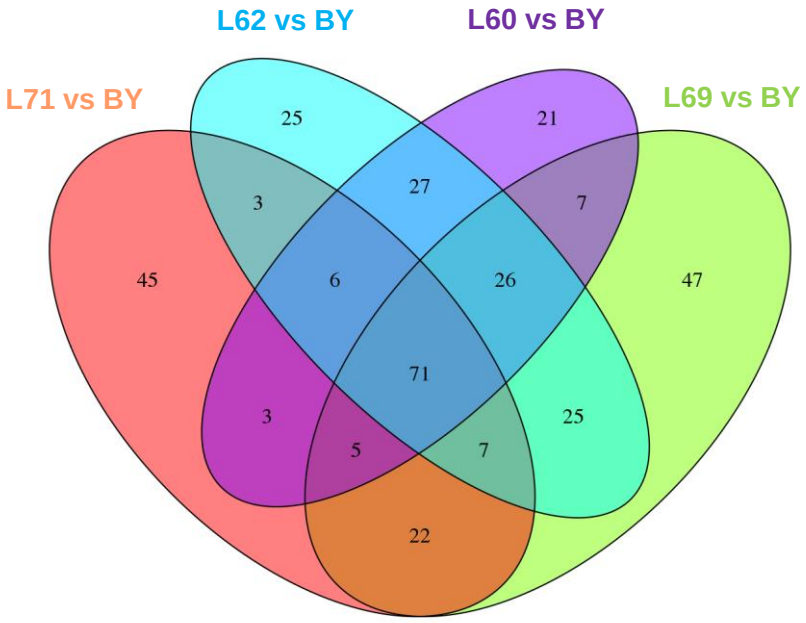

Figure IIIB-4. Representation of differentially expressed genes in the industrial strains compared to reference strains. Number indicates genes differentially expressed.

As shown in Figure IIIB-5, the transcriptomic profile of L71 is different to that of L69 and L60 strains. We observed two parts, noted A and B, were these differences were the most pronounced. In the part A, the genes in this region are mainly downregulated for the L71 strain as compared to the three other industrial strains, whereas in B, they are mainly upregulated, suggesting some biological peculiarity in this L71 strain as compared to the three others industrial strains, even though all being used in wine production.

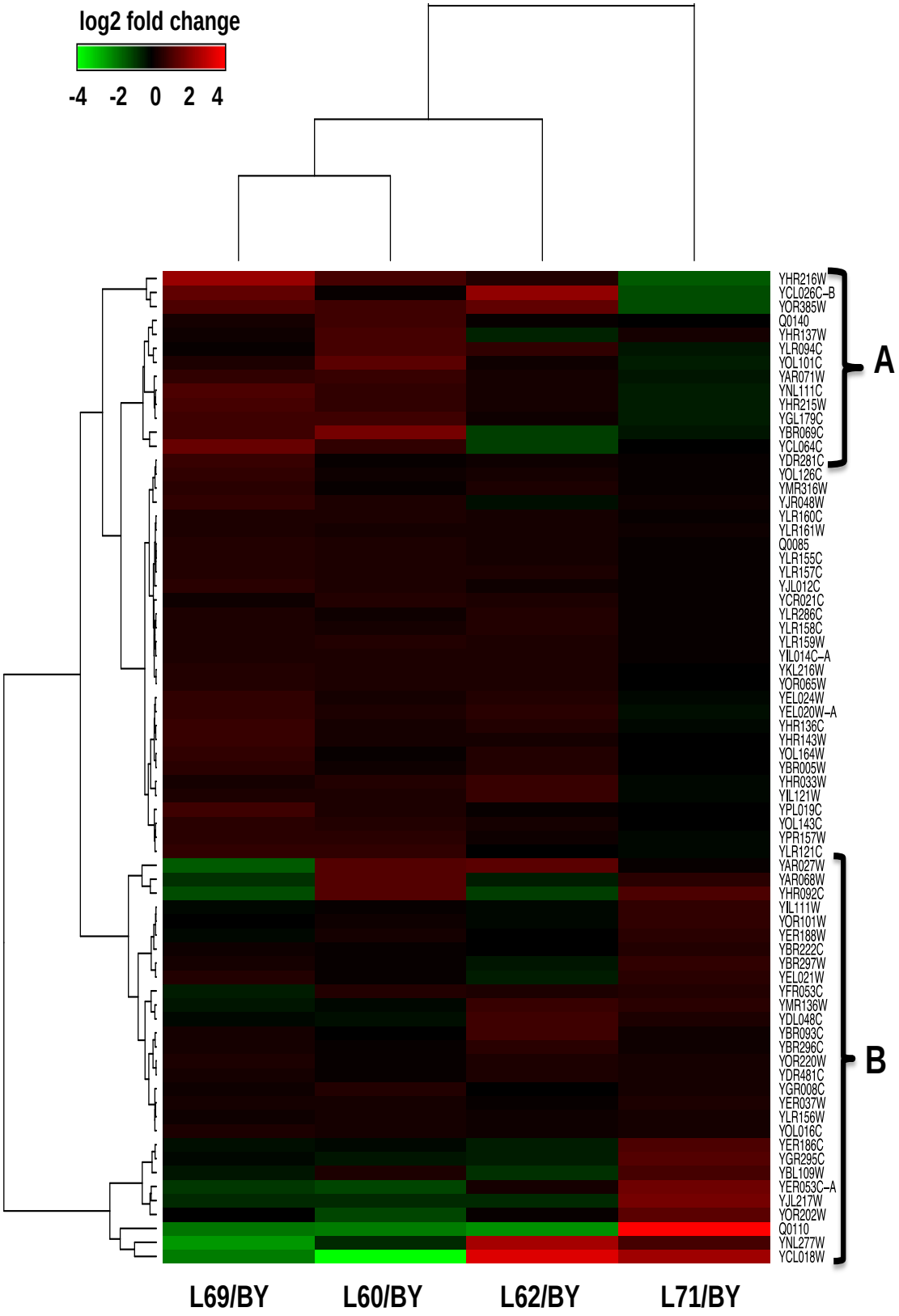

Figure IIIB-5. Heatmap of common genes differentially expressed in wine yeasts as compared to laboratory strain (in yeast peptone dextrose medium).

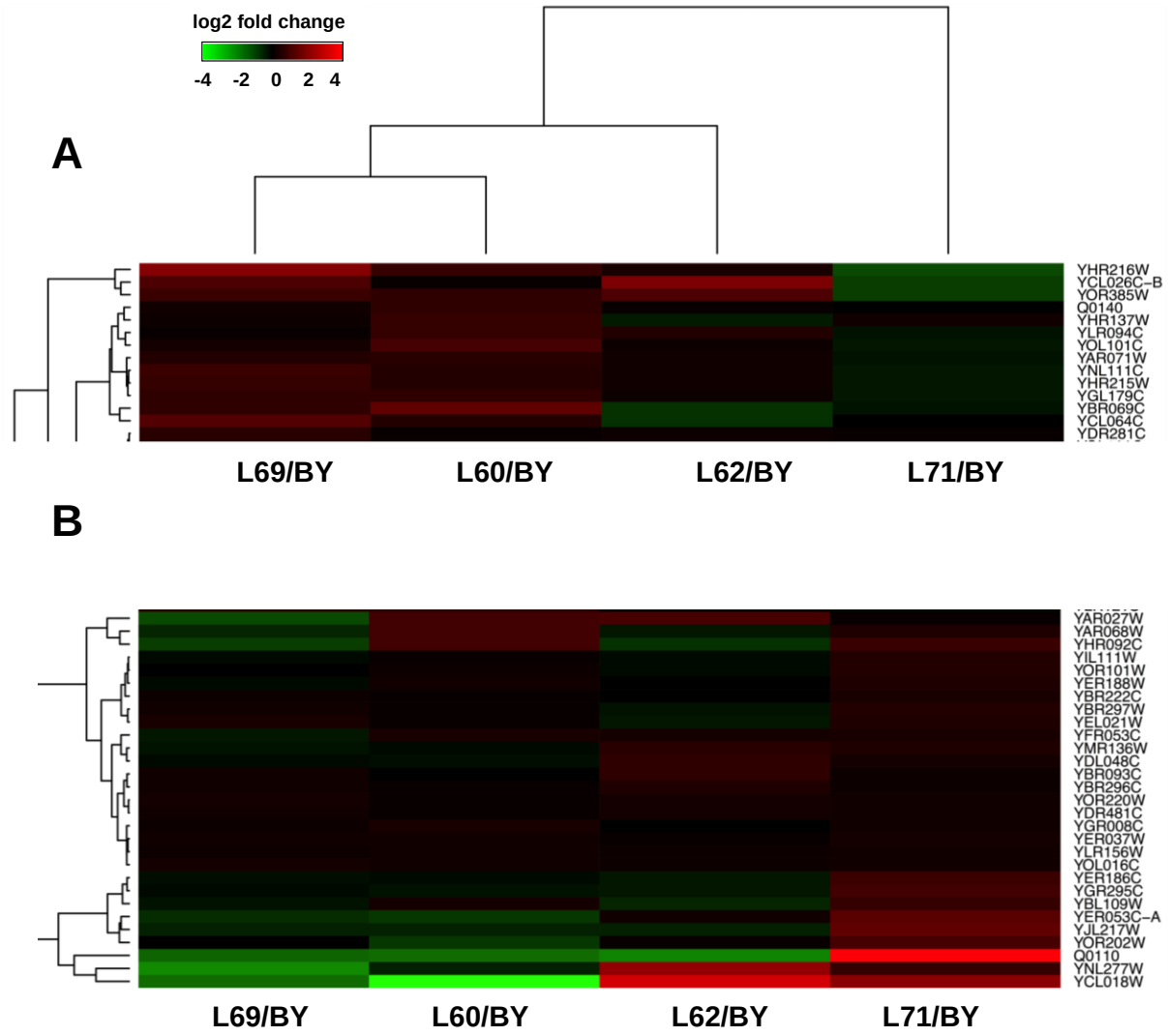

Figure IIIB-6. Upregulated and downregulated genes in wine yeasts as compared to laboratory strain (detailed of the Figure IIIB-5).

In the part A, we identified genes localized in cytoplasm (YHR216W/IMD2, YCL26C-B/HBN1, YOR385W), which were highly downregulated in L71 strain and upregulated in L69, L60 and L62 strains. *HBN1* encoded a NADPH nitroreductase and *IMD2* encoded an inosine monophosphate dehydrogenase that catalyzes the limiting step in GTP biosynthesis (Escobar-Henriques et al., 2003). Genes encoding acid phosphatases (*YAR071W/PHO11 and YHR215W/PHO10),* were downregulated in L71 and upregulated in L60 and L69. We also observed in this cluster *YGL179C/TOS3* encoding a protein kinase localized to the cytoplasm and activate the Snf1p kinase, which is required for the utilization of non-fermentable source. *TOS3* is downregulated in L71 and L62 strain, but upregulated in L60 and L69. In contrast, transcript levels of YBR069C/*TAT1* and YCL064C/*CHA1* were very low in L62 and highly increased in L69, as compared to the reference strain. These genes are required for

amino acids metabolism: YBR069C/*TAT1* encoded a transmembrane transporter and YCL064C/*CHA1* catalyzed the degradation of hydroxyl amino acids (serine and threonine) into pyruvate and α-ketobutyrate.

In the part B, we observed an upregulation in L62 strain of genes encoding acid phosphatases (*YBR093C/PHO5 and YDR481C/PHO8)* and YBR296C/PHO89 encoding a plasma membrane phosphate transporter. The activity of acid phosphatase is easily detectable, because they encode glycoproteins located in the cell wall (*YAR071W/PHO11, YHR215W/PHO10* and *YBR093C/PHO5*) or in the vacuole (*YDR481C/PHO8*). YDR281C/*PHM6* and YER307W/*PHM8* regulated by phosphate levels were also found in the cluster. Although *PHM6* was upregulated in L69, *PHM8* is upregulated in L60 and L71 strains. Expression of genes involved in the PHO system is controlling by the level of inorganic phosphate (Pi) in the growth medium. Therefore, the induction of *PHO* genes in L62 strain indicates an impairment of the Pi levels regulatory system in this strain. We also found in the cluster B some genes important for nutrient assimilation such as *YBR297W/MAL33, YHR092C/HXT4* and *YFR053C/HXK1*, which are regulated in response to carbon source. As *TOS3*, *YBR297W/MAL33* encoded a regulatory protein implied in maltose fermentation responded by an upregulation in L71 and L69 strain, but with lowest level of transcription in L62 strain, as compared to the reference strain. Important for glucose assimilation, *YFR053C/HXK1* encoded a hexokinase, which catalyzed glucose during its metabolism, whereas *YHR092C/HXT4* is one of the sugar transporters. *YFR053C/HXK1* and *YHR092C/HXT4* were downregulated in L69 strain but upregulated in L71 and L60 strains, suggesting that glucose was well metabolized in L71 and L60 than L69 strain. Genes involved in cellular respiration (YIL111W/*COX5B*) and amino acid biosynthesis (YEL021W/*URA3, YNL277W/MET2, YCL018W/LEU2, YOR202W/HIS3*) showed upregulation in L71. Taking together these results suggest that L71 strain would have a better assimilation of both nutrient and glucose as compared to the laboratory strain and the other industrial yeasts.

Furthermore, the genome-wide transcriptomic analysis of industrial strains cultivated in rich medium showed a pronounced difference in the expression of selected genes with the diploid 'wild-type' strain BY4743. Indeed, the ASP gene family (*YLR155C/ASP3-1, YLR157C/ASP3-2, YLR158C/ASP3-3* and *YLR160C/ASP3-4)* was downregulated more than 300-fold upon industrial strains. In budding yeast *Saccharomyces cerevisiae*, the asparagine degradation pathway comprised five asparaginase (*ASP*) genes located at two separated loci. *ASP3* is located on chromosome XII and

is repeated four times to create a gene cluster including *ASP3-1, ASP3-2, ASP3-3* and *ASP3-4*. These four identical genes are induced during nitrogen starvation (Bon et al., 1997) and code for cell-wall asparaginase II, which hydrolyses L- or D-asparagine to aspartate and ammonia (Kim et al., 1988). The depletions of the copies of *ASP3* in industrial strains is in line with previous results, that showed their absence in the genomes of 128 fungal species, with no specificity to clinical, wine or brewing phenotypes (League et al., 2012). By using comparative genome hybridization on array of brewing yeasts (Pope et al., 2007) or wine yeasts including clinical and commercial isolates (Carreto et al., 2008), they have found the absence of *ASP3* genes in all strains, whereas they are present in the laboratory strain S288c, from which BY4743 is a derivative. Therefore, *ASP3* can be used as a discriminant factor for fermentative yeasts, since it can be found in variable copy number (from 0 to 4) in wine and brewing yeasts.

From the transcriptomic profiles of wine yeast strains, we retrieved about 80 genes differentially expressed between industrial and laboratory strain that are linked to cell wall architecture and remodelling (Figure IIIB-7). The representation of the transcription levels of these genes illustrates the proximity between the strains. Again, we could show that the gene profiles of L60 and L69 were similar, whereas that of L71 strain was more distant. From this gene list, we highlighted an area C that corresponded to genes that were either upregulated or downregulated in industrial strain with respect to reference strain. This region is illustrated in Figure IIIB-8. In this heatmap, we found differences in reexpression of *FLO* genes implicated in cell-cell adhesion (*FLO5/YHR211W, FLO10/YKR102W, FLO11/YIR019C*), as well as in the expression of the pseudogene *YHR213W* which shares sequence similarity with *FLO1* (Teunissen and Steensma, 1995). In L60 strain, those floculin-encoded genes are all upregulated, while they are downregulated in strain 71 and only *FLO11* and *YHR231W* are upregulated in L69. However, in previous AFM experiments we only observed highly adhesion properties in L69 strain, and not in L60, which suggest that the adhesion properties could be specific to Flo11 protein that is likely abundant in L69 due to overexpression of its corresponding gene. Also, the fact that no significant adhesion was found in the L60 strain could be explained by the weak up-regulation of *FLO5/FLO10/FLO11* (only a 2-fold increase compared to lab strain). On the other hand upregulation of genes which encode mannoproteins anchored into the cell wall via a glucosylphosphatidylinositol (GPI) anchor (*FIT2/YOR382W, FIT3/YOR383C*) in L60 strain and in L69 strain (*YIL011W/TIR3*) could explain the higher content of mannan in the cell wall of these two strains

(Table IIIB-1).

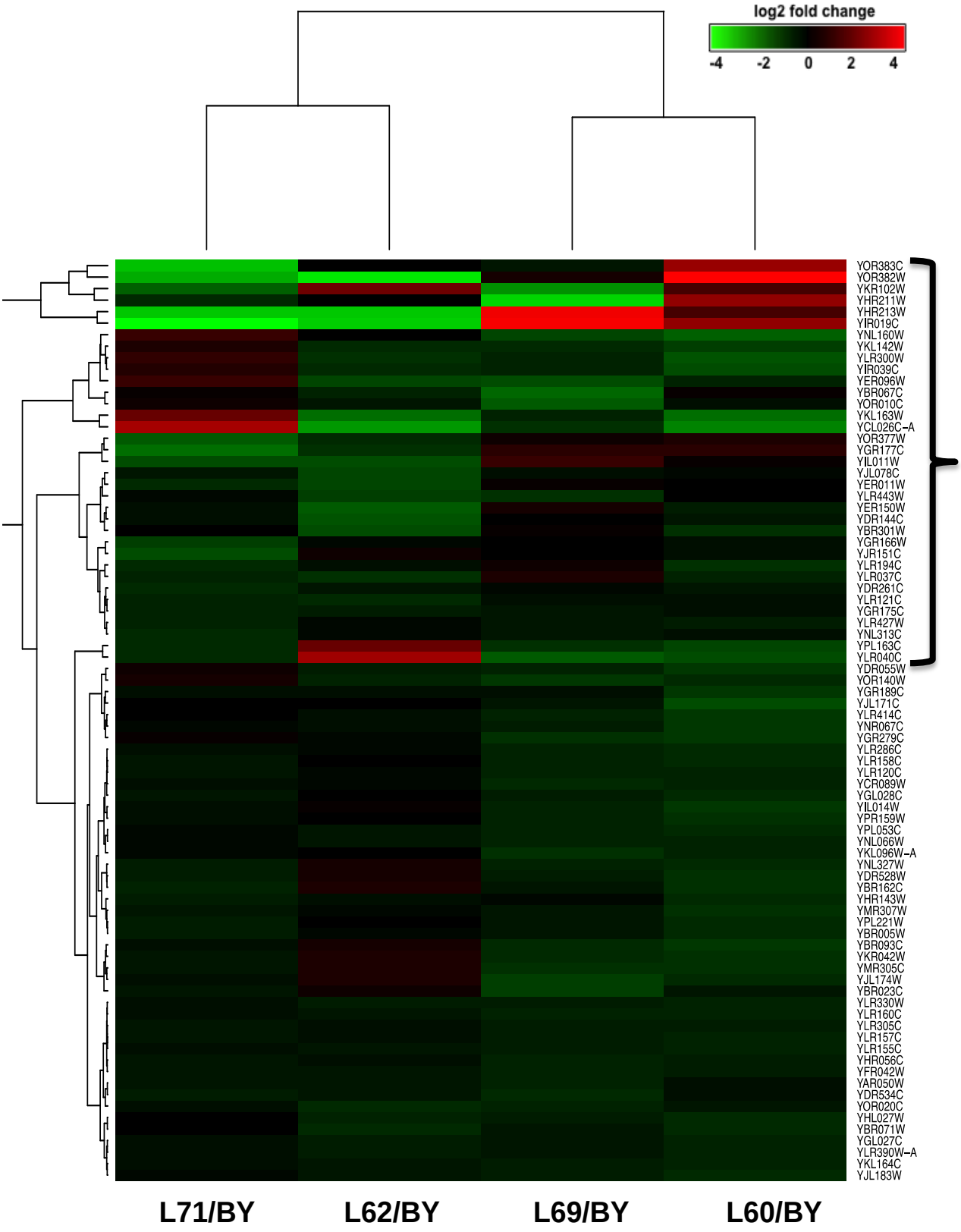

Figure IIIB-7. Differences in expression levels of genes related to cell wall organization between industrial strains and laboratory reference strain

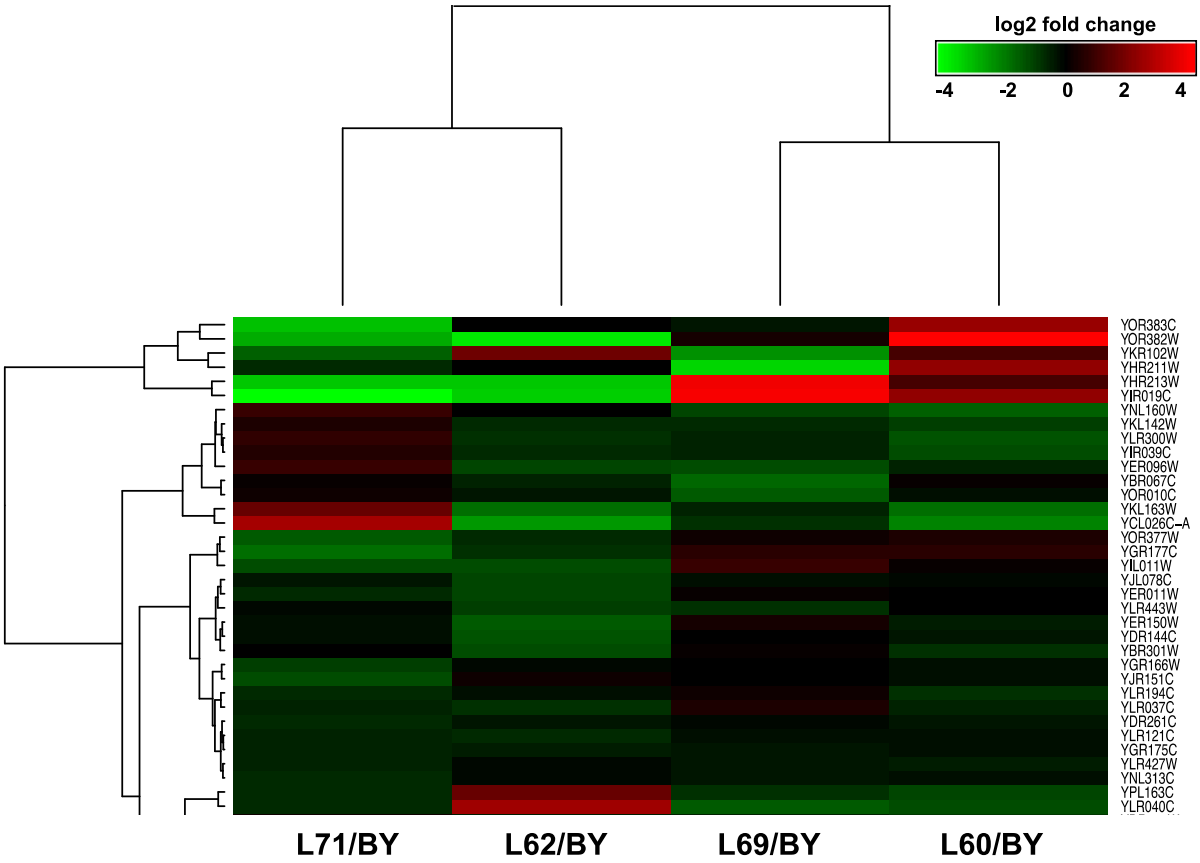

Figure IIIB-8. Differences in expression levels of genes related to cell wall organization between industrial strains and laboratory reference strain (detailed from Figure IIIB-7).

In this group C, we identified a small cluster of 5 to 7 genes in L71 strain that showed higher expression levels than in the three other industrial strains when referred to the laboratory strain. These genes are *YNL160W/YGP1 and YKL163W/PIR3,* which encodes cell wall glycoproteins required for cell wall stability*, YLR300W/EXG1* encoding a β-1,3-glucanosyltransferase*, YER096W/SHC1* encoding a protein that activates Chs3p (chitin synthase III) for the synthesis of the chitosan layer in ascospores*, and YCL026C-A/FRM2* which is implicated in the integration of lipid signaling pathways with cellular homeostasis. Finally, we identified two strongly upregulated genes in L62 strain, *YPL163C/SVS1* and *YLR040C* which encode proteins localized at the cell wall and whose function may denote some strain specificity. Indeed, *YLR040C* also termed *AFB1* encodes a MATα-specific α-factor blocker that can contribute to mating efficiency under certain conditions and the protein is localized to the cell wall through a GPI-anchor (Huberman and Murray, 2013).

To conclude, as it was noticed for our biochemical and biophysical analyses, microarray analysis showed significant differences in the transcriptomic profiles of these four industrial strains. Furthermore, comparative analysis of transcripts levels in industrial strains demonstrated that many of

the differentially expressed genes are involved in metabolism and play an important role in the adaptation of industrial yeasts to new environment. These genes are related to cell wall such as *FLO* genes encoded lectin-like proteins (*FLO5, FLO10 and FLO11*), transporters (*HXT4, TAT1*), to nutrients assimilation (*MAL33, HXK1, PHO5, PHO10, PHO11, PHO89, TOS3*) and amino acid assimilation (*MET2, LEU2, HIS3, URA3, CHA1*).

Correlation analyses between biochemical composition, nanomechanical and adhesive properties of cell wall and global gene expression

To get a comprehensive view of the relationship between changes of gene expression, cell wall composition and cell surface properties at the nanoscale level (nanomechanical properties and SMFS), we used the R package mixOmics. First, we performed a partial least square regression (Sparse PLS) with selection of genes implicated in the associations with the different sets of variables (biophysical and biochemical values from the Figure IIIB-1 and Table 1) (Lê Cao et al., 2009; Gonzalez-Ramos and Gonzalez, 2006). In this study, we have selected 50 genes for each component. The correlation circle plot (Figure IIIB-9) displays all the biochemical variables (β-1,3-glucan, β-1,6-glucan, mannan, chitin), biophysical variables (Young modulus, contour length and percentage of adhesive events detected with the lectin-tip on the yeast cell surface) and the genes selected on each component (a total of 150 in this plot for 3 components). It emphasizes variables that are important to define each component. The group of genes in the right-hand side of the *x-axis* is positively correlated to mannan, while the group on the left-hand side of the *x-axis* is negatively correlated to mannan content. These two groups of genes define the component 1.

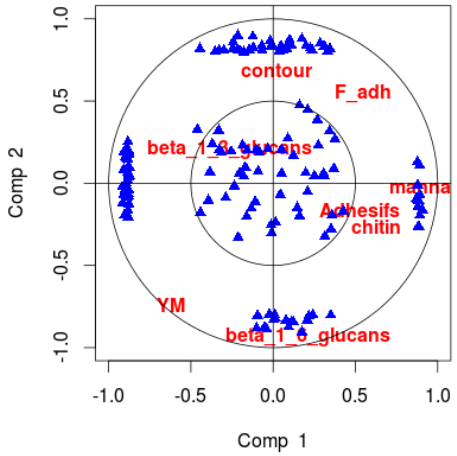

Figure IIIB-9. Correlation circle plot with biochemical-biophysical analysis of industrial yeasts.

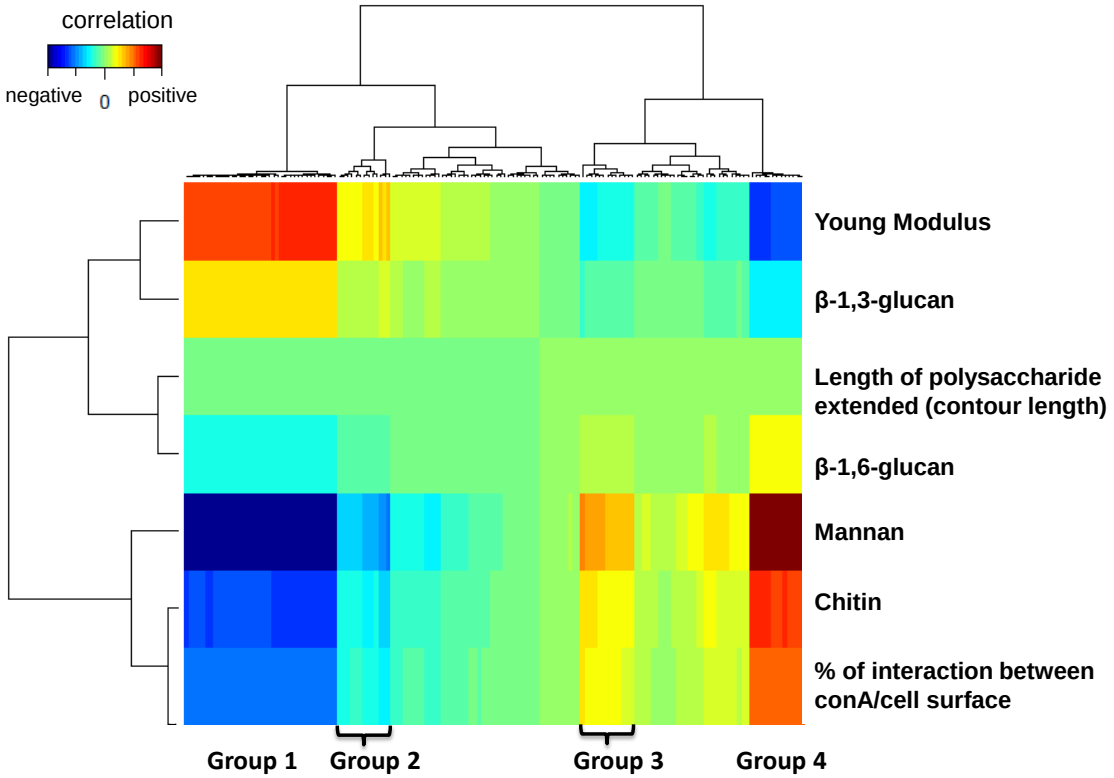

Figure IIIB-10. Representation of associations between biophysical-biochemical variables and transcripts values of genes. Red (blue) indicates high positive (negative) correlation.

For more clarity, the associations found were represented as heatmap (Figure IIIB-10). As shown in Figure IIIB-10, there were some relationships between biochemical and biophysical variables. This heatmap representation allows to find a close relationship between mannans, chitin and the percentage of adhesive events measured with the lectin-tip on the yeast cell surface, whereas the length of the molecule expanded (contour length) is associated to the content of β-1,6-glucan. Moreover, we can notice that the cell elasticity (*i.e.* Young modulus) is related to β-1,3-glucan levels. Each of these variables shared some associations with the 150 genes that were retrieved from this covariance analysis. These genes were divided into 4 groups and their biological functions were described in Table IIIB-3.

Table IIIB-2. Group of genes associated to biophysical-biochemical variables

Group 1		Group 2		Group 3		Group 4	
ORF	**Gene**	**ORF**	**Gene**	**ORF**	**Gene**	**ORF**	**Gene**
YBL007C	SLA1	YKR092C	SRP40	YCR105W	ADH7	YCL026C-B	HBN1
YBL040C	ERD2	YIR022W	SEC11	YCR107W	AAD3	YDR197W	CBS2
YBL109W	YBL109W	YMR214W	SCJ1	YGR039W	YGR039W	YHL026C	YHL026C
YBL112C	YBL112C	YPR006C	ICL2	YNR073C	YNR073C	YHR072W	ERG7
YDR423C	CAD1	YJR086W	STE18	YOL165C	AAD15	YJL156C	SSY5
YDR545W	YRF1-1	YCL038C	ATG22	YPL049C	DIG1	YLR180W	SAM1
YEL074W	YEL074W	YDL248W	COS7	YPL186C	UIP4	YLR313C	SPH1
YER186C	YER186C	YGL203C	KEX1	YPR006C	ICL2	YNL057W	YNL057W
YFL018C	LPD1	YPL049C	DIG1	YPR171W	BSP1	YNL298W	CLA4
YGL053W	PRM8	YDR065W	RRG1	YBR121C	GRS1	YOL091W	SPO21
YGR295C	COS6	YMR132C	JLP2	YGR163W	GTR2	YOL095C	HMI1
YHR219W	YHR219W	YLR113W	HOG1	YKL178C	STE3	YPR191W	QCR2
YIL059C	YIL059C	YML032C	RAD52	YBL076C	ILS1	YJR151C	DAN4
YIL111W	COX5b	YGR166W	TRS65	YGR126W	YGR126W	YBR004C	GPI18
YIL147C	SLN1			YIR022W	SEC11		
YIL173W	VTH1			YJR103W	URA8		
YKR070W	YKR070W			YLR040C	YLR040C		
YLL066C	YLL066C			YLR249W	YEF3		
YLR317W	YLR317W			YMR219W	ESC1		
YLR362W	STE11			YGL203C	KEX1		
YLR399C	BDF1			YBR140C	IRA1		
YLR466W	YRF1-4						
YLR467W	YRF1-5						
YMR092C	AIP1						
YNL336W	COS1						
YNR075W	COS10						
YOR011W	AUS1						
YOR089C	VPS21						
YOR101W	RAS1						
YOR151C	RPB2						
YOR396W	YRF1-8						
YPL231W	FAS2						

Group 1 contained genes that were positively correlated to the cell elasticity (Young Modulus) and β-1,3-glucan level, whereas they were negatively correlated to mannan, chitin and interaction with the lectin. This set of genes encodes transcription factors (*CAD1, SLN1, BDF1, RPB2*), in transmembrane proteins implicated in endocytosis, protein sorting (*ERD2, PRM8, VPS21, VTH1*) or in a process that couples the yeast endocytic machinery to proteins regulating actin (*SLA1*). Thus, interestingly, most of the genes in this group 1 encode membrane-associated proteins (*SLA1, ERD2, PRM8, COS6, COX5, SLN1, VTH1, COS1, COS10, AUS1, VPS21, RAS1*). *STE11* encodes a mitogen activated protein kinase kinase kinase (MAPKKK), which is involved in the MAPK cascade required for both mating and filamentation (Westfall et al., 2004). One of the targets of this cascade is *FLO11* (Rupp et al., 1999)

that is upregulated in L69 strain and encodes a cell wall protein with interesting adhesive properties. In group 2 was found *DIG1, STE18, HOG1* and *KRE11*. As group 1, this second set of genes has a positive correlation with the cell elasticity (Young modulus) and a negative association with mannan and chitin. *DIG1* and *STE18,* as *STE11*, are also implied in the MAPK signaling pathway governing the pheromone response. *DIG1* is a MAP kinase involved in the regulation of mating-specific genes and the invasive growth pathway. Furthermore, *HOG1* encodes a mitogen-activated protein kinase involved in the response to hyperosmolarity condition. When the high osmolarity glycerol (HOG) pathway is activated by osmosensors, such as *SLN1*, the MAP kinase Hog1 can activated genes such as regulators of glycerol synthesis resulting in accumulation of glycerol, which is the main osmoprotector compound of yeast cells. Moreover, activation of the HOG1 MAPK cascade induces expression of several genes through stress response elements (STREs) (Schulleret al. 1994). Furthermore, *TRS65* encoded a subunit of TRAPPII (Sacher et al., 2000) and involved in the Golgi traffic, is positively correlated to cell wall elasticity. Also called *KRE11* (Killer toxin REsistant), based on its identification as a killer toxin resistant mutant, this gene has a role in cell wall β-1,6-glucan biosynthesis but also in the stress response (Brown et al., 1993). Altogether, these data suggest that cell wall β-glucan, MAPK signaling pathway and cytoskeleton assembly are important for the cell wall elasticity. In Figure IIIB-10, we also noticed that the group 3 and 4 are positively correlated to mannan and chitin in the cell wall as well as adhesive properties with the lectin (contour length and percentage of adhesive events). This set of genes is implied in protein processing (*KEX1, SSY5*), ergosterol and phospholipid biosynthesis (*ERG7, URA8*), cell wall mannoprotein (*DAN4, YLR040C*) and *GPI18* encoded a mannosyltransferase that transfers the second mannose in GPI biosynthesis.

To conclude, statistical methodology shown that among the four industrial strains, L71 is more distant that L69, L62 and L60, with some similarities between L62 and L60. Associations between biochemical and biophysical variables demonstrated the relation between Young Modulus and β-1,3-glucan but also the role of β-1,6-glucan in the elongation of polysaccharide with lectin tip. This analysis has highlighted upregulated genes involved in membrane cytoskeleton assembly and remodeling such as (*SLA1, SPH1, CLA4*), mannoprotein glycosylation *(DAN4, GPI18, YLR040C).*

IV. CONCLUSION

In conclusion, cell wall structure and organisation of a laboratory strain and four industrial yeasts strains used in wine fermentation were investigated by biochemical and biophysical methods, and gene expression of these strains were analysed by DNA microarrays. These three sets of data were used to tentatively extract correlations between them using dedicated biomathemical tools. We found difference in the cell wall composition among industrial strains and hence could not connect the content of a specific component to cell wall elasticity. However, we clearly found using AFM tips functionalized with concanavalin A specific adhesion properties in the L69 strain that was associated with an upregulation of *FLO11*. In addition, the use of these functionalized tips showed a longer rupture length of the molecule, indicating that mannoproteins with a different anchorage into the cell wall are stretched on this particular strain. Furthermore, transcriptomic analysis showed also the specificity of each strain. The laboratory strain was very distant to industrial strains. Among them, L71 strain was found to be the most different. In this strain, genes implied in phosphate, amino acid and glucose metabolisms were upregulated, suggesting a better assimilation of nutrient and glucose as carbon source. In addition, the upregulation of genes related to cell wall proteins such as *FLO* genes or *TIR3, FIT2* and *FIT3* would explain the higher amount of mannan. Finally, a new statistical method to integrate all the data shown associations between cell elasticity and β-1,3-glucans with genes implied in membrane, cytoskeleton assembly (*SLA1*), β-1,6-glucan biosynthesis (*KRE11*) and MAPK signalling pathways (*STE11, HOG1, DIG1*). On the other hand, genes involved in protein processing, ergosterol biosynthesis and cell wall mannoproteins biosynthesis were associated to the levels of mannan and chitin in the cell wall as well as lectin-cell surface interactions.

References:

Alsteens, D., Dupres, V., Mc Evoy, K., Wildling, L., Gruber, H.J., and Dufrêne, Y.F. (2008). Structure, cell wall elasticity and polysaccharide properties of living yeast cells, as probed by AFM. Nanotechnology 19, 384005.

Arfsten, J., Leupold, S., Bradtmöller, C., Kampen, I., and Kwade, A. (2010). Atomic force microscopy studies on the nanomechanical properties of Saccharomyces cerevisiae. Colloids Surf. B Biointerfaces 79, 284–290.

Binnig, Quate, and Gerber (1986). Atomic force microscope. Phys. Rev. Lett. 56, 930–933.

Brown, G.D., and Gordon, S. (2003). Fungal β-Glucans and Mammalian Immunity. Immunity 19, 311–315.

Brown, J., Z, K., B, J., and H, B. (1993). A mutational analysis of killer toxin resistance in Saccharomyces cerevisiae identifies new genes involved in cell wall (1-->6)-beta-glucan synthesis. Genetics 133, 837–849.

Bustamante, C., Marko, J.F., Siggia, E.D., and Smith, S. (1994). Entropic elasticity of lambda-phage DNA. Science 265, 1599–1600.

Lê Cao, K.-A., González, I., and Déjean, S. (2009). integrOmics: an R package to unravel relationships between two omics datasets. Bioinforma. Oxf. Engl. 25, 2855–2856.

Lê Cao, K.-A., Boitard, S., and Besse, P. (2011). Sparse PLS discriminant analysis: biologically relevant feature selection and graphical displays for multiclass problems. BMC Bioinformatics 12, 253.

Carreto, L., Eiriz, M.F., Gomes, A.C., Pereira, P.M., Schuller, D., and Santos, M.A. (2008). Comparative genomics of wild-type yeast strains unveils important genome diversity. BMC Genomics 9, 524.

Chalier, P., Angot, B., Delteil, D., Doco, T., and Gunata, Z. (2007). Interactions between aroma compounds and whole mannoprotein isolated from Saccharomyces cerevisiae strains. Food Chem. 100, 22–30.

Chen, J., and Seviour, R. (2007). Medicinal importance of fungal β-(1→3), (1→6)-glucans. Mycol. Res. 111, 635–652.

Chopinet, L., Formosa, C., Rols, M.P., Duval, R.E., and Dague, E. (2013). Imaging living cells surface and quantifying its properties at high resolution using AFM in QITM mode. Micron.

Dague, E., Bitar, R., Ranchon, H., Durand, F., Yken, H.M., and Francois, J.M. (2010). An atomic force microscopy analysis of yeast mutants defective in cell wall architecture. Yeast Chichester Engl. 27, 673–684.

Dague, E., Jauvert, E., Laplatine, L., Viallet, B., Thibault, C., and Ressier, L. (2011). Assembly of live micro-organisms on microstructured PDMS stamps by convective/capillary deposition for AFM bio-experiments. Nanotechnology 22, 395102.

Dallies, N., Francois, J., and Paquet, V. (1998). A new method for quantitative determination of polysaccharides in the yeast cell wall. Application to the cell wall defective mutants of Saccharomyces cerevisiae. Yeast Chichester Engl. 14, 1297–1306.

Escobar-Henriques, M., Collart, M.A., and Daignan-Fornier, B. (2003). Transcription initiation of the yeast IMD2 gene is abolished in response to nutrient limitation through a sequence in its coding region. Mol. Cell. Biol. 23, 6279–6290.

Francius, G., Alsteens, D., Dupres, V., Lebeer, S., De Keersmaecker, S., Vanderleyden, J., Gruber, H.J., and Dufrêne, Y.F. (2009). Stretching polysaccharides on live cells using single molecule force spectroscopy. Nat. Protoc. 4, 939–946.

Francois, J.M. (2006). A simple method for quantitative determination of polysaccharides in fungal cell walls. Nat. Protoc. 1, 2995–3000.

Gibson, B.R., Lawrence, S.J., Leclaire, J.P.R., Powell, C.D., and Smart, K.A. (2007). Yeast responses to stresses associated with industrial brewery handling. FEMS Microbiol. Rev. 31, 535–569.

González, I., Cao, K.-A.L., Davis, M.J., and Déjean, S. (2012). Visualising associations between paired “omics” data sets. BioData Min. 5, 19.

Gonzalez-Ramos, D., and Gonzalez, R. (2006). Genetic determinants of the release of mannoproteins of enological interest by Saccharomyces cerevisiae. J. Agric. Food Chem. 54, 9411–9416.

Gonzalez-Ramos, D., Quirós, M., and Gonzalez, R. (2009). Three Different Targets for the Genetic Modification of Wine Yeast Strains Resulting in Improved Effectiveness of Bentonite Fining. J. Agric. Food Chem. 57, 8373–8378.
Hochberg, Y., and Benjamini, Y. (1990). More powerful procedures for multiple significance testing. Stat. Med. 9, 811–818.

Hutter, J.L., and Bechhoefer, J. (1993). Calibration of atomic- force microscope tips. Rev. Sci. Instrum. 64, 1868–1873.

Janshoff, A., Neitzert, M., Oberdörfer, Y., and Fuchs, H. (2000). Force Spectroscopy of Molecular Systems—Single Molecule Spectroscopy of Polymers and Biomolecules. Angew. Chem. 39, 3212–3237.

Jauvert, E., Dague, E., Séverac, M., Ressier, L., Caminade, A.-M., Majoral, J.-P., and Trévisiol, E. (2012). Probing single molecule interactions by AFM using bio-functionalized dendritips. Sens. Actuators B Chem. 168, 436–441.

Katakura, Y., Sano, R., Hashimoto, T., Ninomiya, K., and Shioya, S. (2010). Lactic acid bacteria display on the cell surface cytosolic proteins that recognize yeast mannan. Appl. Microbiol. Biotechnol. 86, 319–326.

Kim, K.W., Kamerud, J.Q., Livingston, D.M., and Roon, R.J. (1988). Asparaginase II of Saccharomyces cerevisiae. Characterization of the ASP3 gene. J. Biol. Chem. 263, 11948–11953.

Klis, F.M., Boorsma, A., and De Groot, P.W. (2006). Cell wall construction in Saccharomyces cerevisiae. Yeast Chichester Engl. 23, 185–202.

Kogan, G., and Kocher, A. (2007). Role of yeast cell wall polysaccharides in pig nutrition and health protection. Livest. Sci. 109, 161.

Lafon-Lafourcade, S., Geneix, C., and Ribéreau-Gayon, P. (1984). Inhibition of alcoholic fermentation of grape must by Fatty acids produced by yeasts and their elimination by yeast ghosts. Appl. Environ. Microbiol. 47, 1246–1249.

League, G.P., Slot, J.C., and Rokas, A. (2012). The ASP3 locus in Saccharomyces cerevisiae originated by horizontal gene transfer from Wickerhamomyces. FEMS Yeast Res. 12, 859–863.

Lesage, G., and Bussey, H. (2006). Cell wall assembly in Saccharomyces cerevisiae. Microbiol. Mol. Biol. Rev. MMBR 70, 317–343.

Mercadé-Prieto, R., Thomas, C.R., and Zhang, Z. (2013). Mechanical double layer model for Saccharomyces Cerevisiae cell wall. Eur. Biophys. J. 42, 613–620.

Millsap, K. (1998). Adhesive interactions between medically important yeasts and bacteria. FEMS Microbiol. Rev. 21, 321–336.

Nguyen, T.H., Fleet, G.H., and Rogers, P.L. (1998). Composition of the cell walls of several yeast species. Appl. Microbiol. Biotechnol. 50, 206–212.

Novak, M., and Vetvicka, V. (2009). Glucans as biological response modifiers. Endocr. Metab. Immune Disord. Drug Targets 9, 67–75.

Pope, G.A., MacKenzie, D.A., Defernez, M., Aroso, M.A.M.M., Fuller, L.J., Mellon, F.A., Dunn, W.B., Brown, M., Goodacre, R., Kell, D.B., et al. (2007). Metabolic footprinting as a tool for discriminating between brewing yeasts. Yeast Chichester Engl. 24, 667–679.

Reissig, J.L., Storminger, J.L., and Leloir, L.F. (1955). A modified colorimetric method for the estimation of N-acetylamino sugars. J. Biol. Chem. 217, 959–966.

Roduit, C., Saha, B., Alonso-Sarduy, L., Volterra, A., Dietler, G., and Kasas, S. (2012). OpenFovea: open-source AFM data processing software. Nat. Methods 9, 774–775.

Rupp, S., Summers, E., Lo, H.-J., Madhani, H., and Fink, G. (1999). MAP kinase and cAMP filamentation signaling pathways converge on the unusually large promoter of the yeast FLO11 gene. EMBO J. 18, 1257–1269.

Sacher, M., Barrowman, J., Schieltz, D., Yates, J.R., and Ferro-Novick, S. (2000). Identification and characterization of five new subunits of TRAPP. Eur. J. Cell Biol. 79, 71–80.

Schiavone, M., Vax, A., Formosa, C., Martin-Yken, H., Dague, E., and François, J.M. (2014). A combined chemical and enzymatic method to determine quantitatively the polysaccharide components in the cell wall of yeasts. FEMS Yeast Res. n/a – n/a.

Smyth, G.K. (2005). Limma: linear models for microarray data. In Bioinformatics and Computational Biology Solutions Using R and Bioconductor, (New York: R. Gentleman, V. Carey, S. Dudoit, R. Irizarry, W. Huber), pp. 397–420.

Suharja, A.A.S., Henriksson, A., and Liu, S.-Q. (2014). Impact of Saccharomyces Cerevisiae on Viability of Probiotic Lactobacillus Rhamnosus in Fermented Milk under Ambient Conditions. J. Food Process. Preserv. 38, 326–337.

Teunissen, A.W., and Steensma, H.Y. (1995). Review: the dominant flocculation genes of Saccharomyces cerevisiae constitute a new subtelomeric gene family. Yeast Chichester Engl. 11, 1001–1013.

Tirelli, A., Fracassetti, D., and De Noni, I. (2010). Determination of Reduced Cysteine in Oenological Cell Wall Fractions of Saccharomyces cerevisiae. J. Agric. Food Chem. 58, 4565–4570.

Walker, G.M. (1998). Yeast Physiology and Biotechnology (John Wiley & Sons).
Westfall, P.J., Ballon, D.R., and Thorner, J. (2004). When the stress of your environment makes you go HOG wild. Science 306, 1511–1512.

Zyl, W.H. van, Lynd, L.R., Haan, R. den, and McBride, J.E. (2007). Consolidated Bioprocessing for Bioethanol Production Using Saccharomyces cerevisiae. In Biofuels, L. Olsson, ed. (Springer Berlin Heidelberg), pp. 205–235.

Supplementary results: Cell wall composition and transcriptomic analysis of industrial yeasts: Effect of the growth medium

In our investigation, we have raised the question about the effect of the growth medium. Comparative transcriptomic and cell wall composition analyses of the reference strain BY4743 and four industrial strains (L71, L69, L62, L60) were performed to gain insight into transcriptomic changes that may be induced by a modification of growth medium.

Experiment:

Four strains named L71, L69, L62 and L60 were provided by Lallemand Inc. (Montréal, Canada) and three of them are *Saccharomyces cerevisiae* with oenological origin. The strain *Saccharomyces cerevisiae* BY4743 (MAT**a**/α his3Δ1/his3Δ1 leu2Δ0/leu2Δ0 LYS2/lys2Δ0 met15Δ0/MET15 ura3Δ0/ura3Δ) from Euroscarf collection was used as diploid control. Cells were grown at 30°C with agitation in a rich medium (YPD; 2% (w/v) glucose, 1% (w/v) peptone, 1% (w/v) yeast extract) or in a synthetic minimal medium (YNB) containing 0.17% (w/v) yeast nitrogen base (Difco), 0.5% (w/v) ammonium sulfate and 2% (w/v) glucose with amino acid complementation as necessary. The pH was adjusted to 6.0 with sodium hydroxide.

Cell wall isolation, quantification of polysaccharides and DNA microarray analyses were perfomed as described in Material and Methods of chapter IIIB.

The fold change (FC) was defined as: $FC = \frac{Expression\ of\ S\ (YPD)}{Expression\ of\ S\ (YNB)}$ where S is the strain name.

Results:

Growth physiology and cell wall composition during YPD and YNB cultures

Industrial yeasts were grown in two growth medium, yeast peptone dextrose medium 'YPD' (2% w/v glucose, 1% w/v peptone, 1% w/v yeast extract) and a yeast minimal medium 'YNB' (2% w/v glucose, 0.17% w/v yeast nitrogen base without amino acids, 0.5% w/v ammonium sulfate).

From growth curves of the four industrial strains on the two media, we observed that the strains have a higher growth rate in minimal medium, indicating a faster growth in this medium than in YPD medium.

During aerobic growth on rich medium, the specific rate (μ) of the L62 was lower than the others. However, this strain showed a 20 % increase in specific growth rate, when grown in minimal medium (table IIIC-1).

Table IIIC-1. Growth rate μ (h^{-1}) of industrial yeasts strains in two different growth media.

Strain	μ (YPD)	μ (YNB)
L60	0.354	0.359
L69	0.355	0.437
L62	0.256	0.308
L71	0.340	0.402

The cell wall composition of a yeast strain grown in flask at 30°C in rich and in minimal medium was analyzed (Table IIIC-2). As opposite to a growth in rich medium, a severe decrease of the chitin amount accompanied with an increase of β-glucan and a decrease of mannan were observed in the wall of cells prepared from a minimal medium culture. For example, a 10-fold decrease of chitin was observed in the cell wall of L69 strain. Taken into account these results, we could suggest that a modification of medium might affect the cell wall, in particular the levels of mannans, chitin and β-1,3-glucans.

Table IIIC-2. Influence of the growth medium on the cell wall composition.

Strain	medium	chitin	β-1,3-glucans	β-1,6-glucans	mannans
BY4743	YPD	42.2 ± 1.0	340.2 ± 11.4	156.8 ± 89.0	384.5 ± 15.3
	YNB	36.8 ± 4.7	341.8 ± 19.2	227.0 ± 18.3	377.6 ± 20.5
L71	YPD	48.2 ± 21.4	248.2 ± 46.8	197.8 ± 73.9	318.3 ± 62.4
	YNB	28.1 ± 9.8	342.4 ± 23.9	202.7 ± 17.7	378.0 ± 31.4
L69	YPD	30.0 ± 8.6	308.0 ± 46.6	142.0 ± 14.3	370.5 ± 43.6
	YNB	3.1 ± 0.6	373.3 ± 21.4	176.5 ± 31.1	417.0 ± 29.6
L60	YPD	44.4 ± 6.7	297.5 ± 99.8	190.8 ± 54.0	449.4 ± 67.1
	YNB	27.8 ± 12.1	264.1 ± 5.3	300.6 ± 26.5	409.4 ± 5.0
L62	YPD	136.2 ± 59.3	210.6 ± 27.5	187.5 ± 66.4	433.6 ± 48.8
	YNB	42.7 ± 4.1	407.0 ± 31.3	147.0 ± 15.0	390.5 ± 6.3

Yeasts strains were grown in flasks at 30°C under rotation until OD600=1. After growth, cell wall composition of the four industrial strains (L71, L69, L62, L60) from Lallemand Inc. (Montréal, Canada) was determined an acid-enzymatic combined method (Schiavone et al., FEMS Yeast Research, 2014). Mean values ± SD are expressed as μg of chitin, β-1,3-glucans, β-1,6-glucans and mannans per mg of cell wall dry mass and were obtained from two independent experiments made in biological triplicates.

Genome transcriptomic analysis of diploid yeast strains

Transcriptomic profile of each yeast strain grown in the different medium has allowed us to compare the gene expression in the two conditions. In L71 and L62 strains, no significant changes in the transcript levels were found. This result showed that industrial strains L71 and L62 seem to be more tolerant to a modification of growth medium than the laboratory strain. However, we found than a less extended number of genes were differentially expressed in the laboratory strain BY4743 as compared to the industrial strains L69 and L60, indicating the relevance to investigate these conditions in industry. Indeed, we observed 177 and 140 genes were differentially expressed in L69 and L60 strains, but the transcription of only 39 genes was modified in laboratory strain (Figure IIIC-1).

In the case of industrial yeasts, 59 and 40 genes were respectively upregulated in L60 and L69 strains upon the modification of the growth culture. In laboratory strain, upregulated genes were mostly involved in transport, response to stress, cell wall organization and phospholipid metabolism (see table IIIC-3). In L69 strain, we observed an increase of gene expression of genes implied in protein fate, stress response and transport of siderophore and drug (table IIIC-4). In L60 strain, we also observed an upregulation of genes required for transport of siderophore as well as phosphate and metal ions. In addition, in this strain, highest levels of transcription were found for *FLO* genes encoded proteins with binding function and for genes involved in metabolism of lipids and maltose (see table IIIC-5).

To identify the general response to a modification of growth medium in the laboratory strain and industrials strains, we selected genes, whose expression was induced or repressed more than twofold and common to the three strains (see Figure IIIC-1).

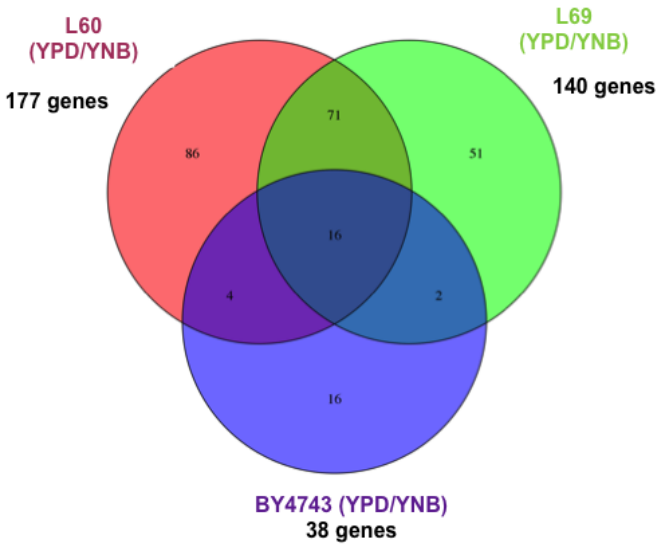

Figure IIIC-1. Representation of the differentially expressed genes between the two growth medium composition. Venn diagram and number indicates genes differentially expressed (pvalue of 5%, Fold Change of 2).

Differences in expression levels of the 16 common genes were shown in Figure IIIC-2. We observed that the main changes in transcription concerned the synthesis of amino acids, in particular the serine synthesis (SER33) and methionine pathway (*MET1, MET2, MET3, MET5, MET6, MET10, MET14, MET16, MET17* and *MET28*), which are both connected, but also the sulfate assimilation pathways (*SUL2, SAM2*). A comparison of the gene transcript profiles of L69, L60 and BY4743 cells exposed to a rich or minimum glucose medium showed that genes involved in the synthesis of methionine were overexpressed in L60 strain, whereas the expression of these genes were down-regulated in L69 strain. In addition, the repression of *SAM2* and *SUL2* linked to the sulfate assimilation pathway, would suggest a requirement for the L60 cells to conserve methionine (Celton et al., 2012).

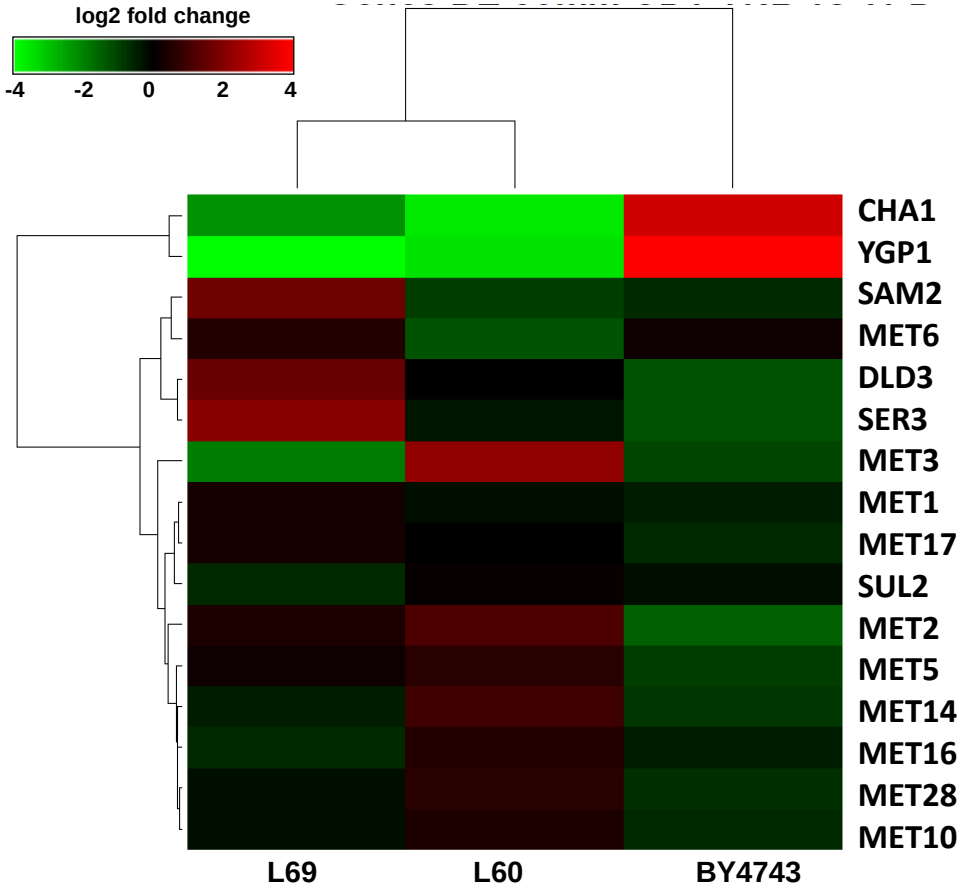

Figure IIIC-2. Differences in expression levels of DE genes in function of growth medium composition (fold change is the relation between gene expression of the strain in YPD and gene expression of the strain in YNB).

Another important result is that the transcript level of *YGP1* was were very low in industrial strains (L69 and L60) and highly increased in laboratory strain grown in rich medium, as compared to minimal

medium. Increased expression of *YGP1* in response to the limitation of nutrients, is in agreement with the fact that the levels of both *YGP1* mRNA and its corresponding protein are increased in response to low nutrient levels (Destruelle et al., 1994). Moreover, this gene encodes a secretory glycoprotein related to the cell wall, which can suggest that nutrient limitation can affect the cell wall.

Therefore, we investigate how a modification of growth medium composition can affect the transcription level of genes related to the cell wall. As shown in figures IIIC-3 and IIIC-4, we selected 80 genes related to cell wall biogenesis and organization, whose expression was different between the two conditions (YPD and YNB medium).

In the figure IIIC-3, we observed a similar transcriptomic profiles for L69 and L60 in response to the modification of the growth medium, while BY4743, L71 and L62 seem to have a similar response.

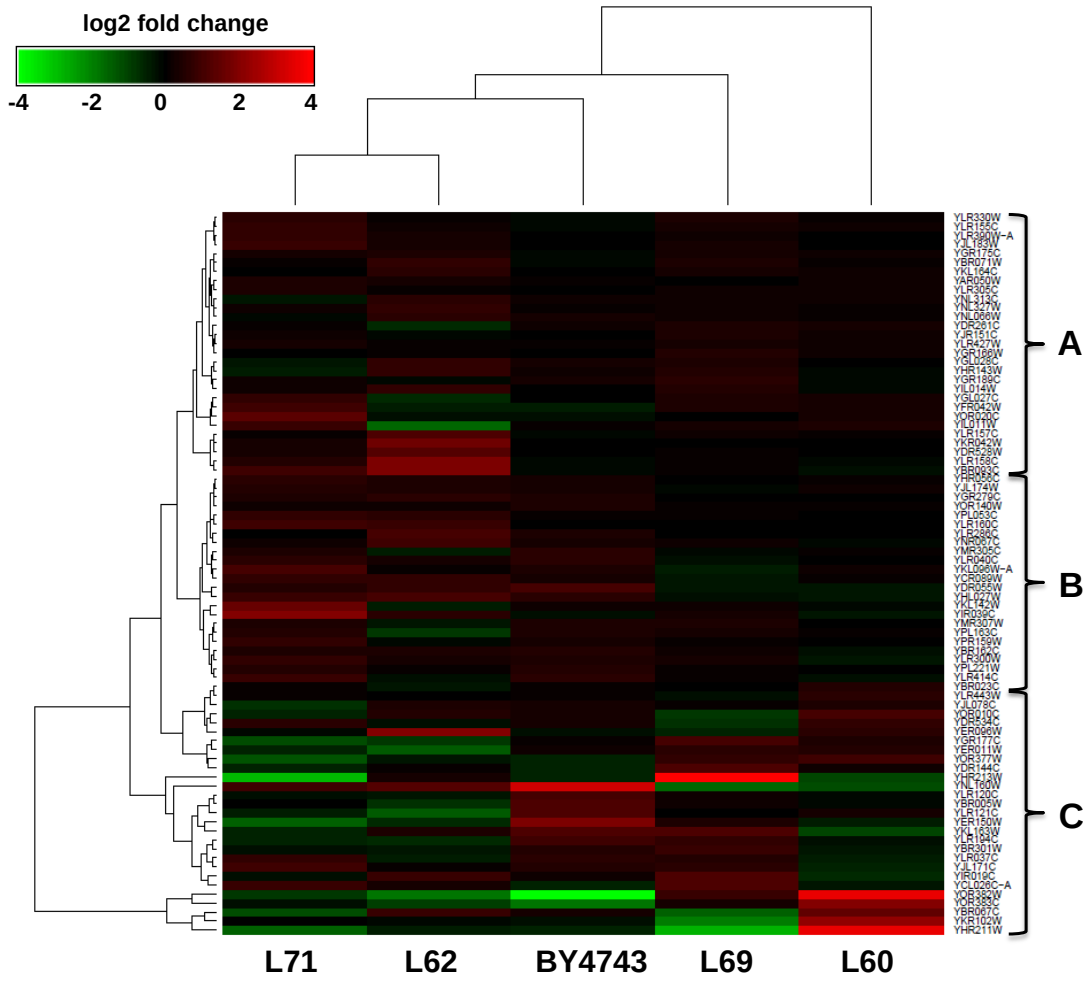

Figure IIIC-3. Differences in expression levels of cell wall-related genes in function of growth medium composition (fold change is the relation between gene expression of the strain in YPD and gene expression of the strain in YNB).

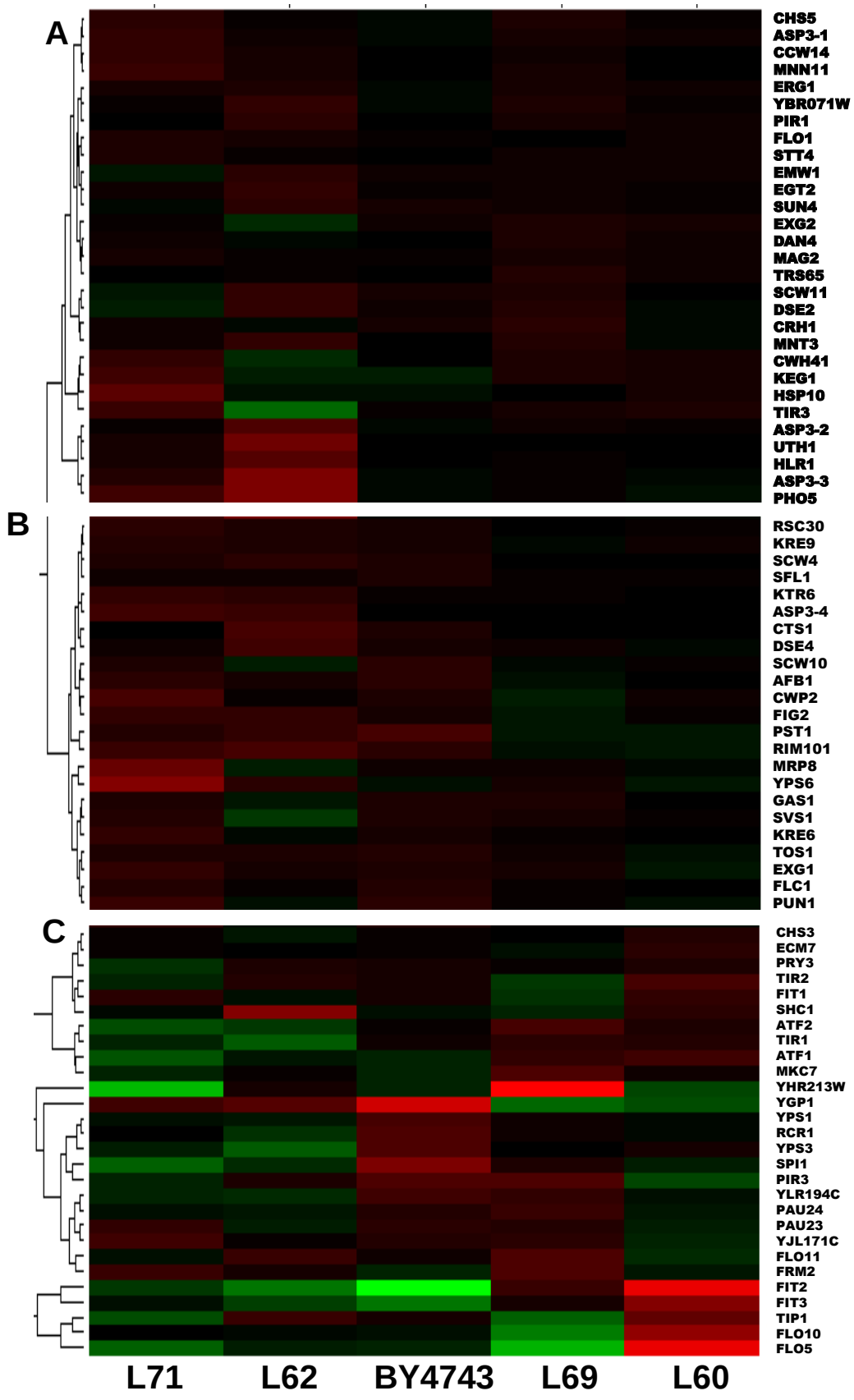

Figure IIIC-4. Differences in expression levels of cell wall-related genes in function of growth medium composition (detailed from figure 3).

For the L71 strain, genes induced in a rich medium are involved in cell wall organization (*YPS6, CWP2, EXG1, CCW14, PUN1, KTR6, KRE6*), reponse to stress such as *PAU23* and *TIR3,* which encode cell wall mannoproteins and *AFB1* whose is expressed under mating conditions. On the contrary, we observed for this same strain a repression of genes implied in flocculation (*FLO5, YHR213W, FLO11*) and in alcohol metabolism process (*ATF1, ATF2*). These two genes encode two alcohol acetyltransferase, which form volatile esters and acetate esters during wine and brewing fermentation. Comparison of L71 and BY4743 profiles showed the same regulation of genes related to the yeast cell wall organization. Additionally, analysis of the transcription levels in rich or minimal medium for the laboratory strain have shown an activation of some genes involved in cell wall organization, but also implied in the synthesis of chitin (*RCR1, CHS1*), mannoprotein (*PAU24*) and glucan (*SCW10*). In L62, *SHC1* is upregulated in YPD medium as compared to the alkaline medium YNB. Paralog to *SKT5*, this gene is required for the synthesis of the chitosan layer of ascospores and activates the chitin synthase Chs3p during sporulation. In L69, genes implied in flocculation have a distinct level of transcription. *FLO11* and *YHR213W* genes are upregulated, whereas *FLO10* and *FLO5* are downregulated in YPD medium. Moreover, we observed in this strain an upregulation of genes involved in chitin synthesis (*SKT5, PCM1, CHS7*) as well as in the cell wall growth and in its maintenance (*MKC7*). The expression of several genes encoding for the cell wall mannoproteins (*PAU24, PIR1, TIR1, CWP2, FIT1*) and a cell wall adhesin (*FIG2*) are also changed. To summarize, we found that the transcripts levels of several GPI-CWPs were changed when the yeast cells are grown in synthetic medium. The effect of growth conditions on transcriptional activation or repression of specific CWPs was previously report on laboratory strains by Wodicka et al. (Wodicka et al., 1997). Moreover, we could suggest that the repression of these genes is in line with a ratio of mannan in the rich medium as compared to it in the minimal medium. In contrary to them, we did not observe a large increase of the transcript level of *FKS2* (*GSC2*) in minimal medium, but our data indicate an increased expression of genes involved in chitin synthesis in rich medium correlated with the higher level of chitin measured in cells grown on rich (YPD) medium.

Table IIIC-3. Upregulated genes (about 1.5-fold and higher) in YPD/YNB, in BY4743 diploid strain, based on microarray analysis.

ORF name	Gene name	Fold change
Response to stress		
YAL068C	PAU8	1,64
YCR021C	HSP30	5,74
YEL049W	PAU2	1,56
YGL179C	TOS3	2,45
YGL261C	PAU11	1,69
YGR294W	PAU12	1,72
YIL176C	PAU14	1,55
YLL064C	PAU18	1,71
YLR099C	ICT1	2,27
YLR461W	PAU4	1,63
YNR076W	PAU6	1,71
YOL161C	PAU20	1,74
YOR049C	RSB1	2,68
YJL144W	YJL144W	1,66
Fungal cell wall organization		
YBR005W	RCR1	2,27
YBR301W	PAU24	1,51
YLR194C	YLR194C	2,56
YMR305C	SCW10	1,69
YNL192W	CHS1	1,66
YLR120C	YPS1	2,01
YLR121C	YPS3	2,25
Phospholipid metabolism		
YDR072C	IPT1	1,52
YKL051W	SFK1	2,00
YMR006C	PLB2	1,65
YOL011W	PLB3	1,59
YLR099C	ICT1	2,27
Actin organization		
YNL020C	ARK1	1,91
YKL051W	SFK1	2,00
Transport		
YER053C	PIC2	2,34
YGR138C	TPO2	5,70
YMR040W	YET2	1,68
YOR049C	RSB1	2,68
YPR138C	MEP3	2,29
YPR149W	NCE102	1,61
YPR156C	TPO3	1,90
YPR157W	TDA6	3,11
YOR036W	PEP12	1,58
YDL234C	GYP7	1,57
Transcription		
YDL070W	BDF2	1,56
YJR127C	RSF2	1,73
Invasive growth in response to glucose limitation		
YMR316W	DIA1	3,32

Table IIIC-4. Upregulated genes (about 1.5-fold and higher) in YPD/YNB, in L60 diploid strain and based on microarray analysis.

ORF name	Gene name	Fold change
Maltose metabolic process		
YIL172C	IMA3	1,70
YJL221C	IMA4	1,70
YOL157C	IMA2	1,46
Floculation		
YAL063C	FLO9	2.67
YHR211W	FLO5	6.64
YKR102W	FLO10	2.84
Transport		
YJL117W	PHO86	1,83
YML123C	PHO84	72,05
YDR534C	FIT1	1,50
YEL065W	SIT1	8,25
YHL040C	ARN1	2,02
YNR060W	FRE4	6,06
YOR381W	FRE3	1,84
YOR382W	FIT2	8,62
YOR383C	FIT3	5,41
YER145C	FTR1	2,72
YJL133W	MRS3	1,44
YLR443W	ECM7	1,64
YMR038C	CCS1	3,14
YMR058W	FET3	3,36
YOL158C	ENB1	2,55
YBR008C	FLR1	1,60
YBR068C	BAP2	28,25
YBR069C	TAT1	10,29
YBR085W	AAC3	2,25
YDR039C	ENA2	13,98
YDR040C	ENA1	2,38
YDR508C	GNP1	38,34
YEL065W	SIT1	8,25
YER145C	FTR1	2,72
YGL162W	SUT1	6,10
YGR224W	AZR1	5,63
YHL035C	VMR1	2,10
YJL212C	OPT1	1,63
YMR058W	FET3	3,36
YOL158C	ENB1	2,55
YOR378W	YOR378W	3,40
YPR198W	SGE1	1,96
Lipid localization		
YGR037C	ACB1	2,43

YIL013C	PDR11	2,02
YJL078C	PRY3	1,66
YKR013W	PRY2	2,15
YMR246W	FAA4	2,12
Cellular metabolic salvage		
YDR399W	HPT1	1,59
YEL038W	UTR4	1,79
YHR128W	FUR1	2,34
YHR137W	ARO9	2,46

Table 5. Upregulated genes (about 1.5-fold and higher) in YPD/YNB, in L69 diploid strain and based on microarray analysis.

ORF name	Gene name	Fold change
maltose metabolic process		
YIL172C	IMA3	1,83
YJL216C	IMA5	1,55
YJL221C	IMA4	1,73
YOL157C	IMA2	1,64
Fungal cell wall biosynthesis		
YBL061C	SKT5	1,53
YEL058W	PCM1	1,91
YHR142W	CHS7	2,23
YLR194C	YLR194C	2.06
Flocculation		
YHR213W	YHR213W	6.50
phospholipid metabolism		
YCR105W	ADH7	2,17
YEL070W	DSF1	2,57
YLR134W	PDC5	1,47
YMR008C	PLB1	2,62
YNR073C	YNR073C	1,98
YOR377W	ATF1	2,32
YPL110C	GDE1	1,65
YLR056W	ERG3	1,80
YLR100W	ERG27	2,30
YML008C	ERG6	1,90
YMR202W	ERG2	1,63
YOL151W	GRE2	1.85
transport		
YEL065W	SIT1	6,70
YHL047C	ARN2	2,19
YNR060W	FRE4	4,79
YOR381W	FRE3	1,96
YBR008C	FLR1	1,86
YGR224W	AZR1	4,99
YHL035C	VMR1	2,29
YOL158C	ENB1	1.95
YBR106W	PHO88	1.43
YML123C	PHO84	101.96
Reponse to stress		
YAL068C	PAU8	2.01
YNR076W	PAU6	1.89
YBR301W	PAU24	1.66
YLL064C	PAU18	1.95
YGR294W	PAU12	2.09
YGL261C	PAU11	2.64

Table IIIC-6. Upregulated genes in YPD/YNB for BY4743 diploid strain and based on microarray analysis.

GOBPID	Term	Pvalue	Genes
GO:0006950	response to stress	1.96E-03	PAU8, PAU24, HSP30, BDF2, PAU2, PHM8, TOS3, PAU11, PAU12, PAU14, YJL144W, PAU16, PAU18, ICT1, PAU4, PAU6, PAU20, RSB1
GO:0006468	protein phosphorylation	2.91E-02	TOS3 HAL5 ARK1 CMK2 HRK1 NCE102
GO:0031505	fungal-type cell wall organization	2.98E-02	RCR1 SPS100 YPS1 YPS3 YLR194C
GO:0006650	glycerophospholipid metabolic process	3.17E-02	IPT1 ICT1 PLB2 PLB3

Table IIIC-7. Upregulated genes in YPD/YNB for L69 strain and based on microarray analysis.

GOBPID	Term	Pvalue	Genes
GO:0000023	maltose metabolic process	1.32E-03	IMA3 IMA5 IMA4 IMA2
GO:0006031	chitin biosynthetic process	2.81E-02	SKT5 PCM1 CHS7
GO:0006066	alcohol metabolic process	3.03E-02	ADH7 DSF1 PDC5 PLB1 YNR073C ATF1 GDE1
GO:0015891	siderophore transport	1.52E-04	SIT1 ARN2 FRE4 FRE3
GO:0015893	drug transport	4.32E-02	FLR1 AZR1 VMR1
GO:0016125	sterol metabolic process	4.35E-02	ERG3 ERG27 ERG6 ERG2 GRE2
GO:0016485	protein processing	1.40E-03	PRE7 RPT2 RPN6 RPN5 MKC7 RPN9 RAD23 RPN3 PUP3 UBP9 DDI1 RPN12 SCL1 RPT6 PRE9 PUP2 RPN1 YIL082W-A TMA108 KAR2 RPN13 UFO1 HRT1 TRE1
GO:0030003	cellular cation homeostasis	4.11E-02	VMA8 SIT1 ARN2 YHC3 VMA6 COS3 YMR134W FRE4 FRE3
GO:0030163	protein catabolic process	2.73E-03	PRE7 RPN6 RPN5 RPN9 RAD23 PUP3 UBP9 DDI1 RPN12 SCL1 RPT6 PRE9 PUP2 KAR2 RPN13 UFO1 HRT1 TRE1
GO:0030811	regulation of nucleotide catabolic process	9.31E-03	RDI1 GLO3 AGE2 YRB2 HCH1 RGA1 GYP5
GO:0033124	regulation of GTP catabolic process	1.51E-02	RDI1 GLO3 AGE2 YRB2 RGA1 GYP5
GO:0043248	proteasome assembly	8.42E-05	RPT2 RPN6 RPN9 RPT6 PRE9 ECM29 HSC82
GO:0051336	regulation of hydrolase activity	4.66E-02	RDI1 GLO3 AGE2 YRB2 HCH1 RGA1 GYP5

Table IIIC-8. Upregulated genes in YPD/YNB for L60 strain and based on microarray analysis.

GOBPID	Term	Pvalue	Genes
GO:0000023	maltose metabolic process	6.75E-03	IMA3 IMA4 IMA2
GO:0000097	sulfur amino acid biosynthetic process	6.75E-03	UTR4 CYS4 ARO9 MDE1 SAM4
GO:0000302	response to reactive oxygen species	4.57E-02	DRE2 CCS1 AIF1
GO:0000501	flocculation via cell wall protein-carbohydrate interaction	5.54E-04	FLO9 FLO5 FLO10
GO:0006177	GMP biosynthetic process	5.49E-03	IMD3 IMD4
GO:0006790	sulfur compound metabolic process	1.61E-02	UTR4 CYS4 ARO9 OPT1 MDE1 MET31 GLR1 SAM4
GO:0006810	transport	8.66E-04	MST28 FLR1 BAP2 TAT1 AAC3 SSB1 ENA2 ENA1 SRP101 GNP1 AGE1 FIT1 SIT1 FTR1 LOC1 ATG18 TIP20 SUT1 ACB1 UTP22 AZR1 YHB1 VMR1 ARN1 MIP6 BZZ1 PDR11 VTC4 VTC4 PRY3 PHO86 MRS3 OPT1 SFT1 PIR1 PRY2 YKR104W ART10 ECM7 PHO84 CCS1 FET3 RNA1 FAA4 SSB2 FRE4 MDY2 ENB1 VPS17 GET4 THI72 YOR378W FRE3 FIT2 FIT3 GUP2 MMT2 SGE1
GO:0006811	ion transport	2.19E-05	BAP2 TAT1 ENA2 ENA1 GNP1 FIT1 SIT1 FTR1 ACB1 ARN1 PHO86 MRS3 ECM7 PHO84 CCS1 FET3 FAA4 FRE4 ENB1 FRE3 FIT2 FIT3 MMT2
GO:0006814	sodium ion transport	3.68E-02	ENA2 ENA1
GO:0006817	phosphate ion transport	4.41E-02	PHO86 PHO84
GO:0006826	iron ion transport	7.12E-04	FTR1 MRS3 FET3 ENB1
GO:0009116	nucleoside metabolic process	4.47E-02	HPT1 AGE1 UTR4 VMR1 FUR1 PDR11 MDE1 YKR104W IMD3 IMD4 RNA1 SAM4
GO:0010035	response to inorganic substance	2.56E-02	VMR1 DRE2 CCS1 FET3 AIF1
GO:0010876	lipid localization	2.56E-02	ACB1 PDR11 PRY3 PRY2 FAA4 SUT1
GO:0010941	regulation of cell death	3.01E-02	DRE2 AIF1
GO:0043094	cellular metabolic compound salvage	2.09E-03	HPT1 UTR4 FUR1 ARO9 MDE1
GO:0045048	protein insertion into ER membrane	9.07E-03	MDY2 GET4
GO:0055085	transmembrane transport	1.68E-02	FLR1 BAP2 TAT1 AAC3 ENA2 ENA1 GNP1 SIT1 FTR1 SUT1 AZR1 VMR1 OPT1 PHO84 FET3 ENB1 YOR378W MMT2 SGE1

Complementary results

Oligo	Sequence
Gas1-SP	CTAGTTATTTTGCAGCAGAT
Gas1-ASP	TCTCGATGAAATCAACAAGT
GPI7-SP	TTCTGCAATGTGAGTGGGTTATG
GPI7-ASP	TTAGTATGGTTGCAATATTT

Colony PCR. Colonies were suspended in 10 µl of NaOH 0.02 N, boiled for 5 minutes at 95°C, centrifuged at 16,000×g for 5 minutes, and 2 µl of the supernatant was used in each amplification. The DNA was amplified by PCR in 25 µl volumes with 2.5 µM of each primer, 10 mM dNTP and 0.5 µl of DNA Polymerase. After an initial denaturation of 30 seconds at 98°C, the amplification profile was 30 cycles of denaturation (98°C for 10 seconds), hybridization (55°C for 20 seconds) and elongation (72°C for 3 minutes). Amplification products (10 µl) were analyzed on a 1% agarose gel.

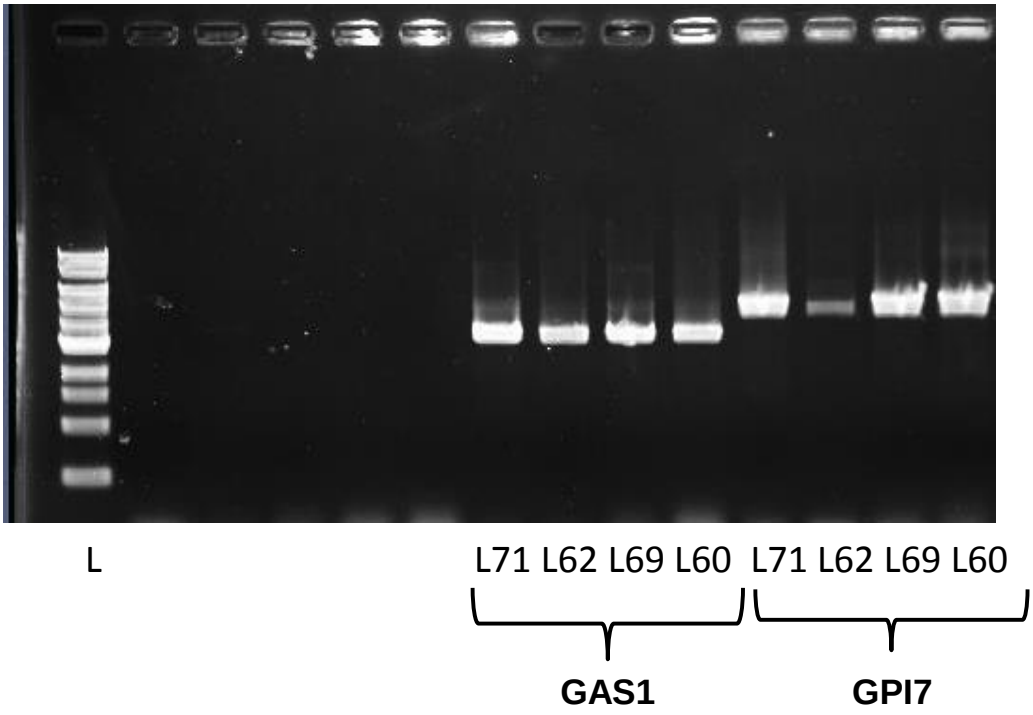

For PCR products, theoretical sizes on BY4743 reference strain were 3600bp for *GAS1* and 4945bp for *GPI7*. Strictly identical amplifications were obtained for industrial background indicating the presence of the corresponding full-size genes in these strains.

Discussion of the results

In this chapter, advanced technologies such as atomic force microscopy (AFM), DNA microarrays and biochemical method were used in order to describe specific properties for each strain. For the L62 strain, which has a lower growth rate (μ =0.256 h^{-1}), we measured high level of chitin and low amount of β-1,3-glucan in the cell wall with a ratio between these two components of 1.5. Concomittently the ratio β-glucan/mannan was found to be of 0.9 and we measured a low cell elasticity (239 kPa as compared to 637 kPa for L71 strain). Interestingly, these results were similar to the one found for *gas1*Δ mutant, suggesting that the phenotype of L62 could be linked to the GAS1 gene. In addition, strains deleted for *GAS1* and *GPI7* released higher amounts of mannoproteins, that have beneficial effects on wine stability and sensorial qualities (Gonzalez-Ramos and Gonzalez, 2006). In addition of transcriptomic data, we checked if the four industrial strains were deleted of these genes (see chapter 3B, complementary results). PCR amplification for *GAS1* and *GPI7* being strictly identical between wild-type and industrial strains, we confirmed the presence of the full size gene in the later strains. However, physiological results obtained on L62 can be explained by a lower transcriptional level of these genes (Fold-change of 0.9 for *GAS1* and 0.8 for *GPI7* as compared to the diploid control BY4743). We can also noticed that *mnn9Δ* and L71 strains, which have the higher value of cell wall elasticity, have a ratio of β-1,3-glucan/chitin above 5. Moreover, we must notice the high value of the ratio β-1,3-glucan/chitin in L69 strain, which results to the decrease of chitin content in the cell wall similar to the strain defective in chitin synthesis (*chs3*Δ). Since chitin is known to play a crucial role in septation during budding and in response to cell wall stress, we investigated *chs3*Δ cells. Unfortunately, transcriptomic data were not available yet for *chs3*Δ, delaying the use of quantitative data in the integrative approach.

The integrative approach was used to combine all the datasets and to compare them in order to unravel association between biochemical composition and biophysical properties of the cell (adhesion and nanomechanical properties) and transcription of genes. Data were divided into two matrices: one gathering quantitative data on cell wall composition and biophysical characteristics, whereas the other consists in the transcriptomic data. Then, the canonical correlation analysis (CCA) has been used to find correlation between the two matrices. It must be noticed that quantitative data were aquired for

industrial strains whereas qualitative data coming from previous studies were analysed in the case of the deleted strains (*gas1*Δ and *mnn9*Δ).

The analysis performed on *gas1*Δ and *mnn9*Δ deleted strains has highlighted a close association between amount of mannans in *gas1*Δ and *mnn9*Δ and adhesion frequency between concanavalin A on the AFM tip and the cell surface. The same correlation was observed in the 4 industrial strains (L71, L69, L62 and L60). Since concanavalin A binds α-glucose and α-mannose, these adhesion results are in agreement with biochemical data sets. We also observed a close association between the length of the molecule stretched with the functionalized tip (contour length) and the chitin amount incorporated into *gas1*Δ and *mnn9*Δ cells. This correlation does not exist in the 4 industrial strains.

However, the analysis performed on the four industrial strains has highlighted a close association between the contour length and β-1,6-glucan. This could be explained by the role of β-1,6-glucan that consists in linking β-1,3-glucan and mannans (Kollar et al., 1997). This correlation cannot be unraveled from *gas1*Δ and *mnn9*Δ as these strains are modified for their glucans and mannans content. The observation that the length of mannan unfolded can be either correlated to chitin in *gas1*Δ or β-1,6-glucan in the other strains can be related to the fact that a fraction of mannoproteins is linked to chitin through a β-1,6-glucan, which account for 40% of covalent cell wall proteins in *gas1*Δ cells (Kapteyn et al., 1997). Thus, the modification of the cross-linkage between the polysaccharides may have an influence on the stretching of mannans. Another association can be found between the cell wall elasticity (*i.e.* Young modulus) and the ratio of β-glucans/mannans in *gas1*Δ and *mnn9*Δ. Young or elastic modulus is the variable parameter in the Hertz (or Sneddon) model. It gives the resistance of a material to deformation and has the same unit as Pressure (Pascals). The higher the value is, the more force is required to deform to the same extent. The correlation of this value with β-1,3-glucan and the ratio of β-glucans/mannans make sense in deleted strains because of the changes in the outer and inner layer of the cell wall mainly composed of mannoproteins and β-glucans respectively. However for the industrial strains, which are enriched in cell wall mannans, Young modulus is no longer associated to this ratio but it is associated to β-1,3-glucan, showing the relevance to distinguish β-1,3-glucan to β-1,6-glucan. Furthermore, the correlation analysis provides correlation between genes and the different physico-chemical variables. We noticed that Young modulus is highly and positively correlated to the transcript level of *GAS1* in the deletion strains *gas1*Δ and *mnn9*Δ, and to several genes in industrial strains. This clusters of genes implied in cytoskeleton

assembly (*SLA1, SPH1, CLA4*), β-1,6-glucan biosynthesis (*KRE11*) and MAPK signaling pathways (*STE11, HOG1, DIG1, STE18*). These results suggest a relation between Young modulus and the budding machinery. Indeed, the process of budding implied many genes required for cell wall biogenesis (*KRE11*) and assembly (*GAS1*) as well as cell polarity, cytoskeleton and cell signaling. Cell wall is an exceptional mechanical structure. It provides mechanical support by being stiff and rigid, and at the same time, allows the cell to grow and elongate. In order to achieve both of these opposed properties, the cell wall needs to be modulated and can be either plastically or elastically deformed. This indicates that the cell to some extent must be able to control the mechanical response and deformation behaviour of its cell wall, which can only be achieved by adjusting and modulating the cross-linking within and between the cell wall components. A modification of the cell wall assembly takes place in order to allow the cell wall to plastically deform for cell growth.

Finally, we found in these two analyses a positive correlation between mannans and genes involved in mannoproteins biosynthesis and glycosylation. Also, five genes related to membrane structure and sterol metabolisms as well as 2 genes implied in ergosterol and phospholipid biosynthesis were correlated to these variables. This latest can be explained by the fact that N-glycosylation, sphingolipid synthesis and sterol esterification, localized in the endosplasmic reticulum are coordinately regulated (Jacquier and Schneiter, 2012).

Chapter IV: IMPACT OF AUTOLYSIS PROCESS ON THE CELL WALL

Objective:

The impact of packaging yeast cells as “YCW” (for Yeast Cell Wall) by autolysis and drying process on the cell wall composition and nanomechanical properties of two industrial strains were investigated. L71 and L69 from Lallemand collection were chosen in this study regarding to their particular interest in wine fermentation.

Material and methods:

Levels of chitin, β-1,3-glucan, β-1,6-glucan and mannan in the cell wall were determined by the acido-enzymatic method. The determination of the cell wall composition was performed on cells grown under standard laboratory condition, which correspond to a growth in a glucose rich medium until exponential phase. Cell wall composition was also investigated on cells propagated under industrial protocol to produce “cream”, which was subjected to autolysis (20 hr at 55°C) followed by separation and by spray-drying in order to produce the dry “YCW”. Atomic force microscopy was used to evaluate the surface properties such as average roughness measurement, stiffness and adhesion. Furthermore, AFM tips were functionalized with concanavalin A that binds α-glucose as well as α-mannose residues, which occur in mannan oligosaccharides of the yeast cell wall. Single-molecule force experiments with concanavalin A tips bring information on the distribution of mannan at the cell surface and on their extension. Transcript levels of genes in L71 and L69 strains were compared to explain the differences between the two strains at genetic level.

Results:

This study has shown that packaging yeast cells as “YCW” by autolysis and drying process does not change the composition of the cell wall but causes a change in topography and surface properties of the cell. However, AFM in this study has a great interest, because this technology brings a specific view of the effects on the cell surface. High resolution imaging of the cell surface showed a modification from a smooth surface for exponential-phase cells to a wrinkled topography for YCW cells, resulting in a 4-fold increase of the average roughness of the YCW cells. In addition, the

observation of some holes of 600 nm diameter localized on the middle of YCW cells in both L69 and L71 strains, would suggest a release of intracellular constituents of the yeast. Furthermore, the L69 strain, which has the highest mannoproteins content, was also characterized by the presence of highly adhesive patches forming nanodomains. Using transcriptomic analyses, we found that the transcript levels of *FLO11* and *YHR213w* were relatively much higher in L69 than in L71 strain. In *S. cerevisiae*, the sequence of the Flo11 protein presents amyloid forming motifs that can lead to partial β-aggregation. Therefore, we can suggest that an upregulation of *FLO11* in L69 strain can lead to massive amounts of Flo11p, which formed β-aggregate amyloids clusters into nanodomains.

Atomic Force Microscopy allows revealing effects of autolysis process and differences on the nanomechanical properties of industrial yeast strains

Marion Schiavone[1,2,3,4,5], Nathalie Sieczkowski[5], Mathieu Castex[5], Etienne Dague[1,4,] and Jean Marie François*[1,2,3]

[1]Université de Toulouse; INSA, UPS, INP, 135 avenue de Rangueil, F-31077 Toulouse, France

[2]INRA, UMR792 Ingénierie des Systèmes Biologiques et des Procédés, F-31077 Toulouse, France ;

[3]CNRS, UMR5504, F-31400 Toulouse, France 135 avenue de Rangueil, F-31077 Toulouse, France ;

[4]CNRS; LAAS ; 7 avenue du colonel Roche, F-31400 Toulouse, France ;

[5]Lallemand SAS, 19, rue des briquetiers, 31702 Blagnac, France

*Correspondance to Jean Marie François; LISBP- INSA, 135 Avenue de Rangeuil, F-31077 Toulouse cedex 04 ; Email: fran_jm@insa-toulouse.fr; Phone: +33(0) 5 61 55 9492

Running Title: Process effects on cell wall composition and nanomechanical properties

Keywords: Cell wall, autolysis, atomic force microscopy, β-glucan, chitin, yeast

ABSTRACT

The *Saccharomyces cerevisiae* cell surface is endowed with several technological properties, among which its effective biosorption capacity to reduce undesirable molecules, such as volatiles phenols in wine or mycotoxins in food. Since cell surface properties are intimately linked to cell wall structure, the aim of this study was to investigate effects of autolyzing/drying process on the biochemical composition of cell wall and on the nanomechanical properties of cell surface. To achieve these goals, we used a recently developed method to analyze the biochemical composition, and we took advantage of Atomic Force Microscopy to access the nanomechanical properties. We choose to work on two industrial strains because of their difference in winemaking applications and sorption properties. We found that the autolysis/drying process of the two strains did not significantly modify the biochemical composition of their cell wall. It, however, caused severe changes in cell surface topography characterized by a 4-fold increase of the roughness and by a global increase in adhesion characteristics of the autolyzed/dried samples. Though this process had some effects on biomechanical properties, the two strains natively harbored differences in biophysical properties that could be accounted by difference in cell wall composition, as the strain with the highest mannoproteins content was also characterized by the presence of highly adhesive patches forming nanodomains,. Comparative transcriptome analysis uncovered a strong upregulation of flocculin encodin*g FLO11* gene in this industrial strain that corroborated with higher interaction to concanavalin A-functionalized AFM tip, leading to the idea that this protein is responsible for the patches formation.

I. INTRODUCTION

The yeast *Saccharomyces cerevisiae* is used since millennia in traditional biotechnological purposes, such as the production of wine, beer and bread. In addition to this role in fermented foods and beverages, this yeast species is attracting increased attention because of other relevant biological properties, such as antimicrobial and biosorption activities, that make them promising candidates for a wide range of applications not limited to the food sector. Indeed, the antimicrobial activities against undesirable bacteria and mold have been recognized since a long time to provide probiotic properties of yeasts, although the mechanisms underlying these antagonistic activities remain unclear (Hatoum et al., 2012). Biosorption is a cell surface property that is defined as the physicochemical process wherein undesirable molecules, which can be a toxin, heavy metals or volatile compounds, interact

and accumulate at the surface of microbial cells (Fomina and Gadd, 2014; Petruzzi et al., 2014). Since this property is displayed by inactive or dead cells and does not require intracellular energy, the physicochemical properties of the microorganism's surface are determining factor in the nature of the interaction and in the sorption capacity. The surface of yeast cell corresponds to a thick wall of about 120-180 nm, exhibiting an ultrastructure of two distinct layers as visualized by electron microscopy (Osumi, 1998): an outer layer mainly constituted of mannoproteins (30-50% of cell wall dry mass) and an inner layer made of chitin (2 - 5 % of cell wall dry mass) and β-glucans (40 - 60 % of cell wall dry mass). Extensive biochemical analysis allowed to propose a supramolecular structure of the mature cell wall in which the chains of β-(1,3) glucose residues are branched to β-(1,6)-glucans, forming a fibrillar network, that serves as backbone to which are linked chitin, β-(1,6)-glucan and mannoproteins. In addition, the outer layer of mannoproteins can be linked to the inner layer through β-(1,6)-glucan via a remnant of a GPI anchor (Lesage and Bussey, 2006). It is therefore suggested that the sorption capacity for a given molecule can be linked to a specific component of the yeast cell wall. This suggestion has been verified in very few cases. For example, a major role of mannoproteins in the retention of volatile aroma by yeast cell walls has been reported (Pradelles et al., 2008), whereas β-glucan was showed as a valuable microbiological binder of the mycotoxin zearalenone (Yiannikouris et al., 2004). However, these studies were mostly carried out with pure fractions of polysaccharides and did take into account neither the complexity and variability of the cell wall composition, that can depend on culture conditions (Aguilar-Uscanga and Francois, 2003) and strains background (Nguyen et al., 1998), nor the process by which yeast cells are prepared and used as biosorbant. In this context, Pradelles and coworkers (Pradelles et al., 2008) investigated effects of cell wall composition on the sorption of the undesirable 4-ethylphenol. While they confirmed a predominant role of mannoproteins in the sorption capacity of this volatile aromatic compound, they also highlighted the fact that drying the yeast biomass greatly increased the sorption capacity of this molecule, which was in part correlated with increased surface hydrophobicity of the dried biomass rehydrated subsequently in water (Pradelles et al., 2009). Taken together, these results indicate that the drying process and more generally the method to prepare yeast cell wall fractions for biosorption applications may have a strong impact on physico-chemical properties of the cell surface. This question is particularly pertinent when we consider that yeast cells employed for biosorption applications are obtained from cultures that are autolysed and air-dried at 55°C, and commercially supplied as 'yeast cell wall' fraction or

YCW. Autolysis is a term that describes the breakdown of cell constituents by action of endogenous enzymes. It can occur naturally when yeast have completed their growth cycle and entered the death phase, or it can be induced at high temperature and low pH (Martínez-Rodríguez et al., 2001; White et al., 2002). Proteases, β-glucanases and chitinases are among autolytic hydrolases that are implicated in this process, and therefore, it can be expected that this process may cause important change in cell wall composition. Accordingly, Martinez-Rodriguez et al (Martínez-Rodríguez et al., 2001) reported important ultrastructural changes during the autolysis of yeast cells using Low Temperature Scanning Electron Microscopy (LTSEM), whereas Aerosol Flow Tube - Fourier Transform Infrared Spectroscopy (AFT-FTIR) was used to monitor global biochemical changes during autolysis revealed hydrolysis of mannans and β-glucans (Cavagna et al., 2010). In spite of these apparent hydrolyses, microscopic observation of autolyzed cells showed that the cell shape was fully retained suggesting that the cell wall structure was not destroyed (Hernawan and Fleet, 1995). Altogether, these studies raised fundamental questions about the effects of industrial processes on structure and properties of yeast cell surface.

These questions can be addressed using Atomic Force Microscope (AFM) which is a very powerful force microscope technology allowing tridimensional images of cell surface and quantitative measurement of nanomechanical properties such as roughness and elasticity (Young modulus) (Dague et al., 2007; Dufrêne, 2010). We used recently this technology to image and quantify surface properties of yeast cell wall mutants (Dague et al., 2010), to investigate effects of antifungal drug caspofungin and heat shock on yeast cells (Formosa et al., 2013; Pillet et al., 2014). These studies led to the finding that the nanomechanical properties of the cell surface are merely dependent on the molecular architecture of the cell wall and not on a specific polysaccharide component of the wall. To gain deeper knowledge on the molecular organization of cell wall, the single molecule force spectroscopy (SMFS) can be employed. This method consists in probing the cell with an AFM tip that is functionalized with a specific ligand that could interact with some proteins present at the cell surface (Hinterdorfer et al., 2012). Accordingly, probing the yeast cell surface with AFM tip functionalized with concanavalin A (conA tip), which is a lectin protein that interacts with α-mannose and α-glucose residues (Sharon and Lis, 2007), has provided quantitative information about distribution, frequency of adhesion events, flexibility and extension of mannans on the surface of different yeast strains. With this approach, Alsteens et al. (Alsteens et al., 2008) investigated the surface properties of a bottom

fermenting and a top-fermenting yeast. They showed that the latter species has higher adhesion frequency and more extended polysaccharides than the former one, consistent with the fact that the surface of top-fermenting yeast cells is richer in proteins and more hydrophobic.

The purpose of this study was therefore to investigate effects of industrial autolysis and drying process on cell wall composition and cell surface nanomechanical properties of two industrial yeast strains that bear differences in winemaking properties. Effects of this process on adhesive properties and on polysaccharides distribution using conA tip of the two strains were also analyzed by comparing whole active living from rehydrated dried yeast cells.

II. MATERIAL AND METHODS

Strains and culture conditions

Two diploid industrial winemaking *Saccharomyces cerevisiae* strains, L71 and L69, from Lallemand Inc. (Blagnac, France) were studied. Differences between the two strain was mainly that the L69 strain has a higher mannoproteins content, expresses different sensorial notes during wine fermentation and presents good capacity to interact with volatile undesirable phenols (Lallemand Inc., unpublished data). The strains were propagated under standard laboratory conditions, which corresponded to growth in 200 ml YPD medium (1% [w/v] yeast extract, 2% [w/v] bactopeptone and 2% [w/v] glucose) in 1 liter shake flasks at 30°C under shaking at 200 rpm. They were also propagated under industrial standard protocol, involving batch and fed-batch growth on molasses based medium, collected, and concentrated to produce packed yeast cells termed ‘cream’. The latter cream was then subjected to autolysis (20 hr at 55°C), followed by separation and then by spray-drying to produce the dry “YCW” (industrial term meaning Yeast Cell Wall fraction that is used for this type of yeast packaging). This autolytic/drying process leads to > 99.9 % of cell mortality as estimated by methylene blue coloration test (Cot et al., 2007). YCW were provided in 30 g packets sealed under vacuum and stored unopened at 4°C until required. Rehydration was performed according to the manufacturer’s guidelines (Lallemand Inc., Blagnac, France): 0.1 g of YCW was sprinkled onto 10× its weight of temperature equilibrated (30°C) sterile water in a tube. The YCW was left to absorb water slowly for 20 min, mixed gently to form slurry and the temperature was maintained at 30°C throughout rehydration.

AFM measurements

Sample preparation

Cells collected from exponential growth in YPD or after rehydration of YCW were washed two times in sodium acetate (18 mM CH_3COONa, 1 mM $CaCl_2$ and, 1 mM $MnCl_2$, pH 5.2), and immobilized on polydimethylsiloxane (PDMS) stamps prepared as described in (Dague et al, 2011). Briefly, freshly oxygen activated microstructured PDMS stamps were covered by 100 µL of yeasts sample at OD_{600} around 1.0. The cells were then deposited into the microstructures of the stamp by convective/capillary assembly.

AFM imaging

Images and force-distance curves were recorded at room temperature in acetate solution using an AFM Nanowizard III (JPK Instruments, Berlin, Germany) and MLCT AUWH cantilevers (Bruker, Santa Barbara, USA). The spring constants of the cantilevers were systematically measured by the thermal noise method according to (Hutter and Bechhoefer, 1993) and were found to be in the range of 0.01-0.02 $N.m^{-1}$. AFM height and adhesion images were recorded in Quantitative Imaging™ mode (Chopinet et al., 2013), and the maximal force applied to the cell was limited to 1.5 nN.

Surface roughness measurements

To measure cell surface roughness, images were obtained by scanning at high resolution (1µm x 1µm areas) on independent cell samples (at least 5) in the contact mode. In contact mode, the tip is in contact with the surface of the sample and scans this surface horizontally with a constant force, which is lower as possible. Height and vertical deflection images were both recorded with the contact mode. Height images with the same center of offset were processed and analyzed with the power spectral density method (JPK data processing software) consisting of average roughness (Ra in nm) measurements on five boxes of five different sizes for each images.

Stiffness measurements

Results were analyzed using the Data Processing software from JPK Instruments. The stiffness value (k_{cell} in $N.m^{-1}$) measured on cells was determined from the cantilever spring constant (k) and the slope (s) of the linear part of the force curve according to (Arnoldi et al., 2000):

$$kcell = k\left(\frac{s}{1-s}\right)$$

Force spectroscopy

For force spectroscopy experiments, the applied force was kept constant at 0.5 nN. To probe cell surface polysaccharides, AFM tips were functionalized with the concanavalin A (ConA) from *Canavalia ensiformis* (Sigma-Aldrich, L7647) via a dendritip as described in (Jauvert et al., 2012). The coupling with the lectin was made by immersion of the dendritip in 100 µL of ConA solution (100 $\mu g.mL^{-1}$ in a 0.1 M carbonate buffer). After 1 hr incubation, 100 µL of $NaBH_4$ 3.5 $mg.mL^{-1}$ solution was added and incubated 15 min in order to reduce the unreacted groups. Finally, the cantilever bearing the functionalized tip was washed three times and stored in acetate buffer. To analyze the stretching of polysaccharides at the surface of the cell, elongation forces were stretched using the worm-like chain (WLC) model introduced by Bustamante (Bustamante et al., 1994) which describes the polymer as a curved filament and the force F *vs* the extension x is given by:

$$F(x) = k_bT/l_p\,[0.25\,(1-x/L_c)^{-2} + x/L_c - 0.25]$$

where l_p represents the persistent length, the contour length (L_c) is the total length of the stretched molecule, k_b is the Boltzmann constant and T is the absolute temperature. This model has already been successfully used for the stretching of polysaccharides of yeasts especially for *S. cerevisiae* and *S. carlsbergensis* (Alsteens et al., 2008) and gives the best fitting of force curves. Blocking control experiments were performed by injecting 100 mM D-mannose solution into the cell surface.

Cell wall isolation and quantification of polysaccharides

Yeast cell walls were extracted and purified from yeast culture of L71 and L69 taken in exponential phase of growth on glucose (OD_{600}=1), rehydrated YCW and 'cream' according to the protocol described in (Francois, 2006). Cell wall polysaccharides mannan, chitin, β-(1,3) and β-(1,6) glucan in the purified cell walls were determined by a combination of acid and enzymatic hydrolysis recently developed (Schiavone et al., 2014) and quantification of the release sugar monomers (mannose, glucose and *N*-acetylglucosamine) was determined by High Performance Anionic Exchange Chromatography (HPAEC) with Pulsed Amperometric Detection (PAD) as described in (Dallies et al., 1998).

Transcriptomic analyses

Three independent biological cultures of industrial strains L71 and L69 were carried out in 50 mL of YPD in a 250 mL shake flasks. Yeast cells (about 10 OD_{600} units) were collected at OD_{600}=1 by centrifugation (3,000 rpm, 4°C, 2 min), followed by a washing step with 1 ml of sterilized water. The

cell pellets were immediately frozen in liquid nitrogen and stored at -80°C until RNA extraction. RNA extraction, quantification and labelling were carried out as described in (Alkim et al., 2013). Labeled cDNA were hybridized on Agilent glass slides microarrays, which bear the whole Saccharomyces cerevisiae genome (see details at http://www.biocompare.com/ProductDetails/760330/S-cerevisiae-Saccharomycescerevisiae-Whole-Genome.html). Hybridization was carried out in an automatic hybridization chamber (Agilent Technologies, Wilmington, USA) for 17 hr at 65°C. The hybridization signals were detected by scanning using Innoscan 900 laser Scanner (Innopsys Instruments), and transformed to numerical values using Feature Extraction V.11.5.1.1. The microarrays hybridization and processing were carried out at the Biochips Platform of Toulouse (http://biopuce.insa-toulouse.fr). Transcriptome analyses were done in R computing environment (www.R-project.org) using the Limma package (Yang and Speed, 2002) (www.bioconductor.org). The estimates used for the foreground and background intensities were the median of pixels intensity. Raw data were imported into R and spot quality weights were performed assigning a weight of 1 or 0 to each spot. Low-quality spots, non-uniform spots, spots with low signal/background ratio or spots with low signal-to-noise ratio and empty or non-validated spots were down weighted. Data were preprocessed by base 2 logarithmic transformation and within-array normalized was performed using the weighted global median (spots with zero weight were not included in the normalization). To achieve consistency of expression values between arrays, normalization across all the microarrays for each strain was performed. After normalization, the expression of a gene was calculated by the median of replicate spots within each microarray. Gene expression data for both strains were pairwise compared using the Limma package (Smyth, 2005). Genes with significant evidence for differential expression were identified with a modified t-test in conjunction with an empirical Bayes method to moderate the standard errors of the estimated log-fold changes. The P-values for the genes of interest were adjusted for multiple testing by the “BH" method (Hochberg and Benjamini, 1990).

III. RESULTS

Effects of autolysis/drying process on cell wall composition of two industrial yeast strains.

Since it is considered that the interaction cell-environment and sorption capacity to undesirable compounds are dependent on the surface properties of yeasts, which are in turn impacted

by the biochemical composition of cell wall (Armando et al., 2012; Pradelles et al., 2008) (Nunez, 2008) we aimed at investigating effects of the industrial autolysis/drying process on cell wall composition of two industrial strains. These strains were chosen on the basis of their different winemaking behavior and content of mannoproteins (Lallemand Inc, unpublished data). To evaluate impact of the process, we compared the polysaccharides composition of cell walls purified from autolyzed/dried yeast cells, which are commercialized as "YCW", with those extracted from the same industrial strains that were cultivated under laboratory standard conditions (Yeast Peptone Dextrose medium) and harvested at the exponential phase of growth. The cell wall composition was also determined on packed yeast cells which are provided as 'cream' and which was obtained from batch fermentation in molasses-based medium. Results of this analysis are reported in Table IV-1.

Table IV-1: Cell wall composition of industrial strain L71 and L69

cell wall polysaccharides	Culture YPD		Cream		Autolysis/drying	
	Strain L71	Strain L69	Strain L71	Strain L69	Strain L71	Strain L69
	% of cell wall dry weight					
β-(1,3)-glucan	30.5 ± 6.0	36.2 ± 5.5*	34 ± 2.3	33.7 ± 5.0	32 ± 3.4	33.3 ± 4.0
β-(1,6)-glucan	24.4 ± 5.4	16.7 ± 1.7**	22.5 ± 5.5	17.3 ± 3.6**	22.5 ± 5.5	15.1 ± 2.7
chitin	6.0 ± 0.5	3.5 ± 1.0**	5.5 ± 1.0	2.8 ± 0.4**	5.5 ± 2.0	2.0 ± 0.4***
mannans	39.2 ± 7.0	43.5 ± 5.0**	37.0 ± 2.0	45.7 ± 5.5**	40.0 ± 2.0	48.5 ± 6.4**

The yeast strains L69 and L71 (Lallemand SAS collection) were cultivated in shake in flask under laboratory condition (Yeast Peptone Dextrose medium, 30°C) or obtained as 'Cream' or 'YCW' (autolysis/drying process (24 h at 55°C). The amounts of chitin, β-1,3-glucan, β-1,6-glucan and mannans in the cell wall are mean values ± SD obtained from three independent biological replicates, each made 2 times. Statistical comparisons in the cell wall composition between strains for each condition were made by one-way analysis of variance followed the Tukey's comparison test (XLstat software), for which *p* values were obtained indicated by an asterisk. *is meaning *p*-value < 0.05, ***p*-value <0.01 and ****p*-value <0.001.

Overall, the polysaccharides content in purified cell wall was between 85 to 90 % of the cell wall dry mass, the remaining 10 to 15 % corresponded to proteins (data not shown). Also, the proportion of β-(1,3), β-(1,6)-glucan, mannan and chitin in cell wall of the two industrial strains were statistically not different (*p* value > 0.05) between the three conditions/ treatments investigated. However, it can be noticed a strain effect on the biochemical composition of the cell wall that was statistically significant. Indeed, strain L71 either in a living, cream or dried stated exhibited two times more chitin (*p* value < 0.001) and a higher proportion of β-(1,6)-glucan in total β-glucan than in strain L69. On the other hand, the mannan content of the L69 strain was roughly 20 -25 % higher than in

strain L71 (p value < 0.01), which agreed with the fact that this industrial winemaking strain was selected on the basis of its higher production of mannoproteins. This high mannan content of strain L69 could be associated with the fact that this strain has a higher surface hydrophobicity than strain L71 (data not shown) as well as to a tendency to hold cells together in small-branched chain during growth and to produce clumps upon rehydration of YCW produced from this strain (data not shown).

Effects of autolysis/drying process on nanomechanical properties of two industrial yeast strains.

In accordance with a previous work (Hernawan and Fleet, 1995), rehydrated YCW regained round to ovoid cell shape like a normal living yeast cell (data not shown). This cell shape retention allowed using our immobilization methodology that is based on trapping of single round/ovoid yeast cell into microchambers made in microstructured PDMS stamp by capillary/convective means(Dague et al., 2011). This methodology is very efficient to readily monitor several isolated cells in liquid environment by AFM. Topographic images using Quantitative Imaging™ mode (Chopinet et al., 2013) of living yeast cells from strain L71 and rehydrated YCW derived from L71 strain is reported in Figure IV-1 (a and b). For both types of yeast samples, height images illustrated a rather round shape of the immobilized object with an apparent smooth surface. However, a closer inspection of the AFM images from the rehydrated sample revealed the presence of a single hole of 600 nm diameter size curiously localized in the middle of immobilized cell (Fig. IV-S1 in supplementary data), and this feature was obtained in at least 15 % of the analyzed cells. At higher resolution, height images (Fig.IV-1 c and d) from contact mode clearly showed significant differences of the surface between living and rehydrated sample from L71 strain, as the surface of the latter was severely fractured. In quantitative terms, the roughness of cell surface (determined on 1 µm x 1 µm areas) was around 1.9 ± 0.2 nm for the living cell and increased to 5.1 ± 1.1 nm for the rehydrated YCW sample (Table IV-2). This surface change could be linked to the ultrastructural changes that were reported by Low Temperature Scanning Electron Microscopy (LSTEM) of a commercial yeast strain after 14 hr of induced autolysis in a model wine medium (Martínez-Rodríguez et al., 2001). Figure IV-1 (e, f) shows adhesion images of a living and rehydrated cell from YCW of L71 strain that were obtained by probing the surface with an AFM tip in QI™ mode. As the tip is made of silicon nitride and the immobilized sample is under an acidic pH (sodium acetate 18 mM at pH 5.2), these conditions most likely favor hydrophobic interactions, which

are however relatively weak with both type of cells, and hence agreed with exposure of 'neutral' cell wall carbohydrates.

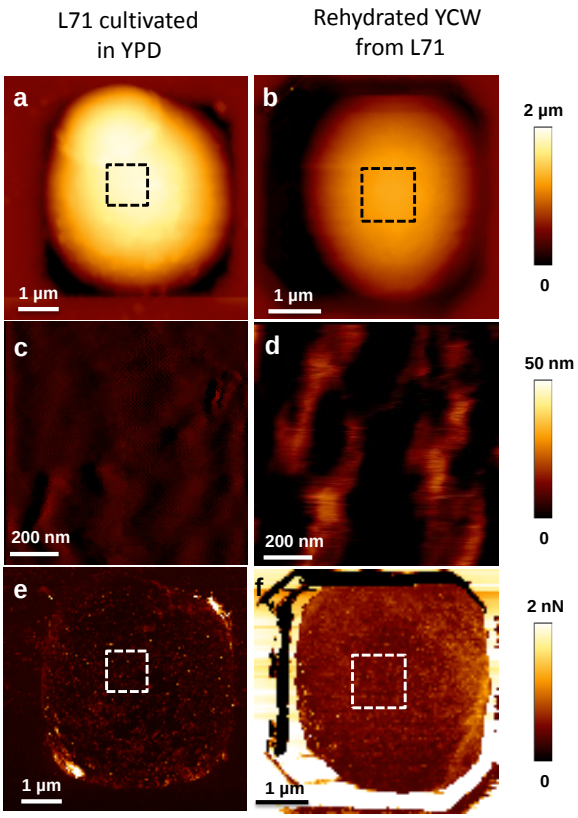

Figure IV-1: Cell surface topography of a living cell and rehydrated sample from strain L71

AFM height (a, b), contact (c,d) and adhesion images (e, f) of a living (a, c, e) and a rehydrated YCW sample (b, d, f) of YCW from strain L71. Living cells were from L71 cultivated exponentially on YPD medium whereas the rehydrated sample was from autolysed/dried sample of L71 obtained as "YCW" and rehydrated according to manufacturer's recommendation as described in Material & Methods.

Table IV-2: Effect of autolysis/drying process on cell surface roughness

Condition/treatment	Roughness (nm)	
	Strain L71	Strain L69
Culture YPD*	1.9 ± 0.2	1.7 ± 0.2
autolysis/drying	5.1 ± 1.1	6.4 ± 1.4

The yeast strain L69 and L71 (Lallemand Inc collection) were cultivated in shake in flask under laboratory condition (Yeast Peptone Dextrose medium, 30°C) or obtained as 'cream' or 'YCW' (autolysis/drying process (24h at 55°C). Surface roughness was calculated on AFM high-resolution images of 1 x 1 µm on a total of 15 cells taken from three independent biological replicates for each condition.

Similar AFM analyses were carried out with active living yeast cells and rehydrated YCW of L69 strain. The topographic images taken at low resolution (Fig IV-2, a and c) did not show difference in both types of cell samples immobilized in PDMS (Fig. IV-2). At higher resolution, some discretional dots could be visualized that were rather larger in rehydrated YCW (Fig IV-2, b and d). In addition, we

found a hole in immobilized rehydrated samples of YCW in about at least 15 % of the AFM images, like it was seen for strain L71 (see Fig.IV-S1 supplementary data).

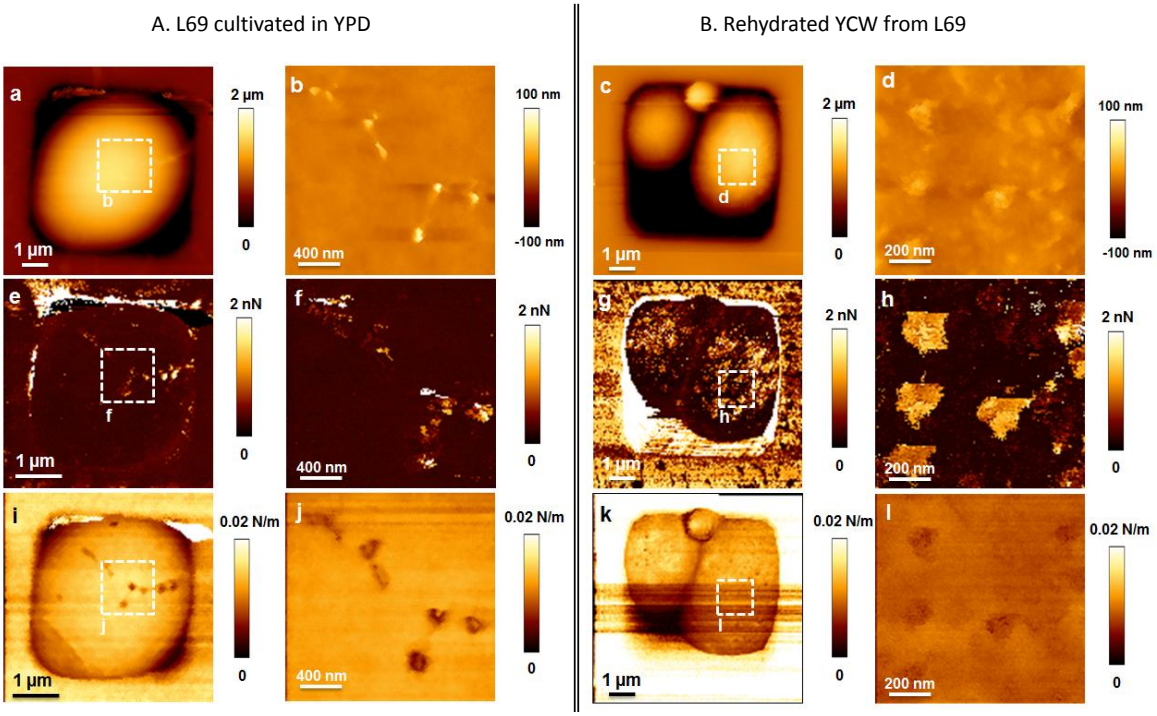

Figure IV-2: Cell surface topography of a living cell and rehydrated cell from strain L69

AFM height (a, b, c, d), adhesion (e, f, g, h) and stiffness (i, j, k, l) images of a living (a, b, e, f, I, j) and a rehydrated YCW sample (c, d, g, h, k, l) from the strain L69. The living cell was from an exponential culture of L69 strain on YPD medium, whereas rehydrated cell was from autolysed/dried sample of L69 obtained as "YCW" and rehydrated according to manufacturer's recommendation as described in Material & Methods.

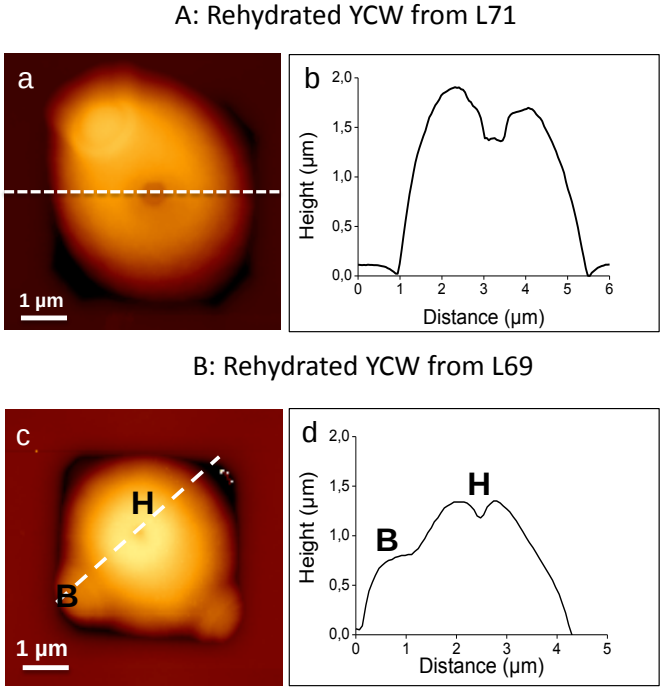

Figure IV-S1: AFM images on rehydrated cell reveal the presence of a hole

AFM height images (a, b) recorded with QI™ mode (JPK instruments) and (c, d) plots of height versus distance of a cross-section represented by white hatched bars for rehydrated cell of strain L71 (a, b) and strain L69 (c, d). The bud and the hole identified of the height image are represented by B and H, respectively.

The force curves acquired in QI mode were also analyzed to obtain adhesion images. This analysis revealed adhesives patches that were not present in L71 strain and which became apparently bigger in the sample from rehydrated YCW (compared Fig. IV-2 a, e, i for active yeast cells with c, g and k for rehydrated YCW). On average, the patches from the rehydrated YCW had a mean area of 156663.4 ± 3904.4 nm^2 (0.016 ± 0.004 μm^2) and a diameter of 141 ± 32 nm (measured from 56 patches on 7 different cells with Image J software). Additional details of the morphology and mechanical properties of these patches are reported in Figure IV-3 and Figure IV-S2 in supplementary data.

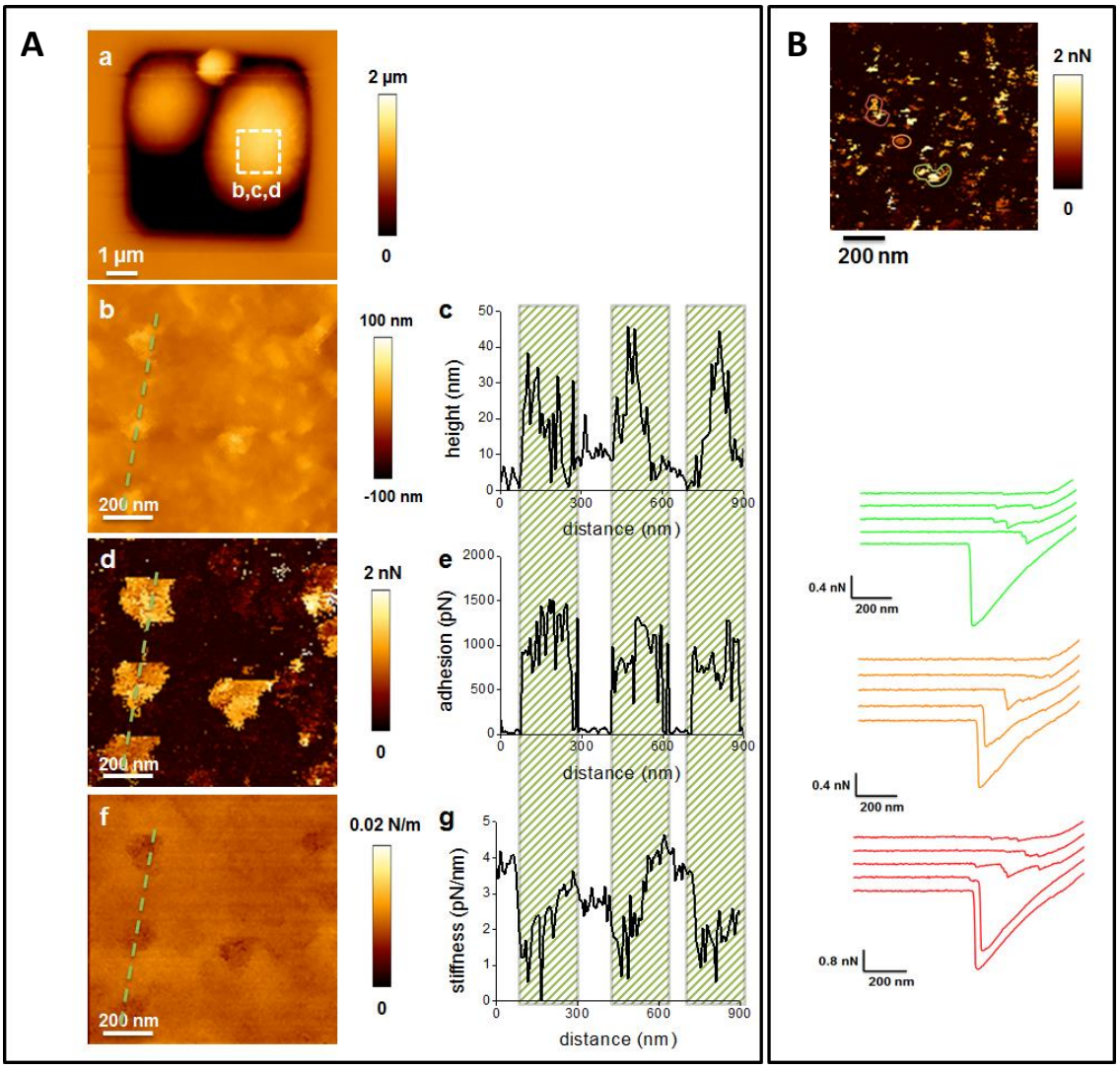

Figure IV-3: Detailed cell surface analysis identified adhesive patches in rehydrated cell from strain L69
On the left panel (A) are shown AFM height (a, b), adhesion (d) and stiffness (f) images. The green hatched lines represent a cross-section drawn over a distance separated three identified patches. The change of height (in nm), adhesion (pN) and stiffness (pN/nm) is quantitatively represented by plotting the value of each of these biophysical parameter over the distance of this cross-section. The right panel (B) illustrates an AFM adhesion image at high resolution (z-scale: 2 nN) and force-distance curves obtained on a green, orange and red patches that are represented by the corresponding color in the bottom of this image.

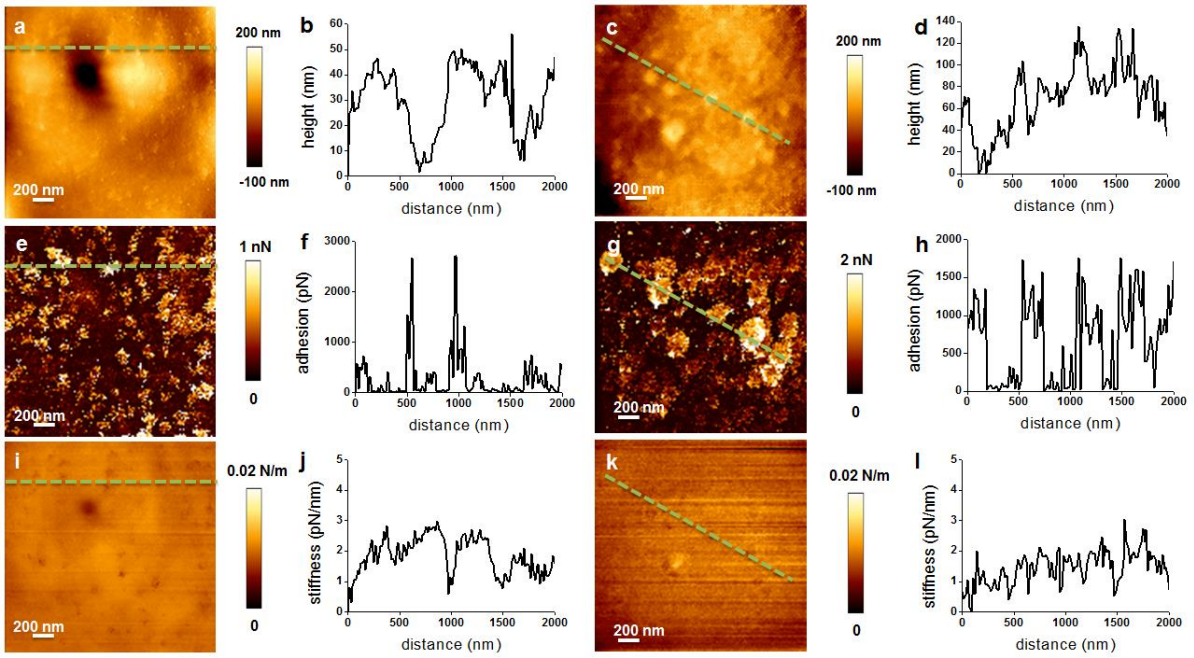

Figure IV-S2: Detail cell surface analysis identified adhesive patches on rehydrated cell from strain L69. AFM height (a, c), adhesion (e, g) and stiffness (I, k) images recorded with Quantitative Imaging mode. The green hatched lines represent a cross-section drawn over a distance separated different patches. The change of height (in nm), adhesion (pN) and stiffness (pN/nm) is quantitatively represented by plotting the value of each of these biophysical parameter over the distance of this cross-section.

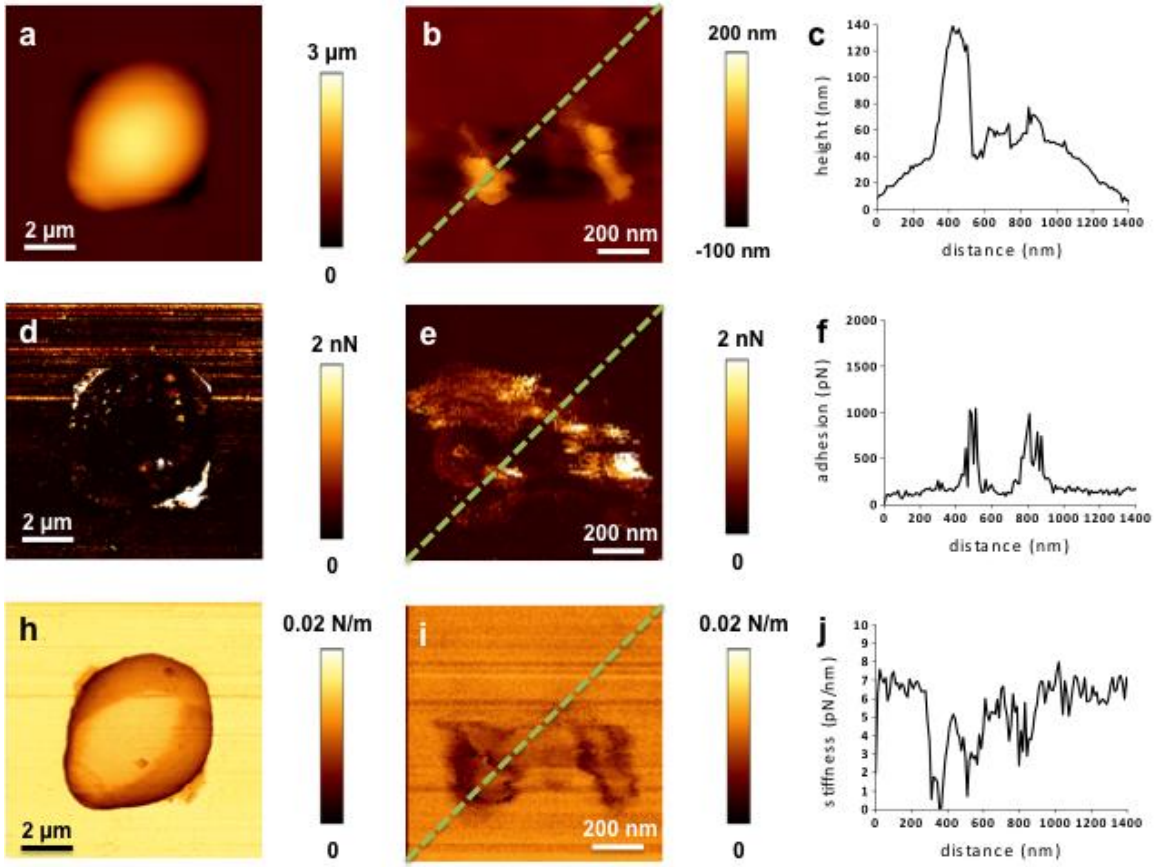

Figure IV-S3: Detailed cell surface analysis identified adhesive patches on living cells from strain L69 AFM height (a, b), adhesion (d, e) and stiffness (h, i) images recorded with Quantitative Imaging mode. The green hatched lines represent a cross-section drawn over a distance separated patches. The change of height (in nm), adhesion (pN) and stiffness (pN/nm) is quantitatively represented by plotting the value of each of these biophysical parameter over the distance of this cross-section.

From a cross-section taken through several patches (see the green dashed line), the corresponding height, adhesion and stiffness values were determined. This detailed AFM analyses showed that these patches corresponded to small protuberances exceeding the cell surface as shown in Figure IV-3Ae (also shown in Figure IV-S2 b and d, in supplementary data). These protuberances strongly interacted with the AFM tip (Fig. IV-3B). Example of adhesion force is schematically illustrated by force-distance curves taken from 3 different patches (Fig. IV-3B). On the contrary, these patches exhibited lower stiffness than the ground surface of the rehydrated YCW sample. Recently, similar observation was made with other *Candida albicans* cells that also harbored nanodomains at its cell surface represented by hydrophobic patches that were likely due to high expression the *ALS1* encoding cell surface protein (Alsteens et al., 2010; Formosa et al*.,* 2014). Taken together, these results provide some clues about the surface properties of L69 strain which were distinct from those of L71 strain.

Probing mannans polysaccharides at the cell surface using an AFM tip functionalized with Concanavalin A.

To go deeper in the analysis of the process effect on cell surface properties and illustrate differences in cell surface between the two industrial strains, we employed the single molecule force spectroscopy (SMFS) using an AFM tip functionalized with ConA. This molecule is a lectin protein that has high affinity to α-mannosyl residues, with an unbinding force, which corresponds to the rupture of a single lectin-mannose, has been estimated in the range of 60 pN (Alsteens et al., 2008). Figure IV-4 shows results of distribution, adhesion and flexibility of mannans at the surface of a living and YCW rehydrated from L71 strain. Adhesion force maps (Fig. IV-4, b and f) obtained with 1024 force-distance curves recorded with the ConA tip showed a relatively homogenous distribution of mannans polysaccharides across the surface of the rehydrated L71 sample, whereas this distribution was apparently less regular for the living cell. However, the adhesion frequency that represents the percentage of single or multiple unbinding forces was in the range of 25 % for both types of yeast samples (Fig. IV-4, c and g) with a mean value of unbinding forces around a maximum of 60 pN (58 ± 21 pN for the living cell and 65 ± 38 pN for the rehydrated sample, this difference being statistically not significant with a calculated p value > 0.05) in accordance with a previous report (Alsteens et al., 2008). Moreover, this binding interaction was blocked at 92.5 % by addition of excess of mannose solution onto the immobilized samples (see Fig.IV-S3, in supplementary data). This result indicated

that the adhesion force merely originates from specific lectin-mannans interactions. However, the 7.5% residual adhesion suggested some unspecific interactions. We also noticed that bud scars in both type of yeast samples were not adhesive (data not shown).

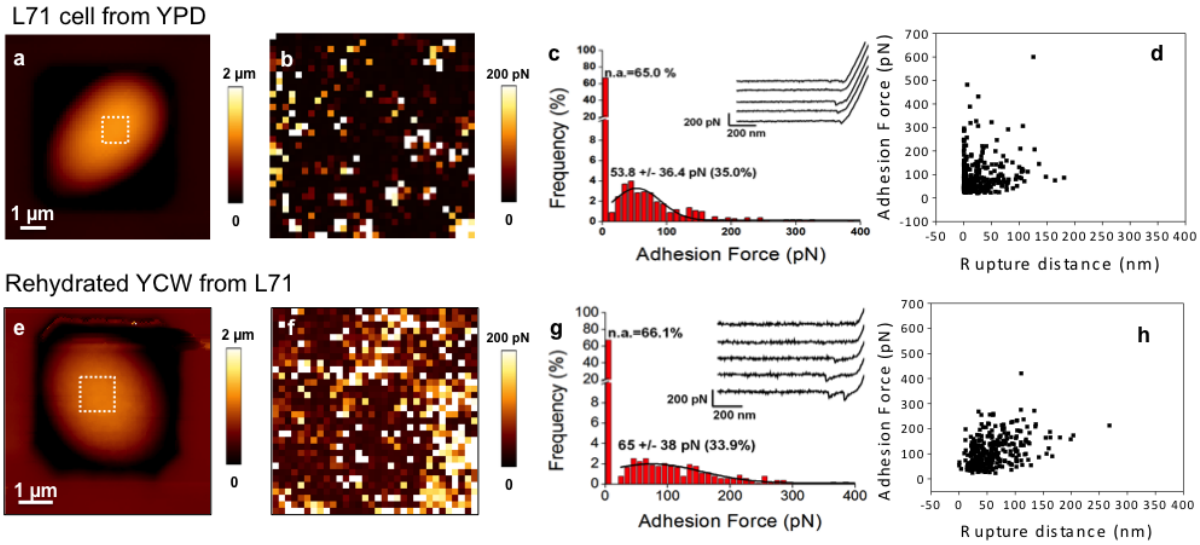

Figure IV-4: Mapping mannan polysaccharides on the surface of a living and rehydrated cell from strain L71 using AFM tips functionalized with ConA

AFM height images (a, e), adhesion force maps (b, f), adhesion force histograms (n=1024) with representative force curves recorded with ConA tip (c, g) and plots of adhesion frequency versus rupture distance (d, h) obtained on a living (a, b, c, d) and rehydrated sample (e, f, g, h) from strain L71. The living cell was from an exponential culture of L71 strain on YPD medium, whereas the rehydrated cell were from autolysed/dried sample of L71 strain obtained as "YCW" and rehydrated according to manufacturer's recommendation as described in Material & Methods.

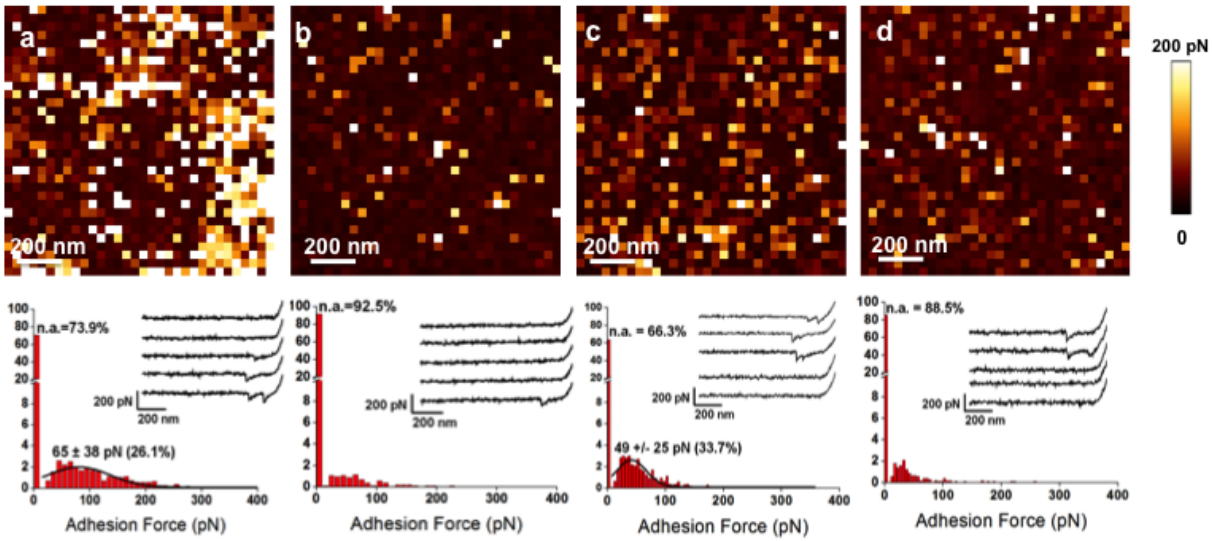

Figure IV-S4. Interaction of conA-tip with surface polysaccharides is abolished by excess of mannose

Adhesion force maps (1 µm x 1 µm) with corresponding adhesion force histograms (n=1024) recorded with a Con A tip on rehydrated cell of L71 (a, b) and L69 (c, d) strain in the absence (a, c) or in the presence of 100 mM mannose (b, d).

An additional property of the mannan polysaccharides that can be obtained using this SMFS approach is the rupture distances which define the distance needed to retract the conA tip from its binding with the mannan polysaccharides. These data can be informative on the flexibility and extension of these macromolecules. As can be seen in Fig. IV-4 (d and h), the rupture distances recorded for both types of samples was comprised between 0 and 250 nm, with a slight wider distribution towards larger lengths for the rehydrated sample suggesting that the polysaccharides chains in this sample were slightly more adhesive and extended than in living cells.

We then carried out a similar experiment with strain L69. Results of this SMFS analysis using ConA tip are reported in Figure IV-5. It can be seen that, like for the previous L71 strain, adhesion force map from the rehydrated YCW of L69 strain was more homogeneous than that of a living cell. However, longer rupture distances (up to 350 nm) were recorded on the living cell of L69 strain as compared to those with living L71 cells (compare Fig. IV-4d and Fig. IV-5d), suggesting difference in the stretching of polysaccharides between these two strains. In addition, longer rupture distances in L69 than in L71 strain were consistent with higher adhesion and presence of patches at the cell surface of the L69 strain. Alternatively or complementary to this explanation, it is possible that L69 strain expressed more and/or different mannoproteins than L71 strain. Also, on average, the rupture distance obtained with living cell of L69 was apparently longer than that of the rehydrated YCW of the same strain (Fig.IV-5 d and h).

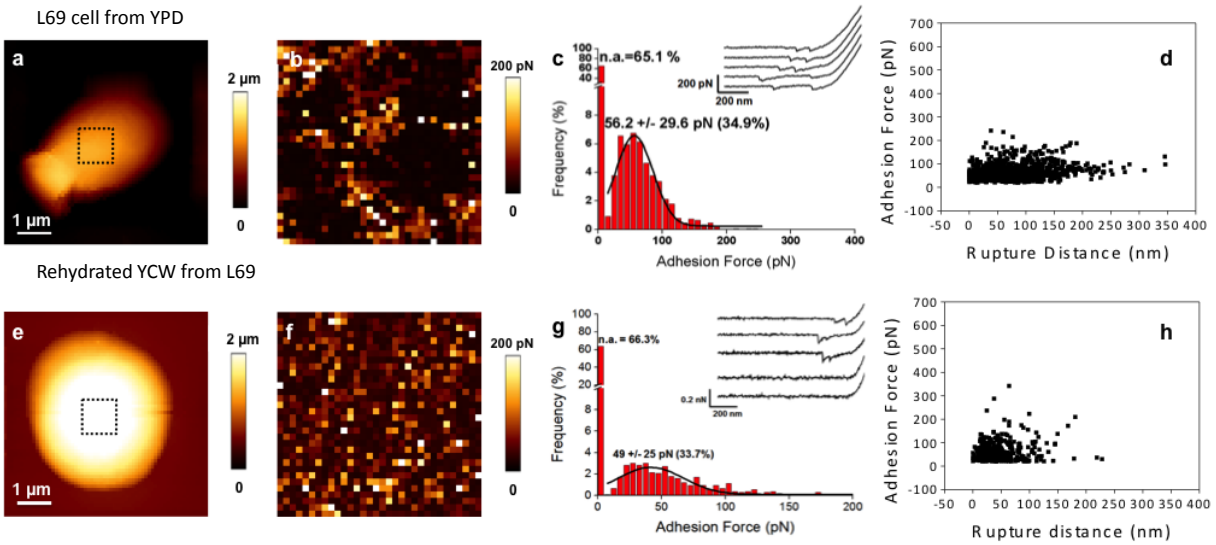

Figure IV-5: Mapping mannan polysaccharides on the surface of a living and rehydrated cell from strain L69 using a AFM tip functionalized with ConA

AFM height images (a, e), adhesion force maps (b, f), adhesion force histograms (n=1024) with representative force curves recorded with ConA tip (c, g) and plots of adhesion frequency versus rupture distance (d, h) obtained on a lived (a, b, c, d) and rehydrated cell (e, f, g, h) from strain L69. The lived cell was from an exponential culture

of L69 strain on YPD medium, whereas rehydrated cells were from “YCW” of strain L69 rehydrated according to manufacturer’s recommendation as described in Material & Methods.

Transcriptomic analyses to infer differences in cell surface properties between the two industrial strains.

To seek for a molecular explanation of the difference between cell surface properties between the two industrial strains, we carried out a genome-wide scale expression analysis using DNA microarrays. On a global view, we obtained 392 differentially expressed genes between L69 versus L71 strain, that were distributed into 175 upregulated and 217 downregulated genes (see table IV-S1 and IV-S2 in supplementary material). Major differences between L69 versus L71 strains were found in the downregulation of several genes implicated in sulfate and methionine metabolism as well as in a relatively increased expression of genes with yet unclear function. We looked more carefully to genes implicated in cell wall biogenesis and assembly to find out potential differentially expressed genes that could be linked to difference in cell surface properties between the two strains. As reported in Table IV-3, strain L69 was characterized by higher expression levels of genes encoding mannoproteins. In particular, FLO11 encoding a mucin-like protein that belongs to the flocculation gene family (Lo et al, 1996; Van Mulders, 2009) was strongly upregulated in L69 strain. Since this protein has a highly hydrophobic character (Karunanithi et al., 2010), this can explain the hydrophobic adhesions recorded by AFM (Fig. IV-3). In addition, the relative higher expression of *YHR213w* encoding a putative flocculin may further contribute to this hydrophobicity property as well as to the presence of patches at the cell surface of L69 strain. There was however some cell wall encoding genes whose expression was slightly more expressed in strain L71 relative to L69 strain, such as *FLO5* encoding a lectin-like cell wall protein, but this differential expression can be considered as insignificant to account for difference in adhesion properties between the two strains.

Table IV-3: Difference in expression levels of genes related to cell wall biogenesis between L69 versus L71 strain

ORF	Gene	Biological function	Fold change
YER011W	*TIR1*	Cell wall mannoprotein	1.9
YGR166W	*KRE11*	β-1,6-glucan biosynthesis	2.0
YHR213W	*YHR213W*	Pseudogenic fragment, similar to flocculin	7.7
YIR019C	*FLO11*	flocculin, GPI-anchored cell surface glycoprotein	11.4
YJR151C	*DAN4*	Cell wall mannoprotein, similar to TIR1, TIR2, TIR3, and TIR4	1.7
YLR037C	*PAU23*	Cell wall mannoprotein, similar to TIR1, TIR2, TIR3, and TIR4	1.5
YLR194C	*YLR194C*	Unknown function and unknown phenotype	1.8
YOR382W	*FIT2*	GPI-anchored cell wall mannoprotein	3.1
YOR383C	*FIT3*	GPI-anchored cell wall mannoprotein	4.1
YER096W	*SHC1*	Sporulation-specific activator of Chs3p (chitin synthase III)	*0.5*
YGR279C	*SCW4*	Soluble cell wall protein with similarity to β-glucanases	*0.6*
YHR211W	*FLO5*	flocculin, lectin-like cell wall protein	*0.5*
YKL163W	*PIR3*	Member of PIR family protein, cell wall structural protein	*0.5*
YLR300W	*EXG1*	Exo-β-1,3-glucanase	*0.4*
YOR010C	*TIR2*	Putative cell wall mannoprotein	*0.5*
YOR140W	*SFL1*	Suppressor of flocculation	*0.7*

IV. DISCUSSION

Combination of biochemical analyses and AFM technology allows us to observe that packaging yeast cells as “YCW” by autolysis and drying process significantly affected the global surface properties of the cells, in spite of the fact that the biochemical composition of the cell wall was barely altered by this packaging process. This result reinforces our previous finding showing no direct relationship between the polysaccharides composition of cell wall and its bionanomechanical properties (Dague et al., 2010; Formosa et al., 2013; Pillet et al., 2014). Also, the finding that cell wall composition remained barely unchanged after autolysis and drying process is at variance to other reports that indicated some loss of β-glucan and mannans during this process (Cavagna et al., 2010; Giovani and Rosi, 2007). However, the discrepancy can be explained by the difference in the autolysis process. In our study, it is an industrial process that consisted in an induced autolysis at high temperature for 20 h, whereas other studies were related to yeast autolysis during wine fermentation that lasted several days and was done at lower temperature (Alexandre and Guilloux-Benatier, 2006; Martínez-Rodríguez et al., 2001). As compared to living or active yeast cells, the main effect of autolysis/drying process was to increase the roughness of the cell surface, which was visualized as a change from a relatively smooth to wrinkled structure. It remains to evaluate whether this modification has some impact in the sorption capacity of the yeast cells.

In a previous work, we showed that the mode of cultivation and medium composition influenced the cell wall composition (Aguilar-Uscanga and Francois, 2003), while other studies demonstrated differences in cell wall composition among different yeasts species (Nguyen et al., 1998). Here, we furthermore showed that even for a same yeast species that is endowed with same genome, the biochemical composition of the cell wall and its cell surface organization can be dramatically different. These differences can be explained in part by difference in gene expression levels. Indeed, we found that the transcript levels of *FLO11* encoding a flocculin and of *YHR213w* that is suggested to code also for a flocculin, were relatively much higher in L69 than in L71 strain. In addition, several patches in the nanometer size were detected at the cell surface of L69 strain by AFM that resembled nanodomains identified at the cell surface of the pathogenic yeast *C. albicans* (Alsteens et al., 2010; Formosa et al., 2014b). In *C. albicans*, these nanodomains were attributed to the presence of massive amount of *ALS1* encoding adhesins which forms amyloid due to seven residues sequence enriched in β-branched amino acids (Ile, Thre, Val) that are predicted to form

intramolecular β-sheet like interactions or amyloids (Lipke et al., 2012). Recently, it was found that the sequence of the *S. cerevisiae* Flo11 protein presents such amyloid forming motifs VVSTTV and VTTAVT that can lead to partial β-aggregation (Ramsook et al., 2010). Therefore, the higher expression for this flocculin encoding gene in L69 strain may account for the formation of the nanodomains, for the difference in the stretching properties of the mannoprotein of this strain as compared to L71 strain, as well as for the tendency of L69 cells to form aggregates (data not shown). Furthermore, the higher content of mannans measured in L69 strain can be also explained by a higher level in Flo11 which is known to be a very highly glycosylated protein as well as by other GPI-anchored mannoproteins, since the expression of their corresponding genes was found increased as compared to strain L71. On the other side, the reduced levels of β-(1,6) glucan and chitin in L69 strain were not associated with reduced expression levels of the main genes related to their biosynthesis or regulation (Lesage et al., 2002) suggesting that these differences between the two strains would be at the post-transcriptional regulation. For chitin, it is well established that chitin synthase 3 (CSIII) encoded by *CHS3* is responsible for > 90 % of the chitin in exponential growing yeast and that this protein is regulated at the post-translational level, which implicated notably an endocytic process mechanism that retrieves CSIII from chitosomes to plasma membrane (review in (Orlean, 2012)). Regulation of β-(1,6)-glucan is also very complex and takes place along the secretory pathway because several of the proteins implicated in the synthesis of this polymer were localized in the ER, Golgi or plasma membrane. Thus, the synthesis of β-glucan can be regulated at the level of any of these enzymatic steps during this process.

In conclusion, our combined biochemical and biophysical analyses of living-active and autolyzed cells confirmed, on the one hand that for a given yeast strain, changes in biomechanical properties of the cell surface caused by the process packaging are not linked to changes in cell wall composition. On the other hand, the significant difference in a particular and specific cell wall component between yeast strains could result in important difference in the biophysical properties of the surface between these strains.

ACKNOWLEDGEMENTS

We thank Henri Durand and Anne Ortiz-Julien from Lallemand Inc. for critical discussions during this work. This work was supported in part by a grant n°10051296 from Region Midi Pyrénées to JMF and an ANR Young Scientist project ANR-11-JSV5-001-01, n° (SD) 30 02 43 31 to ED. ED is researcher at the Centre National de la Recherche Scientifique (CNRS) and MS is supported by a grant from Lallemand SAS (Cifre fellowship).

References

Aguilar-Uscanga, B., and Francois, J.M. (2003). A study of the yeast cell wall composition and structure in response to growth conditions and mode of cultivation. Lett. Appl. Microbiol. 37, 268–274.

Alexandre, H., and Guilloux-Benatier, M. (2006). Yeast autolysis in sparkling wine – a review. Aust. J. Grape Wine Res. 12, 119–127.

Alkim, C., Benbadis, L., Yilmaz, U., Cakar, Z.P., and François, J.M. (2013). Mechanisms other than activation of the iron regulon account for the hyper-resistance to cobalt of a Saccharomyces cerevisiae strain obtained by evolutionary engineering. Met. Integr. Biometal Sci. 5, 1043–1060.

Alsteens, D., Dupres, V., Mc Evoy, K., Wildling, L., Gruber, H.J., and Dufrêne, Y.F. (2008). Structure, cell wall elasticity and polysaccharide properties of living yeast cells, as probed by AFM. Nanotechnology 19, 384005.

Alsteens, D., Garcia, M.C., Lipke, P.N., and Dufrene, Y.F. (2010). Force-induced formation and propagation of adhesion nanodomains in living fungal cells. Proc. Natl. Acad. Sci. 107, 20744–20749.

Armando, M.R., Pizzolitto, R.P., Dogi, C.A., Cristofolini, A., Merkis, C., Poloni, V., Dalcero, A.M., and Cavaglieri, L.R. (2012). Adsorption of ochratoxin A and zearalenone by potential probiotic Saccharomyces cerevisiae strains and its relation with cell wall thickness. J. Appl. Microbiol. 113, 256–264.

Arnoldi, M., Fritz, M., Bäuerlein, E., Radmacher, M., Sackmann, E., and Boulbitch, A. (2000). Bacterial turgor pressure can be measured by atomic force microscopy. Phys. Rev. E 62, 1034–1044.

Bustamante, C., Marko, J.F., Siggia, E.D., and Smith, S. (1994). Entropic elasticity of lambda-phage DNA. Science 265, 1599–1600.

Cavagna, M., Dell'Anna, R., Monti, F., Rossi, F., and Torriani, S. (2010). Use of ATR-FTIR microspectroscopy to monitor autolysis of Saccharomyces cerevisiae cells in a base wine. J. Agric. Food Chem. 58, 39–45.

Chopinet, L., Formosa, C., Rols, M.P., Duval, R.E., and Dague, E. (2013). Imaging living cells surface and quantifying its properties at high resolution using AFM in QITM mode. Micron.

Dague, E., Gilbert, Y., Verbelen, C., Andre, G., Alsteens, D., and Dufrêne, Y.F. (2007). Towards a nanoscale view of fungal surfaces. Yeast 24, 229–237.

Dague, E., Bitar, R., Ranchon, H., Durand, F., Yken, H.M., and Francois, J.M. (2010). An atomic force microscopy analysis of yeast mutants defective in cell wall architecture. Yeast Chichester Engl. 27, 673–684.

Dague, E., Jauvert, E., Laplatine, L., Viallet, B., Thibault, C., and Ressier, L. (2011). Assembly of live micro-organisms on microstructured PDMS stamps by convective/capillary deposition for AFM bio-experiments. Nanotechnology 22, 395102.

Dallies, N., Francois, J., and Paquet, V. (1998). A new method for quantitative determination of polysaccharides in the yeast cell wall. Application to the cell wall defective mutants of Saccharomyces cerevisiae. Yeast Chichester Engl. 14, 1297–1306.

Dufrêne, Y.F. (2010). Atomic force microscopy of fungal cell walls: an update. Yeast 27, 465–471.
Fomina, M., and Gadd, G.M. (2014). Biosorption: current perspectives on concept, definition and application. Bioresour. Technol. 160, 3–14.

Formosa, C., Schiavone, M., Martin-Yken, H., François, J.M., Duval, R.E., and Dague, E. (2013). Nanoscale Effects of Caspofungin against Two Yeast Species, Saccharomyces cerevisiae and Candida albicans. Antimicrob. Agents Chemother. 57, 3498–3506.

Formosa, C., Schiavone, M., Boisrame, A., Richard, M.L., Duval, R.E., and Dague, E. (2014). Multiparametric imaging of adhesive nanodomains at the surface of Candida albicans by atomic force microscopy. Nanomedicine Nanotechnol. Biol. Med.

Francois, J.M. (2006). A simple method for quantitative determination of polysaccharides in fungal cell walls. Nat. Protoc. 1, 2995–3000.

Giovani, G., and Rosi, I. (2007). Release of cell wall polysaccharides from Saccharomyces cerevisiae thermosensitive autolytic mutants during alcoholic fermentation. Int. J. Food Microbiol. 116, 19–24.

Hatoum, R., Labrie, S., and Fliss, I. (2012). Antimicrobial and Probiotic Properties of Yeasts: From Fundamental to Novel Applications. Front. Microbiol. 3.

Hernawan, T., and Fleet, G. (1995). Chemical and cytological changes during the autolysis of yeasts. J. Ind. Microbiol. 14, 440–450.

Hinterdorfer, P., Garcia-Parajo, M.F., and Dufrêne, Y.F. (2012). Single-Molecule Imaging of Cell Surfaces Using Near-Field Nanoscopy. Acc. Chem. Res. 45, 327–336.

Hochberg, Y., and Benjamini, Y. (1990). More powerful procedures for multiple significance testing. Stat. Med. 9, 811–818.

Hutter, J.L., and Bechhoefer, J. (1993). Calibration of atomic‐force microscope tips. Rev. Sci. Instrum. 64, 1868‐1873.

Jauvert, E., Dague, E., Séverac, M., Ressier, L., Caminade, A.-M., Majoral, J.-P., and Trévisiol, E. (2012). Probing single molecule interactions by AFM using bio-functionalized dendritips. Sens. Actuators B Chem. 168, 436–441.

Karunanithi, S., Vadaie, N., Chavel, C.A., Birkaya, B., Joshi, J., Grell, L., and Cullen, P.J. (2010). Shedding of the Mucin-like Flocculin Flo11p Reveals a New Aspect of Fungal Adhesion Regulation. Curr. Biol. CB 20, 1389–1395.

Lesage, G., and Bussey, H. (2006). Cell wall assembly in Saccharomyces cerevisiae. Microbiol. Mol. Biol. Rev. MMBR 70, 317–343.

Lipke, P.N., Garcia, M.C., Alsteens, D., Ramsook, C.B., Klotz, S.A., and Dufrêne, Y.F. (2012). Strengthening relationships: amyloids create adhesion nanodomains in yeasts. Trends Microbiol. 20, 59–65.

Martínez-Rodríguez, A.J., Polo, M.C., and Carrascosa, A.V. (2001). Structural and ultrastructural changes in yeast cells during autolysis in a model wine system and in sparkling wines. Int. J. Food Microbiol. 71, 45–51.

Nguyen, T.H., Fleet, G.H., and Rogers, P.L. (1998). Composition of the cell walls of several yeast species. Appl. Microbiol. Biotechnol. 50, 206–212.

Orlean, P. (2012). Architecture and Biosynthesis of the Saccharomyces cerevisiae Cell Wall. Genetics 192, 775–818.

Osumi, M. (1998). The ultrastructure of yeast: Cell wall structure and formation. Micron 29, 207–233.

Petruzzi, L., Sinigaglia, M., Corbo, M.R., Campaniello, D., Speranza, B., and Bevilacqua, A. (2014). Decontamination of ochratoxin A by yeasts: possible approaches and factors leading to toxin removal in wine. Appl. Microbiol. Biotechnol. 98, 6555–6567.

Pillet, F., Lemonier, S., Schiavone, M., Formosa, C., Martin-Yken, H., Francois, J., and Dague, E. (2014). Uncovering by Atomic Force Microscopy of an original circular structure at the yeast cell surface in response to heat shock. BMC Biol. 12, 6.

Pradelles, R., Alexandre, H., Ortiz-Julien, A., and Chassagne, D. (2008). Effects of yeast cell-wall characteristics on 4-ethylphenol sorption capacity in model wine. J. Agric. Food Chem. 56, 11854–11861.

Pradelles, R., Vichi, S., Alexandre, H., and Chassagne, D. (2009). Influence of the drying processes of yeasts on their volatile phenol sorption capacity in model wine. Int. J. Food Microbiol. 135, 152–157.

Ramsook, C.B., Tan, C., Garcia, M.C., Fung, R., Soybelman, G., Henry, R., Litewka, A., O'Meally, S., Otoo, H.N., Khalaf, R.A., et al. (2010). Yeast Cell Adhesion Molecules Have Functional Amyloid-Forming Sequences. Eukaryot. Cell 9, 393–404.

Schiavone, M., Vax, A., Formosa, C., Martin-Yken, H., Dague, E., and François, J.M. (2014). A combined chemical and enzymatic method to determine quantitatively the polysaccharide components in the cell wall of yeasts. FEMS Yeast Res. 14, 933–947.

Sharon, N., and Lis, H. (2007). Lectins (Springer Science & Business Media).

Smyth, G.K. (2005). Limma: linear models for microarray data. In Bioinformatics and Computational Biology Solutions Using R and Bioconductor, (New York: R. Gentleman, V. Carey, S. Dudoit, R. Irizarry, W. Huber), pp. 397–420.

White, S., McIntyre, M., Berry, D.R., and McNeil, B. (2002). The Autolysis of Industrial Filamentous Fungi. Crit. Rev. Biotechnol. 22, 1–14.

Yang, Y.H., and Speed, T. (2002). Design issues for cDNA microarray experiments. Nat. Rev. Genet. 3, 579–588

Table IV-S1: Classification of genes whose expression was higher in strains L69 compared to L71 into MIPS categories*

Upregulated genes classified according to MIPS Functional Classification (459 categories)							
MIPS category	**Category**	**up-regulated genes in the given category**	**number of genes in MIPS category**	**% genes in each category**	**% genes in this category / total of upregulated genes**	**p-value**	**In category from Cluster**
transport facilitation	siderophore-iron transport	20	1038	1.9	11.4	8E-07	ARN1 ARN2 FET3 FRE4 ENB1 FRE3
	drug/toxin transport					3E-06	FLR1 AZR1 ARN1 ARN2 PDR11 QDR1 ENB1 YRM1 PDR10
	ABC transporters					2E-03	ARB1 PDR11 ENB1 PDR10 PXA1
metabolism & energy	fermentation	41	1881	2.2	23.0	7E-06	ADH7 AAD3 AAD4 AAD6 ALD2 AAD15 ATF1
	tetracyclic and pentacyclic triterpenes (cholesterin, steroids and hopanoids) metabolism					1E-05	ERG28 ERG25 ERG11 ERG7 ERG3 ERG27 ERG6 HMG1
	C-compound and carbohydrate metabolism					3E-04	GPI18 ADH7 AAD3 AAD4 YEL047C AAD6 ATF2 PHO12 FLO11 KTI12 GAL80 ALD2 PGM3 YNR071C YNR073C CSI2 AAD15 ATF1
	metabolism of phenylalanine					6E-04	AAD3 AAD4 AAD6 AAD15
	metabolism of tyrosine					8E-04	AAD3 AAD4 AAD6 AAD15
stress response	detoxification by export	9	554	1.6	5.0	3E-03	QDR1 YRM1 FLR1 AZR1 ARN1 ARN2 YLR046C ENB1 SSU1
unclassified proteins	unclassified proteins	60	1393	4.3	34.0	6E-03	PAU8 YAR064W YBL044W PSY4 YBL055C APD1 YBR242W HBN1 RNQ1 YCR051W YDR056C RTN1 FDC1 YEL057C YER077C AIM11 YER137C YFL051C PAU11 YGR017W ECL1 HGH1 PAU12 YHL042W YHR078W YHR213W YIL086C YIL096C YJL213W YJR039W YJR056C YJR115W DAN4 YKL047W COS9 YLL056C PAU18 PAU23 AVL9 YLR194C YLR326W YLR346C YMR007W YMR178W YMR181C YMR265C RSN1 YNL022C TCB2 YNL095C YNL193W YOL166C YOR012W IRC11 YOR342C YOR385W YOR390W YPL068C YPL279C YPR071W
regulation of metabolism and protein function	protease inhibitor	2	253	0.8	1.1	9E-03	RAD23 TFS1
others	in several non-enriched categories	43			25.0		

* Differential genes expression between L69 and L71 strain were retained on the basis of fold change > 1.5 at *p*-value <0.01

Table IV-S2: Classification of genes whose expression was lower in strains L69 compared to L71 into MIPS categories*

Downregulated genes classified according to MIPS Functional Classification (459 categories)							
MIPS category	**Category**	**down-regulated genes in the given category**	**number of genes in MIPS category**	**% genes in each category**	**% of genes in this category / total of downregulated genes**	**p-value**	**In category from Cluster**
cell cycle and DNA progressing	DNA topology	14	1012	1.4	6.5	7E-06	YBL113C YEL077C YRF1-2 YRF1-3 YIL177C YJL225C YLL067C YRF1-6 YRF1-7 YPR204W
	somatic / mitotic recombination					4E-03	YRF1-2 YRF1-3 YRF1-6 YRF1-7
communication	G-protein mediated signal transduction	6	234	2.6	2.8	5E-03	GPB2 STE18 STE4
	cAMP/cGMP mediated signal transduction					6E-03	PDE1 RAS1 SFL1
metabolism	sulfate assimilation	42	1514	2.8	19.4	3E-10	MET10 MET3 MET5 MET14 MET1 MET22 MET16
	purine nucleotide/nucleoside/nucleobase anabolism					2E-07	ADE1 ADE5,7 ADE3 MTD1 ADE13 IMD3 ADE4 ADE2 SER1
	biosynthesis of methionine					2E-05	CBF1 MET14 MET2 MET22
	metabolism of methionine					5E-04	MET32 MET3 MET1 MET17 MET16
	degradation of glycine					6E-04	GCV3 GCV1 SHM2
	biosynthesis of serine					1E-03	SER33 SHM2 SER1
	biosynthesis of homocysteine					1E-03	MET10 STR3 MET5
	biosynthesis of leucine					2E-03	LEU2 LEU1 BAT1
	tetrahydrofolate-dependent C-1-transfer					8E-03	ADE3 MTD1 SHM2
	C-1 compound catabolism					1E-02	GCV3 GCV1
protein binding	NAD/NADP binding	7	1049	0.7	3.2	1E-04	GPD1 MET10 ADE3 SER33 MET5 MTD1 GPD2
transport facilitation	sulfate/sulfite transport	2	1038	0.2	0.9	3E-03	OAC1, SUL2
others	in several non-enriched categories	143			67.3		

*Differential genes expression between L69 and L71 strain were retained on the basis of fold change < 0.6 at *p*-value <0.01

Chapitre V: CONCLUSION AND PERSPECTIVES

1. Conclusion

Due to increasing yeast biomass production resulting from the expansion of the Biorefinery as an alternative to petrol-based energy, the yeast cell wall is receiving an increased interest as an added value product targeting agro-nutrition markets, such as in animal nutrition and in wine for its probiotic and sorption properties (phenols, mycotoxins). The study of the yeast cell wall composition and its structure is a research topic addressed for more than twenty years. The recent advances in the AFM technology on liquid samples has allowed a remarkable progress in the understanding of the cell wall organization, structure and mechanical properties as well as to view and inspect these properties of the cell wall for the first time from 'outside' of the cells. As an exquisite example of the power of this approach was the investigation of the effect of heat shock on the cell wall which allowed us to observe the formation of a circular structure at the cell surface that propagated in a concentric manner to reach a diameter superior to 3 µm (Pillet et al., 2014). Likewise, effects of an antifugal drug caspofungin on the yeast cell wall of two species *Candida albicans* and *Saccharomyces cerevisiae* unraveled strong impact on the topography and nanomechanical properties of the cell (Formosa et al., 2013).

In this work, we wished to combine three approaches, namely biophysical using AFM, biochemical through a quantitative method of cell wall composition and molecular, using DNA microarray to assess gene expression, of laboratory and industrial strains cultivated under different conditions or subjected to specific process conditions in order to find correlation between nanomechanical properties of the cell wall, biochemical composition, as well as to underscore molecular cues that may account for the cell wall organization, structure and physical properties. To achieve this objective, our work has been divided into three parts:

(i) To develop an accurate and quantitative method to determine all the cell wall components

(ii) To investigate the "strain" effect on cell wall physical and composition, and to compare for each their transcriptome profiles

(iii) To study the effects of the autolysis process that result in a specific packaging of yeast sold as Yeast Cell Wall (YCW) on cell wall biophysical properties and composition.

As a general overview, our data clearly showed the importance of the strain and the culture conditions on the biochemical composition of the cell wall. This is in total agreement with previous works from our group (Aguilar-Uscanga and Francois, 2003) and others (Bzducha-Wróbel et al., 2013; Nguyen et al., 1998) that have shown the impact of the growth medium, mode of culture as well as strain origins on the cell wall composition. These studies showed that there was an approximately 1.5-fold decrease in β-glucan/mannan ratio in the cell wall of *S. cerevisiae* growing in a synthetic minimal medium compared to a rich yeast peptone dextrose medium (Aguilar-Uscanga et al., 2007). Also, glycerol at a concentration of 3% in the medium increased the amount of mannoproteins and β-glucan in cell wall of *S. cerevisiae* (Bzducha-Wróbel et al., 2013). In addition to the effect of nutrients and carbon sources, the culture parameters and environmental conditions influenced the cell wall composition. When the temperature rises from 22°C to 37°C, the amount of β-1,3-glucanase resistant fraction increase significantly (Aguilar-Uscanga et al., 2007), whereas the molecular size of β-1,3-glucan molecules depend on growth phase (Cabib et al., 2012). Here, we provided complementary information because we were able to distinct β-1,3 from β-1,6-glucan and found that this was the β-1,6-glucan content in the total β-glucan that in general was the most affected by these strain/culture conditions as well as in response to an antofungal drug (Formosa et al., 2013). A second general conclusion, which sustained previous works (Dague et al., 2010 and chapter 3A), was the lack of direct connection of the cell wall nanomechanical properties (specifically expressed as the Young modulus, a value that account for elasticity or stiffness) to a specific cell wall component. However, this conclusion may be challenged with the finding of a close correlation between Young modulus and β-1,3-glucan that was obtained from our correlation analysis using dedicated statistical methods (S-PLS and CCA in mixOmics package). This finding supported the general statement that β-1,3-glucan that forms the inner layer of the cell wall may be responsible for the cell shape due to the fibrillar structure of this component. However, this structure alone cannot account for the variations in elasticity properties of the cell wall as indicated by strong alteration of this propertie in mutants defective in cell wall remodeling enzymes such as Gas1, Crh1, Crh2 (Dague et al., 2010).

An interesting result that came out from our study using functionalized AFM tip with concanavalin A was to show tight association between either the mannan content, its type nature/type of mannoproteins in the cell wall and lectin-cell surface interactions. Indeed, long chains of polysaccharides were unfolded on the surface of *gas1*Δ mutant cell using single molecule force

spectroscopy with conA-tips, whereas *mnn9*Δ cells showed small percentage of specific interaction mannan-lectin and shorter rupture lengths (below 100 nm) likely because of their low content of mannan as well as of a different mannosylation decoration on the proteins. Thus our results indicate a difference in the length of polysaccharides stretched on the surface of these mutants. Using the same methodology, we explored the cell surface of the industrial strains and revealed that one of them, namely L69, was strongly adhesive. We were able to unfold molecules of 20-400 nm at the surface of this strain. This behavior agrees with a flexible filament with the worm like chain model (Bustamante et al., 1994; Janshoff et al., 2000), suggesting that chains of mannoproteins with a different anchorage in the cell wall are stretched on this strain. In addition, this strong adhesion event was found to be related to the specific overexpression of *FLO11* which encodes a flocculin protein attached to the cell wall via a GPI anchor and of *YHR213w* those codes for a putative floculin, whereas other flocculin encoded genes *FLO5* and *FLO10* were downregulated in this L69 strain. Moreover this strain, which has the highest mannoproteins content, was unique in displaying at the cell surface highly adhesive patches forming nanodomains, which were highlighted after autolysis process of these cells. Furthermore, we noticed that these nanodomains, which were imaged for the first time on the yeast *S. cerevisiae*, resembled to nanodomains identified at the cell surface of the pathogenic yeast *C. albicans* (Formosa et al., 2014b). These nanodomains in *Candida albicans* cells were attributed to *ALS1* (Formosa et al., 2014b) encoding adhesins. These poteins are known to form amyloid due to a structural motif of seven residues enriched in β-branched amino acids (Ile, Thre, Val), that are predicted to form intramolecular β-sheet like interactions (Ramsook et al., 2010). As written above, the *FLO11* encodes a GPI-anchored cell surface glycoprotein named flocculin and *YHR213W* has been identified as fragment with sequence similarity to *FLO11.* Molecular studies of Flo11 has revealed that the domain structure of this protein includes a N-terminal domain corresponding to a lectin-like adhesion domain, a repetitive and highly glycosylated central domain and a C-terminal domain that carries a GPI anchoring site. Also, the sequence of the Flo11 protein presents amyloid forming motifs that can lead to partial β-aggregation (Ramsook et al., 2010). Therefore, we can suggest that an upregulation of *FLO11* in L69 strain can lead to massive local deposition of Flo11 protein, which leads to β-aggregate amyloids clusters into nanodomains. Amyloids proteins are likely important in adhesion and pathogenicity as many adhesion molecules on the surface of pathogenic fungi such as *Aspergillus*, *Coccidioides*, and *Mucorales*, exhibits these properties. They mediate assembly of fungal

hydrophobins, curli in *Eschierichia coli* and chaplin in *Streptomyces coelicolor* (Syed and Boles, 2014). In yeast, amyloids nanodomains promote formation and maintenance of cell aggregation and biofilm, which can be preventing by mutation in amyloid sequence or by treatment with antiamyloid dyes such as Congo Red, thioflavin S and thioflavin T. In mammalian cells, these amyloids proteins were originally associated as markers of neurodegenerative diseases like Alzheimer, Parkinson or Creutzfeldt-Jakob diseases (Goldschmidt et al., 2010). The characterization, structure and properties of adhesive nanodomains in *S. cerevisiae* required further investigation. Furthermore, their discovery raises the question of their function in the sorption properties in *S. cerevisisae* based on the finding that, in *C. albicans*, the adhesins Als1p and Als5p were shown to bind multivalent ligands. For example, N-terminal domain of Als1p binds α-fucose (Donohue et al., 2011) and Als5p or Als1p adhere to peptides and proteins that display appropriate sequences of amino acids with a bulky hydrophobic amino acid and a cationic amino acid as well as an appropriate steric conformation (Klotz et al., 2004). Thus, both sequences and conformation are important in ligand recognition characteristics.

By integrating biomechanical properties and biochemical composition of cell wall with transcriptome profile of industrial strains using biomathematical methods based on correlation/covariance, we found a close association between cell wall elasticity (*i.e.* Young modulus values) and levels of β-1,3-glucans. The genes that were correlated with this association encoded protein implicated in membrane and cytoskeleton assembly (*SLA1*), β-1,6-glucan biosynthesis (*KRE11*) and in MAPK signaling pathways (*STE11, HOG1, DIG1, STE18*). These results suggest that Young modulus value may be dependent on level of β-glucan and that these two variables can be regulated by MAP kinase signaling implicated in osmotic stress and pseudohyphae growth. Moreover, the levels of mannan as well as lectin-cell surface interactions were associated to genes involved in protein processing (*KEX1, SSY5*), ergosterol and phospholipid biosynthesis (*ERG7, URA8*) and cell wall mannoprotein (*DAN4, YLR040C, GPI18*).

The last part of the thesis was dedicated to address the question of the effect of autolysis on the cell wall composition and nanomechanical properties of two industrial strains (L71 and L69 strains). This study showed that packaging yeast cells as “YCW” (for Yeast Cell Wall) by autolysis and drying process does not change the composition of the cell wall but causes a change in topography and surface properties of the cell. High resolution imaging of the cell surface showed a modification

from a smooth surface for exponential-phase cells to a wrinkled topography for YCW cells, resulting in a 4-fold increase of the average roughness of the YCW cells. An increase of roughness can modify the physicochemical properties of the surface by increasing hydrophobicity of the surface. It may result in an increase of the active surface by enhancing the number of ligands for an interaction with receptor (Hu et al., 2013), but the effects of surface roughness on sorption capacity have now to be accurately measured. Indeed, this measurement of sorption would help us to understand the link between sorption and cell wall properties and composition. Sorption measurements can be made by AFM, optical and magnetic tweezers (Neuman and Nagy, 2008). These techniques are used to study the interactions of a single biomolecule (ligand) with a surface of a living cell. Optical tweezers system used the light to trap microspheres, which can be coated by a ligand. Magnetic tweezers consist in a magnetic field used to turn the microsphere and the ligand attached, leading to study the torsion and conformation of the molecule. In contrast to the tweezers methods, in single molecule force spectroscopy experiments the ligand is linked to the AFM tip and it can be used to stretch the receptor, but also to localize the sites of the ligand-receptor interaction.

In addition, this AFM study showed some holes (600 nm in diameter) localized in the middle of YCW cells in both L69 and L71 strains, that could be due either to an effect of autolysis that may provoke a self-digestion of the yeast material by the intrinsic proteolytic enzymes as it is found in autolysis process during wine fermentation, but it can be also a consequence of the fluid-bed drying used in this process. Whether the autolysis process may impact on sorption capacity of various molecules such as toxins or drugs, remains to be evaluated.

To conclude, besides the development of a specific method to quantify each component of the cell wall, this work may provide relevant results towards industrial applications. On one hand, demonstrating that levels of β-1,3 and β-1,6-glucan in cell wall prepared from various strains (laboratory and industrial strains) and samples (living cells, cream, autolysed fraction) are influenced by strain and culture conditions could have an impact in the production of yeast derivatives for food and health industry. Also, understand the cell wall organization, mechanical and surface properties in *S. cerevisiae* as well as to find molecular cues that are related to these characteristics can suggest molecular or process strategies to favour specific cell wall properties of the yeast that will be dedicated to specific function, such as enhancing sorption capacity, optimizing expression of some specific mannoproteins at the cell surface and finding new antifungal targets. .

2. Perspectives

Short-term outlook:

Since the cell wall nanomechanical properties are highly specific to strains and depend on the cross-linkages between cell wall polysaccharides, one perspective that deserves further study should be to determine and quantify these cross-linkages between all the cell wall components and evaluate their importance in different strains. A characterization by NMR and mass-spectrometry techniques would assess to particular structures, which would explain the differences in nanomechanical measurements. Furthermore, we could improve our understanding on the relationship between gene, nanomechanical properties and cell wall composition by using the integrative approach applied to many other strains from other ecological niche, as well as for a strain that are challenged with different stresses such as heat shock, osmotic shock and ethanol stress. This should refine and extand our integrative analysis with hopefully pointing out genes essential that may dictate the cell wall composition and cell surface biophysical properties (*i.e.* cell wall elasticity and adhesion).

Another important perspective is to evaluate if the sorption ability is impacted by the presence of clusters of amyloids proteins (“nanodomains”). This question could be addressed using functionalized AFM tips with different ligands known to interact and to stretch at the cell surface and doing this, eventually identify potential ‘receptor’ of these ligands. Moreover, the origin of these nanodomains could be confirmed by attaching the amyloid peptide sequence of Flo11 protein to the tips in order to bind the nanodomains and to correlate them with the distribution of Flo11 protein on the cell surface. Another approach could be to functionalize the tip with an antibody that binds Flo11 protein. However anti-Flo11p (or anti-Muc1p) for yeast are not yet commercially available. Therefore, we would tag Flo11p with an HA molecule and map the distribution of this protein among the nanodomains with a tip functionalized with anti-HA (Formosa et al., 2014, Journal of Molecular Recognition, to be published). Control experiments on *flo11*Δ mutant strain derivative from L69 strain or on L69 strain mutated in amyloid sequence woud be required to make sure that measures are specific.

Long-term outlook:

Another approach to study the cell wall biogenesis, assembly and organization would be to investigate at the nanometer level, the progression of cell wall degradation upon treatment by specific hydrolytic enzymes or toxins and conversely the regeneration of the cell wall from these single spheroplasting cells. The use of chitinase, endo and exo-β-glucanases in order to degrade the polysaccharides that constitute the cell wall layers, and AFM imaging would allow following the degradation of the cell surface. For example, chitinase from *Streptomyces griseus* could be used to specifically degrade the bud scar known to be rich in chitin. Moreover, the use of fluorescence microscopy would allow observing the repartition of selected proteins. This technique combined to AFM experiment with functionalized tips would enable to detect and map the specific interactions between a ligand on the AFM tip and a receptor at the cell surface. For example, we could unfold the different polysaccharides of the cell wall. The lectin concanavalin A isolated from jack beans that binds α-glucose and α-mannose residues, could be used to unfold yeast mannan, whereas β-glucan could be unfolded with a banana lectin from *Musa acuminata* (Goldstein et al., 2001). This latest is the first lectin that binds glucosyl residues of β-3-glucose oligosaccharides (such as laminaribiose and its homologs) and interacts with β-6-linked glucose group, which occurs in β-1,3 and β-1,6-glucan of the yeast cell wall (Sharon and Lis, 2007).

Moreover studying the molecular interaction between a mycotoxin (Fumonisin B1 or Aflatoxin) and the yeast cell wall would have direct economic impact because of the commercialization of the yeast cell walls as binder of free-mycotoxins that contaminated animal feeds. This project should provide quantitative data on the molecular interaction in order to evaluate the ability of different industrial strains to bind the toxin. The first part of this investigation would be the development of AFM tips functionalized with the toxin. Then, single molecule force spectroscopy experiments would allow to detect and to measure the specific interactions between the yeast cell wall and the AFM tip functionalized with the toxin. Measuring the specific interaction and then unfolding the receptor involved in this interaction could provide us quantitative data on the type of molecular interactions. First, several mutants would be used to unravel which cell wall components are implicated in the interaction. Secondly, different industrial strains would be tested in order to correlate the data on the molecular interaction with *in vitro* assays performed by Lallemand Inc. on the same strains. To refine our understanding of the molecular interactions between the yeast cell wall and the mycotoxin, optical

tweezers could be used. Polystyrene beads will be functionalized with mycotoxin, and used to monitor single molecule interactions with yeast cells trapped in the laser beam. Using AFM and optical tweezers, we could also study how the industrial process can influence the molecular interaction of a mycotoxin with the cell wall. With these innovative techniques, we will be able to analyze the interactions between the toxin and the surface of different yeasts such as active yeast, cream and autolysed/dried yeast (packaged as ‘YCW’ fraction).

Chapter VI: REFERENCES

Adams, D.J. (2004). Fungal cell wall chitinases and glucanases. Microbiol. Read. Engl. 150, 2029–2035.

Aguilar-Uscanga, B., and Francois, J.M. (2003). A study of the yeast cell wall composition and structure in response to growth conditions and mode of cultivation. Lett. Appl. Microbiol. 37, 268–274.

Aguilar-Uscanga, B., Arrizon, J., Ramirez, J., and Solis-Pacheco, J. (2007). Effect of Agave tequilana juice on cell wall polysaccharides of three Saccharomyces cerevisiae strains from different origins. Antonie Van Leeuwenhoek 91, 151–157.

Ahimou, F., Touhami, A., and Dufrêne, Y.F. (2003). Real-time imaging of the surface topography of living yeast cells by atomic force microscopy. Yeast 20, 25–30.

Aimanianda, V., Clavaud, C., Simenel, C., Fontaine, T., Delepierre, M., and Latge, J.P. (2009). Cell wall beta-(1,6)-glucan of Saccharomyces cerevisiae: structural characterization and in situ synthesis. J. Biol. Chem. 284, 13401–13412.

Alexandre, H., and Guilloux-Benatier, M. (2006). Yeast autolysis in sparkling wine – a review. Aust. J. Grape Wine Res. 12, 119–127.

Alsteens, D., Dague, E., Rouxhet, P.G., Baulard, A.R., and Dufrêne, Y.F. (2007). Direct Measurement of Hydrophobic Forces on Cell Surfaces Using AFM. Langmuir 23, 11977–11979.

Alsteens, D., Dupres, V., Mc Evoy, K., Wildling, L., Gruber, H.J., and Dufrêne, Y.F. (2008). Structure, cell wall elasticity and polysaccharide properties of living yeast cells, as probed by AFM. Nanotechnology 19, 384005.

Alsteens, D., Dupres, V., Yunus, S., Latgé, J.-P., Heinisch, J.J., and Dufrêne, Y.F. (2012). High-Resolution Imaging of Chemical and Biological Sites on Living Cells Using Peak Force Tapping Atomic Force Microscopy. Langmuir 28, 16738–16744.

Arfsten, J., Leupold, S., Bradtmöller, C., Kampen, I., and Kwade, A. (2010). Atomic force microscopy studies on the nanomechanical properties of Saccharomyces cerevisiae. Colloids Surf. B Biointerfaces 79, 284–290.

Armando, M.R., Pizzolitto, R.P., Dogi, C.A., Cristofolini, A., Merkis, C., Poloni, V., Dalcero, A.M., and Cavaglieri, L.R. (2012). Adsorption of ochratoxin A and zearalenone by potential probiotic Saccharomyces cerevisiae strains and its relation with cell wall thickness. J. Appl. Microbiol. 113, 256–264.

Arroyo, J., Bermejo, C., García, R., and Rodríguez-Peña, J.M. (2009). Genomics in the detection of damage in microbial systems: cell wall stress in yeast. Clin. Microbiol. Infect. 15, 44–46.

Azuma, M., Levinson, J.N., Pagé, N., and Bussey, H. (2002). Saccharomyces cerevisiae Big1p, a putative endoplasmic reticulum membrane protein required for normal levels of cell wall β-1,6-glucan. Yeast 19, 783–793.

Baguley, B.C., Rommele, G., Gruner, J., and Wehrli, W. (1979). Papulacandin B: an Inhibitor of Glucan Synthesis in Yeast Spheroplasts. Eur. J. Biochem. 97, 345–351.

Baladron, V., Ufano, S., Duenas, E., Martin-Cuadrado, A.B., del Rey, F., and Vazquez de Aldana, C.R. (2002). Eng1p, an Endo-1,3- -Glucanase Localized at the Daughter Side of the Septum, Is Involved in Cell Separation in Saccharomyces cerevisiae. Eukaryot. Cell 1, 774–786.

Beaussart, A., El-Kirat-Chatel, S., Sullan, R.M.A., Alsteens, D., Herman, P., Derclaye, S., and Dufrêne, Y.F. (2014). Quantifying the forces guiding microbial cell adhesion using single-cell force spectroscopy. Nat. Protoc. 9, 1049–1055.

Bernstein, M., Hoffmann, W., Ammerer, G., and Schekman, R. (1985). Characterization of a gene product (Sec53p) required for protein assembly in the yeast endoplasmic reticulum. J. Cell Biol. 101, 2374–2382.

Bezsonov, E.E., Groenning, M., Galzitskaya, O.V., Gorkovskii, A.A., Semisotnov, G.V., Selyakh, I.O., Ziganshin, R.H., Rekstina, V.V., Kudryashova, I.B., Kuznetsov, S.A., et al. (2013). Amyloidogenic peptides of yeast cell wall glucantransferase Bgl2p as a model for the investigation of its pH-dependent fibril formation. Prion 7, 175–184.

Binnig, Quate, and Gerber (1986). Atomic force microscope. Phys. Rev. Lett. 56, 930–933.

Blanco, N., Reidy, M., Arroyo, J., and Cabib, E. (2012). Crosslinks in the cell wall of budding yeast control morphogenesis at the mother–bud neck. J. Cell Sci. 125, 5781–5789.

Boles, E., Liebetrau, W., Hofmann, M., and Zimmermann, F.K. (1994). A family of hexosephosphate mutases in Saccharomyces cerevisiae. Eur. J. Biochem. FEBS 220, 83–96.

Bom, I.J., Dielbandhoesing, S.K., Harvey, K.N., Oomes, S.J., Klis, F.M., and Brul, S. (1998). A new tool for studying the molecular architecture of the fungal cell wall: one-step purification of recombinant trichoderma beta-(1-6)-glucanase expressed in Pichia pastoris. Biochim. Biophys. Acta 1425, 419–424.

Boone, C. (1990). Yeast KRE genes provide evidence for a pathway of cell wall beta-glucan assembly. J. Cell Biol. 110, 1833–1843.

Boorsma, A., Nobel, H. de, Riet, B. ter, Bargmann, B., Brul, S., Hellingwerf, K.J., and Klis, F.M. (2004). Characterization of the transcriptional response to cell wall stress in Saccharomyces cerevisiae. Yeast 21, 413–427.

Bourdineaud, J.-P., Van Der Vaart, J.M., Donzeau, M., De Sampaïo, G., Verrips, C.T., and Lauquin, G.J.-M. (1998). Pmt1 mannosyl transferase is involved in cell wall incorporation of several proteins in Saccharomyces cerevisiae. Mol. Microbiol. 27, 85–98.

Brown, G.D., and Gordon, S. (2003). Fungal β-Glucans and Mammalian Immunity. Immunity 19, 311–315.

Brown, J., Kossaczka Z, Jiang B, and Bussey H (1993). A mutational analysis of killer toxin resistance in Saccharomyces cerevisiae identifies new genes involved in cell wall (1-->6)-beta-glucan synthesis. Genetics *133*, 837–849.

Brown Jl, and Bussey H (1993). The yeast KRE9 gene encodes an O glycoprotein involved in cell surface beta-glucan assembly. Mol. Cell. Biol. 13, 6346–6356.

Bugli, F., Posteraro, B., Papi, M., Torelli, R., Maiorana, A., Sterbini, F.P., Posteraro, P., Sanguinetti, M., and Spirito, M.D. (2013). In Vitro Interaction between Alginate Lyase and Amphotericin B against Aspergillus fumigatus Biofilm Determined by Different Methods. Antimicrob. Agents Chemother. 57, 1275–1282.

Bulawa, C.E., and Osmond, B.C. (1990). Chitin synthase I and chitin synthase II are not required for chitin synthesis in vivo in Saccharomyces cerevisiae. Proc. Natl. Acad. Sci. U. S. A. 87, 7424–7428.

Burda, P., and Aebi, M. (1999). The dolichol pathway of N-linked glycosylation. Biochim. Biophys. Acta 1426, 239–257.

Burnham, N.A., Chen, X., Hodges, C.S., Matei, G.A., Thoreson, E.J., Roberts, C.J., Davies, M.C., and Tendler, S.J.B. (2003). Comparison of calibration methods for atomic-force microscopy cantilevers. Nanotechnology 14, 1.

Bustamante, C., Marko, J.F., Siggia, E.D., and Smith, S. (1994). Entropic elasticity of lambda-phage DNA. Science 265, 1599–1600.

Byrne, K.P., and Wolfe, K.H. (2005). The Yeast Gene Order Browser: Combining curated homology and syntenic context reveals gene fate in polyploid species. Genome Res. 15, 1456–1461.

Bzducha-Wróbel, A., Kieliszek, M., and Błażejak, S. (2013). Chemical composition of the cell wall of probiotic and brewer's yeast in response to cultivation medium with glycerol as a carbon source. Eur. Food Res. Technol. 237, 489–499.

Cabib, E. (1991). Differential inhibition of chitin synthetases 1 and 2 from Saccharomyces cerevisiae by polyoxin D and nikkomycins. Antimicrob. Agents Chemother. 35, 170–173.

Cabib, E. (2005). Synthase III-dependent Chitin Is Bound to Different Acceptors Depending on Location on the Cell Wall of Budding Yeast. J. Biol. Chem. 280, 9170–9179.

Cabib, E. (2009). Two novel techniques for determination of polysaccharide cross-links show that Crh1p and Crh2p attach chitin to both beta(1-6)- and beta(1-3)glucan in the Saccharomyces cerevisiae cell wall. Eukaryot. Cell 8, 1626–1636.

Cabib, E., and Arroyo, J. (2013). How carbohydrates sculpt cells: chemical control of morphogenesis in the yeast cell wall. Nat. Rev. Microbiol. 11, 648–655.

Cabib, E., Silverman, S.J., and Shaw, J.A. (1992). Chitinase and chitin synthase 1: counterbalancing activities in cell separation of Saccharomyces cerevisiae. J. Gen. Microbiol. 138, 97–102.

Cabib, E., Blanco, N., Grau, C., Rodríguez-Peña, J.M., and Arroyo, J. (2007). Crh1p and Crh2p are required for the cross-linking of chitin to ?(1-6)glucan in the Saccharomyces cerevisiae cell wall. Mol. Microbiol. 63.

Cabib, E., Farkas, V., Kosik, O., Blanco, N., Arroyo, J., and McPhie, P. (2008). Assembly of the Yeast Cell Wall: Crh1p AND Crh2p ACT AS TRANSGLYCOSYLASES IN VIVO AND IN VITRO. J. Biol. Chem. 283, 29859–29872.

Cabib, E., Blanco, N., and Arroyo, J. (2012). Presence of a large β(1-3)glucan linked to chitin at the Saccharomyces cerevisiae mother-bud neck suggests involvement in localized growth control. Eukaryot. Cell 11, 388–400.

Canetta, E., Adya, A.K., and Walker, G.M. (2006). Atomic force microscopic study of the effects of ethanol on yeast cell surface morphology. FEMS Microbiol. Lett. 255, 308–315.
Lê Cao, K.-A., González, I., and Déjean, S. (2009). integrOmics: an R package to unravel relationships between two omics datasets. Bioinforma. Oxf. Engl. 25, 2855–2856.

Cappellaro, C., Mrsa, V., and Tanner, W. (1998). New potential cell wall glucanases of Saccharomyces cerevisiae and their involvement in mating. J. Bacteriol. 180, 5030–5037.

Carreto, L., Eiriz, M.F., Gomes, A.C., Pereira, P.M., Schuller, D., and Santos, M.A. (2008). Comparative genomics of wild type yeast strains unveils important genome diversity. BMC Genomics 9, 524.

Castillo, L., Martinez, A.I., Garcera, A., Victoria Elorza, M., Valentin, E., and Sentandreu, R. (2003). Functional analysis of the cysteine residues and the repetitive sequence ofSaccharomyces cerevisiae Pir4/Cis3: the repetitive sequence is needed for binding to the cell wall ?-1,3-glucan. Yeast 20, 973–983.

Castro, C., Ribas, J.C., Valdivieso, M.H., Varona, R., Rey, F. del, and Duran, A. (1995). Papulacandin B resistance in budding and fission yeasts: isolation and characterization of a gene involved in (1,3)beta-D-glucan synthesis in Saccharomyces cerevisiae. J. Bacteriol. *177*, 5732–5739.

Celton, M., Sanchez, I., Goelzer, A., Fromion, V., Camarasa, C., and Dequin, S. (2012). A comparative transcriptomic, fluxomic and metabolomic analysis of the response of Saccharomyces cerevisiae to increases in NADPH oxidation. BMC Genomics 13, 317.

Cerf, A., Cau, J.C., Vieu, C., and Dague, E. (2009). Nanomechanical properties of dead or alive single-patterned bacteria. Langmuir ACS J. Surf. Colloids 25, 5731–5736.

Chalier, P., Angot, B., Delteil, D., Doco, T., and Gunata, Z. (2007). Interactions between aroma compounds and whole mannoprotein isolated from Saccharomyces cerevisiae strains. Food Chem. 100, 22–30.

Chen, J., and Seviour, R. (2007). Medicinal importance of fungal β-(1→3), (1→6)-glucans. Mycol. Res. 111, 635–652.

Cherry, J.M., Adler, C., Ball, C., Chervitz, S.A., Dwight, S.S., Hester, E.T., Jia, Y., Juvik, G., Roe, T., Schroeder, M., et al. (1998). SGD: Saccharomyces Genome Database. Nucleic Acids Res. 26, 73–79.

Chopinet, L., Formosa, C., Rols, M.P., Duval, R.E., and Dague, E. (2013). Imaging living cells surface and quantifying its properties at high resolution using AFM in QITM mode. Micron.

Cid, V.J., Duran, A., del Rey, F., Snyder, M.P., Nombela, C., and Sanchez, M. (1995). Molecular basis of cell integrity and morphogenesis in Saccharomyces cerevisiae. Microbiol. Rev. 59, 345–386.

Claro, F.B., Rijsbrack, K., and Soares, E.V. (2007). Flocculation onset in Saccharomyces cerevisiae: effect of ethanol, heat and osmotic stress. J. Appl. Microbiol. 102, 693–700.

Comitini, F., Mannazzu, I., and Ciani, M. (2009). Tetrapisispora phaffii killer toxin is a highly specific β-glucanase that disrupts the integrity of the yeast cell wall. Microb. Cell Factories 8, 55.

Dague, E., Bitar, R., Ranchon, H., Durand, F., Yken, H.M., and Francois, J.M. (2010). An atomic force microscopy analysis of yeast mutants defective in cell wall architecture. Yeast Chichester Engl. 27, 673–684.

Dague, E., Jauvert, E., Laplatine, L., Viallet, B., Thibault, C., and Ressier, L. (2011). Assembly of live micro-organisms on microstructured PDMS stamps by convective/capillary deposition for AFM bio-experiments. Nanotechnology 22, 395102.

Dallies, N., Francois, J., and Paquet, V. (1998). A new method for quantitative determination of polysaccharides in the yeast cell wall. Application to the cell wall defective mutants of Saccharomyces cerevisiae. Yeast Chichester Engl. 14, 1297–1306.

Danielson, M.E., Dauth, R., Elmasry, N.A., Langeslay, R.R., Magee, A.S., and Will, P.M. (2010). Enzymatic method to measure Î2-1,3-Î2-1,6-glucan content in extracts and formulated products (GEM assay). J. Agric. Food Chem. 58, 10305–10308.

Daran, J.M., Dallies, N., Thines-Sempoux, D., Paquet, V., and François, J. (1995). Genetic and biochemical characterization of the UGP1 gene encoding the UDP-glucose pyrophosphorylase from Saccharomyces cerevisiae. Eur. J. Biochem. FEBS 233, 520–530.

Davenport, K.R., Sohaskey, M., Kamada, Y., Levin, D.E., and Gustin, M.C. (1995). A Second Osmosensing Signal Transduction Pathway in Yeast HYPOTONIC SHOCK ACTIVATES THE PKC1 PROTEIN KINASE-REGULATED CELL INTEGRITY PATHWAY. J. Biol. Chem. 270, 30157–30161.

Dengis, P.B., and Rouxhet, P.G. (1997). Flocculation Mechanisms of Top and Bottom Fermenting Brewing Yeast. J. Inst. Brew. 103, 257–261.

Denning, D.W. (2003). Echinocandin antifungal drugs. The Lancet 362, 1142–1151.

Destruelle, M., Holzer, H., and Klionsky, D.J. (1994). Identification and characterization of a novel yeast gene: the YGP1 gene product is a highly glycosylated secreted protein that is synthesized in response to nutrient limitation. Mol. Cell. Biol. 14, 2740–2754.

Devrekanli, A., Foltman, M., Roncero, C., Sanchez-Diaz, A., and Labib, K. (2012). Inn1 and Cyk3 regulate chitin synthase during cytokinesis in budding yeasts. J. Cell Sci. 125, 5453–5466.

Dijkgraaf, G.J.P., Abe, M., Ohya, Y., and Bussey, H. (2002). Mutations in Fks1p affect the cell wall content of beta-1,3- and beta-1,6-glucan in Saccharomyces cerevisiae. Yeast Chichester Engl. 19, 671–690.

Donohue, D.S., Ielasi, F.S., Goossens, K.V.Y., and Willaert, R.G. (2011). The N-terminal part of Als1 protein from Candida albicans specifically binds fucose-containing glycans. Mol. Microbiol. 80, 1667–1679.

Douglas, C.M., Foor, F., Marrinan, J.A., Morin, N., Nielsen, J.B., Dahl, A.M., Mazur, P., Baginsky, W., Li, W., and el-Sherbeini, M. (1994). The Saccharomyces cerevisiae FKS1 (ETG1) gene encodes an integral membrane protein which is a subunit of 1,3-beta-D-glucan synthase. Proc. Natl. Acad. Sci. U. S. A. 91, 12907–12911.

Dufrêne, Y.F. (2002). Atomic Force Microscopy, a Powerful Tool in Microbiology. J. Bacteriol. 184, 5205–5213.

Dufrêne, Y.F. (2008). Atomic force microscopy and chemical force microscopy of microbial cells. Nat. Protoc. 3, 1132–1138.

Dünkler, A., Jorde, S., and Wendland, J. (2008). An Ashbya gossypii cts2 mutant deficient in a sporulation-specific chitinase can be complemented by Candida albicans CHT4. Microbiol. Res. 163, 701–710.

Ebner, A., Wildling, L., Zhu, R., Rankl, C., Haselgrübler, T., Hinterdorfer, P., and Gruber, H.J. (2008). Functionalization of probe tips and supports for single-molecule recognition force microscopy. Top. Curr. Chem. 285, 29–76.

Eng, W.-K., Faucette, L., McLaughlin, M.M., Cafferkey, R., Koltin, Y., Morris, R.A., Young, P.R., Johnson, R.K., and Livi, G.P. (1994). The yeast FKS1 gene encodes a novel membrane protein, mutations in which confer FK506 and cyclosporin A hypersensitivity and calcineurin-dependent growth. Gene 151, 61–71.

Escobar-Henriques, M., Collart, M.A., and Daignan-Fornier, B. (2003). Transcription initiation of the yeast IMD2 gene is abolished in response to nutrient limitation through a sequence in its coding region. Mol. Cell. Biol. 23, 6279–6290.

Feldmann, H. (2012). Yeast: Molecular and Cell Biology (John Wiley & Sons).

Fernandez Mp, and Cabib E (1984). Saccharomyces cerevisiae mannoproteins form an external cell wall layer that determines wall porosity., Saccharomyces cerevisiae mannoproteins form an external cell wall layer that determines wall porosity. J. Bacteriol. J. Bacteriol. 159, 159, 1018, 1018–1026.

Firmin, S., Gandia, P., Morgavi, D.P., Houin, G., Jouany, J.P., Bertin, G., and Boudra, H. (2010). Modification of aflatoxin B 1 and ochratoxin A toxicokinetics in rats administered a yeast cell wall preparation. Food Addit. Contam. Part A 27, 1153–1160.

Fleet, G. (1991). Cell walls. Yeasts 4, 199–277.

Fleet, G.H., and Manners, D.J. (1976). Isolation and Composition of an Alkali-soluble Glucan from the Cell Walls of Saccharomyces cerevisiae. J. Gen. Microbiol. 94, 180–192.

Fleet, G.H., and Manners, M. (1977). The enzymic degradation of an alkali-soluble glucan from the cell walls of Saccharomyces cerevisiae. J. Gen. Microbiol. 98, 315–327.

Formosa, C., Schiavone, M., Martin-Yken, H., François, J.M., Duval, R.E., and Dague, E. (2013). Nanoscale Effects of Caspofungin against Two Yeast Species, Saccharomyces cerevisiae and Candida albicans. Antimicrob. Agents Chemother. 57, 3498–3506.

Formosa, C., Pillet, F., Schiavone, M., Duval, R.E., Reissier, L., and Dague, E. (2014a). Generation of living cell arrays for Atomic Force Microscopy studies. Nat. Protoc. in press.

Formosa, C., Schiavone, M., Boisrame, A., Richard, M.L., Duval, R.E., and Dague, E. (2014b). Multiparametric imaging of adhesive nanodomains at the surface of Candida albicans by atomic force microscopy. Nanomedicine Nanotechnol. Biol. Med.

Francius, G., Alsteens, D., Dupres, V., Lebeer, S., De Keersmaecker, S., Vanderleyden, J., Gruber, H.J., and Dufrêne, Y.F. (2009). Stretching polysaccharides on live cells using single molecule force spectroscopy. Nat. Protoc. 4, 939–946.

Francois, J.M. (2006). A simple method for quantitative determination of polysaccharides in fungal cell walls. Nat. Protoc. 1, 2995–3000.

Free, S.J. (2013). Fungal cell wall organization and biosynthesis. Adv. Genet. 81, 33–82.

Friedrichs, J., Helenius, J., and Muller, D.J. (2010). Quantifying cellular adhesion to extracellular matrix components by single-cell force spectroscopy. Nat. Protoc. 5, 1353–1361.

Fuchs, B.B., and Mylonakis, E. (2009). Our paths might cross: the role of the fungal cell wall integrity pathway in stress response and cross talk with other stress response pathways. Eukaryot. Cell 8, 1616–1625.

Gaboriaud, F., and Dufrêne, Y.F. (2007). Atomic force microscopy of microbial cells: Application to nanomechanical properties, surface forces and molecular recognition forces. Colloids Surf. B Biointerfaces 54, 10–19.

Gad, M., and Ikai, A. (1995). Method for immobilizing microbial cells on gel surface for dynamic AFM studies. Biophys. J. 69, 2226–2233.

García, R., Bermejo, C., Grau, C., Pérez, R., Rodríguez-Peña, J.M., Francois, J., Nombela, C., and Arroyo, J. (2004). The Global Transcriptional Response to Transient Cell Wall Damage in Saccharomyces cerevisiae and Its Regulation by the Cell Integrity Signaling Pathway. J. Biol. Chem. 279, 15183–15195.

García, R., Rodríguez-Peña, J.M., Bermejo, C., Nombela, C., and Arroyo, J. (2009). The high osmotic response and cell wall integrity pathways cooperate to regulate transcriptional responses to zymolyase-induced cell wall stress in Saccharomyces cerevisiae. J. Biol. Chem. 284, 10901–10911.

Gasch, A.P., Spellman, P.T., Kao, C.M., Carmel-Harel, O., Eisen, M.B., Storz, G., Botstein, D., and Brown, P.O. (2000). Genomic Expression Programs in the Response of Yeast Cells to Environmental Changes. Mol. Biol. Cell 11, 4241–4257.

Gentzsch, M., and Tanner, W. (1996). The PMT gene family: protein O-glycosylation in Saccharomyces cerevisiae is vital. EMBO J. 15, 5752–5759.

Girrbach, V., and Strahl, S. (2003). Members of the Evolutionarily Conserved PMT Family of ProteinO-Mannosyltransferases Form Distinct Protein Complexes among Themselves. J. Biol. Chem. 278, 12554–12562.

Goffeau, A., Barrell, B.G., Bussey, H., Davis, R.W., Dujon, B., Feldmann, H., Galibert, F., Hoheisel, J.D., Jacq, C., Johnston, M., et al. (1996). Life with 6000 genes. Science 274, 546, 563–567.

Goldschmidt, L., Teng, P.K., Riek, R., and Eisenberg, D. (2010). Identifying the amylome, proteins capable of forming amyloid-like fibrils. Proc. Natl. Acad. Sci. 107, 3487–3492.

Goldstein, I.J., Winter, H.C., Mo, H., Misaki, A., Van Damme, E.J., and Peumans, W.J. (2001). Carbohydrate binding properties of banana (Musa acuminata) lectin II. Binding of laminaribiose oligosaccharides and beta-glucans containing beta1,6-glucosyl end groups. Eur. J. Biochem. FEBS 268, 2616–2619.

Gómez-Esquer, F., Rodríguez-Peña, J.M., Díaz, G., Rodriguez, E., Briza, P., Nombela, C., and Arroyo, J. (2004). CRR1, a gene encoding a putative transglycosidase, is required for proper spore wall assembly in Saccharomyces cerevisiae. Microbiol. Read. Engl. 150, 3269–3280.

Gonzalez-Ramos, D., and Gonzalez, R. (2006). Genetic determinants of the release of mannoproteins of enological interest by Saccharomyces cerevisiae. J. Agric. Food Chem. 54, 9411–9416.

Goossens, K.V.Y., Stassen, C., Stals, I., Donohue, D.S., Devreese, B., De Greve, H., and Willaert, R.G. (2011). The N-Terminal Domain of the Flo1 Flocculation Protein from Saccharomyces cerevisiae Binds Specifically to Mannose Carbohydrates. Eukaryot. Cell 10, 110–117.

Götzinger (2006). Effect of roughness on particle adhesion in aqueous solutions: A study of Saccharomyces cerevisiae and a silica particle 10.1016/j.colsurfb.2006.11.001 : Colloids and Surfaces B: Biointerfaces | ScienceDirect.com.

Guerriero, G., Silvestrini, L., Obersriebnig, M., Salerno, M., Pum, D., and Strauss, J. (2013). Sensitivity of Aspergillus nidulans to the Cellulose Synthase Inhibitor Dichlobenil: Insights from Wall-Related Genes' Expression and Ultrastructural Hyphal Morphologies. PLoS ONE 8, e80038.

Ha, C., Lim, K., Kim, Y., Lim, S., Kim, C., and Chang, H. (2002). Analysis of alkali-soluble glucan produced by Saccharomyces cerevisiae wild-type and mutants. Appl. Microbiol. Biotechnol. 58, 370–377.

Hashimoto, H., Sakakibara, A., Yamasaki, M., and Yoda, K. (1997). Saccharomyces cerevisiae VIG9 encodes GDP-mannose pyrophosphorylase, which is essential for protein glycosylation. J. Biol. Chem. 272, 16308–16314.

Hatoum, R., Labrie, S., and Fliss, I. (2012). Antimicrobial and Probiotic Properties of Yeasts: From Fundamental to Novel Applications. Front. Microbiol. 3.

Heinisch, J.J., Dupres, V., Wilk, S., Jendretzki, A., and Dufrêne, Y.F. (2010). Single-Molecule Atomic Force Microscopy Reveals Clustering of the Yeast Plasma-Membrane Sensor Wsc1. PLoS ONE 5, e11104.

Heinisch, J.J., Lipke, P.N., Beaussart, A., El Kirat Chatel, S., Dupres, V., Alsteens, D., and Dufrene, Y.F. (2012). Atomic force microscopy - looking at mechanosensors on the cell surface. J. Cell Sci. 125, 4189–4195.

Hernawan, T., and Fleet, G. (1995). Chemical and cytological changes during the autolysis of yeasts. J. Ind. Microbiol. 14, 440–450.
Herscovics, A., and Orlean, P. (1993). Glycoprotein biosynthesis in yeast. FASEB J. 7, 540.

Hinterdorfer, P., and Dufrêne, Y.F. (2006). Detection and localization of single molecular recognition events using atomic force microscopy. Nat. Methods 3, 347–355.

Hofmann, M., Boles, E., and Zimmermann, F.K. (1994). Characterization of the essential yeast gene encoding N-acetylglucosamine-phosphate mutase. Eur. J. Biochem. FEBS 221, 741–747.

Hong, Z., Mann, P., Shaw, K.J., and Didomenico, B. (1994). Analysis of beta-glucans and chitin in a Saccharomyces cerevisiae cell wall mutant using high-performance liquid chromatography. Yeast Chichester Engl. 10, 1083–1092.

Howell, A.S., and Lew, D.J. (2012). Morphogenesis and the Cell Cycle. Genetics 190, 51–77.

Hu, J., Lipowsky, R., and Weikl, T.R. (2013). Binding constants of membrane-anchored receptors and ligands depend strongly on the nanoscale roughness of membranes. Proc. Natl. Acad. Sci. U. S. A. 110, 15283–15288.

Huang, L.S., Doherty, H.K., and Herskowitz, I. (2005). The Smk1p MAP kinase negatively regulates Gsc2p, a 1,3-β-glucan synthase, during spore wall morphogenesis in Saccharomyces cerevisiae. Proc. Natl. Acad. Sci. U. S. A. 102, 12431–12436.

Huberman, L.B., and Murray, A.W. (2013). Genetically engineered transvestites reveal novel mating genes in budding yeast. Genetics 195, 1277–1290.

Hutter, J.L., and Bechhoefer, J. (1993). Calibration of atomic- force microscope tips. Rev. Sci. Instrum. 64, 1868–1873.

Imai, K. (2004). A Novel Endoplasmic Reticulum Membrane Protein Rcr1 Regulates Chitin Deposition in the Cell Wall of Saccharomyces cerevisiae. J. Biol. Chem. 280, 8275–8284.

Ishihara, S., Hirata, A., Nogami, S., Beauvais, A., Latge, J.-P., and Ohya, Y. (2007). Homologous Subunits of 1,3-Beta-Glucan Synthase Are Important for Spore Wall Assembly in Saccharomyces cerevisiae. Eukaryot. Cell 6, 143–156.

Jacquier, N., and Schneiter, R. (2012). Mechanisms of sterol uptake and transport in yeast. J. Steroid Biochem. Mol. Biol. 129, 70–78.

Janshoff, A., Neitzert, M., Oberdörfer, Y., and Fuchs, H. (2000). Force Spectroscopy of Molecular Systems—Single Molecule Spectroscopy of Polymers and Biomolecules. Angew. Chem. 39, 3212–3237.

Jauvert, E., Dague, E., Séverac, M., Ressier, L., Caminade, A.-M., Majoral, J.-P., and Trévisiol, E. (2012). Probing single molecule interactions by AFM using bio-functionalized dendritips. Sens. Actuators B Chem. 168, 436–441.

Jena, B.P., and Hörber, J.K.H. (2006). Force Microscopy: Applications in Biology and Medicine (John Wiley & Sons).

Jiang, B., Ram, A.F., Sheraton, J., Klis, F.M., and Bussey, H. (1995). Regulation of cell wall beta-glucan assembly: PTC1 negatively affects PBS2 action in a pathway that includes modulation of EXG1 transcription. Mol. Gen. Genet. MGG 248, 260–269.

Joannis-Cassan, C., Tozlovanu, M., Hadjeba-Medjdoub, K., Ballet, N., and Pfohl-Leszkowicz, A. (2011). Binding of Zearalenone, Aflatoxin B₁, and Ochratoxin A by Yeast-Based Products: A Method for Quantification of Adsorption Performance. J. Food Prot. 74, 1175–1185.

Johnson, M.E., and Edlind, T.D. (2012). Topological and Mutational Analysis of Saccharomyces cerevisiae Fks1. Eukaryot. Cell 11, 952–960.

Jungmann, J., Rayner, J.C., and Munro, S. (1999). The Saccharomyces cerevisiae protein Mnn10p/Bed1p is a subunit of a Golgi mannosyltransferase complex. J. Biol. Chem. 274, 6579–6585.

Kalebina, T.S., Plotnikova, T.A., Gorkovskii, A.A., Selyakh Irina O., Galzitskaya, O.V., Bezsonov, E.E., Gellissen, G., and Kulaev, I.S. (2008). Amyloid-like properties of Saccharomyces cerevisiae cell wall glucantransferase Bgl2p: prediction and experimental evidences., Amyloid-like properties of Saccharomyces cerevisiae cell wall glucantransferase Bgl2p: Prediction and experimental evidences. Prion Prion *2, 2*, 91, 91–96.

Kamada, Y., Jung, U.S., Piotrowski, J., and Levin, D.E. (1995). The protein kinase C-activated MAP kinase pathway of Saccharomyces cerevisiae mediates a novel aspect of the heat shock response. Genes Dev. 9, 1559–1571.

Kapteyn, J.C., Ram, A.F., Groos, E.M., Kollar, R., Montijn, R.C., Van Den Ende, H., Llobell, A., Cabib, E., and Klis, F.M. (1997). Altered extent of cross-linking of beta1,6-glucosylated mannoproteins to

chitin in Saccharomyces cerevisiae mutants with reduced cell wall beta1,3-glucan content. J. Bacteriol. 179, 6279–6284.

Kapteyn, J.C., Van Den Ende, H., and Klis, F.M. (1999). The contribution of cell wall proteins to the organization of the yeast cell wall. Biochim. Biophys. Acta BBA - Gen. Subj. 1426, 373–383.

Karreman, R.J., Dague, E., Gaboriaud, F., Quiles, F., Duval, J.F., and Lindsey, G.G. (2007). The stress response protein Hsp12p increases the flexibility of the yeast Saccharomyces cerevisiae cell wall. Biochim. Biophys. Acta 1774, 131–137.

Katakura, Y., Sano, R., Hashimoto, T., Ninomiya, K., and Shioya, S. (2010). Lactic acid bacteria display on the cell surface cytosolic proteins that recognize yeast mannan. Appl. Microbiol. Biotechnol. 86, 319–326.

Kim, K.S., and Yun, H.S. (2006). Production of soluble β-glucan from the cell wall of Saccharomyces cerevisiae. Enzyme Microb. Technol. 39, 496–500.

Kim, K.S., Chang, J.E., and Yun, H.S. (2004). Estimation of soluble β-glucan content of yeast cell wall by the sensitivity to Glucanex® 200G treatment. Enzyme Microb. Technol. 35, 672–677.

Kim, K.W., Kamerud, J.Q., Livingston, D.M., and Roon, R.J. (1988). Asparaginase II of Saccharomyces cerevisiae. Characterization of the ASP3 gene. J. Biol. Chem. 263, 11948–11953.

Kim, M.-K., Park, H.-S., Kim, C.-H., Park, H.-M., and Choi, W. (2002). Inhibitory effect of nikkomycin Z on chitin synthases in Candida albicans. Yeast Chichester Engl. 19, 341–349.

Kitamura, A., Someya, K., Hata, M., Nakajima, R., and Takemura, M. (2009). Discovery of a small-molecule inhibitor of {beta}-1,6-glucan synthesis. Antimicrob. Agents Chemother. 53, 670–677.

Klebl, F., and Tanner, W. (1989). Molecular cloning of a cell wall exo-beta-1,3-glucanase from Saccharomyces cerevisiae. J. Bacteriol. 171, 6259–6264.

Klis, F.M., Mol, P., Hellingwerf, K., and Brul, S. (2002). Dynamics of cell wall structure in Saccharomyces cerevisiae. FEMS Microbiol. Rev. 26, 239–256.

Klis, F.M., Boorsma, A., and De Groot, P.W. (2006). Cell wall construction in Saccharomyces cerevisiae. Yeast Chichester Engl. 23, 185–202.

Klotz, S.A., Gaur, N.K., Lake, D.F., Chan, V., Rauceo, J., and Lipke, P.N. (2004). Degenerate peptide recognition by Candida albicans adhesins Als5p and Als1p. Infect. Immun. 72, 2029–2034.

Kogan, G., and Kocher, A. (2007). Role of yeast cell wall polysaccharides in pig nutrition and health protection. Livest. Sci. 109, 161.

Kollar, R., Petrakova, E., Ashwell, G., Robbins, P.W., and Cabib, E. (1995). Architecture of the yeast cell wall. The linkage between chitin and beta(1-->3)-glucan. J. Biol. Chem. 270, 1170–1178.

Kollar, R., Reinhold, B.B., Petrakova, E., Yeh, H.J., Ashwell, G., Drgonova, J., Kapteyn, J.C., Klis, F.M., and Cabib, E. (1997). Architecture of the yeast cell wall. Beta(1-->6)-glucan interconnects mannoprotein, beta(1-->)3-glucan, and chitin. J. Biol. Chem. 272, 17762–17775.

Kopecká, M. (1984). Papulacandin B: Inhibitor of biogenesis of (1→3)-β-d-glucan fibrillar component of the cell wall ofSaccharomyces cerevisiae protoplasts. Folia Microbiol. (Praha) 29, 441–449.

Kopecká, M. (2013). Yeast and fungal cell-wall polysaccharides can self-assemble in vitro into an ultrastructure resembling in vivo yeast cell walls. Microscopy 62, 327–339.

Kopecka, M., and Gabriel, M. (1992). The influence of Congo red on the cell wall and (1,3)-beta-d-glucan microfibril biogenesis in Saccharomyces cerevisiae. Arch. Microbiol. 158, 115–126.

Kuranda, M.J., and Robbins, P.W. (1991). Chitinase is required for cell separation during growth of Saccharomyces cerevisiae. J. Biol. Chem. 266, 19758–19767.

Kurita, T., Noda, Y., Takagi, T., Osumi, M., and Yoda, K. (2011). Kre6 Protein Essential for Yeast Cell Wall -1,6-Glucan Synthesis Accumulates at Sites of Polarized Growth. J. Biol. Chem. 286, 7429–7438.

Lafon-Lafourcade, S., Geneix, C., and Ribéreau-Gayon, P. (1984). Inhibition of alcoholic fermentation of grape must by Fatty acids produced by yeasts and their elimination by yeast ghosts. Appl. Environ. Microbiol. 47, 1246–1249.

Lagorce, A. (2003). Genome-wide Analysis of the Response to Cell Wall Mutations in the Yeast Saccharomyces cerevisiae. J. Biol. Chem. 278, 20345–20357.

Lagorce, A., Le Berre-Anton, V., Aguilar-Uscanga, B., Martin-Yken, H., Dagkessamanskaia, A., and François, J. (2002). Involvement of GFA1, which encodes glutamine-fructose-6-phosphate amidotransferase, in the activation of the chitin synthesis pathway in response to cell-wall defects in Saccharomyces cerevisiae. Eur. J. Biochem. FEBS 269, 1697–1707.

Abu-Lail, N.I., and Camesano, T.A. (2003). Polysaccharide properties probed with atomic force microscopy. J. Microsc. 212, 217–238.

Lam, K.K.Y. (2006). Palmitoylation by the DHHC protein Pfa4 regulates the ER exit of Chs3. J. Cell Biol. 174, 19–25.

Larriba, G., Basco, R.D., Andaluz, E., and Luna-Arias, J.P. (1993). Yeast exoglucanases. Where redundancy implies necessity. Arch. Med. Res. 24, 293–299.

League, G.P., Slot, J.C., and Rokas, A. (2012). The ASP3 locus in Saccharomyces cerevisiae originated by horizontal gene transfer from Wickerhamomyces. FEMS Yeast Res. 12, 859–863.

Lesage, G., and Bussey, H. (2006). Cell wall assembly in Saccharomyces cerevisiae. Microbiol. Mol. Biol. Rev. MMBR 70, 317–343.

Levin, D.E. (2005). Cell Wall Integrity Signaling in Saccharomyces cerevisiae. Microbiol. Mol. Biol. Rev. 69, 262–291.

Levin, D.E. (2011). Regulation of Cell Wall Biogenesis in Saccharomyces cerevisiae: The Cell Wall Integrity Signaling Pathway. Genetics 189, 1145–1175.

Li, H., Ma, M.-L., Luo, S., Zhang, R.-M., Han, P., and Hu, W. (2012). Metabolic responses to ethanol in Saccharomyces cerevisiae using a gas chromatography tandem mass spectrometry-based metabolomics approach. Int. J. Biochem. Cell Biol. 44, 1087–1096.

Liu, B.Y., Zhang, G.M., Li, X.L., and Chen, H. (2012). Effect of glutaraldehyde fixation on bacterial cells observed by atomic force microscopy: Effect of glutaraldehyde fixation on bacterial cells. Scanning 34, 6–11.

Lussier, M., Gentzsch, M., Sdicu, A.-M., Bussey, H., and Tanner, W. (1995). Protein O-Glycosylation in Yeast THE PMT2 GENE SPECIFIES A SECOND PROTEIN O-MANNOSYLTRANSFERASE THAT FUNCTIONS IN ADDITION TO THE PMT1-ENCODED ACTIVITY. J. Biol. Chem. 270, 2770–2775.

Lussier, M., White, A.-M., Sheraton, J., Paolo, T. di, Treadwell, J., Southard, S.B., Horenstein, C.I., Chen-Weiner, J., Ram, A.F.J., Kapteyn, J.C., et al. (1997a). Large Scale Identification of Genes Involved in Cell Surface Biosynthesis and Architecture in Saccharomyces cerevisiae. Genetics 147, 435–450.

Lussier, M., Sdicu, A.-M., Winnett, E., Vo, D.H., Sheraton, J., Düsterhöft, A., Storms, R.K., and Bussey, H. (1997b). Completion of the Saccharomyces cerevisiae Genome Sequence Allows Identification of KTR5, KTR6 and KTR7 and Definition of the Nine-Membered KRE2/MNT1 Mannosyltransferase Gene Family in this Organism. Yeast 13, 267–274.

Lussier, M., Sdicu, A.-M., and Bussey, H. (1999). The KTR and MNN1 mannosyltransferase families of Saccharomyces cerevisiae. Biochim. Biophys. Acta BBA - Gen. Subj. 1426, 323–334.

Machi, K. (2004). Rot1p of Saccharomyces cerevisiae is a putative membrane protein required for normal levels of the cell wall 1,6- -glucan. Microbiology 150, 3163–3173.

Magnelli, P., Cipollo, J.F., and Abeijon, C. (2002). A Refined Method for the Determination of Saccharomyces cerevisiae Cell Wall Composition and [beta]-1,6-Glucan Fine Structure. Anal. Biochem. 301, 136.

Manners, D.J., Masson, A.J., and Patterson, J.C. (1973a). The structure of a beta-(1 leads to 3)-D-glucan from yeast cell walls. Biochem. J. 135, 19–30.

Manners, D.J., Masson, A.J., Patterson, J.C., Björndal, H., and Lindberg, B. (1973b). The structure of a beta-(1--6)-D-glucan from yeast cell walls. Biochem. J. 135, 31–36.

Martín-Cuadrado, A.-B., Fontaine, T., Esteban, P.-F., del Dedo, J.E., de Medina-Redondo, M., del Rey, F., Latgé, J.P., and de Aldana, C.R.V. (2008). Characterization of the endo-beta-1,3-glucanase activity of S. cerevisiae Eng2 and other members of the GH81 family. Fungal Genet. Biol. FG B 45, 542–553.

Martin-Yken, H. (2011). Mémoire de l'Habilitation à diriger des recherches.

Mazáň, M., Ragni, E., Popolo, L., and Farkaš, V. (2011). Catalytic properties of the Gas family β-(1,3)-glucanosyltransferases active in fungal cell-wall biogenesis as determined by a novel fluorescent assay. Biochem. J. 438, 275–282.

Meaden, P., Hill, K., Wagner, J., Slipetz, D., Sommer, S.S., and Bussey, H. (1990). The yeast KRE5 gene encodes a probable endoplasmic reticulum protein required for (1----6)-beta-D-glucan synthesis and normal cell growth. Mol. Cell. Biol. 10, 3013–3019.

Meitinger, F., Palani, S., Hub, B., and Pereira, G. (2013). Dual function of the NDR-kinase Dbf2 in the regulation of the F-BAR protein Hof1 during cytokinesis. Mol. Biol. Cell 24, 1290–1304.

Mercadé-Prieto, R., Thomas, C.R., and Zhang, Z. (2013). Mechanical double layer model for Saccharomyces Cerevisiae cell wall. Eur. Biophys. J. 42, 613–620.

Miki Bl, Poon Nh, James Ap, and Seligy Vl (1982). Possible mechanism for flocculation interactions governed by gene FLO1 in Saccharomyces cerevisiae. J. Bacteriol. 150, 878–889.

Milewski, S., Gabriel, I., and Olchowy, J. (2006). Enzymes of UDP-GlcNAc biosynthesis in yeast. Yeast Chichester Engl. 23, 1–14.

Millsap, K. (1998). Adhesive interactions between medically important yeasts and bacteria. FEMS Microbiol. Rev. 21, 321–336.

Mio, T., Yabe, T., Arisawa, M., and Yamada-Okabe, H. (1998). The eukaryotic UDP-N-acetylglucosamine pyrophosphorylases. Gene cloning, protein expression, and catalytic mechanism. J. Biol. Chem. 273, 14392–14397.

Mio, T., Yamada-Okabe, T., Arisawa, M., and Yamada-Okabe, H. (1999). Saccharomyces cerevisiae GNA1, an essential gene encoding a novel acetyltransferase involved in UDP-N-acetylglucosamine synthesis. J. Biol. Chem. 274, 424–429.

Mora, J.F. de, Gil, R., Sentandreu, R., and Herrero, E. (1991). Isolation and characterization of Saccharomyces cerevisiae mutants resistant to aculeacin A. Antimicrob. Agents Chemother. 35, 2596–2601.

Mouyna, I. (2000). Glycosylphosphatidylinositol-anchored Glucanosyltransferases Play an Active Role in the Biosynthesis of the Fungal Cell Wall. J. Biol. Chem. 275, 14882–14889.

Mrsa, V., Klebl, F., and Tanner, W. (1993). Purification and characterization of the Saccharomyces cerevisiae BGL2 gene product, a cell wall endo-beta-1,3-glucanase. J. Bacteriol. 175, 2102–2106.

Nakamata, K., Kurita, T., Bhuiyan, M.S.A., Sato, K., Noda, Y., and Yoda, K. (2007). KEG1/YFR042w Encodes a Novel Kre6-binding Endoplasmic Reticulum Membrane Protein Responsible for beta-1,6-Glucan Synthesis in Saccharomyces cerevisiae. J. Biol. Chem. 282, 34315–34324.

Neuman, K.C., and Nagy, A. (2008). Single-molecule force spectroscopy: optical tweezers, magnetic tweezers and atomic force microscopy. Nat. Methods 5, 491–505.

Nguyen, T.H., Fleet, G.H., and Rogers, P.L. (1998). Composition of the cell walls of several yeast species. Appl. Microbiol. Biotechnol. 50, 206–212.

Novak, M., and Vetvicka, V. (2009). Glucans as biological response modifiers. Endocr. Metab. Immune Disord. Drug Targets 9, 67–75.

Oh, Y., Chang, K.-J., Orlean, P., Wloka, C., Deshaies, R., and Bi, E. (2012). Mitotic exit kinase Dbf2 directly phosphorylates chitin synthase Chs2 to regulate cytokinesis in budding yeast. Mol. Biol. Cell 23, 2445–2456.

Okada, H., Ohnuki, S., Roncero, C., Konopka, J.B., and Ohya, Y. (2014). Distinct roles of cell wall biogenesis in yeast morphogenesis as revealed by multivariate analysis of high-dimensional morphometric data. Mol. Biol. Cell 25, 222–233.

Orlean, P. (1990). Dolichol phosphate mannose synthase is required in vivo for glycosyl phosphatidylinositol membrane anchoring, O mannosylation, and N glycosylation of protein in Saccharomyces cerevisiae. Mol. Cell. Biol. 10, 5796–5805.

Orlean, P. (2012). Architecture and Biosynthesis of the Saccharomyces cerevisiae Cell Wall. Genetics 192, 775–818.

Ostergaard, S., Olsson, L., and Nielsen, J. (2000). Metabolic Engineering of Saccharomyces cerevisiae. Microbiol. Mol. Biol. Rev. 64, 34–50.

Osumi, M. (1998). The ultrastructure of yeast: Cell wall structure and formation. Micron 29, 207–233.

Ovalle, R., Lim, S.T., Holder, B., Jue, C.K., Moore, C.W., and Lipke, P.N. (1998). A spheroplast rate assay for determination of cell wall integrity in yeast. Yeast 14, 1159–1166.

Pagé, N., Gérard-Vincent, M., Ménard, P., Beaulieu, M., Azuma, M., Dijkgraaf, G.J.P., Li, H., Marcoux, J., Nguyen, T., Dowse, T., et al. (2003). A Saccharomyces cerevisiae Genome-Wide Mutant Screen for Altered Sensitivity to K1 Killer Toxin. Genetics 163, 875–894.

Pelling, A.E., Sehati, S., Gralla, E.B., Valentine, J.S., and Gimzewski, J.K. (2004). Local nanomechanical motion of the cell wall of Saccharomyces cerevisiae. Science 305, 1147–1150.

Peneff, C., Mengin-Lecreulx, D., and Bourne, Y. (2001). The crystal structures of Apo and complexed Saccharomyces cerevisiae GNA1 shed light on the catalytic mechanism of an amino-sugar N-acetyltransferase. J. Biol. Chem. 276, 16328–16334.

Pillet, F., Lemonier, S., Schiavone, M., Formosa, C., Martin-Yken, H., Francois, J., and Dague, E. (2014). Uncovering by Atomic Force Microscopy of an original circular structure at the yeast cell surface in response to heat shock. BMC Biol. 12, 6.

Pittet, M., and Conzelmann, A. (2007). Biosynthesis and function of GPI proteins in the yeast Saccharomyces cerevisiae. Biochim. Biophys. Acta BBA - Mol. Cell Biol. Lipids 1771, 405–420.

Plotnikova, T.A., Selyakh, I.O., Kalebina, T.S., and Kulaev, I.S. (2006). Bgl2p and Gas1p are the major glucan transferases forming the molecular ensemble of yeast cell wall. Dokl. Biochem. Biophys. 409, 244–247.

Pope, G.A., MacKenzie, D.A., Defernez, M., Aroso, M.A.M.M., Fuller, L.J., Mellon, F.A., Dunn, W.B., Brown, M., Goodacre, R., Kell, D.B., et al. (2007). Metabolic footprinting as a tool for discriminating between brewing yeasts. Yeast Chichester Engl. 24, 667–679.

Popolo, L., and Vai, M. (1999). The Gas1 glycoprotein, a putative wall polymer cross-linker. Biochim. Biophys. Acta BBA - Gen. Subj. 1426, 385–400.

Popolo, G., Gilardelli D, Bonfante P, and Vai M (1997). Increase in chitin as an essential response to defects in assembly of cell wall polymers in the ggp1delta mutant of Saccharomyces cerevisiae. J. Bacteriol. *179*, 463–469.

Popolo, L., Gualtieri, T., and Ragni, E. (2000). The yeast cell-wall salvage pathway. Med. Mycol. 39 Suppl 1, 111–121.

Pozo-Bayón, M.Á., Andújar-Ortiz, I., and Moreno-Arribas, M.V. (2009). Volatile profile and potential of inactive dry yeast-based winemaking additives to modify the volatile composition of wines. J. Sci. Food Agric. 89, 1665–1673.

Pradelles, R., Alexandre, H., Ortiz-Julien, A., and Chassagne, D. (2008). Effects of yeast cell-wall characteristics on 4-ethylphenol sorption capacity in model wine. J. Agric. Food Chem. 56, 11854–11861.

Pradelles, R., Chassagne, D., Vichi, S., Gougeon, R., and Alexandre, H. (2010). (−)Geosmin sorption by enological yeasts in model wine and FTIR spectroscopy characterization of the sorbent. Food Chem. 120, 531–538.

Ragni, E., Fontaine, T., Gissi, C., Latgè, J.P., and Popolo, L. (2007a). The Gas family of proteins of Saccharomyces cerevisiae: characterization and evolutionary analysis. Yeast Chichester Engl. 24, 297–308.

Ragni, E., Coluccio, A., Rolli, E., Rodriguez-Peña, J.M., Colasante, G., Arroyo, J., Neiman, A.M., and Popolo, L. (2007b). GAS2 and GAS4, a pair of developmentally regulated genes required for spore wall assembly in Saccharomyces cerevisiae. Eukaryot. Cell 6, 302–316.

Ram, A.F.J., and Klis, F.M. (2006). -Identification of fungal cell wall mutants using susceptibility assays based on Calcofluor white and Congo red. Nat. Protoc. 1, 2253–2256.

Ram, A.F.J., Wolters, A., Hoopen, R.T., and Klis, F.M. (1994). A new approach for isolating cell wall mutants inSaccharomyces cerevisiae by screening for hypersensitivity to calcofluor white. Yeast 10, 1019–1030.

Ram, A.F.J., Kapteyn, J.C., Montijn, R.C., Caro, L.H.P., Douwes, J.E., Baginsky, W., Mazur, P., van den Ende, H., and Klis, F.M. (1998). Loss of the Plasma Membrane-Bound Protein Gas1p in Saccharomyces cerevisiae Results in the Release of ?1,3-Glucan into the Medium and Induces a Compensation Mechanism To Ensure Cell Wall Integrity. J. Bacteriol. 180, 1418–1424.

Ramsook, C.B., Tan, C., Garcia, M.C., Fung, R., Soybelman, G., Henry, R., Litewka, A., O'Meally, S., Otoo, H.N., Khalaf, R.A., et al. (2010). Yeast Cell Adhesion Molecules Have Functional Amyloid-Forming Sequences. Eukaryot. Cell 9, 393–404.

Rayner, J.C., and Munro, S. (1998). Identification of the MNN2 and MNN5 mannosyltransferases required for forming and extending the mannose branches of the outer chain mannans of Saccharomyces cerevisiae. J. Biol. Chem. 273, 26836–26843.

Reyes, A., Sanz, M., Duran, A., and Roncero, C. (2007). Chitin synthase III requires Chs4p-dependent translocation of Chs3p into the plasma membrane. J. Cell Sci. 120, 1998–2009.

Van Rinsum, J., Klis, F.M., and Ende, H.V.D. (1991). Cell wall glucomannoproteins of Saccharomyces cerevisiae mnn9. Yeast 7, 717–726.

Rodriguez-Nogales, J.M., Fernández-Fernández, E., and Vila-Crespo, J. (2012). Effect of the addition of β-glucanases and commercial yeast preparations on the chemical and sensorial characteristics of traditional sparkling wine. Eur. Food Res. Technol. 235, 729–744.

Rodriguez-Pena, J.M. (2005). The "yeast cell wall chip" - a tool to analyse the regulation of cell wall biogenesis in Saccharomyces cerevisiae. Microbiology 151, 2241–2249.

Rodríguez-Peña, J.M., García, R., Nombela, C., and Arroyo, J. (2010). The high-osmolarity glycerol (HOG) and cell wall integrity (CWI) signalling pathways interplay: a yeast dialogue between MAPK routes. Yeast 27, 495–502.

Roduit, C., Saha, B., Alonso-Sarduy, L., Volterra, A., Dietler, G., and Kasas, S. (2012). OpenFovea: open-source AFM data processing software. Nat. Methods 9, 774–775.

Roemer, T., and Bussey, H. (1991). Yeast beta-glucan synthesis: KRE6 encodes a predicted type II membrane protein required for glucan synthesis in vivo and for glucan synthase activity in vitro. Proc. Natl. Acad. Sci. 88, 11295–11299.

Roemer, T., Delaney, S., and Bussey, H. (1993). SKN1 and KRE6 define a pair of functional homologs encoding putative membrane proteins involved in beta-glucan synthesis. Mol. Cell. Biol. 13, 4039–4048.

Rolli, E., Ragni, E., Calderon, J., Porello, S., Fascio, U., and Popolo, L. (2009). Immobilization of the Glycosylphosphatidylinositol-anchored Gas1 Protein into the Chitin Ring and Septum Is Required for Proper Morphogenesis in Yeast. Mol. Biol. Cell 20, 4856–4870.

Romero, P.A., Lussier, M., Veronneau, S., Sdicu, A.-M., Herscovics, A., and Bussey, H. (1999). Mnt2p and Mnt3p of Saccharomyces cerevisiae are members of the Mnn1p family of α-1,3-mannosyltransferases responsible for adding the terminal mannose residues of O-linked oligosaccharides. Glycobiology 9, 1045–1051.

Roncero, C., and Duran, A. (1985). Effect of Calcofluor white and Congo red on fungal cell wall morphogenesis: in vivo activation of chitin polymerization. J. Bacteriol. 163, 1180–1185.

Roncero, C., Mh, V., Jc, R., and A, D. (1988). Isolation and characterization of Saccharomyces cerevisiae mutants resistant to Calcofluor white. J. Bacteriol. 170, 1950–1954.

Rupp, S., Summers, E., Lo, H.-J., Madhani, H., and Fink, G. (1999). MAP kinase and cAMP filamentation signaling pathways converge on the unusually large promoter of the yeast FLO11 gene. EMBO J. 18, 1257–1269.

Sacher, M., Barrowman, J., Schieltz, D., Yates, J.R., and Ferro-Novick, S. (2000). Identification and characterization of five new subunits of TRAPP. Eur. J. Cell Biol. 79, 71–80.

San Segundo, P., Correa, J., Vazquez de Aldana, C.R., and Del Rey, F. (1993). SSG1, a gene encoding a sporulation-specific 1,3-beta-glucanase in Saccharomyces cerevisiae. J. Bacteriol. *175*, 3823–3837.

Santos, B., Duran, A., and Valdivieso, M.H. (1997). CHS5, a gene involved in chitin synthesis and mating in Saccharomyces cerevisiae. Mol. Cell. Biol. 17, 2485–2496.

Saravolatz, L.D., Deresinski, S.C., and Stevens, D.A. (2003). Caspofungin. Clin. Infect. Dis. 36, 1445–1457.

Schiavone, M., Vax, A., Formosa, C., Martin-Yken, H., Dague, E., and François, J.M. (2014). A combined chemical and enzymatic method to determine quantitatively the polysaccharide components in the cell wall of yeasts. FEMS Yeast Res. n/a – n/a.

Schmidt, M., Varma, A., Drgon, T., Bowers, B., and Cabib, E. (2003). Septins, under Cla4p Regulation, and the Chitin Ring Are Required for Neck Integrity in Budding Yeast. Mol. Biol. Cell 14, 2128–2141.

Sharon, N., and Lis, H. (2007). Lectins (Springer Science & Business Media).

Shaw, J.A., Mol, P.C., Bowers, B., Silverman, S.J., Valdivieso, M.H., Durán, A., and Cabib, E. (1991). The function of chitin synthases 2 and 3 in the Saccharomyces cerevisiae cell cycle. J. Cell Biol. 114, 111–123.

el-Sherbeini, M., and Clemas, J.A. (1995). Nikkomycin Z supersensitivity of an echinocandin-resistant mutant of Saccharomyces cerevisiae. Antimicrob. Agents Chemother. 39, 200–207.

Shetty, P.H., and Jespersen, L. (2006). Saccharomyces cerevisiae and lactic acid bacteria as potential mycotoxin decontaminating agents. Trends Food Sci. Technol. 17, 48–55.

Shokri, H., Asadi, F., and Khosravi, A.R. (2008). Isolation of beta-glucan from the cell wall of Saccharomyces cerevisiae. Nat. Prod. Res. 22, 414–421.

Soares, E. v. (2011). Flocculation in Saccharomyces cerevisiae: a review. J. Appl. Microbiol. 110, 1–18.

Striebeck, A., Robinson, D.A., Schüttelkopf, A.W., and van Aalten, D.M.F. (2013). Yeast Mnn9 is both a priming glycosyltransferase and an allosteric activator of mannan biosynthesis. Open Biol. 3, 130022.

Suchodolskis, A., Feiza, V., Stirke, A., Timonina, A., Ramanaviciene, A., and Ramanavicius, A. (2011). Elastic properties of chemically modified baker's yeast cells studied by AFM. Surf. Interface Anal. 43, 1636–1640.

Suharja, A.A.S., Henriksson, A., and Liu, S.-Q. (2014). Impact of Saccharomyces Cerevisiae on Viability of Probiotic Lactobacillus Rhamnosus in Fermented Milk under Ambient Conditions. J. Food Process. Preserv. 38, 326–337.

Sumita, T., Yoko-o, T., Shimma, Y. -i., and Jigami, Y. (2005). Comparison of Cell Wall Localization among Pir Family Proteins and Functional Dissection of the Region Required for Cell Wall Binding and Bud Scar Recruitment of Pir1p. Eukaryot. Cell 4, 1872–1881.

Svaldo-Lanero, T., Krol, S., Magrassi, R., Diaspro, A., Rolandi, R., Gliozzi, A., and Cavalleri, O. (2007). Morphology, mechanical properties and viability of encapsulated cells. Ultramicroscopy 107, 913–921.

Syed, A.K., and Boles, B.R. (2014). Fold modulating function: bacterial toxins to functional amyloids. Front. Microbiol. 5.

Tanguler, H., and Erten, H. (2008). Utilisation of spent brewer's yeast for yeast extract production by autolysis: The effect of temperature. Food Bioprod. Process. 86, 317–321.

Teparić, R., and Mrša, V. (2013). Proteins involved in building, maintaining and remodeling of yeast cell walls. Curr. Genet. 59, 171–185.

Teunissen, A.W., and Steensma, H.Y. (1995). Review: the dominant flocculation genes of Saccharomyces cerevisiae constitute a new subtelomeric gene family. Yeast Chichester Engl. 11, 1001–1013.

Tirelli, A., Fracassetti, D., and De Noni, I. (2010). Determination of Reduced Cysteine in Oenological Cell Wall Fractions of Saccharomyces cerevisiae. J. Agric. Food Chem. 58, 4565–4570.

Touhami, A. (2003). Aggregation of yeast cells: direct measurement of discrete lectin-carbohydrate interactions. Microbiology 149, 2873–2878.

Touhami, A., Nysten, B., and Dufrêne, Y.F. (2003). Nanoscale Mapping of the Elasticity of Microbial Cells by Atomic Force Microscopy. Langmuir 19, 4539–4543.

Trilla, J.A., Cos, T., Duran, A., and Roncero, C. (1997). Characterization of CHS4 (CAL2), a gene of Saccharomyces cerevisiae involved in chitin biosynthesis and allelic to SKT5 and CSD4. Yeast Chichester Engl. 13, 795–807.

Trilla, J.A., Durán, A., and Roncero, C. (1999). Chs7p, a new protein involved in the control of protein export from the endoplasmic reticulum that is specifically engaged in the regulation of chitin synthesis in Saccharomyces cerevisiae. J. Cell Biol. 145, 1153–1163.

Vink, E., Rodriguez-Suarez, R.J., Gérard-Vincent, M., Ribas, J.C., de Nobel, H., van den Ende, H., Duran, A., Klis, F.M., and Bussey, H. (2004). Anin vitro assay for (1？6)-?-D-glucan synthesis inSaccharomyces cerevisiae. Yeast 21, 1121–1131.

Walker, G.M. (1998). Yeast Physiology and Biotechnology (John Wiley & Sons).

Watari, J., Takata, Y., Ogawa, M., Sahara, H., Koshino, S., Onnela, M.-L., Airaksinen, U., Jaatinen, R., Penttilä, M., and Keränen, S. (1994). Molecular cloning and analysis of the yeast flocculation geneFLO1. Yeast 10, 211–225.

Westfall, P.J., Ballon, D.R., and Thorner, J. (2004). When the stress of your environment makes you go HOG wild. Science 306, 1511–1512.

Wildling, L., Unterauer, B., Zhu, R., Rupprecht, A., Haselgrübler, T., Rankl, C., Ebner, A., Vater, D., Pollheimer, P., Pohl, E.E., et al. (2011). Linking of Sensor Molecules with Amino Groups to Amino-Functionalized AFM Tips. Bioconjug. Chem. 22, 1239–1248.

Wodicka, L., Dong, H., Mittmann, M., Ho, M.H., and Lockhart, D.J. (1997). Genome-wide expression monitoring in Saccharomyces cerevisiae. Nat. Biotechnol. 15, 1359–1367.

Yiannikouris, A., Andre, G., Buleon, A., Jeminet, G., Canet, I., Francois, J., Bertin, G., and Jouany, J.P. (2004a). Comprehensive conformational study of key interactions involved in zearalenone complexation with beta-D-glucans. Biomacromolecules 5, 2176–2185.

Yiannikouris, A., Francois, J., Poughon, L., Dussap, C.G., Bertin, G., Jeminet, G., and Jouany, J.P. (2004b). Alkali extraction of beta-d-glucans from Saccharomyces cerevisiae cell wall and study of their adsorptive properties toward zearalenone. J. Agric. Food Chem. 52, 3666–3673.

Yiannikouris, A., Andre, G., Poughon, L., Francois, J., Dussap, C.G., Jeminet, G., Bertin, G., and Jouany, J.P. (2006). Chemical and conformational study of the interactions involved in mycotoxin complexation with beta-D-glucans. Biomacromolecules 7, 1147–1155.

Yoda, K., Kawada, T., Kaibara, C., Fujie, A., Abe, M., Hitoshi, Hashimoto, Shimizu, J., Tomishige, N., Noda, Y., et al. (2000). Defect in cell wall integrity of the yeast saccharomyces cerevisiae caused by a mutation of the GDP-mannose pyrophosphorylase gene VIG9. Biosci. Biotechnol. Biochem. 64, 1937–1941.

Zhang, G., Kashimshetty, R., Ng, K.E., Tan, H.B., and Yeong, F.M. (2006). Exit from mitosis triggers Chs2p transport from the endoplasmic reticulum to mother-daughter neck via the secretory pathway in budding yeast. J. Cell Biol. 174, 207–220.

Ziman, M., Chuang, J.S., and Schekman, R.W. (1996). Chs1p and Chs3p, two proteins involved in chitin synthesis, populate a compartment of the Saccharomyces cerevisiae endocytic pathway. Mol. Biol. Cell 7, 1909–1919.

Chapter VII: APPENDIX

1. List of figures

2. List of tables

Table IIIA-S3. Genes upregulated in gas1Δ mutant as compared to the wild-type strain (BY4741).

Table IIIA-S4. Genes downregulated in gas1Δ mutant as compared to the wild-type strain (BY4741).

Table IIIA-S5: Median ratio value between mutant/wild-type of biophysical and biochemical data

Table IIIA-S6: Medain ratio value between mutant/wild-type of biophysical and biochemical data.

Table IIIB-1. Cell wall composition of wine yeasts.

Table IIIB-2. Group of genes associated to biophysical-biochemical variables

Table IIIC-1. Growth rate μ (h-1) of industrial yeasts strains in two different growth media.

Table IIIC-2. Influence of the growth medium on the cell wall composition.

Table IIIC-3. Upregulated genes (about 1.5-fold and higher) in YPD/YNB, in BY4743 diploid strain, based on microarray analysis

Table IIIC-4. Upregulated genes (about 1.5-fold and higher) in YPD/YNB, in L60 diploid strain and based on microarray analysis.

Table IIIC-5. Upregulated genes (about 1.5-fold and higher) in YPD/YNB, in L69 diploid strain and based on microarray analysis.

Table IIIC-6. Upregulated genes in YPD/YNB for BY4743 diploid strain and based on microarray analysis.

Table IIIC-7. Upregulated genes in YPD/YNB for L69 strain and based on microarray analysis.

Table IIIC-8. Upregulated genes in YPD/YNB for L60 strain and based on microarray analysis.

Table IV-1: Cell wall composition of industrial strain L71 and L69

Table IV-2: Effect of autolysis/drying process on cell surface roughness

Table IV-3: Difference in expression levels of genes related to cell wall biogenesis between L69 versus L71 strain

Table IV-S1: Classification of genes whose expression was higher in strains L69 compared to L71 into MIPS categories

Table IV-S2: Classification of genes whose expression was lower in strains L69 compared to L71 into MIPS categories

3. Abbreviations

ATP: Adenosine Triphosphate

AFM: Atomic Force Microscopy

BRM: Biological Response Modifier

CAZY: Carbohydrate-active enzymes

CDK: Cyclin Dependent Kinase

Clns: Cyclins

Clbs: B-type Cyclins

CRD: Cysteine-Rich Domains

CWI: Cell Wall Integrity

CWP: Cell Wall Protein

DNA: Deoxyribonucleic Acid

DTT: dithiothreitol

EDTA: Ethylenediaminetetraacetic acid

ER: Endoplasmic Reticulum

FDA: Food and Drug Administration

FJC: Freely Jointed Chain

FJC+: extensive Freely Jointed Chain

GC: Gaussian Chain

GH: Glycosyl Hydrolases

GPI: Glycosylphosphatidylinositol

GTP: Guanosine Triphosphate

HCl: chlorhydric acid

H_2O_2: hydrogen peroxide

HOG: High Osmolarity Glycerol

MAPK: mitogen-activated protein kinase

MAPKKK: mitogen activated protein kinase kinase kinase

MIC: Minimal Inhibitory Concentration

PDMS: Polydimethylsiloxane

PIR: Proteins with Internal Repeats

PKC: Protein Kinase C

PM: Plasma Membrane

QI: Quantitative Imaging

RNA: Ribonucleic Acid

SCFS: Single-Cell Force Spectroscopy

SCW: Soluble Cell Wall

SDS: Sodium Dodecyl Sulfate

SMFS: Single Molecule Force Spectroscopy

STRE: Stress Response Elements

TFA: Trifluoroacetic Acid

TLC: Thin-Layer Chromatography

WLC: Worm-Like Chain

WLC+: extensive Worm-Like Chain

YCW: Yeast Cell Wall

YKO: Yeast Knock-Out

4. Material and methods

4.1. Strains

Strain	ORF	Genotype	Source or Reference
BY4741		MAT***a*** *his3Δ1 leu2Δ0 met15Δ0 ura3Δ0*	EUROSCARF
*kre6*Δ	YPR159W	BY4741 *kre6::KanMX4*	Open Biosystem
*gas1*Δ	YMR307W	BY4741 *gas1::KanMX4*	Open Biosystem
*fks1*Δ	YLR342W	BY4741 *fks1::KanMX4*	Open Biosystem
*mnn9*Δ	YPL050C	BY4741 *mnn9::KanMX4*	Open Biosystem
*chs3*Δ	YBR023C	BY4741 *chs3::KanMX4*	Open Biosystem
L71			Lallemand collection (Blagnac, France)
L69			Lallemand collection (Blagnac, France)
L60			Lallemand collection (Blagnac, France)
L62			Lallemand collection (Blagnac, France)

4.2. Proteins measurement

4.2.1. Bradford assay

The Bovine Serum Albumin standard curve from 50 to 6.25 µg.ml^{-1} was prepared from the stock solution (5 mg.ml^{-1} in water).

200 µl of each standard or unknown sample and 50 µl of Bradford reagent were dropped on microplate. The reaction mixture was mixed gently.

The reaction was let for 5 min in dark room at room temperature.

Absorbance was read at 550 nm on a microplate reader.

4.2.2. Bicinchoninic acid (BCA) assay

The BCA Reagent was prepared as recommended by the supplier (Intron Biotechnology)

The Bovine Serum Albumin (BSA) standard curve from 20 to 2000 µg.ml^{-1} was prepared from the stock solution (2 mg.ml^{-1} in water). 25 µl of each standard or unknown sample and 200 µl of BCA reagent were dropped on microplate. The reaction mixture was mixed gently.

Absorbance was read at 550 nm on a microplate reader.

4.2.3 Measurement of enzymatic activities

4.2.3.1. Glucose oxidase-peroxidase assay: glucose measurement

The reagent of glucose oxidase-peroxidase was prepared as recommended by the supplier (Sigma-Aldrich). A seal of o-dianisidine was dissolved in 1 ml of water and 400 µl of this solution was added to the reagent of glucose oxidase.

The glucose standard curve from 0.5 mg.ml $^{-1}$ to 31.25 µg.ml $^{-1}$ was prepared from the stock solution of 1 mg.ml^{-1}.

20 µl of each standard or unknown sample and 200 µl of glucose oxidase-peroxidase reagent were deposited on each well.

The microplate was incubated 30 minutes at 37°C and absorbance was measured at 490nm on a plate reader with respect to a control solution consisting of 20 µl of distilled water and 200µl of reagent.

4.2.3.2. DNS assay: determination of β-1,6-glucanase activity

A solution of pustulan at 8 mg.ml^{-1} was prepared in 50 mM potassium acetate pH 5.0.

Dinitrosalicyclic acid (DNS) reagent was prepared as follow: 30 g of tartrate double of sodium and potassium, 1.6 g of sodium hydroxide dissolve and 1 g of DNS were dissolved in 100 ml of water.

In glass tubes set at 37°C, 0.5 ml of enzyme and 0.5 ml of pustulan were mixed. At different time (0, 30 min, 1hr), 100 µl of the reaction mixture and 100 µl of DNS were mixed. Then, the tubes were heated 10 min at 100°C. Absorbance was measured at 490nm on a plate reader with respect to a control solution consisting of 100 µl of distilled water and 100µl of DNS.

The glucose standard curve from 2 mg.ml^{-1} to 0.25 mg.ml^{-1} was prepared from the stock solution.

Activity is determined as unit of glucose in µmol released per min at pH 5.0 and at 37°C.

4.3. Analysis of sugars : HPAEC-PAD

High Performance Anionic Exchange Chromatography coupled to Pulsed Amperometric Detection (HPAEC-PAD) was carried out on an ICS 5000 system (Thermofisher Scientific, Courtaboeuf, France) to analyze monosaccharides and/or oligosaccharides released after enzymatic hydrolysis.

Separation of the released monosaccharides (glucose, N-acetylglucosamine, glucosamine) and oligosaccharides (gentiooligosaccharides and laminarioligosaccharides) were performed on a CarboPac PA100 analytical column (250 x 4 mm) with a guard column CarboPac PA100 using NaOH

(100 mM) and NaOAc (500 mM in NaOH 100 mM) as solvent A and B, respectively. Chromatographic conditions developed by (Aimanianda et al., 2009) were applied. The column was pre-equilibrated by 98% A and 2% B. Following sample injection, a gradient run (flow rate 1 ml/min) was performed as follows: 0–2 min, isocratic step (98%A-2% B), 2–15 min 98% A-2% B to 65% A-35% B, 15–22 min 65% A 35% B to 57% A-43% B, 22–23 min 57% A-43% B to 100% B, and 23–25 min 100% B. Residues were detected on a pulsed amperometric system equipped with a gold electrode.

For a better resolution and separation of glucose and mannose peaks, we used CarboPac PA 10 column (Thermofisher Scientific, Courtaboeuf, France) specifically dedicated to monosaccharides analysis. Glucose, mannose, N-acetylglucosamine and glucosamine were separated and quantified on a CarboPac PA10 analytical column (250 x 4 mm) with a guard column CarboPac PA10, by an isocratic elution of NaOH 18 mM at 25°C and a flow rate of 1 ml/min. Residues were detected on a pulsed amperometric system equipped with a gold electrode.

4.4. Production of endo-β(1,6)-glucanase from Trichoderma harzianum

4.4.1. Growth condition and enzyme preparation

Medium	Composition
Buffered Glycerol Medium (BMG)	2% peptone, 1% yeast extract, 100 mM K_2PO4 pH 6.0, 1.34% YNB, 400 µg/l biotin, 1% glycerol
Buffered Methanol Medium (BMM)	2% peptone, 100 mM K_2PO_4 pH 6.0, 1,34% YNB, 400 µg/l biotin, 1% methanol

4.4.2. Purification of the enzyme from (Bom et al., 1998)

Hydrophobic interaction chromatography (HIC) was carried out on a Phenyl Sepharose column.

Reagents:

50 mM Potassium acetate buffer pH 5.0 with 1.5 M Ammonium Sulfate

5 mM Potassium acetate buffer pH 5.0

50 mM Potassium acetate buffer pH 5.0 with 50% ethylene glycol

Material:

Column Sephadex G-25 (1x10 cm)

Column Phenyl Sepharose 6 Fast Flow (2.6x15cm) (XK 26/20-GE Healthcare)

Experiment:

System: AKTA Prime plus (Amersham Biosciences)

Flow: 25 ml/min

Column: XK 26 with Phenyl Sepharose FF (GE Healthcare)

Phase A: 50 mM Potassium Acetate and 1.5 M Ammonium Sulfate

Phase B: 5 mM Potassium Acetate

Phase C: 50 mM Potassium Acetate and 50% Ethylene glycol

The column was equilibrated with 50 mM potassium acetate buffer pH5.0 and 1.5M ammonium sulfate.

The supernatant concentrated was dropped-off.

The column was eluted with 5 mM potassium acetate buffer pH 5.0 (decreased gradient) then, 50 mM potassium acetate pH 5.0 containing 50% ethylene glycol (increased gradient).

2 peaks were observed: peak 1 was in potassium acetate and ammonium sulfate and the second was in 50% ethylene glycol.

Fractions (of 4 ml) from the second peak containing β-1,6 glucanase activity were pooled.

To remove ethylene glycol:

1 ml of those fractions (purified enzyme) was filtered on Sephadex G-25 column. The column was preliminary equilibrated with 50 mM potassium acetate pH 5.0.

The enzyme solution was finally concentrated by ultrafiltration on 10 kDa Amicon-Ultra (Milipore).

The enzyme was stored at -80°C until 12 months without any loss of activity and after filtration at 4°C for 2 weeks.

4.5. Atomic force microscopy

4.5.1. System

The atomic force microscope used was Nanowizard III (JPK Instruments, Berlin, Germany). This AFM is coupled to an inverted microscope Zeiss Axio Vert Observer D1.m (Carl Zeiss, France) and a camera Jenoptik ProfRes MF-Cool (Jenoptik, Jena, Germany). Before each experiment, the spring constant of the cantilevers (k_{cant} in $mN.m^{-1}$) and the sensibility (S in $m.V^{-1}$) have to be measured.

These parameters of calibration were determined in acetate buffer used for the experiment (18 mM CH_3COONa, 1 mM $CaCl_2$, 1 mM $MnCl_2$, pH 5.2) on a glass slide by the thermal noise method (Burnham et al., 2003; Hutter and Bechhoefer, 1993). The cantilevers used were MLCT (Brucker, Camarillo, USA) and the cantilever with a spring constant of 0.01 $N.m^{-1}$ indicated by the manufacturer was used (values measured were between 0.01 and 0.02 $N.m^{-1}$).

4.5.2. Immobilization of yeast cell in PDMS stamps from (Dague et al., 2011)

Immobilization of living cells in polydimethylsiloxane (PDMS) stamps involves three steps. The first one consists in generating a glass/chromium mask presenting microstructured patterns, and transferring these patterns onto a silicium wafer. The generation of a silicium wafer was performed in LAAS-CNRS by photolithography.

The microstructured patterns of the silicon master are squares, ranging from 1.5 to 6 µm wide, with a pitch of 0.5 µm and a depth ranging from 1 µm to 4 µm.

Preparation of PDMS stamps:

A solution of PDMS polymer containing 10:1 (w/w) of PDMS oligomers and a reticular agent (Sylgart® kit 184) was prepared. The PDMS solution was degased under vacuum and deposited on the silicium wafer. Bubbles were removed by degasing again under vacuum the silicium wafer with the PDMS. Finally, the PDMS was cured for 1 hour at 80°C and cooled down at room temperature.

Preparation of yeast cell and immobilization into PDMS:

Cells were harvested at exponential phase (DO_{600}=1) by centrifugation and washed two times in acetate buffer (18 mM CH_3COONa, 1 mM $CaCl_2$, 1 mM $MnCl_2$, pH 5.2). Then, yeast cells were resuspended in the same buffer, and immobilized on polydimethylsiloxane (PDMS) stamps.

A microstructured PDMS motif was cut with a scalpel and removed. Then, the PDMS stamp was covered by a total of 100 µL of cell suspension. The cells were then deposited into the microstructures of the stamp by convective/capillary assembly.

4.5.3. Functionalization of AFM tips from (Jauvert et al., 2012)

Reagents:

Acetone, ethanol, dichloromethane, ethanolamine, DMSO, THF, dendrimer, lectine (concanavalin A), 0.1M carbonate buffer, sodium borohydride ($NaBH_4$), acetate buffer (sodium acetate 18mM pH 5.2 with 1 mM $MnCl_2$ and 1 mM $CaCl_2$)

Material: UV-cleaner, Nitrogen steam, Crystallizer

Experiment:

- Preparation of AFM tips with amino groups

Cantilevers were washed with dichloromethane, acetone, 95% ethanol (5 min each), then placed in UV-ozone cleaner for 15 min and immersed 14 hours in ethanolamine solution in DMSO (3.3 g in 6.6 ml of DMSO) to generate amino groups. After incubation, tips are washed with DMSO and 95% ethanol (3 times for 5 min each wash).

Finally, tips functionalized with amino groups were dried under nitrogen steam.

- Preparation of dendritip

AFM tips functionalized with amino groups were incubated with 58 µM of dendrimer in THF for 5-6 hours at room temperature. Tips were washed in THF and ethanol (3 times for 5 min each). The dendritips can be stored in a desiccator at room temperature.

- Dendritip functionalization with lectin

The coupling with the lectin was made by immersion of the dendritip in 100 µL of lectine solution (100 $\mu g.ml^{-1}$ in a 0.1 M carbonate buffer). After 1 hour of incubation, 100 µl of $NaBH_4$ 3.5 $mg.ml^{-1}$ solution was added and incubated 15 min in order to reduce the unreacted groups. Finally, the cantilever was washed three times and stored in acetate buffer.

4.5.4. Experiment: imaging and force spectroscopy

Quantitative imaging

JPK Instruments has developed recently the QI mode (QI for quantitative imaging): the tip moves from point to point across the surface, the AFM tip being completely detached from the surface before moving to the next point (Chopinet et al., 2013). This mode is similar to the tapping mode; it allows damaging the cell surface and avoiding the lateral deflections. Moreover to the tapping mode, with this mode the force curves can be collected at the same speed and resolution as normal imaging.

The yeast cell was firstly localized on an optical image with a camera set on the inverted microscope (Zeiss), and then we used the QI mode to obtain a tridimensional image of the cell. The cell was scanned with the AFM tip with a constant force of 1.5 nN and a speed of 250 µm/s (extend) or 300 µm/s (retract).

Height image

Height image with QI mode was obtained by analyzing the deflection of the cantilever. The tip oscillates until to get contact with the surface and the modification of the amplitude of oscillation leads to measure the topography.

Adhesion image

The force curves obtained with QI mode were analyzed. When the retract force curve was presented a hysteresis, the adhesion force was determined and resulted in an image of adhesion (in nN).

Contact mode

In contact mode, the tip is in contact with the surface of the sample and scans this surface horizontally with a constant force. Since the contact mode can damage the cell, this mode is used on a small area of the surface (1 µm x 1 µm) and the maximal force applied to the sample was limited to 0.2 nN. The contact mode was used to obtain high resolution of the cell surface of 512 x 512 pixels and a line rate of 1 Hz.

Force spectroscopy

After imaging the yeast cell, a square of 1 µm x 1 µm was selected on the center of the cell. On this area, the tip was pushed on the surface with a constant force of 0.5 nN on different locations (32 x 32 squares), leading to record 1024 force-distance curves. When the tip was interacted with the surface, an adhesion peak was observed on the retract force curve. Force spectroscopy experiments allow to localize adhesion event (force map image) and record force distance curve at the same time.

Parameters used to measure force in force spectroscopy mode: force=0.5 nN; z-length=1 µm; speed=5µm/s.

4.5.5. Data analysis

Elasticity measurement: Openfovea software

Openfovea software developed by (Roduit et al., 2012) was used to determine the elasticity of the cell. By applying the Hertz model, we can calculate the Young modulus (E in Pascal), which gives information on the elasticity of the cell.

The Hertz model is: $$F = \frac{2E \tan \alpha}{\pi\,(1-\nu^2)} . \delta^2$$

Where indentation depth (δ in nm) is the deformation of the sample under the tip, the value of the opening angle (α in rad) is a parameter of the tip geometry and the Poisson ratio (ν in degree). For this

analysis, the parameters applied were : an indentation of 50 nm; model tip as cone; Poisson ratio of 0.5; 0.31 rad for the half-opening angle of the tip.

Thus, fitting each force curve of a batch, e.g. of 1024 force curves, with the Hertz model generates a distribution of Young modulus values that can be adjusted to a Gaussian law with Origin8 in order to describe the mean Young modulus value (E) and standard deviation.

JPK Data processing software

Height image

Height image were analyzed with JPK Data processing. A flatten of 1 was applied on each image and the scale of height was adjusted.

Roughness

Images recorded in contact mode with the same center of offset were processed and analyzed with the power spectral density method (JPK data processing software) consisting of average roughness (Ra in nm) measurements on five boxes of five different sizes for each images (1 µm x 1 µm; 750 nm x 750 nm; 500 nm x 500 nm; 250 nm x 250 nm; 100 nm x 100 nm).

Slope and stiffness images

An image of the slope (s) can also be recorded with the QI™ mode by analyzing the slope of the linear part of the force curve with the Data Processing software from JPK Instruments. The value of the slope leads to determine the stiffness (the cellular spring constant) of the sample k_{cell} in $N.m^{-1}$. The stiffness of the cell was calculated from the calibrated cantilever spring constant (k_{cant}) and the slope (s): $k_{\text{cell}} = k_{\text{cant}}\left(\frac{s}{1-s}\right)$

4.6. Canonical correlations of cell wall physico-chemical traits and transcriptomic profile

The set of cell wall traits (*i.e.* 3 biophysical properties and 4 biochemical data) is represented by the matrix X in which rows correspond to the yeast strains and columns correspond to the 7 cell wall measurements. Likewise, matrix Y refers to the set of transcriptomic data whereas rows also correspond to the yeast strains and columns correspond to the obtained genes.

In Canonical Correlation Analysis (CCA) :

$a^1 = \left(a_1^1, \ldots, a_p^1\right)^T$ and $b^1 = \left(b_1^1, \ldots, b_p^1\right)^T$ are the basis vectors where a and b are the data.

$U^1=Xa^1$ and $V^1=Yb^1$ are the projection of the variates (columns in the matrices X and Y) onto the basis vectors (a^1 and b^1). These derived linear projections U^1 and V^1 are also called the first *canonical variates.*

In CCA, the two basis vectors a^1 and b^1 are such that the correlation (corr) between their projection U^1 and V^1 are both maximised. The coefficient of correlation is definied as :

$$\rho = corr(U^1, V^1) = \max corr\,(Xa^1, Yb^1) = \frac{cov\,(U^1, V^1)}{\sigma_{U^1}\sigma_{V^1}}$$

where σ_{U^1} and σ_{V^1} are standard deviations of the U^1 and V^1

$corr(U^1, V^1)$ and $cov\,(U^1, V^1)$ are respectively the correlation and the covariance of the two projection U^1 and V^1

If ρ is equal to 0, the matrices are not correlated. The matrices are more correlated if ρ is distant to 0 (near -1 and +1). The value of the coefficient of correlation is positive (neagtive), it indicates a positive (negative) correlation. The correlation is high if $0.5 < \rho < 1$ and low if $0 < \rho < 0.5$

To investigate association between individual variables, *i.e.* genes and cell wall traits, the similarity between variables in X and Y is quantified based on the Pearson correlations of their initial representation and the determined canonical variates. This form of correlations is known as canonical structure correlations and can be further visualized by means of a relevance network. Both, the CCA analysis as well the network are derived using the mixOmics package (http://www.math.univ-toulouse.fr/~biostat/mixOmics/). The threshold τ_{CCA} for obtaining edges between genes and cell wall traits in the relevance network was chosen as $\tau_{CCA} \geq 0$. ensuring that all the 7 cell wall parameters are not isolated in this network.

5. List of Publications

Atomic Force Microscopy allows revealing effects of autolysis process and differences on the nanomechanical properties of industrial yeast strains
Schiavone M., Sieczkowski N., Castex M., Dague E., François J. M.
Submitted in october 2014 in FEMS Yeast Research.

A combined chemical and enzymatic method to determine quantitatively the polysaccharide components in the cell wall of yeasts.
Schiavone M., Vax A., Formosa C., Martin-Yken H., Dague E., François J. M.
FEMS Yeast Research (2014). Volume 14, pages 933–947.
doi:10.1111/1567-1364.12182.

Nanoscale effects of Caspofungin against two yeast species; *Saccharomyces cerevisiae* and *Candida albicans.*
Formosa C.*, Schiavone M*., Martin-Yken H, François JM, Duval R.E., Dague E. (*co-authors)
Antimicrobial Agents and Chemotherapy (2013). Vol. 57 n° 8, pages 3498-3506.
doi: 10.1128/AAC.00105-13

Uncovering by Atomic Force Microscopy of an original circular structure of the yeast cell surface in response to heat shock.
Pillet F., Lemonnier S., Schiavone M., Formosa C., Martin-Yken H., François J. M, Dague E.
BMC Biology (2014). Vol. 12, n° 1, page 6.
doi: 10.1186/1741-7007-12-6

Use of Atomic Force Microscopy (AFM) to explore cell wall properties and response to stress in the yeast *Saccharomyces cerevisiae*.
François J. M., Formosa C., Schiavone M., Pillet F., Martin-Yken H., Dague E.
Current Genetics (2013). Vol. 59, n° 4, pages 187‑196.
doi:10.1007/s00294-013-0411-0.

Multiparametric imaging of adhesive nanodomains at the surface of Candida albicans by atomic force microscopy.
Formosa C., Schiavone M., Boisrame A., Richard M.L., Duval R.E., Dague E., 2014. Nanomedicine Nanotechnology, Biol. Med.
doi:10.1016/j.nano.2014.07.008

6. List of Communications

Oral presentations

“Impact of caspofungin and gene deletions on yeast cell wall architecture”
Schiavone M., Formosa C., Martin-Yken H., François J. M., Dague E.
Linz Winter Workshop 2014, 31 January - 3 Februray 2014, Linz, Austria.

“A simple method to determine Saccharomyces cerevisiae cell wall composition by combined chemical and enzymatic hydrolysis”
Schiavone M., Martin-Yken H., François J. M.
Vth International conference on molecular mechanism of fungal cell wall biogenesis, 6-9 June 2012, Primosten, Croatia.

“Biochemical and biophysical study of *Saccharomyces cerevisiae* cell wall”
Microbiotoul 2013, 21-22 October 2013, Toulouse, France.

Posters

« Nanoarchitecture de la paroi de levures stressées » M. Schiavone, C. Formosa, H. Martin-Yken, J. M. François, E. Dague.
Forum de microscopie à sonde locale, February 2014, Montauban, France.

« Imaging of adhesive nanodomaines at the surface of Candida albicans by Atomic Force Microscopy»
Formosa, M. Schiavone, R. E. Duval, E. Dague.
Linz Winter Workshop 2014, 31 January - 3 February 2014, Linz, Austria.

« A method to determine *Saccharomyces cerevisiae* cell wall composition by combined chemical and enzymatics hydrolysis »
M. Schiavone, H. Martin-Yken, E. Dague et J.M. François.
Vth Conference on physiology of yeast and filamentous fungi, 4-7 June 2013, France.

« A simple method to determine *Saccharomyces cerevisiae* cell wall composition by combined chemical and enzymatic hydrolysis » M. Schiavone, H. Martin-Yken, J.M. François.
Vth International conference on molecular mechanism of fungal cell wall biogenesis, 6-9 June 2012, Primosten, Croatie.

« A method to determine *Saccharomyces cerevisiae* cell wall composition by combined chemical and enzymatics hydrolysis » M. Schiavone, H. Martin-Yken, J.M. François.
Levures Modèles et Outils (10ème édition), 2-4 April 2012, Toulouse, France.

AAC
Journals.ASM.org

Nanoscale Effects of Caspofungin against Two Yeast Species, *Saccharomyces cerevisiae* and *Candida albicans*

C. Formosa,[a,b,c,d] M. Schiavone,[a,b,e] H. Martin-Yken,[b,e] J. M. François,[b,e] R. E. Duval,[c,d,f] E. Dague[a,b]

CNRS, LAAS, Toulouse, France[a]; Université de Toulouse, LAAS, Toulouse, France[b]; CNRS, SRSMC, UMR 7565, Vandœuvre-lès-Nancy, France[c]; Université de Lorraine, SRSMC, UMR 7565, Nancy, France[d]; INRA, UMR 972 LISBP, Toulouse, France[e]; ABC Platform, Nancy, France[f]

***Saccharomyces cerevisiae* and *Candida albicans* are model yeasts for biotechnology and human health, respectively. We used atomic force microscopy (AFM) to explore the effects of caspofungin, an antifungal drug used in hospitals, on these two species. Our nanoscale investigation revealed similar, but also different, behaviors of the two yeasts in response to treatment with the drug. While administration of caspofungin induced deep cell wall remodeling in both yeast species, as evidenced by a dramatic increase in chitin and decrease in β-glucan content, changes in cell wall composition were more pronounced with *C. albicans* cells. Notably, the increase of chitin was proportional to the increase in the caspofungin dose. In addition, the Young modulus of the cell was three times lower for *C. albicans* cells than for *S. cerevisiae* cells and increased proportionally with the increase of chitin, suggesting differences in the molecular organization of the cell wall between the two yeast species. Also, at a low dose of caspofungin (i.e., 0.5× MIC), the cell surface of *C. albicans* exhibited a morphology that was reminiscent of cells expressing ad- hesion proteins. Interestingly, this morphology was lost at high doses of the drug (i.e., 4× MIC). However, the treatment of *S. cerevisiae* cells with high doses of caspofungin resulted in impairment of cytokinesis. Altogether, the use of AFM for investigat- ing the effects of antifungal drugs is relevant in nanomedicine, as it should help in understanding their mechanisms of action on fungal cells, as well as unraveling unexpected effects on cell division and fungal adhesion.**

The yeast cell wall is composed of 50 to 60% β-glucans (glucose residues attached by 1,3-β- and 1,6-β-linkages), 40 to 50% mannoproteins (highly glycosylated polypeptides), and 1 to 3% chitin (1, 2). It is an essential dynamic structure playing roles in maintaining cell shape and integrity, sensing the surrounding environment, and interacting with surfaces and other cells (3). The cell wall represents 15 to 25% of the cell dry mass, the chemical composition of which is well established. *Saccharomyces cerevisiae*, also called baker's yeast, is the best-characterized eukaryotic model for scientific and biomedical research. Although the chemical composition of the yeast cell wall is well known, its molecular ultrastructure (organization or assembly) has not been extensively studied at nanoscale (4, 5), although there are a few reports on the nanomechanical and adhesive properties of the yeast cell wall under native conditions or under stress conditions (6–8). As for *Candida albicans*, it is by far the most common human-pathogenic fungal species. It can cause a range of pathogenic effects, including painful superficial infections, severe surface infections, and life-threatening bloodstream infections (9). It is a major cause of morbidity and mortality in immunocompromised patients as a result of AIDS, cancer chemotherapy, or organ transplantation (10).

Given its medical relevance, *C. albicans* has been the subject of extensive research to find new antifungal drugs to fight it. To date, only three classes of antifungal drugs are available for systemic *C. albicans* infections: the polyenes (such as amphotericin B), the azoles (ketoconazole, itraconazole, fluconazole, and voriconazole), and flucytosine. Although many of these drugs have advanced the management of fungal infections, failure rates remain high (11), and the emergence of resistant fungal strains is a growing problem (12). In this context, a new class of antifungal drugs, the echinocandins, was very welcome in the biomedical domain (13). There are currently three drugs belonging to the class that are available for clinical use: caspofungin, micafungin, and anidulafungin. The echinocandins are large polypeptide molecules that inhibit β-1,3-glucan synthase, an enzyme involved in cell wall synthesis. The disruption of this polysaccharide results in the loss of cell wall integrity. The activity of echinocandins is generally opposite to that of the azoles in that they are fungicidal against yeasts and fungistatic against molds (13). As echinocandins have been used only recently in the clinic, the mechanism of resistance to the drugs is still poorly documented, although a few cases of resistant isolates from patients treated with the antifungal implicating mutations in the *FKS1* gene encoding β1,3-glucan synthase (14–17) have been reported.

Whereas the target of echinocandins (i.e., β-1,3-glucan synthase) is well characterized, the global effects of this antifungal drug class on the cell wall of yeasts at nanoscale have not been studied. Such a study is now becoming feasible with the recent advances in atomic force microscopy (AFM) under liquid conditions. Since its invention in 1986 (18), AFM has proven to be a powerful tool in biology (19) for evaluating the effects of antimicrobial drugs against live bacteria or fungi (20, 21). In this study, we used AFM under liquid conditions to investigate nanomechanical effects caused by caspofungin on *S. cerevisiae* and *C. albicans*. Furthermore, we used biochemical methods to determine the cell wall composition in order to evaluate a potential correlation between these biophysical properties and cell wall modifications in response to caspofungin for the two yeast species.

Received 15 January 2013 Returned for modification 27 February 2013
Accepted 4 May 2013
Published ahead of print 13 May 2013
Address correspondence to E. Dague, edague@laas.fr.
C.F and M.S. contributed equally to the work.

doi:10.1128/AAC.00105-13

MATERIALS AND METHODS

Yeast growth conditions. *S. cerevisiae* strain BY4741 (MAT**a** *his3*Δ*1 leu2*Δ*10 met15*Δ*0 ura3*Δ*0*) (22) and *C. albicans* (from ABC Platform Bugs Bank, Nancy, France) were stocked at −80°C, revivified on yeast extract-peptone-dextrose (YPD) agar (Difco; 242720-500g), and grown in yeast extract-peptone-dextrose broth (Difco; 242820-500g) for 20 h at 30°C under static conditions. For caspofungin treatment, caspofungin was added for 20 h before the experiments. Before AFM experiments were conducted, the yeasts were grown in yeast extract-peptone-dextrose broth containing caspofungin at a concentration of 0.063 μg/ml (0.5× MIC) and 0.5 μg/ml (4× MIC) for *S. cerevisiae* and 0.047 μg/ml (0.5× MIC) and 0.37 μg/ml (4× MIC) for *C. albicans*.

MIC determination for caspofungin. The MIC values for caspofungin were determined using commercially available Etest strips containing a gradient of caspofungin (bioMérieux; 532400). For the diffusion test, a yeast solution (optical density at 590 nm [OD_{590}] = 0.150) was applied to the yeast extract-peptone-dextrose agar plates. The plates were allowed to dry for 15 min before the Etest stripes were applied in a radial fashion onto the agar surface. The MIC was determined after 24 h at 30°C by the intersection of the lower part of the elliptical growth inhibition area with the Etest strip.

We chose to use Etest from bioMérieux, as it gave repeatable results compared to the EUCAST (23) or CLSI (24) method. It must be noted that EUCAST does not publish clinical breakpoints for caspofungin for *C. albicans* "due to significant interlaboratory variation in MIC ranges for caspofungin."

We used yeast extract-peptone-dextrose agar (Difco; 242720-500g) and incubation at 30°C in order to determine the caspofungin MIC for the conditions under which we performed the AFM and biochemical experiments of the study. However, we also performed the Etest at 35°C for 24 h, and we found the same results for both *S. cerevisiae* and *C. albicans* as with incubation at 30°C. The common applications for the caspofungin Etest would be to use agar containing RPMI 1640, glucose, and MOPS (morpholinepropanesulfonic acid). However, under these conditions in liquid, the cells of *C. albicans* behave differently, since they form hyphae. In our study, we focused on cells with a spherical shape, the one that *C. albicans* assumes in bloodstream infections. This is why we performed all the experiments in YPD, and thus, we made the choice to determine the MICs in YPD also.

Sample preparation for AFM experiments. Yeast cells were concentrated by centrifugation, washed two times in acetate buffer (18 mM CH_3COONa, 1 mM $CaCl_2$, 1 mM $MnCl_2$, pH 5.2), resuspended in acetate buffer, and immobilized on polydimethylsiloxane (PDMS) stamps prepared as described by Dague et al. (25). Briefly, freshly oxygen-activated microstructured PDMS stamps were covered with a total of 100 μl of the solution of cells and allowed to stand for 15 min at room temperature. The cells were then deposited into the microstructures of the stamp by convective/capillary assembly. For *S. cerevisiae* cells treated with caspofungin at 4.0× MIC, polyethylenimine (PEI)-coated glass slides were used to immobilize the cells, as described previously (26). Briefly, freshly oxygen-activated glass slides were covered with a 0.2% PEI solution in deionized water and left for incubation overnight. Then, the glass slides were rinsed with 20 ml of Milli-Q water and nitrogen dried. A total of 1 ml of the yeast suspension was then applied to the PEI-coated glass slide, allowed to stand for 1 h, and rinsed with acetate buffer. Images were recorded in acetate buffer in quantitative-imaging mode (27, 28) with MLCT AUWH cantilevers (nominal spring constants, 0.01, 0.1, and 0.5 N/m). For imaging, cantilevers with a spring constant of 0.01 N/m were used. For force spectroscopy experiments, cantilevers with spring constants of 0.1 and 0.5 N/m were used. The applied force was kept at 0.5 nN for both imaging and force spectroscopy. For imaging and force spectroscopy, we used an AFM Nanowizard III (JPK Instruments, Berlin, Germany). The cantilevers' spring constants were determined by the thermal-noise method (29). For elasticity measurements, force maps of 32-by-32 force curves were recorded on a small area on top of the cells. The force-distance curves recorded were transformed into force-indentation curves by subtracting the cantilever deflection on a solid surface. The indentation curves were then fitted to the Hertz model, which links force (F) as a function of the Young modulus (E) and the square of the indentation (δ) for a conical indenter according to the following equation: $F = [2E \tan\alpha/\pi(1 - \nu^2)]\delta^2$, where α is the tip opening angle (17.5°) and ν is the Poisson ratio, assumed to be 0.5.

Isolation of cell walls for acid hydrolysis and chitinase assays. Cells from three independent cultures were collected at the exponential phase, harvested by centrifugation (5 min; 4,500 × *g*; 4°C), and washed two times with sterilized water. The pellet was resuspended in 0.5 ml of cold water and transferred to lysing matrix tubes (MPBio; 6960-500) containing 0.5-mm glass beads. The cells were disrupted by 8 cycles of 20 s at 6.5 m/s using a Fastprep system (Mp Biomedicals). Cell walls were isolated by centrifugation and extensive washing, as described by Francois (2), and then lyophilized.

Determination of cell wall polysaccharides by acid hydrolysis and quantification by HPAEC-pulsed amperometric detection. Sulfuric acid hydrolysis of the cell wall and quantification of glucosamine, glucose, and mannose residues released after chitin, β-glucan, and mannan hydrolysis were determined as described by Dallies et al. (30) with modifications according to the method of Francois (2). High-performance anionic chromatography (HPAEC) was carried out on an ICS 5000 system (Thermofisher Scientific, Courtaboeuf, France). Separation and quantification of the released monosaccharides were performed on a CarboPac PA10 analytical column (250 by 4 mm), with a CarboPac PA10 guard column, by isocratic elution of 18 mM NaOH at 25°C and a flow rate of 1 ml/min. Detection was performed on a pulsed amperometric system equipped with a gold electrode.

Chitin determination. A solution of 200 μl of 50 mM potassium acetate, pH 5.0, was added to purify cell walls (10 mg dry mass). After incubation at 65°C for 5 min, 1 U of chitinase from *Streptomyces griseus* (Sigma-Aldrich; C6137) was added. The enzymatic mixture was then incubated for 16 h at 37°C. Chitin levels from yeast cell walls were determined by the colorimetric method, as described by Reissig et al. (31) and adapted for the micromethod (a method performed in a microtiter plate, i.e., 96-well plate), using *N*-acetylglucosamine (Sigma-Aldrich; A8625) as a standard. A volume of 125 μl of the enzymatic mixture was heated with 25 μl of 0.8 M potassium tetraborate, pH 9.0 (Sigma-Aldrich; P1463), at 100°C for 8 min. After cooling at room temperature, 750 μl of Reissig reagent diluted 10 times was added, and tubes were incubated for 40 min at 37°C. The absorbance was read at 585 nm.

RESULTS

Caspofungin affects the morphology and cell division of *S. cerevisiae*. Our innovative method of cell trapping and immobilization in microstructured PDMS stamps (25) allowed us to image yeast cells and obtain morphological and mechanical properties at nanoscale (Fig. 1a and b). For each condition, five cells from three independent cultures were analyzed. The MIC determined with the Etest was 0.125 $\mu g \cdot ml^{-1}$. As shown in Fig. 1c, native cells of *S. cerevisiae* are roughly ovoid, with a mean diameter of 4.5 ± 0.2 μm (Fig. 1e). Upon treatment for 16 h with caspofungin at 0.5× MIC, the cells keep their round shape (Fig. 1b and d), and their mean size is decreased by about 25% ± 2.5% (Fig. 1f). A small dose of caspofungin, therefore, reduces the size of cells, apparently without any other modifications. When yeast cells were treated for 16 h with a high dose of caspofungin (4× MIC), the *S. cerevisiae* cells were no longer spherical but elongated, resembling *Schizosaccharomyces pombe* cells. The cross section taken along the line in Fig. 2b indicated a length of about 2.3 μm (Fig. 2f), which is 50% shorter than the untreated cells. However, two cells that remained connected are distinctly seen in Fig. 2d; they present a surprising feature on their surfaces, at the center of each one.

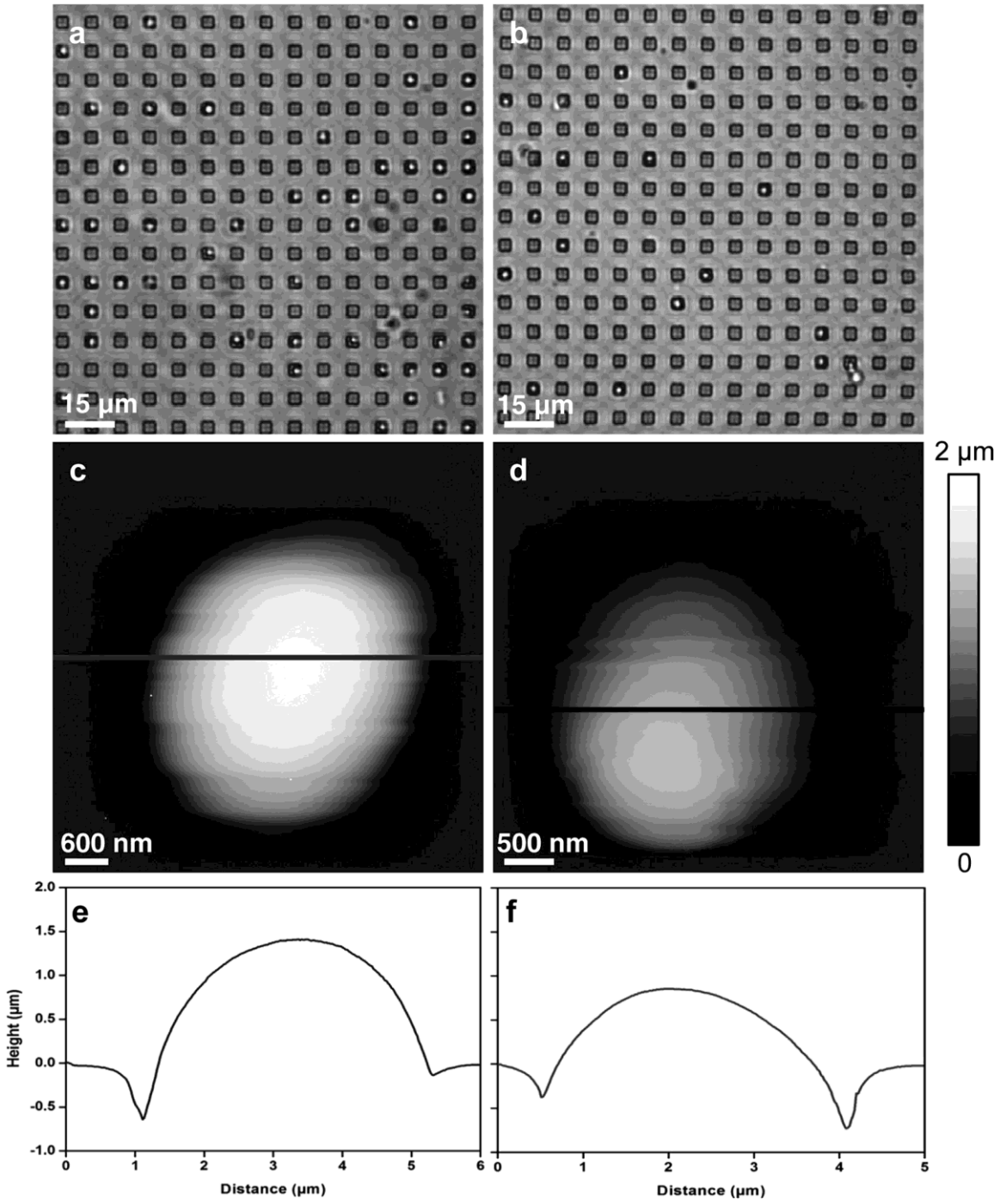

FIG 1 Images of *S. cerevisiae* cells (strain BY4147) trapped in microstructured PDMS stamps. (a and b) Optical images of live native cells (a) and of cells treated with caspofungin at 0.5X MIC (0.063 jLg/ml) (b). (c and d) AFM height images of a native cell (c) and of a cell treated with caspofungin at 0.5X MIC (0.063 jLg/ml) (d). (e and f) Cross sections taken along the lines on the height images.

When we took a closer look at this feature (Fig. 2e and g), we could visualize two rings that were 15 nm high and that were separated by a groove of approximately 200 nm. These results suggest that the morphology and cell division process of *S. cerevisiae* are altered at high doses of caspofungin. How can we explain such an effect?

It is known that caspofungin is an inhibitor of 13-1,3-glucan synthase (13). Thus, cells treated with this antifungal drug should present a reduced percentage of the cell wall polysaccharide. Accordingly, we found a reduction in the 13-glucan content, from 54% of cell dry mass in untreated *S. cerevisiae* cells to 49 and 45% in cells treated with caspofungin concentrations of 0.5X and 4X MIC, respectively (Table 1). The reduction of glucans was compensated for by an increase of mannans, from 45% of dry mass in untreated cells to 50 and 53% in cells treated at 0.5X and 4X MIC,

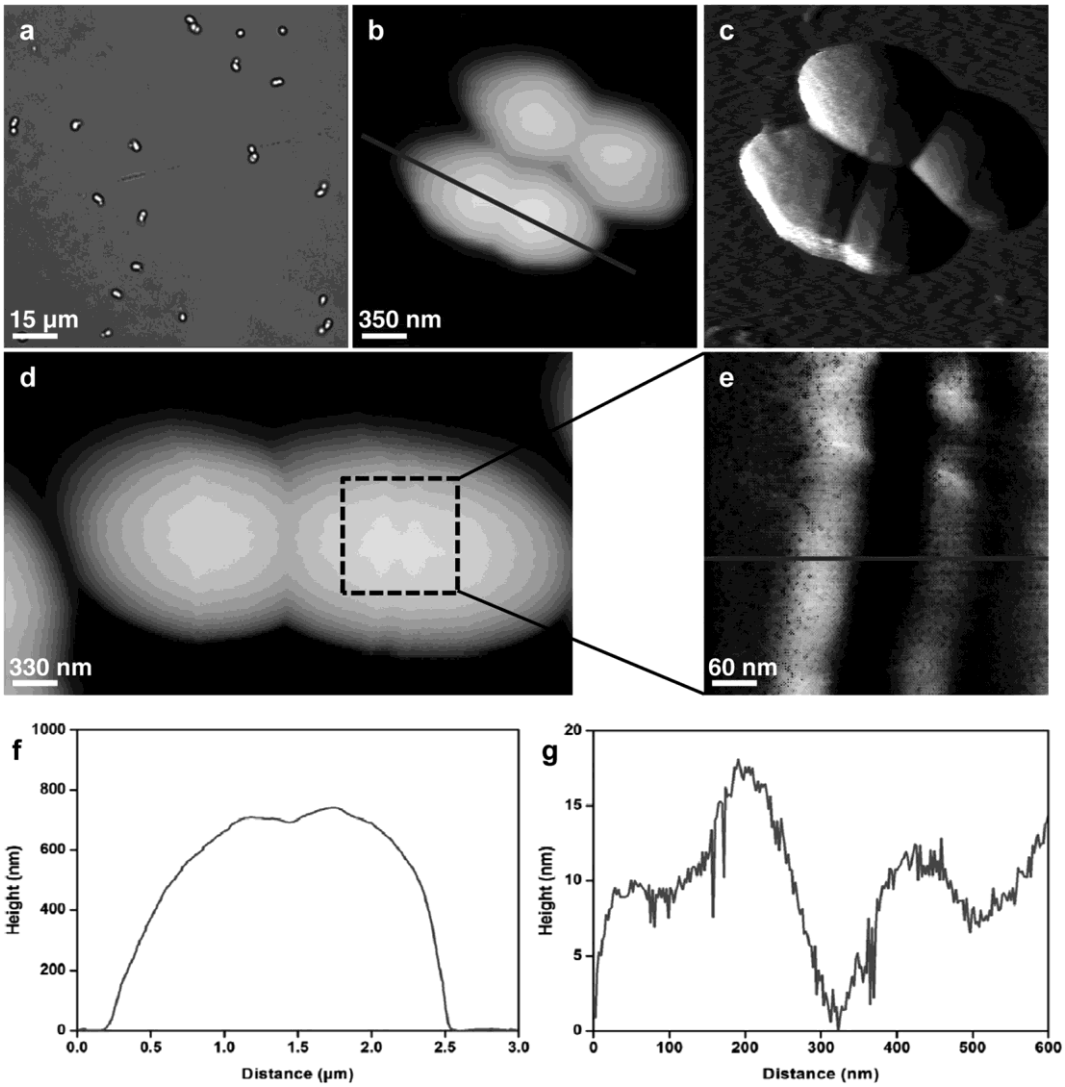

FIG 2 Images of *S. cerevisiae* (strain BY4741) cells treated with caspofungin at 4X MIC (0.5 jLg/ml). (a) Optical image of living cells immobilized on a PEI-coated glass slide. (b) AFM height image (z range = 1.2 jLm) of two cells. (c) Vertical-deflection image corresponding to the height image in panel b. (d) AFM height image of a single cell (z range = 1.2 jLm). (e) Height image of the boxed area in panel d (z range = 20 nm). (f and g) Cross-sections taken along the lines in panels b (f) and e (g).

respectively (Table 1). This cell wall remodeling in response to caspofungin treatment was also accompanied by changes in chitin. However, only at high doses of caspofungin (4X MIC) was an increase in chitin content found, from 5% in untreated cells or cells treated with 0.5X MIC of caspofungin to 14% of cell wall mass with a caspofungin dose of 4X MIC (Table 1). These results are in agreement with previous works of Juchimiuk et al. (32), who showed that *S. cerevisiae* cells treated with 3.0 jLg/ml caspofungin had their contents of 13-1,3-glucans reduced by 50% and their chitin contents increased by 3- to 5-fold. These data are in agreement with the general view that the response of *S. cerevisiae* cells to cell wall stress results in a deep reorganization of the cell wall as a

TABLE 1 Biochemical analysis of glucans and mannans of the cell wall of yeasts by acid hydrolysis and of chitin by the Reissig method[a]

	Content (% dry mass ± SD) in cells treated with caspofungin at:					
	S. cerevisiae			*C. albicans*		
Component	0X MIC	0.5X MIC	4X MIC	0X MIC	0.5X MIC	4X MIC
Glucans	54.1 ± 4.9	48.5 ± 6.5	45.0 ± 7.6	52.0 ± 3.2	48.5 ± 5.5	30.9 ± 8.6
Mannans	45.3 ± 2.9	50.4 ± 6.2	53.7 ± 7.1	46.5 ± 3.3	44.2 ± 3.0	59.3 ± 7.5
Chitin	4.8 ± 0.2	5.1 ± 0.8	13.8 ± 5.2	6.6 ± 2.6	12.8 ± 4.1	17.9 ± 5.3

[a] For each species and set of conditions, cells from 3 independent cultures were analyzed.

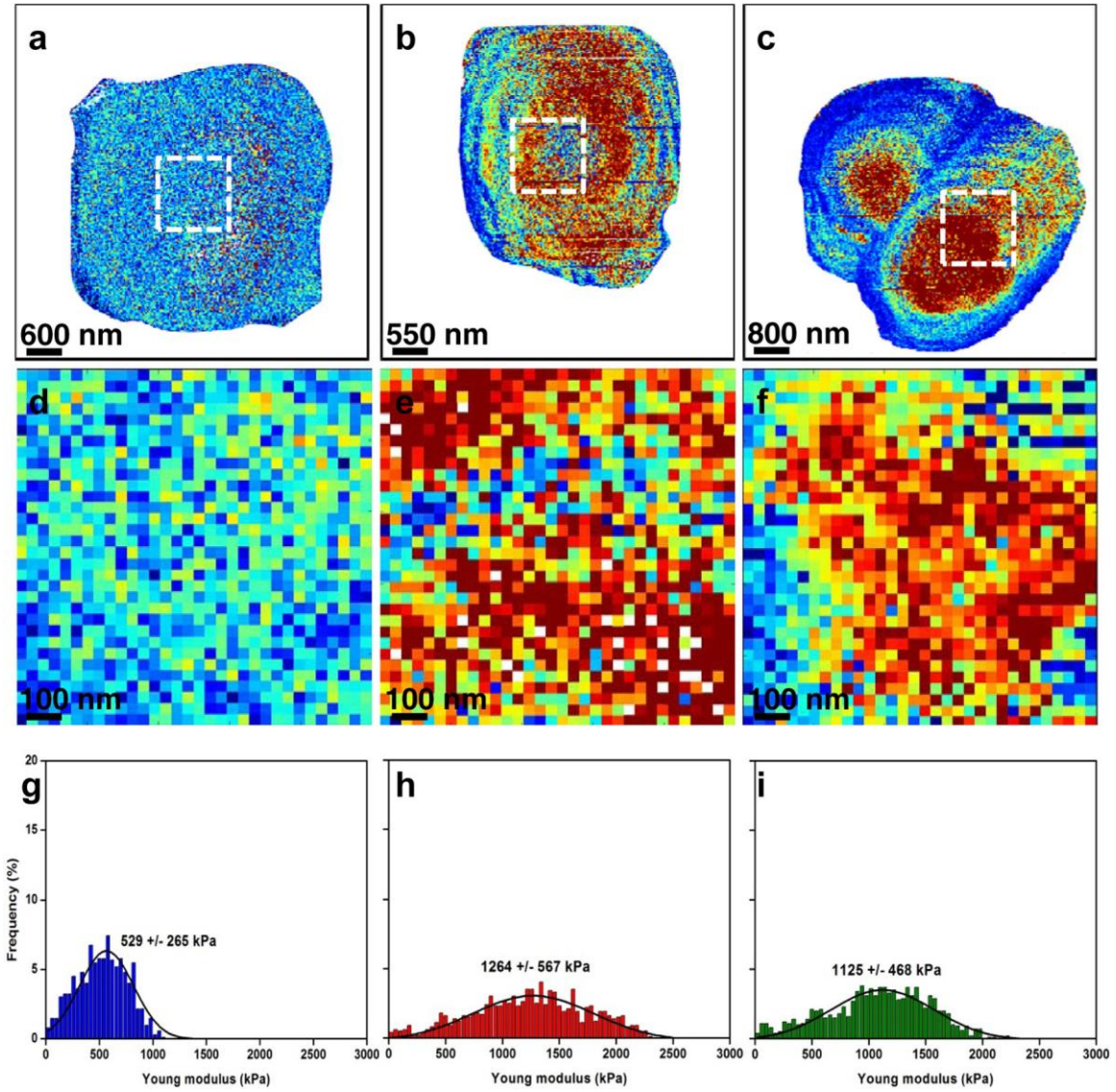

FIG 3 Mapping of *S. cerevisiae* (strain BY4741) cell surface elasticity. (a to c) Elasticity maps (z range = 1.5 MPa) of a native cell (a), of a cell treated with caspofungin at 0.5X MIC (0.063 jLg/ml) (b), and of a cell treated with caspofungin at 4X MIC (0.5 jLg/ml) (c). (d, e, and f) Local elasticity maps (z range = 1.5 MPa) recorded on a 1-jLm area (white dashed squares) on the tops of cells in panels a to c, respectively. (g, h, and i) Distributions of Young modulus values (n = 1,024) corresponding to the local elasticity maps in panels d to f, respectively.

means to rescue cell wall integrity (33) and, in the case of antifungal stress, in the overproduction of mannans and reduction of 13-glucans.

Nanomechanical properties of *S. cerevisiae*. In view of the role of the cell wall in conferring rigidity and protection on the yeast cell, we next addressed the pertinent question of whether the observed changes in cell morphology and chitin content were correlated with modifications in cell wall mechanical properties. To this end, *S. cerevisiae* cells exposed to two different concentrations of caspofungin were probed using nanoindentation measurements. The results of this experiment are shown in Fig. 3. The images of the cells recorded in quantitative-imaging mode (27, 28) allow analysis of all the force curves recorded in a single image (n = 65,536). By applying a mask, thanks to the analysis software (OpenFovea [34, 35]), only the force curves corresponding to the cells are extracted, leading to the elasticity maps presented in Fig. 3a, b, and c. In all the elasticity maps presented in this study, each pixel corresponds to a force curve that has been converted into an indentation curve and fitted with a Hertz model, from which a Young modulus (YM) value was extracted. The redder the pixel, the higher the YM value. These elasticity maps showed artifacts due to the spherical shape of the cells; the edges of the cells seem to have decreased YM values compared to the centers of the cells. However, these elasticity maps give a global view of the elasticity of the whole cells, with untreated cells that appear to be softer than caspofungin-treated cells. These observations were confirmed by local nanoindentation measurements performed on a 1-jLm^2 area on the surface of each cell (Fig. 3d, e, and f). These areas on the tops of the cells are flatter, so the YM artifacts are avoided. Untreated cells had a YM value of 529 ± 265 kPa (Fig. 3g), whereas

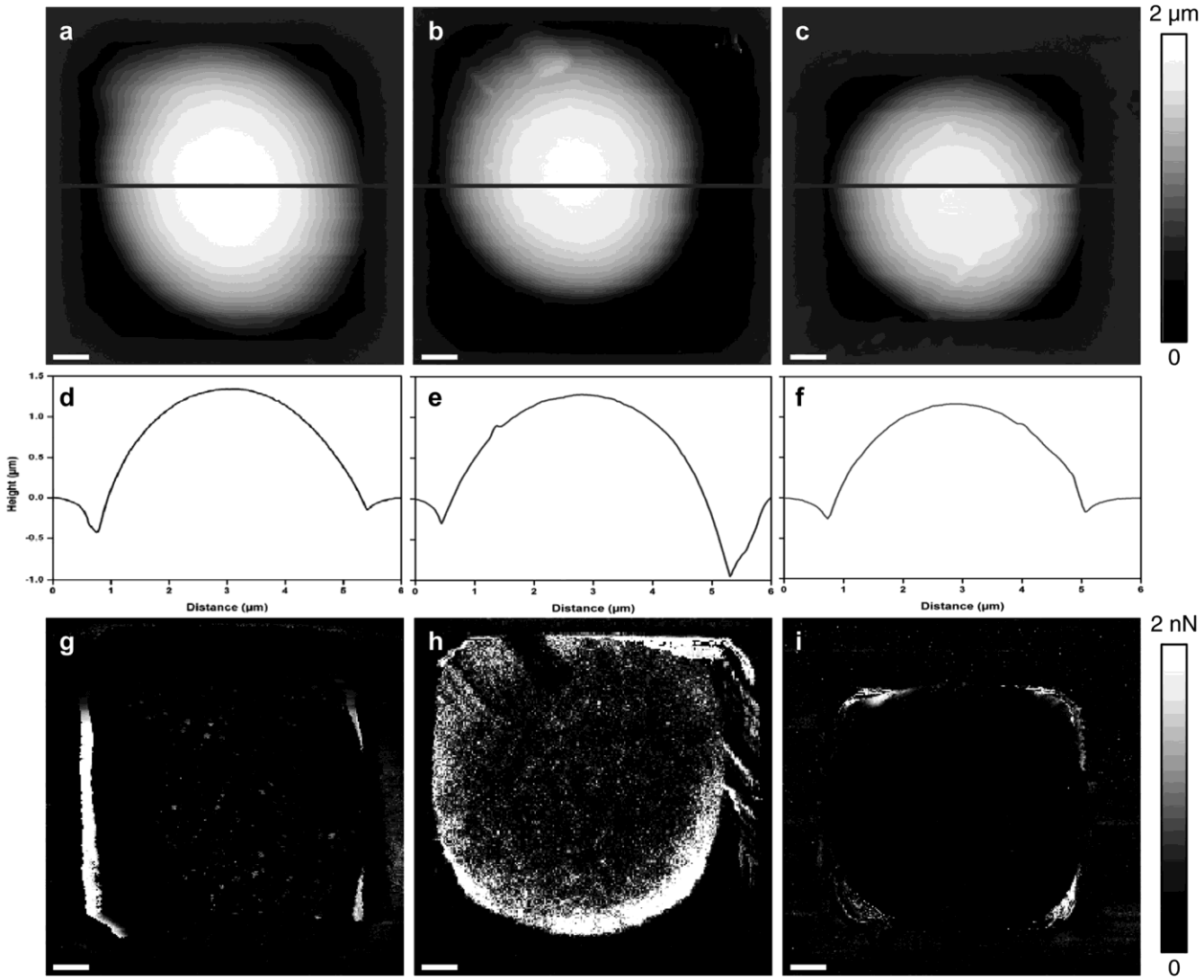

FIG 4 Imaging of *C. albicans* cells trapped in microstructured PDMS stamps. (a to c) AFM height images of a native cell (a), of a cell treated with caspofungin at 0.5X MIC (0.047 jLg/ml) (b), and of a cell treated with caspofungin at 4X MIC (0.376 jLg/ml) (c). (d, e, and f) Cross sections taken along the lines on the images in panels a to c, respectively. (g, h, and i) adhesion images corresponding to the height images in panels a to c, respectively.

cells treated with caspofungin at 0.5X MIC and 4X MIC (Fig. 3h and i) had YM values that increased to 1,264 ± 567 and to 1,125 ± 468 kPa, respectively.

Effects of caspofungin treatment on *C. albicans*. Using the Etest assay, we determined a MIC of about 0.094 jLg · ml^{-1}. The doses that were used in this study (0.5X MIC and 4X MIC) were therefore lower than the one reported to induce paradoxical growth effects (36). Caspofungin treatment does not cause morphology modification in *C. albicans*; the cells are spherical, with a mean diameter of 4.1 ± 0.2 jLm, as shown in Fig. 4a, b, and c. However, caspofungin treatment induced other modifications of the surfaces of *C. albicans* cells. The results presented in Fig. 4g, h, and i are adhesion images of the cells. Native cells are not adhesive, whereas cells treated with caspofungin at 0.5X MIC present adhesions homogeneously distributed over the surface of the cell, as indicated in the adhesion map presented Fig. 4h. However, cells treated with caspofungin at 4X MIC do not show adhesion at all, like native cells.

Probing the cell surface of *C. albicans* using nanoindentation measurements (Fig. 5), we unexpectedly found a YM value for the untreated *C. albicans* cells of 186 ± 89 kPa, which is three times lower than that of *S. cerevisiae* cells. Taking into account that the proportions of mannans, 13-glucans, and chitin in the cell wall are very similar for the two yeast species (1, 37), a likely explanation for the difference in YM values may reside in a difference in the molecular architectures of the cell wall between the two yeast species, notably in cross-linking between the components. Treatment of *C. albicans* cells with caspofungin at 0.5X MIC or 4X MIC for 16 h resulted in an increase of the YM value to 399 ± 147 kPa and 1,326 ± 340 kPa, respectively (Fig. 5h and i). Quite remarkably, this increase in YM values was correlated with the increase in the chitin level in *C. albicans* cells upon treatment with caspofungin (Fig. 6b and Table 1). In addition, the rise of chitin in the walls of *C. albicans* cells treated with caspofungin was accompanied by a decrease in 13-glucans and an increase of mannans, as already noticed for *S. cerevisiae* cells, but the effects of caspofungin were

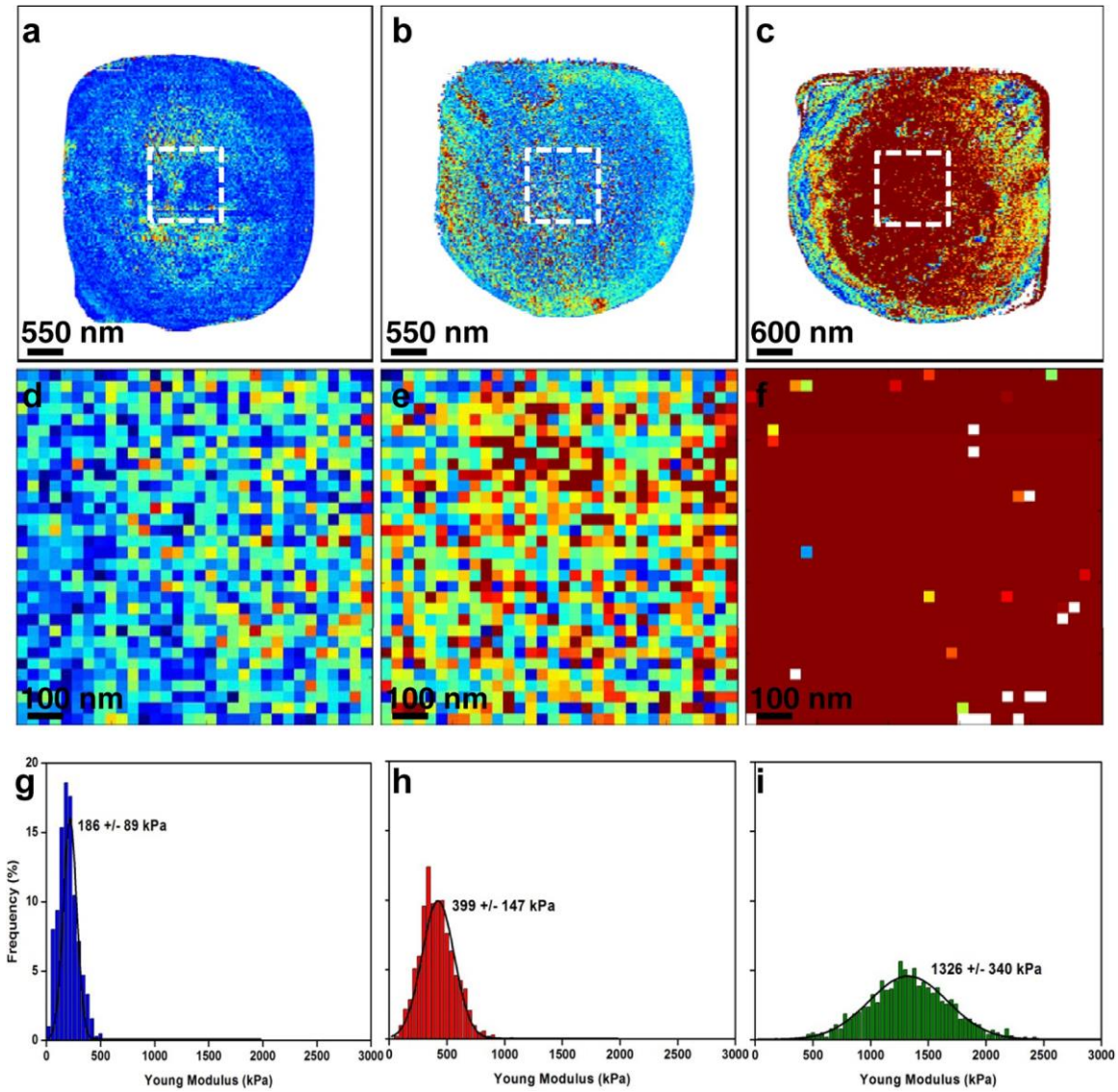

FIG 5 Mapping of *C. albicans* cell surface elasticity. (a to c) Elasticity maps (z range = 0.5 MPa) of a native cell (a), of a cell treated with caspofungin at 0.5X MIC (0.047 jLg/ml) (b), and of a cell treated with caspofungin at 4X MIC (0.376 jLg/ml) (c). (d, e, and f) Local elasticity maps (z range = 0.5 MPa) recorded on a 1-jLm area (white dashed squares) on the tops of the cells in panels a to c, respectively. (g, h, and i) Distributions of Young modulus values (n = 1,024) corresponding to the local elasticity maps in panels d to f, respectively.

apparently more prominent. Notably, untreated cells displayed a 13-glucan content of 52% of the cell wall mass. This proportion was reduced to 49% upon treatment with 0.5X MIC and to 31% when the cells were treated with 4X MIC of caspofungin. As for mannans, the proportion in untreated cells was close to 46% and increased to 59% when the cells were cultivated in the presence of a dose of 4X MIC of caspofungin.

DISCUSSION

We used AFM to investigate the effects of caspofungin on the morphology and nanomechanical properties of two yeast species, *S. cerevisiae* and *C. albicans*. With respect to *S. cerevisiae*, our results indicated that caspofungin at high doses alters the cell division process by perturbing cytokinesis. These modifications were observed along with a diminution of the 13-1,3-glucan content and an increase in the chitin content. Studies by Cabib and coworkers have shown the importance of chitin and 13-1,3-glucans during the cell division of yeasts (38–40). Their work focused on the remodeling of the cell wall during cell division, and particularly on the neck at the mother-bud interface. This crucial region is the site where cytokinesis and septation take place (41). Cabib et al. showed that control of growth at the neck is exerted by a septin ring and a chitin ring present at the location. A defect in either one of the rings leads to only minor morphological abnormalities. However, when both are faulty, control of growth is lost, the neck widens, and cytokinesis does not take place (38). They also showed that the chitin ring at the neck is specifically bound to 13-1,3-glucans (42) and that this linkage is necessary for the control of growth at the mother-daughter neck. As indicated in Fig. 2, the apparent impairment in cytokinesis in yeast treated with a high

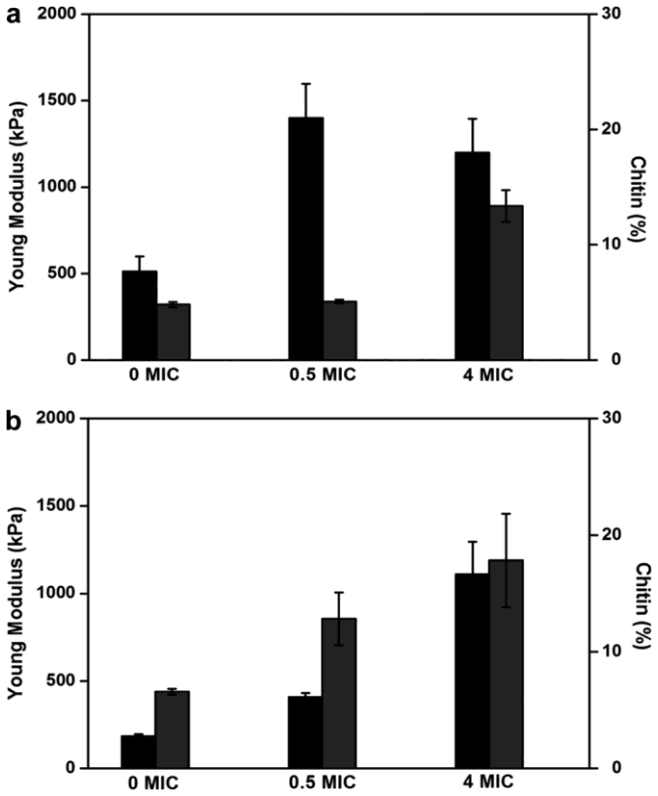

FIG 6 Quantitative analysis of chitin compositions of the yeast cell wall, correlated with Young modulus values. The histograms show Young modulus values (black bars) and chitin (gray bars) for *S. cerevisiae* (strain BY4741) (a) and for *C. albicans* (b) under different caspofungin conditions. The analyses for Young modulus values were performed on five cells from 3 independent cultures.

dose of caspofungin might be due to excess chitin that is present at the bud neck and that is not linked to 13-1,3-glucans, as the content of the latter is reduced.

While the increase in the YM value of the cell wall of *S. cerevisiae* could be correlated with the increase in chitin induced at a high dose of caspofungin, this was not the case for a lower dose of caspofungin, for which the YM value was already the same as at the higher dose of the antifungal drug. These results suggest that the force measurements performed with atomic force microscopy are not solely linked to changes in the cell wall composition but may unravel deep reorganization of the cell wall architecture without significant change in its cell wall components (43). A recent study conducted by our team (43) focused on *S. cerevisiae* mutants defective in, among other things, 13-glucan elongation (*gas1*Δ), chitin synthesis (*chs3*Δ), and cross-linkages between chitin and 13-glucans (*chr1chr2*Δ). This AFM study showed that cell wall elasticity was mainly dependent on the architecture and molecular composition of the cell wall. Moreover, chitin was identified as playing an important role in the nanomechanical properties of the cell wall. Our results are therefore in line with this previous study, and the amount of chitin in the cell wall could be directly correlated with the increase in the YM values. The difference in the nanomechanical properties of the two yeast species suggests a difference in the molecular architectures of their cell walls, even though the cell wall compositions were seemingly comparable.

With respect to *C. albicans* cells, global morphology and cell division do not appear to be affected, even at high doses of caspofungin. The modifications induced by the treatment concern the adhesive properties of the cells. As we saw, cells treated with a low dose of caspofungin present adhesions on their surfaces. *C. albicans* cells display adhesion proteins on their surfaces when cultivated under particular conditions (44). A key adhesin family identified is the Als (for agglutinin-like sequence) family (45, 46), which includes eight large cell surface glycoproteins. Als proteins play major roles in the processes of infection and colonization of the host. Since their discovery, many studies have been dedicated to understanding their functions and localization on the surfaces of cells. A recent study by Alsteens et al. (47) has characterized the localization of Als5 at the surface of mutant strains of *S. cerevisiae* using atomic force microcopy; in 2012, Beaussart et al. (48) characterized the localization of Als3 on the surfaces of *C. albicans* cells during morphogenesis. Their work provides confirmation that Als proteins can be mapped at the surfaces of living cells. Among these proteins is Als1p, which is involved in different processes, such as adherence to endothelial cells, flocculation, and filamentation (49). Gregori et al. (50) showed that Als1 is a critical factor required for caspofungin-induced flocculation. The authors show that cells treated by caspofungin present levels of *ALS1* mRNA that are strongly upregulated. Following these sets of data, we could hypothesize that the adhesion shown in Fig. 3h is due to expression of Als1. However, at high doses, the expression of the gene could be inhibited, leading us to think that the expression of Als1 under antifungal stress is a complex dynamic process that needs further study. Perhaps, at high doses of caspofungin, either the cells are dying or the transcriptional and translational machinery at this level of drug is strongly impaired, so that synthesis of new components at the cell wall, such as adhesion proteins, is inhibited. This hypothesis awaits further work, for instance, by measuring the expression of genes encoding some of these adhesion proteins in *C. albicans* cells challenged at different concentrations of caspofungin. These results were recorded on living cells of wild-type *C. albicans*, which gives us an insight into the physiological localization of the protein. Further work must be done to probe these adhesions with functionalized AFM tips under different conditions of growth and stress.

ACKNOWLEDGMENTS

E.D. is a researcher of the Centre National de la Recherche Scientifique (CNRS). This work was supported by a grant from the Young Scientist Program of ANR (Agence Nationale de la Recherche), project ANR-11-JSV5-001-01, no. (SD) 30 02 43 31, and by a grant from Region Midi Pyrenees (project no. 10051296) to J.M.F. C.F. is supported by a grant from Direction Générale de l'Armement (DGA) for her 3-year Ph.D. study and M.S. by Lallemand SAS.

We thank Charles Roduit for providing us with updated Fovea software. We thank Merck for providing caspofungin and Claire Murzeau for her help in the experiments.

C.F., R.E.D., J.M.F, and E.D. designed the experiments. C.F., M.S., H.M.-Y., and E.D. performed the experiments. C.F. and E.D. wrote the paper. Critical analysis and discussion of the results were carried out by all the authors, who also helped in critical reading of the manuscript and approved its final version.

REFERENCES

1. Lipke PN, Ovalle R. 1998. Cell wall architecture in yeast: new structure and new challenges. J. Bacteriol. 180:3735–3740.

2. Francois JM. 2006. A simple method for quantitative determination of polysaccharides in fungal cell walls. Nat. Protoc. 1:2995–3000.
3. Chaffin WL. 2008. Candida albicans cell wall proteins. Microbiol. Mol. Biol. Rev. 72:495–544.
4. Dague E, Gilbert Y, Verbelen C, Andre G, Alsteens D, Dufrêne YF. 2007. Towards a nanoscale view of fungal surfaces. Yeast 24:229–237.
5. Dufrêne YF. 2010. Atomic force microscopy of fungal cell walls: an update. Yeast 27:465–471.
6. Alsteens D, Dupres V, McEvoy K, Wildling L, Gruber HJ, Dufrene YF. 2008. Structure, cell wall elasticity and polysaccharide properties of living yeasts cells, as probed by AFM. Nanotechnology 19:384005. doi:10.1088/0957-4484/19/38/384005.
7. Adya AK, Canetta E, Walker GM. 2006. Atomic force microscopic study of the influence of physical stresses on Saccharomyces cerevisiae and Schizosaccharomyces pombe. FEMS Yeast Res. 6:120–128.
8. Canetta E, Adya AK, Walker GM. 2006. Atomic force microscopic study of the effects of ethanol on yeast cell surface morphology. FEMS Microbiol. Lett. 255:308–315.
9. Sudbery P, Gow N, Berman J. 2004. The distinct morphogenic states of Candida albicans. Trends Microbiol. 12:317–324.
10. Gow NA, Hube B. 2012. Importance of the Candida albicans cell wall during commensalism and infection. Curr. Opin. Microbiol. 15:406–412.
11. Denning DW. 1998. Invasive aspergillosis. Clin. Infect. Dis. 26:781–803.
12. Sanglard D, Odds FC. 2002. Resistance of Candida species to antifungal agents: molecular mechanisms and clinical consequences. Lancet Infect. Dis. 2:73–85.
13. Denning DW. 2003. Echinocandin antifungal drugs. Lancet 362:1142–1151.
14. Park S, Kelly R, Kahn JN, Robles J, Hsu M-J, Register E, Li W, Vyas V, Fan H, Abruzzo G, Flattery A, Gill C, Chrebet G, Parent SA, Kurtz M, Teppler H, Douglas CM, Perlin DS. 2005. Specific substitutions in the echinocandin target Fks1p account for reduced susceptibility of rare laboratory and clinical Candida sp. isolates. Antimicrob. Agents Chemother. 49:3264–3273.
15. Balashov SV, Park S, Perlin DS. 2006. Assessing resistance to the echinocandin antifungal drug caspofungin in Candida albicans by profiling mutations in FKS1. Antimicrob. Agents Chemother. 50:2058–2063.
16. Garcia-Effron G, Park S, Perlin DS. 2009. Correlating echinocandin MIC and kinetic inhibition of fks1 mutant glucan synthases for Candida albicans: implications for interpretive breakpoints. Antimicrob. Agents Chemother. 53:112–122.
17. Garcia-Effron G, Lee S, Park S, Cleary JD, Perlin DS. 2009. Effect of Candida glabrata FKS1 and FKS2 mutations on echinocandin sensitivity and kinetics of 1,3-β-D-glucan synthase: implication for the existing susceptibility breakpoint. Antimicrob. Agents Chemother. 53:3690–3699.
18. Binnig G, Quate CF, Gerber C. 1986. Atomic force microscope. Phys. Rev. Lett. 56:930–934.
19. Müller DJ, Dufrêne YF. 2011. Atomic force microscopy: a nanoscopic window on the cell surface. Trends Cell Biol. 21:461–469.
20. Formosa C, Grare M, Jauvert E, Coutable A, Regnouf-de-Vains JB, Mourer M, Duval RE, Dague E. 2012. Nanoscale analysis of the effects of antibiotics and CX1 on a Pseudomonas aeruginosa multidrug-resistant strain. Sci. Rep. 2:575.
21. Formosa C, Grare M, Duval RE, Dague E. 2012. Nanoscale effects of antibiotics on P. aeruginosa. Nanomedicine 8:12–16.
22. Baker Brachmann C, Davies A, Cost GJ, Caputo E, Li J, Hieter P, Boeke JD. 1998. Designer deletion strains derived from Saccharomyces cerevisiae S288C: a useful set of strains and plasmids for PCR-mediated gene disruption and other applications. Yeast 14:115–132.
23. EUCAST. 18 February 2012. Document E.DEF 7.2. Method for the determination of broth dilution of antifungal agents for fermentative yeasts; revised March 2012. EUCAST, Basel, Switzerland.
24. CLSI.2008. Reference method for broth dilution antifungal susceptibility. Testing of yeasts. Approved standard, 3rd ed. CLSI document M27-A3, vol. 28, no. 14. CLSI, Wayne, PA.
25. Dague E, Jauvert E, Laplatine L, Viallet B, Thibault C, Ressier L. 2011. Assembly of live micro-organisms on microstructured PDMS stamps by convective/capillary deposition for AFM bio-experiments. Nanotechnology 22:395102. doi:10.1088/0957-4484/22/39/395102.
26. Francius G, Tesson B, Dague E, Martin-Jézéquel Dufrêne VYF. 2008. Nanostructure and nanomechanics of live Phaeodactylum tricornutum morphotypes. Environ. Microbiol. 10:1344–1356.
27. JPK Instruments. 2011. QI™ mode-quantitative imaging with the NanoWizard 3 AFM. http://www.jpk.com/afm.230.en.html.
28. Chopinet L, Formosa C, Rols MP, Duval RE, Dague E. 2013. Imaging living cells surface and quantifying its properties at high resolution using AFM in QI™ mode. Micron 48:26–33.
29. Hutter JL, Bechhoefer J. 1993. Calibration of atomic-force microscope tips. Rev. Sci. Instruments 64:1868–1873.
30. Dallies N, François J, Paquet V. 1998. A new method for quantitative determination of polysaccharides in the yeast cell wall. Application to the cell wall defective mutants of Saccharomyces cerevisiae. Yeast 14:1297–1306.
31. Reissig JL, Strominger JL, Leloir LF. 1955. A modified colorimetric method for the estimation of N-acetylamino sugars. J. Biol. Chem. 217:959–966.
32. Juchimiuk M, Pasikowska M, Zatorska E, Laudy AE, Smoleńska-Sym G, Palamarczyk G. 2010. Defect in dolichol-dependent glycosylation increases sensitivity of Saccharomyces cerevisiae towards anti-fungal drugs. Yeast 27:637–645.
33. Ram AFJ, Kapteyn JC, Montijn RC, Caro LHP, Douwes JE, Baginsky W, Mazur P, Van den Ende H, Klis FM. 1998. Loss of the plasma membrane-bound protein Gas1p in Saccharomyces cerevisiae results in the release of β1,3-glucan into the medium and induces a compensation mechanism to ensure cell wall integrity. J. Bacteriol. 180:1418–1424.
34. Radotić K, Roduit C, Simonović J, Hornitschek P, Fankhauser C, Mutavdžić D, Steinbach G, Dietler G, Kasas S. 2012. Atomic force microscopy stiffness tomography on living Arabidopsis thaliana cells reveals the mechanical properties of surface and deep cell-wall layers during growth. Biophys. J. 103:386–394.
35. Roduit C, Saha B, Alonso-Sarduy L, Volterra A, Dietler G, Kasas S. 2012. OpenFovea: open-source AFM data processing software. Nat. Methods 9:774–775.
36. Bizerra FC, Melo ASA, Katchburian E, Freymüller E, Straus AH, Takahashi HK, Colombo AL. 2011. Changes in cell wall synthesis and ultrastructure during paradoxical growth effect of caspofungin on four different Candida species. Antimicrob. Agents Chemother. 55:302–310.
37. Chaffin WL, López-Ribot JL, Casanova M, Gozalbo D, Martínez JP. 1998. Cell wall and secreted proteins of Candida albicans: identification, function, and expression. Microbiol. Mol. Biol. Rev. 62:130–180.
38. Schmidt M, Varma A, Drgon T, Bowers B, Cabib E. 2003. Septins, under Cla4p regulation, and the chitin ring are required for neck integrity in budding yeast. Mol. Biol. Cell 14:2128–2141.
39. Cabib E, Blanco N, Arroyo J. 2012. Presence of a large β(1–3)glucan linked to chitin at the Saccharomyces cerevisiae mother-bud neck suggests involvement in localized growth control. Eukaryot. Cell 11:388–400.
40. Blanco N, Reidy M, Arroyo J, Cabib E. 2012. Cross-links in the cell wall of budding yeast control morphogenesis at the mother-bud neck. J. Cell Sci. 125:5781–5789.
41. Lippincott J, Li R. 1998. Sequential assembly of myosin II, an IQGAP-like protein, and filamentous actin to a ring structure involved in budding yeast cytokinesis. J. Cell Biol. 140:355–366.
42. Cabib E, Durán A. 2005. Synthase III-dependent chitin is bound to different acceptors depending on location on the cell wall of budding yeast. J. Biol. Chem. 280:9170–9179.
43. Dague E, Bitar R, Ranchon H, Durand F, Yken HM, François JM. 2010. An atomic force microscopy analysis of yeast mutants defective in cell wall architecture. Yeast 27:673–684.
44. Sundstrom P. 2002. Adhesion in Candida spp. Cell. Microbiol. 4:461–469.
45. Hoyer LL, Green CB, Oh S-H, Zhao X. 2008. Discovering the secrets of the Candida albicans agglutinin-like sequence (ALS) gene family—a sticky pursuit. Med. Mycol. 46:1–15.
46. Hoyer LL. 2001. The ALS gene family of Candida albicans. Trends Microbiol. 9:176–180.
47. Alsteens D, Garcia MC, Lipke PN, Dufrêne YF. 2010. Force-induced formation and propagation of adhesion nanodomains in living fungal cells. Proc. Natl. Acad. Sci. U. S. A. 107:20744–20749.
48. Beaussart A, Alsteens D, El-Kirat-Chatel S, Lipke PN, Kucharíková S, Van Dijck P, Dufrêne YF. 2012. Single-molecule imaging and functional analysis of Als adhesins and mannans during Candida albicans morphogenesis. ACS Nano. 6:10950–10964.
49. Coleman DA, Oh S-H, Zhao X, Hoyer LL. 2010. Heterogeneous distribution of Candida albicans cell-surface antigens demonstrated with an Als1-specific monoclonal antibody. Microbiology 156:3645–3659.
50. Gregori C, Glaser W, Frohner IE, Reinoso-Martín C, Rupp S, Schüller C, Kuchler K. 2011. Efg1 controls caspofungin-induced cell aggregation of Candida albicans through the adhesin Als1. Eukaryot. Cell 10:1694–1704.

BMC Biology

RESEARCH ARTICLE Open Access

Uncovering by Atomic Force Microscopy of an original circular structure at the yeast cell surface in response to heat shock

Flavien Pillet[1,2†], Stéphane Lemonier[1,2,3†], Marion Schiavone[1,2,4,5,6], Cécile Formosa[1,2,7,8], Hélène Martin-Yken[4,5,6], Jean Marie Francois[4,5,6*] and Etienne Dague[1,2,3*]

Abstract

Background: Atomic Force Microscopy (AFM) is a polyvalent tool that allows biological and mechanical studies of full living microorganisms, and therefore the comprehension of molecular mechanisms at the nanoscale level. By combining AFM with genetical and biochemical methods, we explored the biophysical response of the yeast Saccharomyces cerevisiae to a temperature stress from 30°C to 42°C during 1 h.

Results: We report for the first time the formation of an unprecedented circular structure at the cell surface that takes its origin at a single punctuate source and propagates in a concentric manner to reach a diameter of 2–3 μm at least, thus significantly greater than a bud scar. Concomitantly, the cell wall stiffness determined by the Young's Modulus of heat stressed cells increased two fold with a concurrent increase of chitin. This heat-induced circular structure was not found either in wsc1Δ or bck1Δ mutants that are defective in the CWI signaling pathway, nor in chs1Δ, chs3Δ and bni1Δ mutant cells, reported to be deficient in the proper budding process. It was also abolished in the presence of latrunculin A, a toxin known to destabilize actin cytoskeleton.

Conclusions: Our results suggest that this singular morphological event occurring at the cell surface is due to a dysfunction in the budding machinery caused by the heat shock and that this phenomenon is under the control of the CWI pathway.

Keywords: Atomic Force Microscopy (AFM), Saccharomyces cerevisiae, Heat-shock, Cell wall, Chitin, Budding

Background

The yeast Saccharomyces cerevisiae is a unicellular eukaryotic microorganism surrounded by a 100–120 nm thick cell wall [1]. The fungal cell wall is an essential structure that maintains cell shape and cell integrity, ensures resistance to internal turgor pressure and thereby prevents cell lysis [2]. The cell wall of Saccharomyces cerevisiae, which represents 10 - 25% of the cell dry mass according to the culture and process conditions [3], consists of three types of polymers that are interconnected to produce a modular complex structure [4]. The inner layer of the cell wall is composed of a β-1,3-glucan network (80 - 90% of the total β-glucan) branched with chitin (1–2% of the cell wall). Together, they form a structure that is largely responsible for the mechanical strength of the whole cell wall [5,6]. In addition, β-1,6-linked glucans (8 - 18% of total β-glucans) are branched on the β-1,3-glucan network, and also linked to the mannoproteins that compose the outer layer [7,8]. The yeast cell wall is a dynamic structure, the molecular architecture of which is continuously remodeled during morphogenetic processes and growth [9]. It also undergoes remodeling in response to environmental stresses, such as ethanol and oxidative stress [10,11], thermal and osmotic stress [12-14], and in response to antifungal drugs such as allicin or caspofungin [15,16]. These

* Correspondence: fran_jm@insa-toulouse.fr; edague@laas.fr
†Equal contributors
[4]Université de Toulouse, INSA, UPS, INP, 135 avenue de Rangueil, F-31077 Toulouse, France
[1]CNRS, LAAS, 7 avenue du colonel Roche, F-31077 Toulouse, France
Full list of author information is available at the end of the article

remodeling processes are organized by a "cell wall rescue-mechanism" that relies on a combination of several signaling pathways, with a major role played by the PKC1-dependent cell wall integrity (CWI) pathway (reviewed in [9,17]). Important biochemical modifications identified so far during stresses were i) massive deposition of chitin that takes place in the lateral walls of both the mother cells and the growing buds, ii) an increased cross-linkage between chitin and β-1,3-glucan and iii) the appearance of novel linkages between cell wall proteins and chitin through β-1,6-glucan [18,19]. Altogether, these cell wall repair mechanisms have been considered as a mean to combat cell wall weakening caused by these stresses [4,20]. However, a direct visualization of the topography and nanomechanical changes associated to these biochemical and molecular changes induced by stresses was still missing to better understand the cell wall biogenesis and remodeling mechanism. The remarkable development of the Atomic Force Microscopy (AFM) technology, combined with genetical and molecular tools, is therefore powerful to fulfil this gap and investigate the dynamics of microbial cell surfaces in response to external cues [21,22].

In this study, we have investigated the effects of heat shock on the nanomechanical properties of the yeast cell wall. We chose this stress condition because of the large body of data available on the heat shock response in the yeast Saccharomyces cerevisiae (reviewed in [23]). In brief, this response is characterized at the genome level by an intense program of changes in gene expression leading to repression of protein biosynthetic machinery and the induction of a battery of genes encoding heat shock proteins (HSPs). The main metabolic and physiological changes reported in response to heat stress are an accumulation of trehalose and an inhibition of glycolysis [24,25], associated with a transient arrest of cell division. Heat shock also triggers the activation of the CWI pathway, resulting in a global transcriptomic change including the overexpression of genes encoding cell wall remodeling enzymes [26]. Although AFM analysis of temperature stress on yeast cells has been previously addressed by Adya et al. [27], we have revisited this stress because of two major technical concerns in the study reported by the latter authors. Firstly, the immobilization procedure they used could likely alter the cell viability and integrity since yeast cells were immobilized on glass slides by air-drying for more than 5 hr. Secondly, the stress was carried out at temperature ranging from 50 to 90°C, which is incompatible with yeast life and irrelevant in a biotechnological viewpoint.

Using a recent immobilization method that ensures the viability and integrity of the yeast cells [28], we showed that a temperature shift from 30 to 42°C induced the singular formation of circular rings that initiate at a single point on the yeast cell surface and expanded in a concentric manner to reach a diameter of 2 to 3 μm after 1 h of incubation. Appearance of this circular structure was accompanied by a twofold increase of chitin and by a raise of the cell wall stiffness. Furthermore, we showed that the formation of this unique circular structure was dependent on the budding process and was regulated by the CWI pathway.

Results

Heat shock induces the formation of a circular structure at the yeast cell surface

To explore the heat shock effects on the yeast cell surface by AFM, a culture sample from exponentially growing yeast cells on YPD cultivated at 30°C was shifted at 42°C for 1 h. Both unstressed and heat shocked cells were then trapped in polycarbonate porous membrane (Figure 1, top panel) or immobilized in holes of a PDMS stamp (Figure 1; lower panel). The presence of two typical bud scars on the unstressed yeast cell was clearly identified on AFM deflection images (Figure 1A & A'). In contrast, the heat-shocked yeast cell presented beside a bud scar, a circular structure (CS) that had a size larger than the bud scar on its cell surface. This CS was not an epiphenomenon since it was observed over 20–25 individual heat shocked cells analyzed from three independent experiments. In addition, the formation of this unique CS was time dependent, since small concentric rings started to be observed after 20 min incubation at 42°C, and their number and size increased with time to finally covered the whole observable cell surface after 2 hr (data not shown). Also, we always observed only one CS per cell, although it could not be excluded that another circular structure was formed underside, since this side of the cells was not accessible to AFM study. This singular event was clearly associated with the heat shock response as witnessed by a rapid and huge accumulation of trehalose (Additional file 1: Figure S1), a key marker of the response of yeast to a thermal stress [24,29]. Also, the viability of heat shocked yeast cells after 1 h of treatment at 42°C was more than 99% as evaluated by methylene blue staining method (Additional file 2: Table S1).

Ultrastructure of the cell surface CS using high resolution AFM imaging

To show that bud scar and CS were morphologically different, we carried out a detailed analysis of AFM height images on unstressed and heat shocked cells. A first difference was in the diameter of the two features, which was around 1 μm maximum for the bud scar but exceeded 2.5 μm for the cell surface CS (Figure 2). Also, the cross section taken on the AFM height image of the

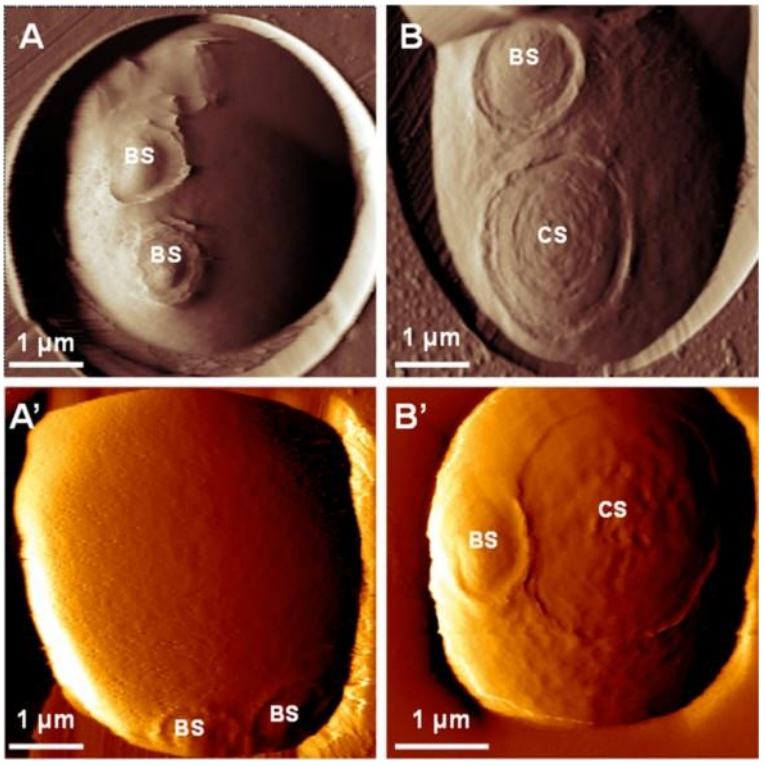

Figure 1 Heat-shock exposition of yeast cells leads to the formation of an unexpected circular structure. AFM deflection images of surface topology of a living yeast cell at 30°C (unstressed) (A, A') or exposed to heat shock during 1 h at 42°C (heat-shocked) (B, B'). Yeast cells were trapped in polycarbonate porous membrane (top panel) or within the patterns of a PDMS stamp (back panel). Bud scar (BS) and circular structure (CS) are indicated on AFM images.

unstressed yeast cell confirmed the typical convex structure of the bud scar (Figure 2B & C), followed by a depression and terminated by an apparent rigid ring which corresponds to a local accumulation of chitin [30]. In contrast, the cell surface CS identified on the heat shocked cells showed a different morphology, being relatively smooth inside the structure and terminated by a sharp ring. At a higher resolution, the AFM deflection image allowed identifying a succession of circular rings that originated from a single point and expanded in a concentric manner to end up by one last sharp ring (Figure 3).

Heat shock increases the yeast cell wall stiffness

Quantitative data on the effects of heat shock were obtained by scanning a given area of the cell surface with the AFM tip. To this end, we choose an area on the cell that was elsewhere from bud and CS. Thousands of Force Volume (FV) measurements were recorded, translated into pixel units to yield an elasticity map from which Young's Modulus (YM) values (expression of cell wall stiffness) could be calculated (Figure 4A & B). Qualitatively, the elasticity map of an unstressed yeast cell was homogeneous, while for the heat shocked cells, there was clearly a central region on the chosen area exhibiting higher pixel intensities, suggesting a difference in the elasticity or stiffness between the unstressed and the heat shocked cells. The YM values were extracted from all the force curves (e.g. 19443 FV curves from 19 unstressed cells, and 15307 FV curves from 15 heat-shocked yeast cells) and expressed as histograms that followed a Gauss distribution (Figure 4C and C'). The median values of the Gauss model fitting curve were used to determine YM from unstressed and heat-shocked cells. An unpaired t-test applied on the obtained YMs data (Additional file 3: Figure S2) allowed concluding that the YM from heat shocked was statistically two-fold higher than that of unstressed yeast cells (p value < 0.0001). The same methodology was used to evaluate the YM at the CS vicinity of the heat shocked cells. As shown in Figure 5, the YM was even higher at the CS, reaching more than 2 MPa inside this structure. Taking into account that cell wall stiffness is generally correlated with changes in chitin level, this finding raised the question whether this increase of stiffness at the CS is linked to increase of chitin or to some other cell wall remodeling events.

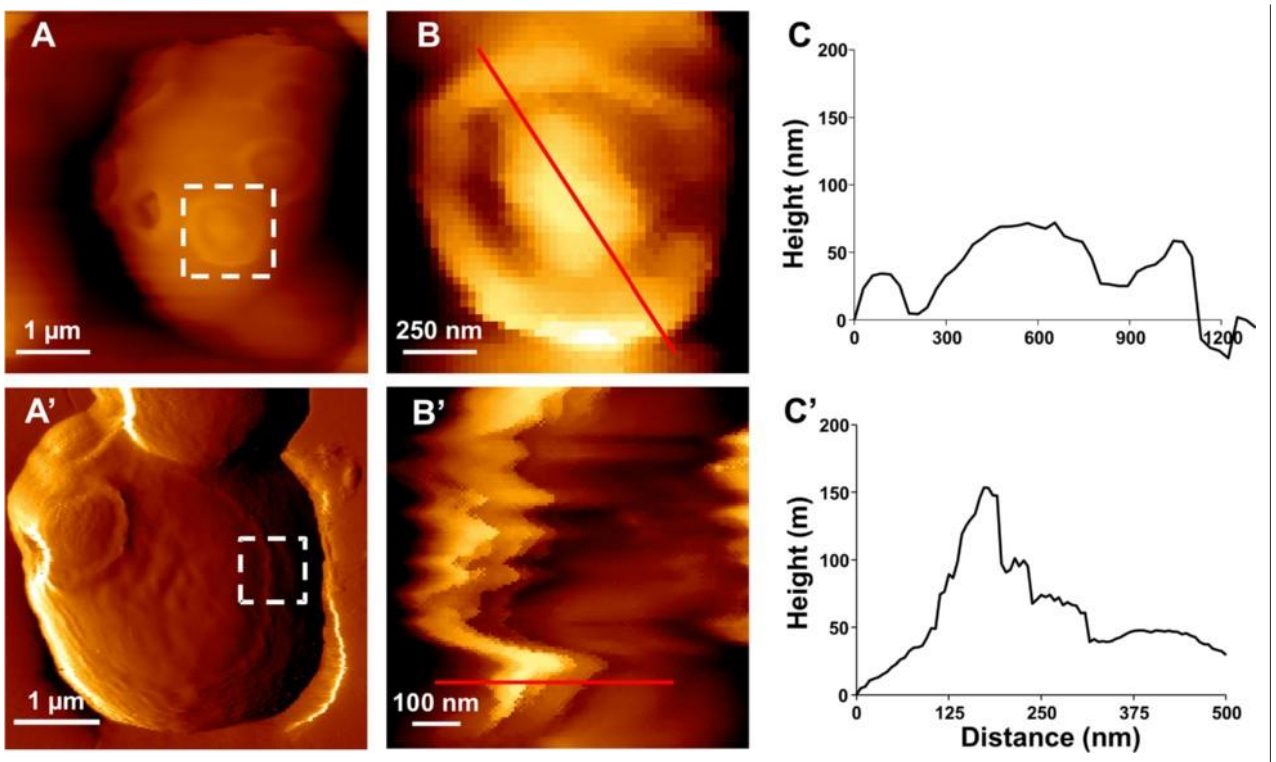

Figure 2 Morphological differences between a bud scar (BS) and circular structure (CS) at the cell surface. In (A, A'), AFM deflection image of an unstressed and of a heat-shocked yeast cell after 1 hr at 42°C at a z range of 2.5 µm. The white dotted squares indicated AFM height image analysis for the BS (A) and for part of the CS (A'). In (B & B') are zoomed height images of these squares area (at z range of 200 nm). In (C & C') are cross sections taken across the red lines, respectively in B and B' respectively.

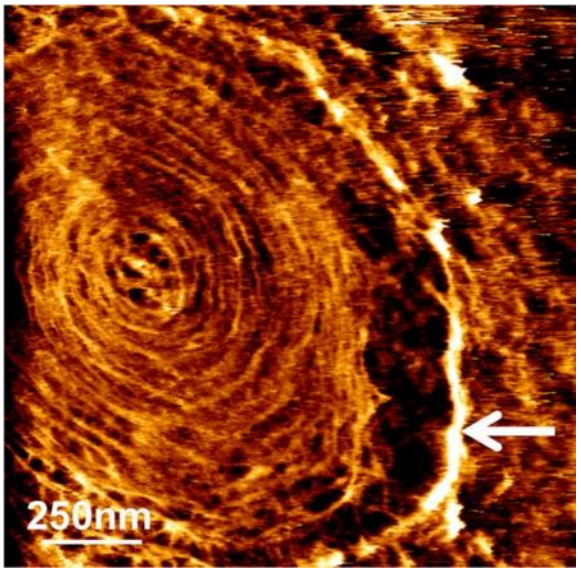

Figure 3 Exploring the ultrastructure of a CS by AFM. High-resolution deflection image shows a succession of concentric rings, followed by 1 major ring (white arrow).

Chitin content in cell wall and link with cell wall stiffness

The formation of a cell surface CS and the increased stiffness suggested that the biochemical composition of the cell wall could have been modified in response to heat shock. To explore this hypothesis, we performed biochemical measurements of carbohydrate composition of the cell wall. As reported in Table 1, levels of β-glucan and mannans were not different between un-stressed yeast cells and cells incubated at 42°C for 1 h. In contrast, the heat shock treatment clearly induced a 45% increase in the chitin content (from 46.2 µg/mg in unstressed cells to 68.3 µg/mg in cells after 1 h incubation at 42°C). To verify that this increase of chitin was preferentially associated with the formation of the CS, we visualized this polymer after staining it with calcofluor white (CFW). As expected, the presence of bud scars with a diameter around 1 µm was clearly visible on a yeast cell cultivated at 30°C (Figure 6A). However, it was interesting to notice that a ring of chitin with a diameter above 2 µm roughly co-localized with the CS in a heat shocked cell for 1 hr at 42°C (Figure 6B & C). Taken together, these result suggested that the increase of cells stiffness in response to heat shock may be linked to chitin levels.

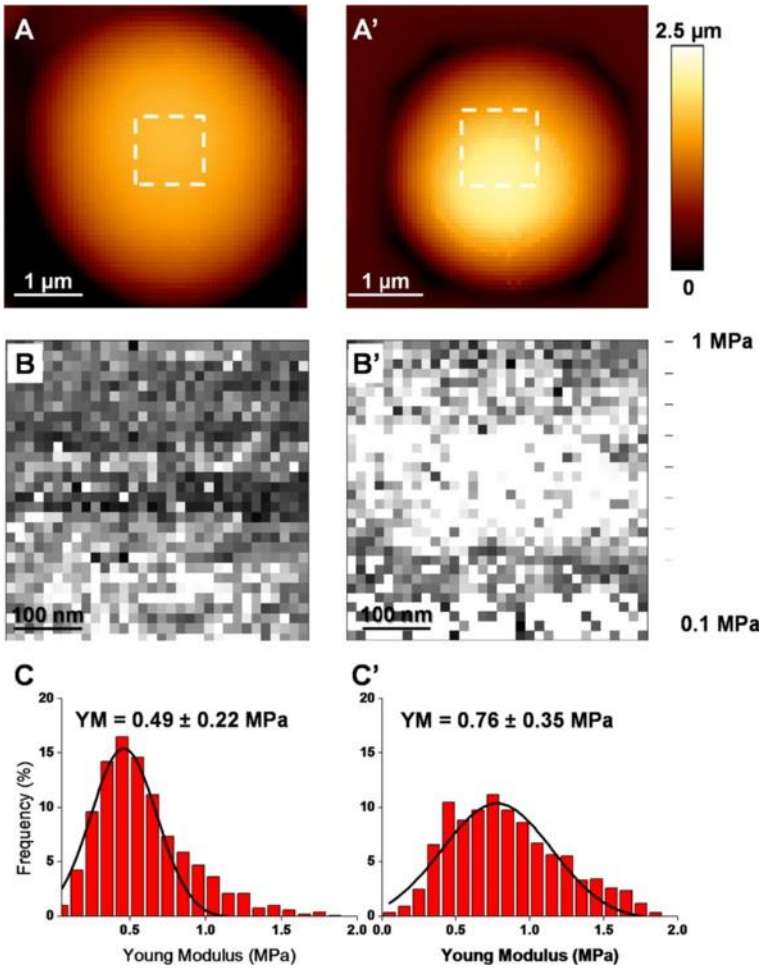

Figure 4 Yeast stiffness is increased by heat-shock at 42 °C. Young's Modulus (YM) determinations on an unstressed (A–C) and a heat-shocked cells (A'-C'). The white squares showed in the height images, (z range = 2 µm) (A, A'), indicate the localization of the elasticity maps shown in (B, B'). Histograms of the YM distributions (C, C') associated with the elasticity maps. YM medians were calculated by fitting a Gauss model (indicated by the black curves).

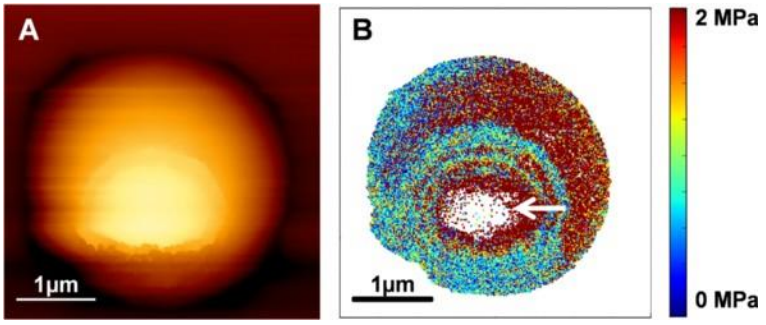

Figure 5 Stiffness map of a heat-shocked yeast cell. Height image (z range of 2.5 µm) (A), with the corresponding elasticity map in quantitative mode, (B) at the z range of 2 MPa. A higher young modulus was characterized in the central part of CS (white arrow).

Table 1 The chitin content in cell wall is increased upon heat-shock

	Chitin	β-glucans	Mannans
30°C	46.2 ± 9.5	440 ± 115	293 ± 24
42°C	68.3 ± 3.3	408 ± 99	301 ± 17

Carbohydrate composition of cell wall from unstressed (30°C) and heat-shocked cells during 1 h at 42°C were determined by acid hydrolysis for β-glucans and mannans and by enzymatic digestion for chitin. Values reported in μg per mg of dry cell wall are the mean ± SD of 3 biological independent experiments technically repeated 2 times.

The formation of the cellular surface CS is dependent on the budding process

The finding that this singular CS was found on about 40% of the heat-shocked cells, showing some morphological signs of a bud, and produced at the vicinity of a previous bud, raised the hypothesis that this structure might be dependent upon the budding machinery system. The process of budding has been thoroughly investigated at the biological, genetic and molecular levels, and showed the implication of many genes and many structural and regulatory networks that encompass cell polarity, cytoskeleton, secretory pathway, cell signaling, etc. [31]. To provide a first biological evidence that the CS formation is dependent on the budding process, we used latrunculin A (LatA), a toxin known to destabilize the actin cytoskeleton [32] that is implicated in the budding process. Exponentially growing cells were subjected to a heat shock at 42°C for 1 hr in the presence of 200 μM LatA. On a sampling of 10 independent yeast cells, we were unable to observe any CS at the cell surface, as compared to results with heat-shocked cells not treated with LatA (Additional file 4: Figure S3A). Furthermore, in the absence of heat shock, the perturbation of the actin cytoskeleton by LatA did not lead to the formation of CS (Additional file 4: Figure S3BC). To get additional biological evidence that the CS involves the budding process, we performed heat shock experiments with exponentially growing yeast cells that were incubated in a nitrogen-depleted medium for 72 hr. This condition results in growth arrest in G1 phase of the cell cycle with virtually all the cells unbudded [33] They were then subjected to heat shock at 42°C for one hour and AFM analysis was carried out on 10 starved cells before and 1 hr after heat-shock. In none of the heat-shocked cells, could we find any CS at the cell surface (Additional file 5: Figure S4). This result can be taken as indirect evidence that CS is depending on the budding process, because of the inability of the nitrogen-starved yeast cells to bud both at 30 and 42°C. Thus, the circular structure only forms during active cell growth and this cannot be separated from a cell-cycle phase specific defect.

At the genetic level, we addressed this question using targeted mutants such as chs3Δ that is defective in chitin ring formation during bud emergence [34], chs1Δ since the loss of this gene impairs septum reparation during cytokinesis [35] as well as a mutant deleted for BNI1 because this gene encodes a formin protein that is required for the proper initiation of bud growth and the proper shape of vegetative buds through formation of actin cables [36]. High resolution AFM imaging carried out on 15 cells from 3 independent experiments did not reveal any formation of singular cell surface CS in these different mutants after a heat shock at 42°C for 1 h (Additional file 6: Figure S5).

The formation of the cellular surface CS is regulated by CWI pathway

Heat shock is known to activate the CWI pathway, and the surface sensor Wsc1 is one of the sensors that detect and transmit this cell wall stress to the signaling cascade [37]. To evaluate whether the formation of the cell surface CS was under the control of the CWI signaling and whether Wsc1 could be implicated in this response, both bck1Δ mutant defective in the MAP kinase of the CWI pathway [38] and wsc1Δ mutant cells were analyzed by

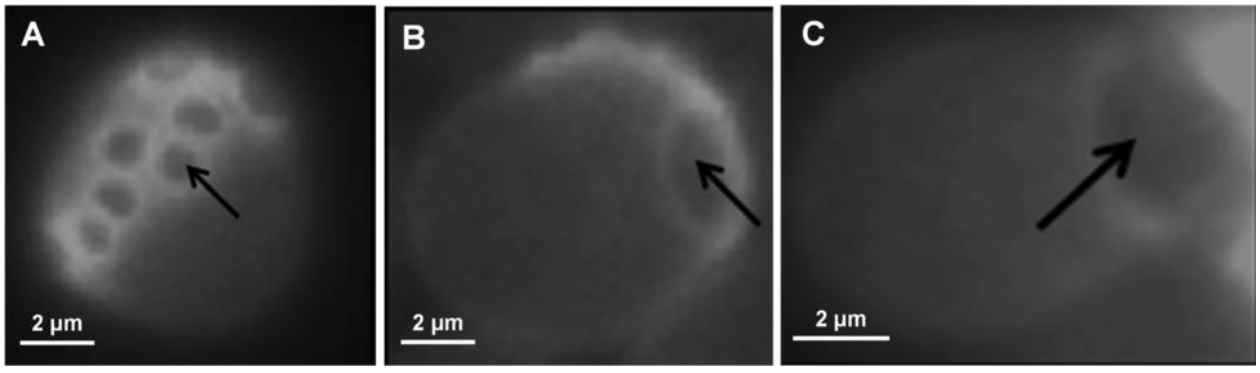

Figure 6 Fluorescence images of calcofluor white stained yeast cells. In (A), BY4741 cells cultivated at 30 °C showing bud scars. (B & C), BY4741 cells after 1 h of heat shock showing the circular structure B and C.

AFM before and after 1 hr heat shock at 42°C. As compared to the wild-type cells, which under this heat stress condition exhibited a large cell surface CS, neither the *bck1Δ* nor *wsc1Δ* cells imaged by AFM presented this singular structure (Additional file 7: Figure S6). The failure to identify any CS formation on these mutants upon 1 hr incubation at 42°C could not be due to cell death nor loss of heat shock response, since loss of viability of *wsc1Δ* and *bck1Δ* mutants was only 1 and 25% respectively (Additional file 2: Table S1), and both mutants readily accumulated trehalose in response to the thermal stress as wild-type cells (Additional file 1: Figure S1). In addition, we failed to identify this structure on more than 20 independent analyzed *wsc1Δ* and *bck1Δ* mutant cells. Therefore, these results support an implication of CWI pathway in the formation of the cell surface CS. We also noticed that the YM of the unstressed *wsc1Δ* was comparable to the one determined on heat-shocked wild-type cells (Additional file 8: Figure S7). Also, these unstressed *wsc1Δ* cells exhibited a chitin content twofold higher than the wild-type cells (Additional file 9: Table S2), arguing in favor of a correlation between chitin content and stiffness of the cell wall. After exposure to 42°C for 1 h, the YM values and the chitin content in the *wsc1Δ* mutant were not significantly affected (Additional files 8 and 9: Figure S7 and Table S2).

Discussion

The Atomic Force Microscopy (AFM) is nowadays the most powerful scanning microscopy tool used to visualize and to explore the dynamics of living cells at the nanometer resolution under physiological conditions. Being also a force machine, it allows force spectroscopy measurements of the cell mechanics [39]. Therefore, it is a superb method for investigating the biomechanical consequences of a heat shock on the yeast cell, with the eventual aim to correlate the putative biophysical changes observed using this methodology to the largely documented molecular and metabolic responses to heat shock [23]. In this study, we reported for the first time the formation of a circular structure (CS) that is induced upon exposure of yeast cell to 42°C. The high resolution AFM imaging clearly indicated that this singular feature takes its origin from a single point and propagates in concentric rings during the time of incubation at 42°C. In addition, this singular CS was observed in yeast cells immobilized by two different methods, which further supports the idea that the formation of this feature is a true morphological event induced by heat shock. The reason why Adya *et al.* [27] did not find this morphological event in their heat shock study by AFM could be explained by the immobilisation technique these authors used, which likely destroyed the integrity of the cell surface.

The discovery of only one singular CS per cell (although we could not preclude that another one was formed underside of the cell since this was not accessible to the AFM analysis), together with the close vicinity of this structure to a previous bud and with the fact that it appeared on about 40% of the heat shocked cells were indications that this amazing structure may be related to a failure in the budding emergence and/or in the budding process. This suggestion is supported by the inability of a mutant defective in *BNI1* encoding a formin protein that is needed for proper bud pattern formation to produce the CS in response to heat shock. The function of this protein is to assemble linear actin cables along the mother daughter axis and at the bud neck [40]. The polarization of the actin cytoskeleton is an essential process for cell expansion and budding in the yeast *S. cerevisiae*, and a defect in this process results in abnormal morphology characterized either by elongated buds or spherical buds [36]. Delley & Hall [41] have reported that a mild heat shock from 24 to 37°C induces a transient depolarization of the actin cytoskeleton that is accompanied by a transient depolarized distribution of the β-glucan synthase complex, composed of the catalytic subunits Fks1 or Fks2 and the regulatory subunit Rho1. They further showed that this depolarization of the actin cytoskeleton and β-glucan synthase was mediated by the plasma membrane protein Wsc1. Interestingly, we found that heat-induced formation of CS was abolished when latrunculin A, a toxin molecule known to disrupt actin cystokeleton [32], was added prior to the thermal stress, as well as in *wsc1Δ* mutant cells. In addition, the use of Calcofluor white staining method highlighted the presence of chitin rings at the vicinity of the CS outer ring. This finding is reminiscent of the presence of the chitin ring that delimitate the bud scars on the yeast cell surface [30]. Taken together, these results support the idea that the heat-induced formation of CS is a morphological consequence at the cell surface of a defective budding process due to perturbation of the actin cytoskeleton depolarization process.

It is known that the CWI pathway is activated under heat stress and although the cell surface mechanosensor Wsc1 is important in detecting this cell wall stress and to transmit the signal to the Pkc1 MAP kinase cascade [42], it is not the sole sensor implicated in the heat stress response [43]. Therefore, the finding that *bck1Δ* mutant cells, defective in the MAP kinase of the CWI pathway, could not produce this structure in response to the thermal stress indicates that the morphological process that leads to CS formation is indeed under the control of the CWI pathway.

The nanomechanical properties of yeast cells obtained from the AFM force volume curves showed that the heat stress caused a twofold increase in the Young's Modulus

values, indicating that the stiffness of the cell wall was increased (or its elasticity decreased). Interestingly, the measurement of cell wall β-glucans, mannans and chitin in yeast cells exposed to 42°C only showed an increase of approximately twofold of the chitin content. Moreover, the loss of WSC1 resulted also in a twofold increase of both the chitin content and the Young's Modulus. Taken together, these results suggest that the cell wall elasticity is mainly linked to the relative changes in the chitin content as described recently by Formosa et al. [44]. This result does not contradict our previous work showing that the cell wall elasticity was merely dependent on cross-linkages between chitin and β-glucans rather than on a particular cell wall component [6], since chitin content is in fact the most critical component that ensures strength of the cell wall through the covalent connection that it makes with the other cell wall components.

Conclusions

The powerful technology AFM allowed identifying and precisely describing an unexpected morphological phenomenon occurring at the cell surface, which may explain physically how yeast cells are damaged by temperature stress and could eventually lead to cell death. Our results are also relevant in regards to the rough industrial growth conditions and processes which the yeast S. cerevisiae has to cope with, and which may cause comparable morphological defects at the cell surface.

Materials and methods

Yeast strains and growth conditions

Yeast strain BY4741 (MATa his3Δ1 leu2Δ10 met15Δ0 ura3Δ0) [45] and its isogenic deletion mutants wsc1Δ, bck1Δ, chs1Δ, chs3Δ and bni1Δ obtained from Open Biosystem (USA) were used in this study. Yeast cells were routinely cultivated at 30°C in a standard rich YEPD (Yeast Extract Peptone Dextrose) medium containing 10 g/l of yeast extract, 20 g/l of peptone and 20 g/l of dextrose. Heat shock experiments were carried out with exponentially growing cells (OD_{600} at 1–2 unit) by putting part of the yeast culture (10 mL in 50 mL Erlen flask) in a water bath set at 42°C during 1 h.

Latrunculin A and nitrogen starvation experiments

Latrunculin [32] was added at 200 μM to exponentially growing cells cultivated at 30°C or just before transferring yeast culture cells at 42°C. For nitrogen starvation experiment, exponentially growing cells in YEPD (collected at OD_{600} at 1.0 unit) were washed 3 times in nitrogen-depleted medium (50 mM of phosphate without nitrogen, 2% of glucose, pH 6.2) and resuspended at OD_{600} of 1.0 unit in this medium for 72 h at 30°C before heat shock as described above.

AFM sample preparation

Yeast cells were immobilized according to two different protocols. The first method consisted in filtering a small volume of yeast culture (1 to 5 mL) through a polycarbonate membrane pore sizes of 5 μm in order to trap cells into the micrometer size pores of the nylon filter (Merck Millipore, Darmstadt, Germany). After filtration, the filter was washed once with 4 mL of acetate buffer 20 mM, pH 5.5. In the second method, the cells were captured in microstructured polydimethylsiloxane (PDMS) stamps according to [28]. Briefly, 1 mL of the cell culture were washed quickly 3 times with 1 mL of AFM buffer (18 mM CH_3COONa, 1 mM $CaCl_2$ and 1 mM $MnCl_2$, pH 5.2), resuspended in 1 mL of the same buffer, and 100 μl of this cell suspension was deposited on a freshly oxygen activated microstructured PDMS stamp. The cells were allowed to stand for 15 min at room temperature and then forced to enter the microstructures of the stamp by convective/capillary assembly [28]. A typical example of cells immobilized in holes of a PDMS stamp is given in Additional file 10: Figure S8. To get statistical significance of the AFM data, about 10–12 cells have been analyzed from three independent experiments. In addition, three independent investigators performed AFM experiments. Each investigator has analyzed 10–12 cells.

AFM imaging and Force spectroscopy experiments

AFM images of yeast cells trapped in polycarbonate membrane were recorded with a Nanowizard II form JPK (JPK Instruments, Berlin, Germany), in contact mode, using OTR4 (Olympus provided by Bruker) cantilevers. AFM experiments on yeasts immobilized on PDMS stamps were performed with a Nanowizard III form JPK (JPK Instruments, Berlin, Germany) in contact mode, Quantitative Imaging mode (QI) [46] and Force Volume mode (FV). The cantilevers used (OTR4 and MLCT) had a spring constant measured by the thermal noise method [47] ranging from 0.01 to 0.5 N/m. Cell wall elasticity was deduced from the Young's modulus which was calculated from FV measurement using the Hertz model [48].

Extraction of cell wall and determination of β-glucan and mannan polysaccharides

Yeast cells (about 50 mg dry mass or 10^9 cells) were collected by centrifugation (5 min, 3000 g), washed once with 10 mL of cold sterilized water, and after a second centrifugation, cell pellet was resuspended in cold water. The cell walls (about 10 mg dry mass) obtained from control and heat shocked yeast cells were extracted

according to the protocol described by Dallies et al. [49]. The content of β-glucans and mannans in the S. cerevisiae cell walls were determined by acid sulfuric hydrolysis method as described by François [50]. The released monosaccharides (glucose and mannose) were quantified by HPAEC-PAD on a Dionex-ICS 5000 system (Thermofisher Scientific, France). Separation was performed on a CarboPac PA10 analytical column (250 × 4 mm) with a guard column CarboPac PA10, by an isocratic elution of NaOH 18 mM at 25°C and a flow rate of 1 mL/min. Detection was performed by pulsed amperometric system equipped with a gold electrode.

Analytical methods

Intracellular trehalose level was determined as previously described [51]. For accurate chitin determination in the yeast cell wall, an enzyme assay has been used as follows. Lyophilized cell walls (about 10 mg) were suspended in 200 µl of 50 mM potassium acetate buffer, pH 5.0 and boiled at 65°C for 5 min. After mixing and cooling to ambient temperature, the cell wall suspension was treated with 1U of chitinase from Streptomyces griseus (Sigma-Aldrich, France) for 24 h at 37°C. The N-acetyl glucosamine released by the chitinase action was then determined using a colorimetric method as described by Reissig et al. [52] and adapted for a micro method. Briefly, 125 µl of the enzymatic mixture was heated with 25 µl of 0.8 M potassium tetraborate pH 9.0 at 100°C for 8 minutes. After cooling at room temperature, 750 µl of Reissig reagent (10 g of 4-dimethylaminobenzaydedyde dissolve in 12.5 mL 10 N HCl and 87.5 mL of glacial acetic acid) diluted ten times in deionized water was added, and the tubes were incubated 40 minutes at 37°C. The absorbance was read at 585 nm. The chitin content was obtained from N-acetylglucosamine standard curve (from 0 to 100 µg/mL) made in the same condition.

Miscellaneous methods

Calcofluor white treatment of yeast cells before and 1 hr after heat shock was carried out as following the procedure described in [53]. Cell viability was performed using methylene blue according to [54].

Additional files

Additional file 1: Figure S1. The accumulation of trehalose is correlated with survival of cells under heat stress condition. Comparison of trehalose accumulation in the wild-type yeast BY4741 and the defective mutants wsc1Δ and bck1Δ. Control (full bar) and heat-shocked condition (hachured bar) are represented.

Additional file 2: Table S1. Evaluation of viability by blue methylene test. The percentage of mortality was evaluated before and after heat shock with the defective mutants wsc1 and bck1, and the wild-type yeast with or without nitrogen starvation during 72 h.

Additional file 3: Figure S2. Young modulus increase with heat-shock. Distribution of Young modulus values calculate with 19 elasticity maps (n_{curves} = 19443) from individual yeasts unstressed (A), in comparison with 15 elasticity maps (n_{curves} = 15307) from individual yeasts heat-shocked at 42°C (B). YM medians were indicated on diagrams and calculated from fits in gauss model (red curves). (C) Statistic unpaired t test between averages and standard deviations calculated from young modulus values. The 3 asterisks shown significant differences between elasticity of unstressed yeasts (full bar) and heat-shock yeasts (hachured bar) at the P value < 0.0001.

Additional file 4: Figure S3. The absence of F-Actin prevent the formation CS. AFM high resolution images of wild-type cells after heat shock in absence (A) or in presence of 200 µM Latrunculin A (B). Cells incubated 1 hr at 30°C with 200 µM of Latrunculin A (C).

Additional file 5: Figure S4. The formation of CS require budding process. High-resolution deflection images of wild-type incubate 72 h at 30°C in nitrogen starvation, without (A) or with heat shock 1 hr at 42°C (B).

Additional file 6: Figure S5. The heat-induced formation of the cell surface circular structure is abolished in mutants defective in the budding process. High-resolution AFM deflection images of bni1Δ (A), chs3Δ (B) and chs1Δ (C) mutants after heat shock.

Additional file 7: Figure S6. The CWI controls the stiffness of the cell wall and the formation of the cell surface circular structure in response to heat shock. High-resolution AFM deflection images of wild-type cell (A), wsc1Δ (B) and bck1Δ (C) cell defective in the CWI pathway imaged after 1 hr of incubation at 42°C.

Additional file 8: Figure S7. The stiffness of wsc1Δ unstressed was similar to wild-type yeast exposed at 42°C during 1 h. Distribution of Young modulus values calculate with 4 elasticity maps (n = 4096) from individual wsc1Δ yeasts unstressed.

Additional file 9: Table S2. Chitin rate was similar in wsc1Δ mutant with or without heat-shock at 42°C. Carbohydrate composition of wsc1Δ mutant was determinated by acid hydrolysis and enzymatic method and expressed in µg/mg of cell wall dry mass.

Additional file 10: Figure S8. Yeast immobilization on PDMS stamp. (A) AFM height image of a PDMS stamp containing some immobilized yeasts. The z range is 2.5 µm. (B) 3D projection associated to the height image.

Competing interests

We declare that we have no competing interest.

Authors' contributions

ED and JMF are the lead authors of the paper. FP and SL carried out the most of the AFM experiments. MS performed extraction and analysis of carbohydrates contents in yeast. CF worked on complementary AFM experiments. HMY participated in writing the paper and performed the biological part of the experiments. All authors read and approved the final manuscript.

Acknowledgement

We thank the team of J.M François for fruitful discussions and experimental help. We are grateful to Louise Chopinet for collaboration in statistical analysis. This work was supported by an ANR young scientist program (AFMYST project ANR-11-JSV5-001-01 n° SD 30024331) to ED and by a grant n°10051296 from Region Midi Pyrénées to JMF. ED is researcher at the Centre National de Recherche Scientifique (CNRS). CF and MS are respectively supported by a grant from "Direction Générale de l'Armement" (DGA) and from Lallemand SAS.

Author details

[1]CNRS, LAAS, 7 avenue du colonel Roche, F-31077 Toulouse, France. [2]Université de Toulouse, UPS, INSA, INP, ISAE, LAAS, F-31077 Toulouse, France. [3]CNRS, ITAV-USR 3505, F31106 Toulouse, France. [4]Université de Toulouse, INSA, UPS, INP, 135 avenue de Rangueil, F-31077 Toulouse, France. [5]INRA, UMR792 Ingénierie des Systèmes Biologiques et des Procédés, F-31077 Toulouse, France. [6]CNRS, UMR5504, F-31400 Toulouse, France. [7]CNRS, UMR 7565, SRSMC, Vandoeuvre-lès-Nancy, France. [8]Université de Lorraine, UMR 7565, Faculté de Pharmacie, Nancy, France.

Received: 9 December 2013 Accepted: 10 January 2014
Published: 27 January 2014

References

1. Dupres V, Dufrêne YF, Heinisch JJ: Measuring Cell Wall Thickness in Living Yeast Cells Using Single Molecular Rulers. ACS Nano 2010, 4:5498–5504.
2. Klis FM, Mol P, Hellingwerf K, Brul S: Dynamics of cell wall structure in Saccharomyces cerevisiae. FEMS Microbiology Reviews 2002, 26:239–256.
3. Aguilar-Uscanga B, François J m: A study of the yeast cell wall composition and structure in response to growth conditions and mode of cultivation. Letters in Applied Microbiology 2003, 37:268–274.
4. Klis FM, Boorsma A, De Groot PWJ: Cell wall construction in Saccharomyces cerevisiae. Yeast 2006, 23:185–202.
5. Smits JG, Kapteyn CJ, van den Ende H, Klis MF: Cell wall dynamics in yeast. Current Opinion in Microbiology 1999, 2:348–352.
6. Dague E, Bitar R, Ranchon H, Durand F, Yken HM, François JM: An atomic force microscopy analysis of yeast mutants defective in cell wall architecture. Yeast 2010, 27:673–684.
7. Kollár R, Reinhold BB, Petráková E, Yeh HJC, Ashwell G, Drgonová J, Kapteyn JC, Klis FM, Cabib E: Architecture of the Yeast Cell Wall β(1 → 6)-glucan interconnects mannoprotein, β(1 → 3)-glucan, and chitin. J Biol Chem 1997, 272:17762–17775.
8. Shahinian S, Dijkgraaf GJ, Sdicu AM, Thomas DY, Jakob CA, Aebi M, Bussey H: Involvement of protein N-glycosyl chain glucosylation and processing in the biosynthesis of cell wall beta-1,6-glucan of Saccharomyces cerevisiae. Genetics 1998, 149:843–856.
9. Levin DE: Cell Wall Integrity Signaling in Saccharomyces cerevisiae. Microbiol Mol Biol Rev 2005, 69:262–291.
10. Gibson BR, Lawrence SJ, Leclaire JPR, Powell CD, Smart KA: Yeast responses to stresses associated with industrial brewery handling. FEMS Microbiology Reviews 2007, 31:535–569.
11. Canetta E, Walker GM, Adya AK: Nanoscopic morphological changes in yeast cell surfaces caused by oxidative stress: an atomic force microscopic study. J Microbiol Biotechnol 2009, 19:547–555.
12. Kobayashi N, McEntee K: Evidence for a heat shock transcription factor-independent mechanism for heat shock induction of transcription in Saccharomyces cerevisiae. PNAS 1990, 87:6550–6554.
13. Yeh J, Haarer BK: Profilin is required for the normal timing of actin polymerization in response to thermal stress. FEBS Letters 1996, 398:303–307.
14. Zhao XQ, Bai FW: Mechanisms of yeast stress tolerance and its manipulation for efficient fuel ethanol production. Journal of Biotechnology 2009, 144:23–30.
15. Kim KS, Kim Y-S, Han I, Kim M-H, Jung MH, Park H-K: Quantitative and Qualitative Analyses of the Cell Death Process in Candida albicans Treated by Antifungal Agents. PLoS ONE 2011, 6:e28176.
16. El-Kirat-Chatel S, Beaussart A, Alsteens D, Jackson DN, Lipke PN, Dufrêne YF: Nanoscale analysis of caspofungin-induced cell surface remodelling in Candida albicans. Nanoscale 2013, 5:1105–1115.
17. Levin DE: Regulation of Cell Wall Biogenesis in Saccharomyces cerevisiae: The Cell Wall Integrity Signaling Pathway. Genetics 2011, 189:1145–1175.
18. Cabib E, Durán A: Synthase III-dependent Chitin Is Bound to Different Acceptors Depending on Location on the Cell Wall of Budding Yeast. J Biol Chem 2005, 280:9170–9179.
19. Valdivieso M-H, Ferrario L, Vai M, Duran A, Popolo L: Chitin Synthesis in a gas1 Mutant ofSaccharomyces cerevisiae. J Bacteriol 2000, 182:4752–4757.
20. Lesage G, Bussey H: Cell Wall Assembly in Saccharomyces cerevisiae. Microbiol Mol Biol Rev 2006, 70:317–343.
21. Dague E, Gilbert Y, Verbelen C, Andre G, Alsteens D, Dufrêne YF: Towards a nanoscale view of fungal surfaces. Yeast 2007, 24:229–237.
22. Dufrêne YF: Atomic force microscopy of fungal cell walls: an update. Yeast 2010, 27:465–471.
23. Verghese J, Abrams J, Wang Y, Morano KA: Biology of the Heat Shock Response and Protein Chaperones: Budding Yeast (Saccharomyces cerevisiae) as a Model System. Microbiol Mol Biol Rev 2012, 76:115–158.
24. Neves MJ, Francois J: On the mechanism by which a heat shock induces trehalose accumulation in Saccharomyces cerevisiae. Biochem J 1992, 288 (Pt 3):859–864.
25. Postmus J, Canelas AB, Bouwman J, Bakker BM, van Gulik W, de Mattos MJT, Brul S, Smits GJ: Quantitative Analysis of the High Temperature-induced Glycolytic Flux Increase in Saccharomyces cerevisiae Reveals Dominant Metabolic Regulation. J Biol Chem 2008, 283:23524–23532.
26. Gasch AP, Spellman PT, Kao CM, Carmel-Harel O, Eisen MB, Storz G, Botstein D, Brown PO: Genomic Expression Programs in the Response of Yeast Cells to Environmental Changes. Mol Biol Cell 2000, 11:4241–4257.
27. Adya AK, Canetta E, Walker GM: Atomic force microscopic study of the influence of physical stresses on Saccharomyces cerevisiae and Schizosaccharomyces pombe. FEMS Yeast Research 2006, 6:120–128.
28. Dague E, Jauvert E, Laplatine L, Viallet B, Thibault C, Ressier L: Assembly of live micro-organisms on microstructured PDMS stamps by convective/capillary deposition for AFM bio-experiments. Nanotechnology 2011, 22:395102.
29. Virgilio C, Hottiger T, Dominguez J, Boller T, Wiemken A: The role of trehalose synthesis for the acquisition of thermotolerance in yeast. I. Genetic evidence that trehalose is a thermoprotectant. European Journal of Biochemistry 1994, 219:179–186.
30. Cabib E, Roh D-H, Schmidt M, Crotti LB, Varma A: The Yeast Cell Wall and Septum as Paradigms of Cell Growth and Morphogenesis. J Biol Chem 2001, 276:19679–19682.
31. Drees BL, Sundin B, Brazeau E, Caviston JP, Chen G–C, Guo W, Kozminski KG, Lau MW, Moskow JJ, Tong A, Schenkman LR, McKenzie A, Brennwald P, Longtine M, Bi E, Chan C, Novick P, Boone C, Pringle JR, Davis TN, Fields S, Drubin DG: A protein interaction map for cell polarity development. J Cell Biol 2001, 154:549–576.
32. Sahin A, Daignan-Fornier B, Sagot I: Polarized Growth in the Absence of F-Actin in Saccharomyces cerevisiae Exiting Quiescence. PLoS ONE 2008, 3:E2556.
33. Futcher B: Metabolic cycle, cell cycle, and the finishing kick to Start. Genome Biol 2006, 7:107.
34. Ziman M, Chuang JS, Schekman RW: Chs1p and Chs3p, two proteins involved in chitin synthesis, populate a compartment of the Saccharomyces cerevisiae endocytic pathway. Mol Biol Cell 1996, 7:1909–1919.
35. Cabib E, Silverman SJ, Shaw JA: Chitinase and chitin synthase 1: counterbalancing activities in cell separation of Saccharomyces cerevisiae. J Gen Microbiol 1992, 138:97–102.
36. Pruyne D, Bretscher A: Polarization of cell growth in yeast. I. Establishment and maintenance of polarity states. J Cell Sci 2000, 113:365–375.
37. Lodder AL, Lee TK, Ballester R: Characterization of the Wsc1 protein, a putative receptor in the stress response of Saccharomyces cerevisiae. Genetics 1999, 152:1487–1499.
38. Lee KS, Levin DE: Dominant mutations in a gene encoding a putative protein kinase (BCK1) bypass the requirement for a Saccharomyces cerevisiae protein kinase C homolog. Mol Cell Biol 1992, 12:172–182.
39. Dufrêne YF, Pelling AE: Force nanoscopy of cell mechanics and cell adhesion. Nanoscale 2013, 5:4094–4104.
40. Pruyne D, Legesse-Miller A, Gao L, Dong Y, Bretscher A: Mechanisms of Polarized Growth and Organelle Segregation in Yeast. Annual Review of Cell and Developmental Biology 2004, 20:559–591.
41. Delley P-A, Hall MN: Cell Wall Stress Depolarizes Cell Growth via Hyperactivation of Rho1. J Cell Biol 1999, 147:163–174.
42. Verna J, Lodder A, Lee K, Vagts A, Ballester R: A family of genes required for maintenance of cell wall integrity and for the stress response in Saccharomyces cerevisiae. PNAS 1997, 94:13804–13809.
43. Winkler A, Arkind C, Mattison CP, Burkholder A, Knoche K, Ota I: Heat Stress Activates the Yeast High-Osmolarity Glycerol Mitogen-Activated Protein Kinase Pathway, and Protein Tyrosine Phosphatases Are Essential under Heat Stress. Eukaryotic Cell 2002, 1:163–173.
44. Formosa C, Schiavone M, Martin-Yken H, François JM, Duval RE, Dague E: Nanoscale effects of caspofungin against two yeast species, Saccharomyces cerevisiae and Candida albicans. Antimicrob Agents Chemother 2013, 57:3498–3506.
45. Baker Brachmann C, Davies A, Cost GJ, Caputo E, Li J, Hieter P, Boeke JD: Designer deletion strains derived from Saccharomyces cerevisiae S288C: A useful set of strains and plasmids for PCR-mediated gene disruption and other applications. Yeast 1998, 14:115–132.
46. Chopinet-Mayeux L, Formosa C, Rols M-P, Duval RE, Dague E: Imaging living cells surface and quantifying its properties at high resolution using AFM in QITM mode. Micron. In press.
47. Hutter JL, Bechhoefer J: Calibration of atomic force microscope tips. Review of Scientific Instruments 1993, 64:1868–1873.
48. Hertz H: Ueber die Berührung fester elastischer Körper. Journal für die reine und angewandte Mathematik 1882, 1881:156–171.

49. Dallies N, François J, Paquet V: A new method for quantitative determination of polysaccharides in the yeast cell wall. Application to the cell wall defective mutants of Saccharomyces cerevisiae. Yeast 1998, 14:1297–1306.
50. François JM: A simple method for quantitative determination of polysaccharides in fungal cell walls. Nat Protoc 2006, 1:2995–3000.
51. Parrou JL, François J: A Simplified Procedure for a Rapid and Reliable Assay of both Glycogen and Trehalose in Whole Yeast Cells. Analytical Biochemistry 1997, 248:186–188.
52. Reissig JL, Strominger JL, Leloir LF: A Modified Colorimetric Method for the Estimation of N-Acetylamino Sugars. J Biol Chem 1955, 217:959–966.
53. Baggett J j, Shaw J d, Sciambi C j, Watson H a, Wendland B: Fluorescent Labeling of Yeast. In Current Protocols in Cell Biology. John Wiley & Sons, Inc; 2001.
54. Teparić R, Stuparević I, Mrša V: Increased mortality of Saccharomyces cerevisiae cell wall protein mutants. Microbiology 2004, 150:3145–3150.

doi:10.1186/1741-7007-12-6
Cite this article as: Pillet et al.: Uncovering by Atomic Force Microscopy of an original circular structure at the yeast cell surface in response to heat shock. BMC Biology 2014 12:6.

Résumé

L’intérêt pour la paroi de la levure s’est accru récemment par l’explosion des activités de bioraffineries augmentant la production de biomasse, et par le besoin de valoriser cette biomasse notamment dans d’autres débouchés comme en nutrition animale et en œnologie pour leurs propriétés probiotiques et de sorption. L’étude de la composition et de la structure de la paroi des levures est maintenant un sujet de recherche abordé depuis plus d’une vingtaine d’années. Les données acquises à ce jour montrent l’importance de la souche, des conditions de cultures et des procédés sur la composition biochimique et les propriétés biophysiques de la paroi cellulaire. Cependant, les relations entre la composition et la structure moléculaire d'une part, et entre les propriétés mécaniques et l'architecture moléculaire de la paroi cellulaire, d'autre part, sont largement incomplètes. Cela est notamment dû au manque (i) de méthodes capables de déterminer quantitativement la composition exacte de la paroi cellulaire de la levure et (ii) d’outils biomathématiques permettant de clarifier ces relations. Le but de cette thèse était donc de combiner des approches biochimiques, biophysiques et les puces à ADN afin d'étudier les relations entre ces paramètres ainsi que de mettre en évidence l'impact des souches, des conditions de croissance et des procédés sur la composition et les propriétés biophysiques de la paroi cellulaire. Pour atteindre cet objectif, une méthode acido-enzymatique a été développée pour quantifier spécifiquement chacun des quatre composants de la paroi cellulaire de la levure, à savoir les mannanes, la chitine, les β-1,3-glucanes et les β-1,6-glucanes. Cette méthode a été validée sur des souches mutantes délétées de gènes, codant pour des protéines essentielles à la biosynthèse de la paroi cellulaire, ainsi que par l'étude de divers stress. Ultérieurement, l'utilisation de la microscopie à force atomique (AFM) a permis l'étude des mêmes souches et de quatre souches utilisées dans la fermentation industrielle. Ils ont démontré des propriétés nanomécaniques et adhésives distinctes, en raison de différences dans la composition et la structure de la paroi cellulaire. Par une analyse biostatistique, l'interaction entre une pointe d'AFM fonctionnalisée avec une lectine et la surface des cellules a été associée aux quantités de mannanes dans la paroi cellulaire. Comme la lectine concanavalin A se lie aux α-mannose et aux α-glucose, ces résultats d’adhésion sont en accord avec les données biochimiques. Le contenu en mannanes et la fréquence d’adhésion de l’interaction paroi-lectine ont également été corrélées à des gènes impliqués dans la maturation des protéines, la biosynthèse d’ergostérol et de mannoprotéines de la paroi cellulaire. En outre, nous avons trouvés une association étroite entre l'élasticité de la paroi (*i.e.* les valeurs de module de Young) et les niveaux de β-1,3-glucanes. Les gènes qui ont été corrélés avec cette association encodent des protéines impliquées dans la membrane et l'assemblage du cytosquelette, la biosynthèse et l'assemblage des β-glucanes, ainsi que dans les voies de signalisation MAPK. Dans la dernière partie, les effets du procédé d’autolyse et du séchage à lit fluidisé sont présentés. Les résultats montrent que ce conditionnement spécifique de levure, vendu en tant que paroi cellulaire de levure, ne modifie pas la composition de la paroi cellulaire, mais induit une modification de la topographie et des propriétés de surface de la cellule. En outre, en utilisant l'AFM nous avons imagés sur *S. cerevisiae* des patchs hautement adhésifs formant des nanodomaines à la surface de la cellule. Par les données transcriptomiques, ces nanodomaines ont été attribués aux protéines Flo11 probablement agrégés en amas β-amyloïdes.

Thèse présentée par :

Marion SCHIAVONE

Intitulée :

Impact du fond génétique de la souche et du procédé industriel sur la paroi de la levure par des approches biochimiques, biophysiques et moléculaires

La cellule de levure possède une paroi de 150-200 nm d'épaisseur qui est indispensable pour l'intégrité cellulaire et lui confère une protection vis-à-vis de l'environnement extérieur. Cette paroi est une structure complexe de polysaccharides liés entre eux. Les mannanes, les β-glucanes et la chitine constituent les 4 principaux polysaccharides de la paroi. Les β-glucanes sont des chaînes d'unités de glucose qui peuvent être liés soit en β(1→3) soit en β(1→6). De nombreuses publications sur ce sujet ont montré que cette interface est dynamique, cependant certaines questions importantes restent encore sans réponse. Des études biochimiques et moléculaires ont démontrées que la structure et la composition pariétale de la levure peuvent varier en fonction des souches de levure, de leur cycle cellulaire et des conditions de culture. Toutefois ces études ont apportées des réponses partielles sur l'influence de l'environnement sur la paroi et en particulier sur son organisation au niveau biochimique, structural et topographique. La compréhension de ce mécanisme est très importante au niveau de la recherche scientifique mais aussi au niveau industriel, puisqu'elle permettrait d'optimiser la production de composés pariétaux et leur utilisation comme cibles antifongiques ou d'additifs alimentaire (en vinification et en nutrition animale). Le but des travaux de recherche sur la paroi de levures consiste à acquérir des données biochimiques de composition de la paroi ainsi que des données topographiques et structurales à l'échelle nanoscopique grâce à la microscopie à force atomique (AFM), afin d'étudier l'impact du fond génétique de la souche de levure. Finalement, l'impact d'un procédé industriel spécifique, tel que l'autolyse et le séchage, sur la composition et l'architecture de la paroi cellulaire de levures industrielles a été évalué.

Partie 1 : Détermination de la composition de la paroi

Pour améliorer notre compréhension, une nouvelle méthode permettant de déterminer les quantités de chaque polysaccharide contenues dans la paroi de levure a été développée. Il existe actuellement plusieurs méthodes d'analyse de la composition de la paroi de la levure utilisant des traitements chimiques ou des hydrolyses enzymatiques. Contrairement aux méthodes chimiques qui permettent d'avoir une estimation des quantités des polysaccharides pariétaux, les méthodes enzymatiques existantes sont utilisées jusqu'alors pour l'analyse structurale des polysaccharides mais ne permettent pas la quantification de chaque composé. Les méthodes chimiques les plus utilisées emploient des acides forts afin d'hydrolyser les polysaccharides pariétaux en monomères, qui sont alors analysés par chromatographie liquide. Cependant, elles présentent différents inconvénients : les monomères libérés peuvent être dégradés par l'acide, tandis que la chitine n'est pas entièrement

hydrolysée ce qui conduit à une sous-estimation de sa quantité et les β-1,3-glucanes ne peuvent pas être distingués des β-1,6-glucanes par ce type de méthode. L'emploi de 11 différentes enzymes commerciales capables d'hydrolyser différent substrats (mannanes, chitine, laminarine comme β-1,3-glucane et le pustulan comme β-1,6 glucane) a permis de sélectionner 4 enzymes commerciales spécifiques dénuées d'activités secondaires. De plus, la production et la purification dans notre laboratoire d'une endo-β(1,6)-glucanase de *Trichoderma harzianum* selon (Bom et al., 1998) a été faite puisqu'aucune enzyme commerciale de ce type n'existe. L'analyse des lipides par chromatographie à couche mince (TLC) a permis de déterminer qualitativement que les phospolipides présents dans les parois purifiées sont des phopshotidylcholines et des phosphotidylinositols. L'utilisation de la méthode de micro-Kejdahl a permis de montrer que les quantités de protéines contenues dans les parois purifiées sont différentes selon les mutants. Finalement, différentes configurations enzymatiques ont été étudiées, ce qui a permis d'établir une procédure enzymatique, capable d'hydrolyser la chitine, les β-1,3-glucanes et les β-1,6-glucanes restants, combiné à un traitement acide afin de déterminer les mannanes.

Ainsi, la méthode développée sur des parois purifiées de levure est basée sur 2 étapes : la chitine et les β-1,3-glucanes sont hydrolysés en leurs monomères respectifs, N-acetylglucosamine et glucose, par l'action combinée de la chitinase de *Streptomyces griseus* avec une exo et une endo-β-1,3 glucanase de *Trichoderma.* Les β-glucanes sont quantifiés à la suite de l'hydrolyse par le mélange endo-β(1,6)-glucanase de *Trichoderma harzianum* et β-glucosidase d'*Aspergillus niger*. La quantité de β-1,6 glucanes est alors déterminée par soustraction entre la quantité de β-glucanes et la quantité de β-1,3 glucanes déterminée à la première étape. L'hydrolyse du β-1,6-glucane par l'endo-β(1,6)-glucanase conduit au gentiobiose, un disaccharide lié en β(1→6), qui est à son tour clivé en glucose par addition de la β-glucosidase. Parallèlement, à la méthode enzymatique une hydrolyse acide des parois purifiées de levure est effectuée. La méthode à l'acide sulfurique bien que destructive est indispensable pour la détermination des mannanes et permet de déterminer des quantités de β-glucanes totaux équivalentes à celle obtenues par la méthode enzymatique. La méthode enzymatique a l'avantage d'être quantitative pour la chitine (sous-estimée à > 50 % par la méthode chimique). De plus, cette méthode acido-enzymatique permet de distinguer les β-1,3 des β-1,6 glucanes. Elle a été validée par l'analyse de la composition pariétale de la souche de référence du laboratoire (BY4741) et des souches mutantes délétées de gènes codant pour la synthèse de chitine (*chs3Δ*), de β-1,3

glucanes (*fks1Δ*), de β-1,6 glucanes (*kre6Δ*), de ramification/élongation des chaînes de β-glucanes (*gas1Δ*) et de mannanes (*mnn9Δ*), cultivés en conditions standard de laboratoire. Ces différents mutants ont montrés une diminution sévère d'un de leurs composés dans la paroi quand un gène impliqué dans sa synthèse est délété. Dans le même temps, des tests de sensibilité aux drogues Congo Red, un colorant interagissant avec les β-1,3 glucanes (Kopecka and Gabriel, 1992) et le Calcofluor White, un colorant fluorescent qui se lie à la chitine (Roncero and Duran, 1985; Roncero et al., 1988) ont été effectués pour corréler les observations phénotypiques avec les résultats obtenus des dosages des β-1,3 glucanes et de la chitine. Nous avons observé une corrélation positive entre la teneur en chitine et les observations phénotypiques, démontrant ainsi que le test de sensibilité au Calcofluor White peut servir de test qualitatif simple.

Finalement, nous avons montré que cette méthode sert à évaluer les effets de l'environnement extérieur sur la composition pariétale de la levure. Par l'emploi de cette méthode, nous avons constaté qu'un changement de température (42°C, 1h) conduit à une augmentation de 2 fois de la quantité de chitine dans la paroi tandis que l'ajout de 9% d'éthanol dans le milieu de culture des levures, n'a apparemment aucun effet sur la composition pariétale.

Partie 2: Effet du fond génétique de la souche de levure sur la paroi cellulaire

La deuxième partie des travaux de recherche a consisté à évaluer l'influence de la souche sur la composition de la paroi, son organisation et ses propriétés biophysiques. Ces travaux ont été faits sur 3 souches mutantes délétées de gène codant pour la synthèse de la paroi et 4 souches industrielles de levure (L71, L69, L62, L60) fournies par la société Lallemand (Blagnac, France). Ces souches diploïdes ont été sélectionnées par la société pour leur intérêt dans les applications œnologiques et nutritionnelles. Les souches de laboratoire et industrielle ont été cultivées dans des conditions standard de laboratoire en milieu riche (Yeast Peptone Dextrose : 2% Glucose, 1% Peptone, 1% Extrait de levure), puis la méthode développée au cours de nos recherches a été employée afin de caractériser la composition polysaccharidique de la paroi purifiée de ces levures.

Par comparaison avec les souches de laboratoire, les parois cellulaires des souches industrielles ont montré une plus forte concentration en mannanes. Nous avons observé que parmi ces souches industrielles, leurs compositions pariétales possèdent différents profiles. En effet, dans le

cas de la souche L69 on détecte très peu de résidus de glucosamine après hydrolyse acide, ce qui est confirmé par la méthode enzymatique, par laquelle une très faible quantité de chitine dans la paroi est mesurée (respectivement 3% et 0.3%) mais aussi par les tests de sensibilité au Calcofluor White, cette souche étant très résistante à cette drogue. Les 3 autres souches ont des quantités plus importantes de chitine, en particulier la souche L62 qui contient de forte teneur en chitine. Grâce à cette nouvelle méthode acido-enzymatique, nous avons également pu déterminer les proportions des β-1,3 et des β-1,6-glucanes. En milieu riche, les souches les plus riches en β-1,3-glucanes sont L71 et L60, ce qui est aussi confirmé par la plus grande sensibilité de ces deux souches au Congo Red.

Ces différences de composition de la paroi cellulaire se reflètent dans des différences entre les propriétés de surface et le comportent mécanique. Ces propriétés ont été observées et mesurées par la microscopie à force atomique (AFM) afin de rechercher un lien possible entre la composition biochimique et les propriétés nanomécaniques de la paroi cellulaire de la levure. Cette technologie récente, développée en 1986 par Binnig et Quate (Binnig et al., 1986), a été préférée à la microscopie électronique (MEB et MET), parce qu'elle permet d'étudier des cellules vivantes dans leurs conditions physiologiques à l'échelle nanoscopique. Avec cet outil, nous avons imagé les cellules, mais aussi nous avons mesuré la force entre la pointe de l'AFM et la surface de la cellule afin de quantifier les interactions qui peuvent exister. Ceci à permis d'observer la morphologie des cellules et de caractériser les propriétés biophysiques de la surface de chaque souche de levure en termes de rugosité, élasticité et adhésion.

L'analyse AFM a montré que les souches industrielles L71, L62 et L60 ne sont pas adhésives tout comme les souches de laboratoire (souches sauvage BY4741 et mutantes *chs3Δ, gas1Δ, mnn9Δ)*. Cependant, la souche œnologique L69, utilisée pour sa forte production en mannoprotéines en fermentation alcoolique, a montré une forte adhésion avec notamment l'observation de patchs sur la paroi. Si l'on compare les valeurs du module de Young, qui donne une information sur l'élasticité des cellules, aux données biochimiques de la paroi obtenues par la méthode acide-enzymatique ; nous observons une tendance entre la valeur de chitine et l'élasticité pour les souches L71, L69, L60 et la souche haploïde de référence de laboratoire (BY4741), à l'exception de la souche L62 et du mutant *gas1*Δ qui présentent de forte teneur en chitine et un faible module de Young. On en conclut que la teneur en chitine mais également l'architecture moléculaire pariétale influencent très fortement ces propriétés nanomécaniques. Pour sonder l'organisation les polysaccharides à la surface de la cellule,

les pointes AFM ont été fonctionnalisées à la concanavaline A suivant un protocole élaboré au LAAS-CNRS (Jauvert et al., 2012). La concanavaline A est une lectine qui se lie spécifiquement aux unités de mannose qui forment les mannanes et constituent la majorité de la couche externe de la paroi. Pour décrire l'étirement des polysaccharides à la surface des cellules de levure, les forces d'élongation ont été ajustées à l'aide d'un modèle physique dit modèle du ver (Worm Like Chain) qui décrit un polymère comme un filament courbé, irrégulier et semi-flexible. 30 à 35% des interactions détectées sont de l'ordre de 55-60 pN, confirmant la spécificité de l'interaction entre la concanavaline A et les mannoprotéines à la surface des cellules des 4 souches industrielles. La répartition entre la force d'adhésion de ces interactions spécifiques et la distance d'étirement est hétérogène et montrent que les longueurs de molécules étirés sont courtes pour les souches L71 et L60 tandis pour la souche L69 la longueur est plus importante (97 nm).

Pour compléter notre étude, nous avons réalisé grâce aux puces à ADN une analyse transcriptomique afin de mesurer les changements dans l'expression relative des ARNm entre les 4 souches diploïdes industrielles, cultivées dans les mêmes conditions que pour les analyses biochimiques et biophysiques. Par comparaison avec les souches industrielles, nous avons obtenus un profil transcriptomique très différent pour la souche diploïde de référence du laboratoire (BY4743), par conséquent nous avons choisi la souche L71 de chez Lallemand comme référence. Cette souche étant utilisée comme référence au niveau industriel. Les résultats ont été acquis à partir de 3 expériences indépendantes et les gènes ont été considérés comme étant sous ou sur exprimés lorsque qu'après normalisation le ratio d'intensité est modifié par au moins un facteur de 1.5. Cette analyse a montré qu'un nombre important des 6256 gènes analysés sont différentiellement exprimés dans ces souches de levure. Parmi ces gènes, 175, 161 et 236 gènes sont surexprimés chez L69, L62 and L60 par rapport à la souche industrielle de référence L71. La distribution de ces gènes surexprimés en catégories fonctionnelles (Funspec database) a montré que ces gènes sont impliqués dans le métabolisme, le transport et la réponse au stress. Par exemple, pour la souche L69, la plupart de ces gènes surexprimés par rapport à la référence L71 encodent des protéines de fonctions inconnues (34% des 175 gènes) et participent au métabolisme (19%), le transport (12%), la réponse au stress (5%) et l'énergie (4%).

A partir des profils transcriptomiques, 80 gènes différentiellement exprimés entre les souches industrielles et la souche de laboratoire ont été retenus. Ces gènes sont liés à la l'architecture et le

remodellage de la paroi cellulaire. La représentation des niveaux de transcrits de ces gènes a illustré la proximité entre les souches L69 et L60, tandis que la souche L71 est plus distante. Des différences significatives ont été observées entre les niveaux de transcrits des gènes *FLO*, notamment les gènes *FLO5, FLO10, FLO11* et le pseudogène *YHR213W* qui partage des homologies de séquence avec FLO1. D'autre part, une sur-expression des gènes *FIT2, FIT3* et *TIR3* codant pour la synthèse des mannoprotéines ancrées à la paroi via une ancre glucosylphosphatidylinositol (GPI) peuvent expliquer une forte proportion de mannanes dans les parois des souches industrielles. Les gènes *YGP1* et *PIR3*, codant pour des glycoprotéines de la paroi et qui participent à la stabilité de paroi, ainsi que *EXG1*, codant pour une β-1,3-glucanosyltransférase, sont également sur-exprimés dans ces souches industrielles. Finalement, *SVS1* et *YLR040C* sont fortement sur-exprimés dans la souche L62. Ces gènes codant des protéines localisées à la paroi, montre une certaine spécificité de cette souche. En effet, *YLR040C* également nommé *AFB1*, code un inhibiteur d'α-factor spécifique de MATα pouvant contribuer sous certaines conditions à l'efficacité du mating et à la localisation de la protéine à la paroi via une ancre GPI. Parmi les 80 gènes, nous avons également constaté une différence prononcée dans l'expression de certains gènes avec la souche diploïde de référence du laboratoire BY4743 et les souches industrielles. En effet, les gènes de la famille *ASP* (*ASP3-1, ASP3-2, ASP3-3* et *ASP3-4*) sont sous-exprimés plus de 300 fois dans les souches industrielles. Chez la levure *Saccharomyces cerevisiae*, la cascade de dégradation de l'asparagine comprend 5 gènes asparaginase dont *ASP3* localisé sur le chromosome XII et répété pour créer un cluster de 4 gènes identiques. Ces gènes encodent l'asparaginase II qui hydrolyse l'asparagine en aspartate et ammoniaque. La délétion des copies du gène *ASP3* est en lien avec des résultats précédents qui rapportent son absence dans le génome de 128 espèces fongiques (League et al., 2012) et dans des souches œnologiques (Carreto et al., 2008), tandis que ces gènes sont présents dans la souche de laboratoire S288c, à partir de laquelle la souche BY4743 est dérivé.

Finalement, afin d'avoir une vue d'ensemble des relations qui peuvent exister entre les changements d'expression des gènes, la composition biochimique de la paroi et les propriétés de surface (nanomécanique et propriétés d'élongation des mannoprotéines), nous avons utilisés le package mixOmics (Lê Cao et al., 2009; Gonzalez-Ramos and Gonzalez, 2006) du logiciel R. Cette analyse a permis de montrer une association entre les quantités de mannanes et la fréquence d'adhésion entre la concanavalin A attaché à la pointe AFM et la surface de la cellule. Puisque la

lectine concanavalin A lie les unités α-glucose et α-mannose, ces résultats montrent la pertinence de l'approche intégrative pour nos données biochimiques et biophysiques. Une association entre la longueur de molécule étirée avec la pointe AFM fonctionnalisée et la quantité des β-1,6-glucanes contenue dans les parois des souches industrielles, a également été observée. Ce résultat est en accord avec des études biochimiques qui ont prouvés que les différents composants de la paroi sont reliés *in vivo* par des liaisons covalentes en complexes macromoléculaires afin de former des blocs flexibles dans lesquels les mannoprotéines sont liés aux β-1,6-glucanes, lesquels sont liés aux chaînes de β-1,3-glucane (Kollar et al., 1997). Ainsi la modification des liaisons entre polysaccharides de la paroi peut avoir une influence sur l'étirement des mannoprotéines. Une association entre le module de Young et les β-glucanes a également été constatée grâce à cette analyse intégrative. Le module de Young ou module élastique est une constante de la loi de Hooke. Il reflète la résistance à la paroi à une déformation élastique et a comme unité le pascal (Pa). Plus la valeur est élevée, plus un stress important est nécessaire pour déformer la paroi. L'analyse intégrative a permis d'établir des associations entre les données biophysiques et biochimiques, mais également de relier toutes ces données aux données transcriptomiques. Par conséquent, l'association module de Young et β-1,3-glucane a été associé à un groupe de gènes impliqués dans l'assemblage du cytosquelette (*SLA1, SPH1, CLA4*), la synthèse β-1,6-glucan (*KRE11*) et des voies de signalisation MAPK (*STE11, HOG1, DIG1, STE18*). En effet, la paroi cellulaire de la levure est une structure rigide et dure, qui apporte un support mécanique à la cellule. Toutefois, la paroi cellulaire peut également être déformé ou modulé, permettant ainsi à la cellule de s'allonger et de se diviser lors de la méiose. Finalement, nous avons observés une association entre les quantités de mannanes dosées biochimiquement et des gènes impliqués dans la synthèse des mannoprotéines et dans la glycosylation. 5 gènes reliés à la structure de la membrane et au métabolisme du stérol, ainsi que 2 gènes liés à la biosynthèse de l'ergostérol et des phospholipides ont également été associés à la quantité de mannanes. Ceci peut être expliquer par le fait que la N-glycosylation, la synthèse des sphingolipides et l'estérification du stérol sont localisés dans le réticulum endoplasmique et sont régulés de manière coordinative. (Jacquier and Schneiter, 2012).

Dans notre investigation, nous avons aussi évalué l'effet du milieu de culture sur la composition biochimique de la paroi et du profile transcriptomique des souches de levure. Dans cette

partie, nous avons cultivées les souches diploïdes industrielles dans un milieu riche (Yeast Peptone Dextrose : 2% Glucose, 1% Peptone, 1% Extrait de levure) et un milieu minimum synthétique (Yeast Nitrogen Base : 2% Glucose, 0.17% Yeast Nitrogen Base, 0.5% Sulfate d'ammonium). A partir des courbes de croissance des 4 souches industrielles sur ces deux milieux, nous avons constaté que les souches ont des temps de génération plus courts sur le milieu synthétique tandis que la souche L62 a un temps plus long dans les 2 milieux. L'analyse de la composition en polysaccharides de la paroi a démontré que ces 4 souches industrielles ont des quantités de mannanes équivalentes (environ 40%) en milieu minéral. Contrairement à une croissance en milieu riche, une augmentation de la quantité de mannanes est observée en milieu synthétique pour la souche industrielle L71 et la souche de référence de laboratoire (BY4743). On constate également qu'il y a une diminution d'au moins 2 fois de la quantité de chitine dans la paroi des souches industrielles et de la souche de laboratoire en milieu synthétique. L'analyse des niveaux des transcrits de la souche de laboratoire BY4743 en milieu synthétique par rapport au milieu riche a montré une activation des gènes impliqués dans l'organisation de la paroi ainsi que dans la synthèse de la chitine (*RCR1, CHS1*), des mannoprotéines (*PAU24*) et des β-glucanes (*SCW10*). L'augmentation de la quantité de mannanes mesurée chez BY4743 peut être corrélée avec une surexpression des protéines pariétales à ancre GPI (GPI-CWP) quand cette souche de levure est cultivée dans le milieu synthétique. Ce résultat est en accord avec les travaux de (Wodicka et al., 1997) qui a montré l'effet du milieu sur l'activation ou la répression des protéines pariétales (CWP) spécifiques.

Partie 3 : Impact de procédé industriel spécifique sur la composition et l'architecture de la paroi cellulaire de levures industrielles.

Dans une dernière partie, nous avons étudié les effets d'un procédé industriel spécifique tel que l'autolyse/séchage, sur la composition biochimique de la paroi et sur les propriétés nanomécaniques de la surface cellulaire. Dans cette investigation, nous avons choisi de travailler sur 2 souches industrielles (L71 et L69) qui confèrent des propriétés œnologiques différentes.

Nous avons comparé la paroi des cellules de ces souches cultivées en condition standard de laboratoire (milieu riche glucosé), à celle des cellules de ces mêmes souches provenant de conditions industrielles. Les conditions industrielles impliquent une croissance en fermenteur et une concentration des cellules pour produire des cellules de levures sous forme de 'crème de levure', qui est à son tour autolysée pendant 20h à 55°C, suivie d'une séparation et d'un séchage par atomisation

afin de produire des fractions séchées de levures appelées 'Yeast Cell Wall' (YCW). L'analyse de la composition pariétale des levures vivantes, de la crème et de la fraction YCW de ces deux souches industrielles a montré que les proportions en β-1,3-glucans, β-1,6-glucans, mannanes et chitine ne sont pas significativement différentes entre les différentes conditions. Cependant, nous avons observé un effet de la souche de la levure sur la composition de la paroi. En effet, la paroi des cellules de la souche L71 contient une proportion en β-1,6-glucanes et en chitine plus importante que celle de la souche L69. Toutefois, la souche L69 contient 20-25% plus de mannanes dans sa paroi que la souche L71, ce qui est en accord avec le fait que cette souche œnologique se différencie par sa forte production en mannoprotéines durant la fermentation alcoolique et peut expliquer le fait que les cellules de cette souche s'agrègent pour former des chaînes de cellules pendant leur croissance en milieu glucosé mais aussi après réhydratation de leur fraction YCW.

L'analyse biophysique par la microscopie à force atomique (AFM) de ces deux souches dans leurs différentes conditions, a permis de montrer que l'autolyse affecte la morphologie des levures et leur surface. La présence de trou de 600 nm de diamètre au milieu d'une cellule provenant de la fraction YCW réhydratée a été observée sur au moins 15% des cellules analysées et avec les deux souches industrielles. Les images AFM de déflection à haute résolution ont également permis de montrer que la surface des fractions autolysées sont plus fracturées que celle des levures vivantes cultivées en condition de laboratoire. La rugosité de la surface cellulaire est ainsi augmentée de 4 fois entre une levure vivante et une levure provenant de la fraction YCW (respectivement 1.9 nm à 5.1 nm). Cette augmentation de la rugosité peut avoir différentes conséquences comme la modification des propriétés physico-chimiques et l'augmentation de la surface active, ce qui peut conduire à une meilleure sorption des molécules néfastes. Une analyse par AFM a aussi été réalisée sur la souche L69. Celle-ci a montré une forte adhésion avec la présence de « patchs » adhésifs à la surface des cellules qui ne sont pas présents chez la souche L71. Ces patchs apparaissent plus grands à la surface de la fraction YCW, avec une aire moyenne de 20 nm^2 et un diamètre de 141 ± 32 nm. Une analyse plus détaillée a montré que ces patchs correspondent à des petites protubérances moins rigide et plus haute de 30-40 nm que la surface de la cellule. Récemment, des observations similaires ont été effectuées à la surface de cellules de *Candida albicans*, qui présentent des nanodomaines du fait de la surexpression de *ALS1*, un gène qui encode une protéine de surface (Alsteens et al., 2010; Lipke et al., 2012). Pour révéler les différences de surface de ces deux souches de levure, nous avons

employé des pointes AFM fonctionnalisées avec la lectine concanavaline A à la surface d'une cellule vivante et de la fraction YCW réhydratée. Ainsi, ces expériences ont permis d'étudier la distribution, l'adhésion et la flexibilité des mannanes. Avec ce type de pointe, nous avons obtenu une force d'interaction de 60 pN, qui est caractéristique de la rupture entre la lectine et un seul résidu de mannose. Dans le cas de la souche L71, pour chaque condition on détecte 25% d'événements adhésifs, mais on observe une longueur d'étirement des polysaccharides plus importante (de 0 à 250 nm) et une distribution des mannanes plus homogène à la surface de la fraction YCW que sur celle d'une cellule vivante. La souche L69 a également présenté une distribution des polysaccharides plus homogène sur la surface des cellules 'YCW', avec une longueur d'étirement des polysaccharides supérieur à 350 nm, indiquant un dépliement des polysaccharides différent entre les souches L71 et L69.

Grâce à l'utilisation de puces à ADN, nous avons pu analyser l'expression relative des gènes dans les deux souches industrielles. Lorsque l'on compare leur profiles transcriptomiques, nous observons que 392 gènes sont différentiellement exprimés entre la souche L69 et la souche L71, dont 175 gènes sont surexprimés tandis que 217 gènes sont sous-exprimés. Parmi les gènes sous-exprimés chez L69, plusieurs gènes sont impliqués dans le métabolisme de la méthionine et du sulfate, tandis que des gènes surexprimés sont impliqués dans la biosynthèse de la paroi et son assemblage. En effet, la souche L69 est caractérisée par une surexpression des gènes encodant les mannoprotéines, en particulier FLO11 qui appartient à la famille multigénique de floculation et encode une protéine hautement glycosylée.

Pour conclure, nous avons observé que le procédé industriel d'autolyse/séchage par atomisation ne modifie pas significativement la composition biochimique de la paroi de deux levures industrielles œnologiques L69 et L71, qui ont des profils sensoriels différents, mais induit des changements de propriétés de surface. Le procédé modifie la topographie de surface de la cellule, ce qui conduit à une augmentation de la rugosité et augmente les propriétés adhésives des cellules. La souche L69 possédant une importante proportion en mannoprotéines dans sa paroi est aussi caractérisée par la présence de patchs adhésifs et qui forment des nanodomaines. Une analyse comparative des profils transcriptomiques de ces deux souches a révélé une forte surexpression des flocculins encodés par le gène *FLO11* dans la souche L69, qui peut être à l'origine de la formation des nanodomaines. Finalement, cette étude a permis de montrer que les modifications biophysiques

induites par le procédé d'autolyse/séchage ne sont pas corrélées aux changements dans la composition de la paroi. De plus, la nature d'un composé pariétal, tel que les mannoprotéines, peut différer en fonction de la souche, et grandement influer les propriétés de surface des levures.

Pour conclure, dans ces travaux de thèse plusieurs approches ont été employées. La microscopie à force atomique (AFM) a permis d'étudier l'organisation de la paroi, sa structure et son organisation, ainsi que de mettre en évidence des particularités à la surface des cellules après différents stress. Par exemple, cette technologie a permis d'observer la formation d'une structure circulaire de 3 µm de diamètre à la surface de cellule soumis à un choc thermique d'1h à 42°C (Pillet et al., 2014). L'AFM a aussi permis de mettre en évidence l'impact important d'un antifongique, la Caspofungin from Merck™, sur la morphologie et les propriétés nanomécaniques des cellules de *Candida albicans* et *Saccharomyces cerevisiae* (Formosa et al., 2013). Des méthodes biochimique et moléculaire (puces à ADN) ont aussi été employées afin d'accéder à la composition de la paroi et à l'expression des gènes de souches de laboratoire et de souches industrielles cultivées sous différentes conditions ou soumises à des procédés industriels spécifiques. Ces approches ont été utilisées afin de mettre en évidence des corrélations entre les propriétés nanomécaniques de la paroi, la composition biochimique et des gènes qui pourraient être déterminant pour l'organisation, la structure et les propriétés physiques de la paroi. Ce travail a donc été divisé en 3 parties : le développement d'une méthode quantitative des différents composants de la paroi, l'étude de l'effet du fond génétique sur la composition et les propriétés de surface des cellules de différentes souches, et finalement l'étude d'un procédé d'autolyse utilisé pour obtenir des levures spécifiques et vendus sous forme de paroi de levures (Yeast Cell Wall).

Les données montrent clairement l'importance du fond génétique de la souche et des conditions de culture sur la composition biochimique de la paroi cellulaire. Ces résultats sont en accord total avec les travaux précédents de notre groupe (Aguilar - Uscanga et François , 2003) et d'autres (Bzducha - Wróbel et al , 2013; . Nguyen et al., 1998) qui ont montré l'impact du milieu de croissance le mode de culture ainsi que les origines de la souche de levure sur la composition de la paroi cellulaire. Ces études ont montré qu'il y avait une diminution d'environ 1,5 fois du ratio β-glucane/mannane dans la paroi cellulaire de *S. cerevisiae* lorsqu'elle est cultivée dans un milieu minimal synthétique par rapport à un milieu peptone dextrose riche en levure (Aguilar- Uscanga et al.,

2007). Par ailleurs, le glycérol à une concentration de 3% dans le milieu conduit également à une augmentation des quantités de mannoprotéines et β-glucane dans la paroi cellulaire de *S. cerevisiae* (Bzducha-Wróbel et al., 2013). Tout comme les éléments nutritifs et les sources de carbone, les conditions de culture et environnementales influencent la composition de la paroi cellulaire. Lorsque la levure est soumise à une augmentation de température, de 22°C à 37°C, la quantité de fraction résistante à une β-1,3-glucanase augmente significativement (Aguilar-Uscanga et al., 2007), tandis que la taille des chaînes de β-1,3-glucane dépendent de la phase de croissance (Cabib et al., 2012). Ici, des informations complémentaires ont été apportées, du fait que l'on a distingué la fraction de β-1,3-glucane des β-1,6-glucane. Ainsi, nous avons observé que la teneur en β-1,6-glucane, contenue dans la fraction de β-glucanes totaux, est en général modifiée en fonction des souches de levure et des conditions de culture. Les β-1,6-glucanes contenues dans la paroi cellulaire est également modifiée en réponse à exposition à un antifongique tel que la Caspofungin (Formosa et al., 2013). Une deuxième conclusion générale qui a soutenu les travaux précédents (Dague et al., 2010 et chapitre 3A), était le manque de connexion directe des propriétés nanomécaniques de la paroi cellulaire (spécifiquement exprimés comme le module de Young qui est une valeur qui compte pour l'élasticité ou la rigidité) à un composant spécifique de celle-ci. Toutefois, cette conclusion peut être contestée avec le constat d'une corrélation étroite entre le module de Young et la teneur en β-1,3-glucane, qui a été obtenu à partir de notre analyse de corrélation par l'utilisation de méthodes statistiques dédiés (S-PLS et CCA dans le pack mixOmics). Cette observation appuie le fait que les chaînes de β-1,3-glucane, qui constituent la couche intérieure de la paroi cellulaire, peuvent être responsables de la forme de la cellule en raison de leur structure fibrillaire. Cependant, une forte altération de l'élasticité dans des mutants défectueux des enzymes de remodelage de la paroi cellulaire telles que Gas1, Crh1, Crh2 (Dague et al., 2010) montre que les variations de l'élasticité de la paroi cellulaire ne peuvent pas être uniquement expliquer par la structure des β-1,3-glucanes.

Un autre résultat intéressant qui est ressorti des travaux est l'association étroite entre le contenu de mannanes et la nature des mannoprotéines dans la paroi de la cellule avec le nombre d'interactions surface-concanavalin A. En effet, l'utilisation d'une pointe AFM fonctionnalisée avec la lectine concanavaline A a permis d'étirer à la surface de la souche mutante *gas1*Δ de longues chaînes de polysaccharides, tandis qu'à la surface de *mnn9*Δ un faible pourcentage d'interaction spécifique mannane-lectine et des longueurs de rupture plus courtes (inférieures à 100 nm) ont été mesurées.

Ce résultat est probablement dû à la faible teneur en mannane dans *mnn9*Δ, ainsi qu'à une mannosylation différente des protéines dans la paroi de cette souche. Ainsi, nos résultats indiquent une différence dans la longueur des polysaccharides étirés à la surface de ces mutants. En utilisant la même méthodologie, nous avons exploré la surface des cellules des souches industrielles et avons montré que la souche L69 était fortement adhésive. Nous avons pu déplier des molécules de 20-400 nm à la surface de cette souche. Ce comportement est en accord avec le modèle du ver (Worm Like Chain), qui décrit un polymère comme un filament flexible courbé (Bustamante et al., 1994;. Janshoff et al, 2000), suggérant que les chaînes de mannoprotéines étirées à la surface de la souche L69 possèdent un ancrage différent dans la paroi cellulaire. En outre, la forte adhésion de cette souche a été associée à la surexpression spécifique de *FLO11*, qui code pour une protéine dite flocculin fixée à la paroi cellulaire via une ancre GPI, ainsi qu'à *YHR213w* qui code pour un floculin putatif. Cependant, d'autres gènes de la famille des flocculines, tels que *FLO5* et *FLO10*, sont réprimés dans la souche L69 par rapport à la souche de laboratoire non adhésive BY4743. En outre, la paroi de cette souche, qui comporte la plus haute teneur en mannoprotéines, présente des patchs hautement adhésifs formant des nanodomaines et qui ont également été mis en évidence après le processus de l'autolyse. Nous avons constaté que ces nanodomaines, imagés pour la première fois sur la levure *S. cerevisiae*, ressemblaient à ceux identifiées à la surface de la levure pathogène *Candida albicans* (Formosa et al., 2014b). Les nanodomaines à la surface de *Candida albicans* ont été attribués à *ALS1* (Formosa et al., 2014b) codant pour des adhésines. En effet, ces protéines sont connues pour former des amyloïdes en raison de la présence d'un motif structural de sept résidus et enrichis en acides aminés β-ramifiés (Île, Thre, Val), qui forment un β-feuillet (Ramsook et al., 2010). Comme écrit plus haut, le gène *FLO11* code pour une glycoprotéine à ancre GPI nommée flocculin, tandis que *YHR213W* a été identifié comme un fragment possédant une similarité de séquence avec *FLO1*. Des études moléculaires sur *FLO11* ont révélé que le domaine de structure de la protéine Flo11 comprend un domaine N-terminal correspondant à un domaine d'adhésion lectine, un domaine central répétitif et hautement glycosylé, ainsi qu'un domaine C-terminal qui porte un site d'ancrage GPI. Cette séquence comporte aussi des motifs pouvant conduire à une β-agrégation partielle (Ramsook et al., 2010). Par conséquent, nous avons suggéré qu'une surexpression de *FLO11* dans la souche L69 peut être à l'origine d'un dépôt localisé important de protéines Flo11, conduisant à l'agrégation des protéines β-amyloïdes en nanodomaines. Ces protéines amyloïdes sont à l'origine de l'adhérence de plusieurs

champignons pathogènes tels qu'*Aspergillus*, *Coccidioides*, et *Mucorales*. Chez la levure, les nanodomaines amyloïdes favorisent la formation de biofilm et le maintien de l'agrégation, mais qui peut être empêché par des mutations dans la séquence d'amyloïde ou par un traitement avec des colorants antiamyloïdes tels que le rouge Congo ou les thioflavines S et T. Dans les cellules de mammifères, ces protéines amyloïdes sont des marqueurs de maladies neurodégénératives comme Alzheimer, Parkinson ou les maladies de Creutzfeldt-Jakob (Goldschmidt et al., 2010). La caractérisation de la structure et des propriétés adhésives des nanodomaines présents chez *S. cerevisiae* nécessitent des analyses complémentaires, mais leur découverte soulève la question de leur fonction dans les propriétés de sorption à *S. cerevisisae*. En effet, chez *C. albicans* les adhésines Als1p et Als5p ont montrés une capacité à lier divers ligands. Par exemple, le domaine N-terminal de Als1p peut lier les résidus de α-Fucose (Donohue et al., 2011), tandis que Als5p ou Als1p peuvent adhérer à des peptides et des protéines présentant des séquences d'acides aminés comportant un acide aminé hydrophobe et un acide aminé cationique ainsi qu'une conformation stérique appropriée (Klotz et al., 2004). Ainsi, la structure de séquences et la conformation sont deux facteurs importants dans la reconnaissance du ligand.

En intégrant les données biochimiques et biophysiques relatives à la paroi cellulaire avec les données transcriptomiques des souches industrielles grâce une méthode biomathématique basée sur des calculs de corrélation, nous avons trouvé une association étroite entre l'élasticité de la paroi cellulaire (c'est-à-dire les valeurs module de Young) et les niveaux de β-1,3-glucanes. Les gènes qui ont été corrélés à cette association codent pour des protéines impliquées dans l'assemblage de la membrane et du cytosquelette (*SLA1*), la biosynthèse des β-1,6-glucanes (*KRE11*) et dans les voies de signalisation MAPK (*STE11, HOG1, DIG1, STE18*). Ces résultats suggèrent que la valeur du module de Young ou d'élasticité peut être fonction du niveau de β-glucane et que ces deux variables peuvent être régulées par la voie de signalisation MAPK, qui est impliquée dans le stress osmotique et la croissance des pseudohyphes. En outre, les niveaux de mannanes ainsi que les interactions de la surface des cellules avec la lectine ConA ont été associées à des gènes impliqués dans la maturation des protéines (*KEX1, SSY5*), ainsi que dans la biosynthèse de l'ergostérol et des phospholipides (*ERG7, URA8*) et des mannoprotéines (*DAN4, YLR040C, GPI18*).

La dernière partie de la thèse a été consacrée à aborder la question de l'effet d'autolyse sur la composition de la paroi cellulaire et les propriétés nanomécaniques de deux souches industrielles

(L71 et L69). Cette étude a montré que le conditionnement des cellules de levure en tant que « YCW » (Yeast Cell Wall dit paroi cellulaire de levure) par autolyse et un procédé de séchage ne modifie pas la composition de la paroi cellulaire, mais entraîne une modification de la topographie et des propriétés de surface de la cellule. L'imagerie à haute résolution de la surface cellulaire a révélé un changement d'une surface lisse, pour des cellules en phase exponentielle, en une surface plissée pour les cellules issues de la fraction YCW. Cette modification conduit alors à une augmentation de 4 fois de la valeur moyenne de rugosité pour des cellules issues d'YCW. Une augmentation de la rugosité peut entraîner une modification des propriétés physico-chimiques en augmentant l'hydrophobicité de la surface. Il peut en résulter une augmentation de la surface active par accroissement du nombre de ligands interagissant avec le récepteur (Hu et al., 2013), mais les effets de rugosité de surface sur la capacité de sorption doivent maintenant être mesuré avec précision. En effet, cette mesure de sorption nous aiderait à comprendre le lien entre la sorption et les propriétés de la paroi cellulaire et la composition. Les mesures de sorption peuvent être faites par l'AFM ou le système de pinces optiques et magnétiques (Neuman et Nagy, 2008). Ces techniques sont utilisées pour étudier les interactions d'une biomolécule unique (ligand) avec la surface d'une cellule vivante. Le système de pinces optiques utilise la lumière pour piéger les microsphères qui peuvent être fonctionnalisées par un ligand. Le système de pinces magnétiques consiste à utiliser un champ magnétique pour piéger la microsphère, sur laquelle le ligand fixé, afin d'étudier la torsion et la conformation de la molécule. Contrairement aux méthodes des pinces, dans des expériences de spectroscopie de force à molécule unique (SMFS) par AFM, le ligand est lié à la pointe de l'AFM et il peut être utilisé pour étirer sur la surface le récepteur et de localiser les sites de l'interaction ligand-récepteur. Dans cette dernière partie, l'AFM nous a permis également de mettre en évidence des trous de 600 nm de diamètre localisés au milieu des cellules, dans les deux souches L69 et L71, qui pourraient être due à 2 phénomènes : soit à un effet de l'autolyse provoquant une autodigestion du contenu intracellulaire de la levure par des enzymes protéolytiques intrinsèques, comme on le trouve dans le processus d'autolyse pendant la fermentation du vin, soit au séchage en lit fluidisé utilisé dans ce procédé.

Finalement, outre le développement d'une méthode spécifique pour quantifier chacun des composants de la paroi cellulaire, ce travail peut fournir des résultats pertinents pour des applications industrielles. D'une part, démontrer que les niveaux de β-1,3 et β-1,6-glucane dans la paroi cellulaire

issues de différentes souches (souches de laboratoire et industrielles) et de divers échantillons (cellules vivantes, crème, fraction autolysée) sont influencés par le fond génétique de la souche et des conditions de culture pourraient avoir un impact dans la production de dérivés de levure pour l'industrie agroalimentaire. De même, comprendre l'organisation de la paroi cellulaire, ses propriétés mécaniques et de surface dans la levure modèle *S. cerevisiae*, ainsi que trouver quels gènes sont liés à ces caractéristiques peuvent suggérer des stratégies moléculaires ou de procédés. Ces stratégies permettraient de favoriser des propriétés spécifiques de la paroi cellulaire de la levure pour des applications particulières, telles que le renforcement des capacités de sorption, l'optimisation de l'expression de certaines mannoprotéines spécifiques à la surface de la cellule ou rechercher de nouvelles cibles antifongiques.